YOUNES LEYSI-DERILOU

MONITORING AND MATHEMATICAL MODELING OF *IN VITRO* HUMAN MEGAKARYOCYTE EXPANSION AND MATURATION DYNAMICS

Thèse présentée
à la Faculté des études supérieures de l'Université Laval
dans le cadre du programme de doctorat en génie chimique
pour l'obtention du grade de Philosophiae doctor (Ph.D.)

DEPARTMENT DE GÉNIE CHIMIQUE
FACULTÉ DE SCIENCES ET GÉNIE
UNIVERSITÉ LAVAL
QUÉBEC

2011

Résumé

La mégakaryopoïèse est un processus complexe, qui prend naissance à partir des cellules souches hématopoïétiques (HSC). Ces dernières se différencient par étapes successives en mégakaryocytes (MKs) qui, suite à leur maturation, libèrent les plaquettes. Afin de modéliser le sort des HSCs lors de la mégakaryopoïèse en culture, un nouveau modèle mathématique a été développé, basé sur un programme de différenciation tridimensionnelle (3-D) où chaque sous-population est représentée par un compartiment. Dans le but d'évaluer la prolifération, la différenciation des MKs immatures puis matures, la cinétique de mort cellulaire ainsi que le nombre de plaquettes produites, à partir des cellules de sang de cordon (CB) ombilical enrichies en $CD34^+$, un ensemble d'équations différentielles a été déployé. Les cellules $CD34^+$ ont été placées en culture dans un milieu optimisé pour la différenciation mégakaryocytaire. Les paramètres cinétiques ont été estimés pour deux températures d'incubation (37°C versus 39°C). Les résultats des régressions ont été validés par l'évaluation de l'estimabilité des paramètres, en utilisant des analyses de sensibilité locale et globale, puis la détermination d'un intervalle de confiance. Ceux-ci ont été comparés par le biais de tests statistiques et d'analyses en composante principale (ACP). Le modèle proposé pourrait permettre de mieux comprendre les phénomènes complexes observés.

Les MKs sont uniques parmi les cellules hématopoïétiques, étant les seules à devenir polyploïdes au cours de leur développement par l'entremise de l'endomitose, un processus mitotique qui se termine prématurément durant la cytocinèse. Pour obtenir une image plus complète et exhaustive de la mégacaryopoïèse, une approche d'imagerie cellulaire à grand champ et à long terme a été développée permettant de suivre individuellement l'évolution des HSCs lors de leur différenciation *ex vivo*. Cela a permis de démontrer que les MKs polyploïdes sont encore capables de se diviser et de produire des cellules filles polyploïdes, et que ce processus est plus fréquent chez les MKs issues de CB que de moelle osseuse d'adulte. De plus, le processus de formation des proplaquettes semble également réversible. Les phénomènes énoncés plus haut étaient inversement proportionnels au niveau de ploïdie des MKs. En conclusion, cette étude a dévoilé de nouvelles propriétés jusqu'ici inconnues des MKs.

Abstract

Megakaryopoiesis is a complex process, which is initiated with the proliferation and the differentiation of hematopoietic stem cells (HSC) into megakaryocytes (MK), followed by the maturation of MK and ended by platelet release. To describe the fates of HSC during *ex vivo* megakaryopoiesis, a new mathematical model was developed based on a 3-dimensional kinetic developmental program. To address this, a set of differential equations was applied to analyze the proliferation, differentiation and death kinetic rates of purified cord blood (CB)-CD34$^+$ cells, immature and mature MKs, as well as platelet number and productivity. CB-CD34$^+$ cells were placed in culture optimized for MK differentiation. The kinetic parameters were estimated for two incubation temperatures (37°C vs. 39°C). The regression results have been validated by assessing the parameter identifiability using local and global sensitivity analyses and confidence intervals, and compared using statistical tests and principal component analysis (PCA). Furthermore, PCA was applied on the solution matrix to construct a simplified MK differentiation pathway model, and to reveal dependencies among the model parameters. The proposed model provides insight into phenomena that would be otherwise difficult to interpret.

MKs are unique among mammalian marrow cells as they polyploidize during their natural development. It is universally accepted that MK becomes polyploid by repeatedly deviating from normal cell cycling, where it ceases to complete cytokinesis and divide. To challenge this long-standing hypothesis and to obtain a more comprehensive picture of megakaryopoiesis, a long-term and large-field live cell imaging approach of *in vitro* MK culture was developed. Using CB- and bone marrow (BM)-CD34$^+$ as starting cells, the direct observation of cells undergoing differentiation and maturation over a 5-day culture period is reported for the first time. Herein, direct visual proof that polyploid MKs can complete cytokinesis during its normal development is presented. This phenomenon was found not restricted to CB- as the BM-derived polyploid MK also underwent division. However the latter showed significantly lower proliferation rate. This new finding explains in part the unresolved issue of low ploidy levels observed in CB-MK and contests the notion that polyploid MKs do not divide.

Avant-Propos

Dr. Alain Garnier supervised the graduate student for the entire research work; helped designing the experiments, and provided expertise in cell culture engineering; gave advice on live cell imaging approach, its development, and consultation on digital image processing; proposed and developed mathematical models and sensitivity analyses, and helped programming with MATLAB® and ImageJ softwares; helped, guided, criticized, and corrected the manuscripts and thesis. Dr. Garnier's lab in chemical engineering department supported financially the graduate student and the required materials and tools, provided the environment for some cell manipulation and live cell imaging apparatus.

Dr. Nicolas Pineault cosupervised the graduate student, provided expertise in stem cell and megakaryocyte biology; helped experimental designs, and provided expertise in cell culturing, flow cytometry, and cell assays; helped, guided, criticized, and corrected the manuscripts and thesis. All CB-cells were provided and manipulated in Dr. Pineault's lab at Héma-Québec R&D department.

Dr. Carl Duchesne cosupervised the graduate student, provided expertise in mathematical modeling, sensitivity analysis of the models, statistical analysis, and programming using MATLAB® software. Dr. Duchesne's lab in chemical engineering department provided the live cell imaging apparatus.

Ms. Lucie Boyer, co-author of the paper on polyploid cell division, helped design the experiments and provided technical assistance on cell culturing, CB-cell purification, flow cytometry, and cell assays in Dr. Pineault's lab at Héma-Québec R&D department.

Ms. Amélie Robert, co-author of the paper on polyploid cell division, performed the confocal microscopy experiment, interpreted the related results and edited the manuscript.

Younes Leysi-Derilou, designed and performed the experiments of cell culturing, flow cytometry, microscopy, cell tracking, data storage, data management, statistical analysis and mathematical modeling; wrote the programs for cell segmentation, image analysis, mathematical modeling, and flow cytometry using ImageJ, MATLAB®, ImagePro Plus, QED InVivo, FCS Express softwares and analyzed the results; and is the principal author of the manuscripts and the author of this thesis.

Acknowledgements

I wish to express my hearty gratitude to Dr. Alain Garnier, for his guidance and inspiration during the time of my graduate study and research. I would like to thank Dr. Nicolas Pineault for serving as my co-advisor and for his valuable guidance and suggestions on biological aspects of this research, and Dr. Carl Duchesne, my other co-director for his help on mathematical modeling.

Dr. Nicolas Pineault's lab in Héma-Québec R&D department has been a very warm environment. I have wonderful memory with my colleagues who worked, studied and discussed together during my graduate studies, Lucie Boyer, Jean-François Boucher, Amélie Robert, Valérie Cortin, Marie-Christine Hains, and Marichou Boulette.

I deeply thank my family, my wife, her family and my friends for their endless support and encouragement. Without their emotional and spiritual support, completion of this PhD degree might have been impossible. Last but not least, this thesis is dedicated to my wife, Sanaz Haratifar, and my brother, Rustam Salimi, and his family members, who have given me their love and concern during my school life.

Table of Contents

List of Tables

List of Figures

Lists of Movies

These movies are available on the attached CD.

Movie 5.1B: Ploidy levels of tracked CB-cells were determined by Hoechst staining.

Movie 5.2A: A CB-4N undergoes endomitosis and forms an 8N cell.

Movie 5.2B: Symmetrical division of a CB-4N cell into two tetraploid cells.

Movie 5.2C: Asymmetrical division of a CB-4N cell into one 2N and one 6N cells.

Movie 5.2D: Asymmetrical division of a CB-8N MK into two 4Ns and one 8N.

Movie 5.3A: Z-stack slices of trilobular hexaploid CB-MK stained with Hoechst (cell nuclei/blue) and phalloidin ALEXA 488 (actin filaments/green).

Movie 5.3B: Z-stack slices of trilobular hexaploid CB-MK stained with Hoechst (cell nuclei/blue) and anti-gamma tubulin (centrioles/red).

Movie 5.6A: A CB-tetraploid cell divides to two tetraploids. One of the tetraploids then enters cell cycle and eventually undergoes endomitosis and gives an 8N cell. Two parts.

Movie 5.6B: A CB-tetraploid cell, after 30 hours, undergoes mitosis and divides gradually into three cells (one 4N and two 2Ns). The newly formed tetraploid enters cell cycle and eventually divides into two tetraploids. Two parts.

Movie 5.6C: A tetraploid BM-MK, after 16 hours, undergoes mitosis and divides gradually into two 4Ns. Two parts.

Movie 5.S3A: Symmetrical division of a BM-tetraploid cell into two tetraploid cells.

Movie 5.S3B: Asymmetrical division of a BM-tetraploid cell produces one diploid and one hexaploid cells.

Movie 5.S4: A tetraploid cell divides to a diploid (2N) and hexaploid (6N). The hexaploid then enters cell cycle and eventually divides into one tetraploid and one octaploid cell. Two parts.

Movie 6.4B: Example of a mature CB-MK undergoing proplatelet that ends with programmed cell death.

Movie 6.4C: Reversible proplatelet formation. A mature tetraploid CB-MK that has already formed proplatelets regress to a regular round shape. Later, this cell undergoes further endomitosis and becomes octaploid.

Movie 6.S1: NIC-treated CB-MKs undergoes several continuous rounds of endomitosis.

List of Abbreviations

APC	Allophycocyanin (fluorochrome)
BIT	Bovine serum albumin, Insulin and Transferrin mixture
BM	Bone Marrow
BS1	Best platelet production culture medium found at Héma-Québec
BSA	Bovine Serum Albumin
c-MPL	cloned-Myeloproliferative Leukemia virus oncogene
CB	Cord Blood
CCD	Charge-Coupled Device (camera)
CFSE	Carboxyfluorescein Succinimidyl Ester
CSF	Colony Stimulating Factor
DMS	Demarcation Membrane System
DMSO	Dimethylsulfoxide
DNA	Deoxyribonucleic Acid
DT	Division Time or mitosis cycling time (hour) in cell lineage tree
EPO	Erythropoietin
FACS	Fluorescence Activated Cell Sorting
FBS	Fetal bovine serum
FITC	Fluorescein Isothiocyanate (fluorochrome)
FL	Flt3/Flk2 Ligand
FSC	Forward Scatter
G0	Resting phase, quiescence
G1	Gap1 phase, pre-synthetic phase and post-mitotic phase
G2	Gap2 phase, post-synthetic phase
GP	Glycoprotein
G-CSF	Granulocyte-Colony Stimulating Factor
GM-CSF	Granulocyte-macrophage colony stimulating factor
HQ	Héma-Québec
HSC	Hematopoietic Stem Cells
ID	Identification

IL	Interleukin
IMDM	Iscove's Modified Dulbecco's Medium
LDL	Low density Lipoprotein
LIF	Leukemia Inhibitory Factor
LT	Living Time (hour) in cell lineage tree
M	Mitosis phase, mitotic phase, phase of cell division
MAb	Monoclonal Antibody
MAPK	Mitogen-activated protein (MAP) kinases
MC	Methylcellulose
ME	Mercaptoethanol
MK	Megakaryocyte
MKLP	Mitotic Kinesin-Like Protein
MNC	Mononuclear cells
NIC	Nicotinamide
ODE	Ordinary Differential Equation
PB	Peripheral Blood
PBS	Phosphate Buffered Saline
PC	Principal Component
PCA	Principal Component Analysis
PE	Phycoerythrin (fluorochrome)
PFA	Paraformaldehyde
PI	Propidium Iodide
PT	Ploidy Time or endomitosis cycling time (hour) in cell lineage tree
R&D	Research and Development
R	Region (Cell event region in flow cytometry)
ROI	Region of Interest
RNA	Ribonucleic Acid
RT	Room Temperature
RT-PCR	Reverse Transcription Polymerase Chain reaction
S	DNA Synthesis Phase
SCF	Stem Cell Factor

Src	Sarcoma
SSC	Side scatter
TCN	Total Cell Number
TPO	Thrombopoietin

Glossary

The following definitions have been obtained from these web pages:

http://www.isscr.org/glossary/printversion.htm

http://stemcells.nih.gov/info/glossary.asp

http://www.wikipedia.org/

Adult stem cells: Stem cells found in different tissues of the developed organism that remain in an undifferentiated or unspecialized state. These stem cells can give rise to specialized cell types of the tissue from which they came.

Apoptosis: Physiologically regulated or programmed cell death; opposite to *necrosis*.

Bone marrow stromal cell: Also known as mesenchymal stem cells, bone marrow stromal cells are a mixed population of cells derived from the non-blood forming fraction of bone marrow. Bone marrow stromal cells are capable of growth and differentiation into a number of different cell types including bone, cartilage and fat.

Cell division: A process by which a single cell divides to create two cells. There are two main types of cell division depending on what happens to the chromosomes: mitosis and meiosis (see below the description of each).

Cell line: Cells that can be maintained and grown in culture and display an immortal or indefinite life span.

Chemokines: Cytokines with chemotactic activities.

Chromosome: A structure consisting of DNA and regulatory proteins found in the nucleus of the cell. The DNA in the nucleus is usually divided up among several chromosomes. The number of chromosomes in the nucleus varies depending on the species of the organism. Humans have 46 chromosomes.

Cytoplasm: The internal part of the cell excluding the nucleus.

Differentiation: The process of development with an increase in the level of organization or complexity of a cell or tissue, accompanied with a more specialized function. Differentiation is controlled by the interaction of a cell's genes with the physical and chemical conditions outside the cell.

Embryonic stem cell: Also called ES cells, embryonic stem cells are cells derived from the inner cell mass of developing blastocysts and can differentiate into several tissue types in a dish. An ES cell is self-renewing (can replicate itself), pluripotent (can form all cell types found in the body) and theoretically is immortal. Human embryonic stem cells are similar to ES cells from the mouse. However, in the mouse, it is possible to inject those cells into a blastocyst, to generate so called transgenic mice, while this is not, and should not, be possible in humans for ethical reasons.

Erythrocytes: Known as red blood cells, which carry oxygen from the lunges to tissues.

Hematopoietic stem cell: are multipotent stem cells that give rise to all the blood cell types including myeloid (monocytes and macrophages, neutrophils, basophils, eosinophils, erythrocytes, megakaryocytes/platelets, dendritic cells), and lymphoid lineages (T-cells, B-cells, natural killer cells). Hematopoietic stem cells are found in adult bone marrow, umbilical cord blood, and peripheral blood when mobilized with granulocyte-colony stimulating factor and in fetal liver.

Humoral: Relating to bodily fluids, especially serum; relating to or arising from any of the bodily humors.

Interleukin: cytokine made by one leukocyte and acting on other leukocytes.

Leukocytes: known as white blood cells, which are responsible for killing any micro-organisms that invade the body.

Meiosis: The type of cell division a diploid germ cell undergoes to produce gametes (sperm or eggs) that will carry half the normal chromosome number. This is to ensure that when fertilization occurs, the fertilized egg will carry the normal number of chromosomes rather than causing aneuploidy (an abnormal number of chromosomes).

Microenvironment: The molecules and compounds such as nutrients and growth factors in the fluid surrounding a cell in an organism or in the laboratory, which play an important role in determining the characteristics of the cell.

Mitosis: The type of cell division that allows a population of cells to increase its numbers or to maintain its numbers. The number of chromosomes remains the same in this type of cell division.

Multipotent stem cells: An unspecialized cell that gives rise to a specific specialized cell, but all within a particular tissue, organ, or physiological system. For example, blood-forming (hematopoietic) stem cells are single multipotent cells that can produce all cell types that are normal components of the blood.

Necrosis: The death of living cells or tissues. Necrosis can be due, for example, to age, accident, ischemia (lack of blood flow); from the Greek "nekros" (dead body).

Nucleus: A cell organelle, which is surrounded by a specialized membrane and contains the DNA of the cell. The DNA is packaged into structures called chromosomes, which is the genetic, inherited material of cells.

Plasticity: A characteristic of a cell that is capable of becoming a specialized cell type of different tissue. For example, when the same stem cell can make both new blood cells and new muscle cells.

Pluripotent stem cells: Stem cell that can become all the cell types that are found in an implanted embryo, fetus, or developed organism, but not embryonic components of the trophoblast and placenta (these are usually called extra-embryonic).

Progenitor cell: A progenitor cell, often confused with stem cell, is an early descendant of a stem cell that can differentiate and has a limited self-renewal potential inferior to that of a stem cell. A progenitor cell is often more limited in the kinds of cells it can become than a stem cell. In scientific terms, it is said that progenitor cells are more differentiated than stem cells.

Regenerative medicine: Medical interventions that aim to repair damaged organs, most often by using stem cells to replace cells and tissues damaged by aging and by disease.

Stem cells: Cells that have both the capacity to self-renew (make more stem cells by cell division) as well as to differentiate into mature, specialized cells (other type). See definitions of adult stem cell, hematopoietic stem cells, and embryonic stem cells, for further definition.

Stochastic: Random, probabilistic, opposite to deterministic process.

Thrombocytopenia: Low level of circulating platelets in individuals due to trauma or deficiencies.

Totipotent stem cells: Stem cells that can give rise to all cell types that are found in an embryo, fetus, or developed organism, including the embryonic components of the trophoblast and placenta required to support development and birth. The zygote and the cells at the very early stages following fertilization (i.e., the 2-cell stage) are considered totipotent.

Umbilical cord blood stem cells: Stem cells collected from the umbilical cord at birth that can produce all of the blood cells in the body (hematopoietic). Cord blood is currently used to treat patients who have undergone chemotherapy to destroy their bone marrow due to cancer or other blood-related disorders.

Undifferentiated: A cell that has not yet developed into a specialized cell type.

Unipotent stem cells: Stem cells that self-renew as well as give rise to a single mature cell type; e.g. spermatogenic stem cells.

Zygote: The cell that results from the union of sperm and egg during fertilization. Cell division begins after the zygote forms.

1. Introduction

The first report on blood platelets dates back to a paper by Osler in 1873[1], recognizing their disk-like shape, their circulation in the blood, and their rapid aggregation when they are removed from the blood vessels. However, at the time the researcher was not certain whether the platelets were normal blood elements. A century ago, James Homer Wright described that megakaryocyte (MK) cytoplasmic pseudopodia stained similarly to platelets and concluded that platelets originated from MKs[2]. In 1999, the first movie of platelet birth from MK was shown[3]. Over these years, the understanding of megakaryopoiesis and platelets has been vastly increased. This chapter reviews recent studies on platelet biology, with a focus on the step preceding platelet production, megakaryopoiesis and imaging the cellular events during megakaryopoiesis.

Cell therapy has recently fascinated many biologists, clinicians and bioengineers. The ability to manipulate cells to generate functional platelets outside the human body has important fundamental and therapeutic applications. A significant portion of population and cancer patients after chemotherapy experiences a significant reduction in platelet levels, a condition known as thrombocytopenia. Platelets are released into blood circulation by MKs which are generated through gradual commitment of hematopoietic stem cells (HSC). To understand the whole process which is initiated in marrow, called megakaryopoiesis, flow cytometry is commonly used to monitor MK growth and development.

Imaging and mathematical biology are two of the fastest growing areas of interdisciplinary research[4,5]. Application of time-lapse video microscopy can increase our understanding of cell behaviour and give the vital handle required to better control the growth, differentiation and maintenance of cells such as MK. Together with quantitative analysis of cell fates, this could lead to new breakthroughs toward future clinical application. In this thesis, imaging and mathematical modeling-based tools were used and developed to better describe and understand the complex process of megakaryopoiesis.

The overall objective of this research is to better understand the process of MK expansion and maturation, through the *ex vivo* expansion of CD34^{+} cells from cord blood (CB) or

bone marrow (BM), and to construct quantitative analyses of cell fates as a function of culture conditions and time. First, a flow cytometry-based quantitative model of the process of megakaryopoiesis was constructed to estimate the proliferation, differentiation and death rates of MKs and their progenitors. The second main objective was to challenge the long-standing hypothesis that polyploid MKs do not complete cytokinesis. For this purpose, a long-term and large-field live cell imaging approach of *in vitro* MK differentiation in the presence of thrombopoietin (TPO) was developed and sophisticated statistical data was applied to analyze the cell fates. Both tools provided means to check hypotheses and to gain new insights into MK development and increase our understanding of the mechanisms governing MK maturation.

Overview of the thesis; *Chapter 1* reviews the literature about megakaryopoiesis, in brief this covers the basics of cell cycle (section 1.1), biological point of view of the process (section 1.2), available and relevant biomathematical models (section 1.3), live cell imaging (section 1.4). *Chapter 2* summarizes the objectives and hypotheses of this thesis. *Chapter 3* describes the experimental procedures. *Chapters 4-6* present the results obtained throughout this thesis work, in the form of three manuscripts about the results of model development and microscopy study of *ex vivo* megakaryopoiesis. Some complementary results are presented in *Chapter 7*. Finally, *Chapter 8* discusses the results, concludes and gives future directions. *Appendix* contains a short communication manuscript.

1.1. Cell Cycle

The first step for controlling and modeling the dynamic process of cellular development is to understand the process of cell division referred to as cell cycle. The term cell cycle is generally used to describe the series of phases that occur during the cellular division process, as shown in Figure 1.1. Some of these phases are recognized for self-renewing cells, and thus by measuring the occurrence frequency of these phases, one can evaluate the self-renewal activity of a cell population. The cell cycle phases can be described as follows[6-8]:

Interphase: this phase represents the time between ("inter") two mitoses and can be sub-divided into three phases of G1, S and G2. In the **G1 phase** (Gap1, pre-synthetic phase and

post-mitotic phase), the cell performs specific functional activities, like synthesis of proteins and RNA. The time spent in this phase is extremely variable and depends on many factors, like cell type, stimulation and inhibition. Highly proliferative cells show a short G1 phase, non-proliferating cells have a long G1 phase. In **S phase** (DNA synthesis), the cell synthesizes deoxyribonucleic acid (DNA) for the cell genome duplication. The time interval needed for the S phase is approximately constant within a cell type. To measure DNA synthesis times, cells can be labelled with radioactive DNA precursors such as 3H-thymidine. **G2 phase** (Gap2, post-synthetic phase) is a short period before the subsequent division.

M phase (Mitosis, mitotic phase, phase of cell division); within this phase the cell undergoes nucleus and cell division. M phase is traditionally divided into six stages: **1) Prophase,** during which the chromatin condenses into chromosomes and the bipolar mitotic spindles begin to form. Microtubules of the cytoskeleton, responsible for cell shape, motility and attachment to other cells during interphase, disassemble; **2) Prometaphase**, which starts with the nuclear envelope break down, so there is no longer a recognizable nucleus. Spindle fibers elongate but instead of attaching to chromosomes, overlap each other at the cell center; **3) Metaphase**, tension due to the spindle fibers aligns all condensed and highly coiled chromosomes in one plane at the center of the cell; **4) Anaphase**, spindle fibers shorten, the kinetochores separate, and the chromatids (daughter chromosomes) are pulled apart and begin moving to the cell poles. Anaphase is also divided into two sub-phases of early Anaphase or Anaphase A (the chromatids abruptly separate and move towards the spindle poles) and late Anaphase or Anaphase B (involves the polar microtubules elongating and sliding relative to each other to drive the spindle poles further apart); **5) Telophase**, the daughter chromosomes arrive at the poles and the spindle fibers that have pulled them apart disappear; and **6) Cytokinesis**, the spindle fibers not attached to chromosomes begin breaking down until only that portion of overlap is left. During this phase, a contractile ring (made of non-muscle myosin and actin filaments) forms, also called cleavage furrow formation, and cleaves the cell into two daughter cells.

G0 phase (resting phase, quiescence), some cells stop to proliferate within the G1 phase and get "arrested" in the G0 phase, until they are activated again ("triggered") by a special stimulus and go back to cell cycling. This feature is characteristic for stem cells.
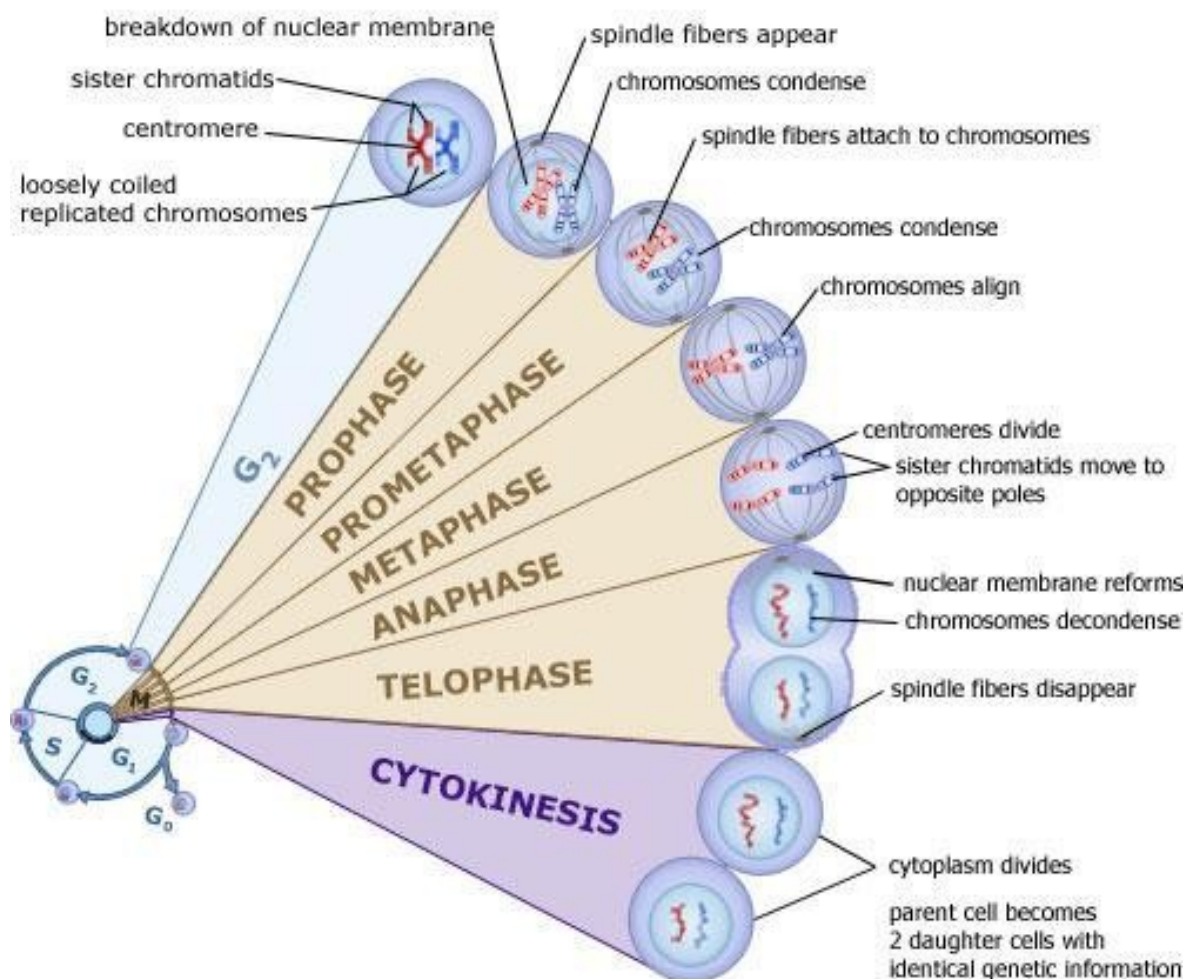
Figure 1.1: Cell cycle and mitosis (source: http://santasusana.org/pakelly/AP%20Bio/cell_cycle.htm).

1.2. Hematopoiesis

The production of blood cells is an enormous task. The normal adult produces daily around 2.5 billion platelets, 2.5 billion erythrocytes (red blood cells) and 1.0 billion granulocytes (white blood cells) per kg of body weight[9]. Since mature blood cells have a limited life span and little or no capacity to self-renew, all of these circulating cells are continuously generated from multipotent HSC. The term *"multipotent"* means the ability to generate

multiple cell types (but limited number of lineages) from undifferentiated stem cells. HSCs have the capacity to either self-renew (meaning being able to produce themselves without differentiation) or differentiate to specific cellular lineages that ultimately give rise to mature blood cells (Figure 1.2), a process termed *hematopoiesis*. This biological model of hematopoiesis is derived from morphological observations, cell colony experiments, labelling experiments, transplantation experiments, cytometry and other functional characterization. According to this model, committed HSCs give rise to two principal lineage-committed progenitors, a common lymphoid progenitor (capable of producing lymphocytes) and a common myeloid progenitor (with developmental potential to feed myeloid, macrophage, eosinophil, basophil, erythroid and MK lineages)[10]. MK and erythrocyte lineages arise from a common progenitor (megakaryocyte-erythroid progenitor) derived from the common myeloid progenitor[11].

HSCs can be identified and enriched using a combination of cell surface markers. Weisman et al. evaluated a set of protein markers on the surface of mouse and human blood cells and suggested CD34^{+}, Thy1^{+}, CD59^{+}, Lin^{-} are the closest markers for human HSCs[12,13]. The classic source of HSC is BM as doctors performed BM transplantations over the last 5 decades. However, granulocyte-colony stimulating factor (G-CSF) mobilized CD34^{+} peripheral blood (PB) cells is now more commonly used since this procedure is less invasive for the donors[10,14,15]. Also increasingly popular, another source is the use of HSC isolated from CB[14]. Else, fetal hematopoietic system, embryonic stem cells and embryonic germ cells are widely used in research as HSC sources[16]. Impacts of these sources on MK development are discussed in section *1.2.5*. Although there is no specific surface marker to recognize HSC population, CD34 is a universally accepted marker in this regard. CD34 expression has been found around 1 - 2% in isolated mononuclear cells (MNC) of CB or BM and below 0.1% in PB, which is increased by mobilization procedures[17].

The process of platelet production by MK, called thrombopoiesis, is complex and relies on a series of events that result in the release of thousands of platelets from each single mature MK[18]. The mechanism by which MKs develop and give rise to platelets have fascinated hematologists for over a century and cell engineers for a decade. The following sections describe in details the biology of MK as well as the platelet assembly process and review

the literature results and lessons from both *in vivo* studies, including preclinical and clinical trials, and *ex vivo* experiences on how to generate platelets from MK.
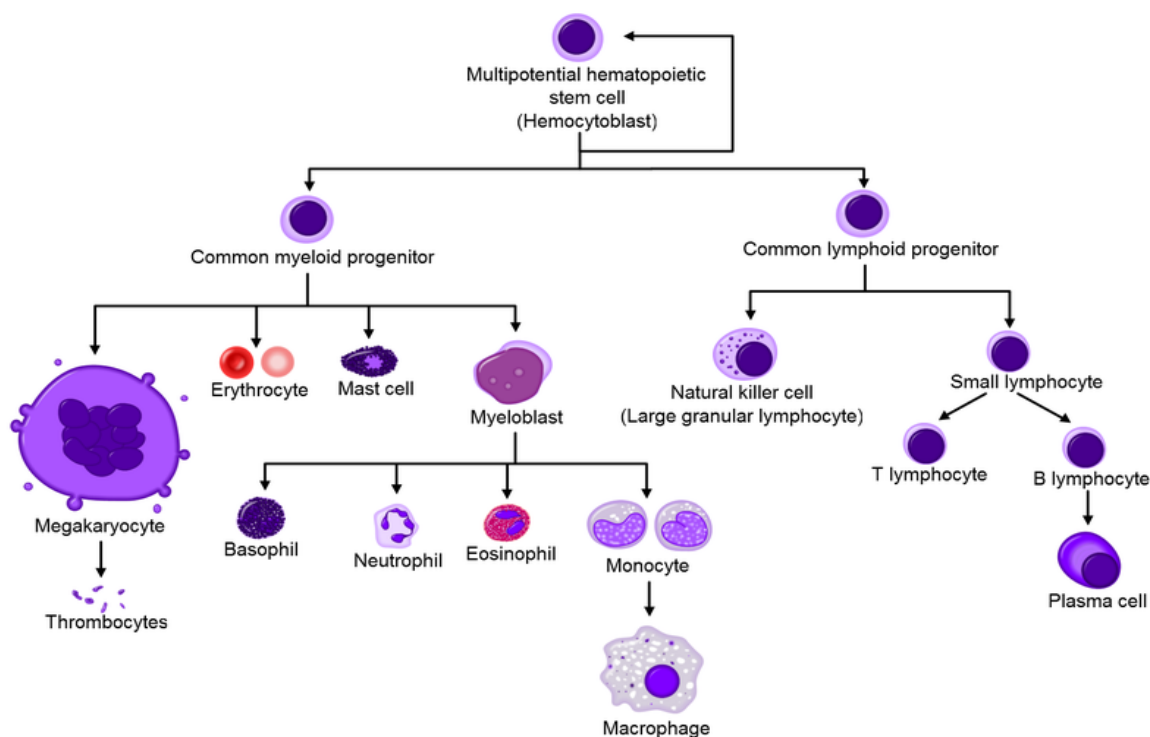
Figure 1.2: Hematopoietic stem cell potential commitments (Source: http://www.lifeethics.org/www.lifeethics.org/2007/10/review-what-we-know-about-stem-cells.html).

1.2.1. Megakaryocyte Characteristics

Megakaryopoiesis, a branch of hematopoiesis, is a process that initiates with the differentiation of multipotent HSCs to megakaryocytic cells, proliferation of MK precursors, maturation through polyploidization at different levels, and followed by proplatelets formation from mature MKs. This process is ended by platelet release from proplatelets into blood stream[18,19]. Each of these steps affects the platelet output and hence each is potentially a regulatory control.

MKs have several unique properties that distinguish them from other marrow cells including larger size, polyploid nucleus, demarcation membrane system (DMS), cytoplasmic dense and α-granules, and expression of platelet surface proteins[18,19]. MKs are the largest marrow cells, which make them easy to recognize from other hematopoietic

cells. For this reason, their development is very well studied. MKs grow up to 10 times larger than other cells in the blood[20] and mature MKs have diameter up to around 150 μm. MKs at a specific stage during maturation undergo polyploidization. During this developmental process, the cell progresses through most of the cell cycle but does not undergo cell division (an aborted mitosis) and hence increases its ploidy (see next section). Several plasma proteins found in platelets (albumin, fibrinogen, and others) are localized in α-granules[21] and synthesized during MK maturation[22]. Deficiency in α-granules of MK results in diseases, such as gray platelet syndrome[23].

MK differentiation can be followed using monoclonal antibodies (MAb) against platelet surface that can be detected by flow cytometry. All MK progenitors usually co-express on their surface the CD34 and CD41 antigens, and are either CD38$^-$ or CD38$^+$, depending upon their maturation stage[18]. The most primitive progenitors (the mixed erythro-megakaryocyte progenitors) are CD38$^-$, while the cells after this stage are CD38^{+}[11]. Another marker is CD61 (integrin β3, glycoprotein (GP) IIIa) which appears during the differentiation of CD34$^+$ cells[18] but it is not specific to MK as it is expressed on non-MK cells including endothelial cells, activated macrophages and osteoclasts[18]. On the opposite, CD41 (platelet integrin αIIb, GPIIb) expression in adult is specific to the MK lineage. Hence, CD41 can be used to select a subset of MK that essentially correspond to either immature or mature MK. CD42 (platelet GPIbα) expression appears at a slightly later stage of maturation and only on the cells that already express CD41[24]. CD42 is dominantly specific to mature MK lineage as some late erythroid progenitors may also express this marker[18]. CD42 expression is initiated slightly later than CD41, but co-expression of CD41 and CD42 are well correlated[18]. Thus, MK differentiation proceed through different stages as shown in Figure 1.3: 1) CD34$^+$CD38$^-$CD41$^-$CD42$^-$, 2) CD34$^+$CD38$^+$CD41$^-$CD42$^-$, 3) CD34$^+$CD38$^+$CD41$^+$CD42$^-$, 4) CD34$^-$CD38$^+$CD41$^+$CD42$^-$, and 5) CD34$^-$CD38$^+$CD41$^+$CD42$^+$. To model the megakaryopoiesis process using these markers, a simplified version of megakaryopoiesis is proposed in *Chapter 4*.

MK development process can be subdivided into several differentiation stages. These stages are difficult to classify since they vary in terminologies and biological criteria used by different authors and thus are in general not easy to compare. It is generally accepted that

MKs originate from a bipotent progenitor cell which can also commit to erythrocyte lineage[11].
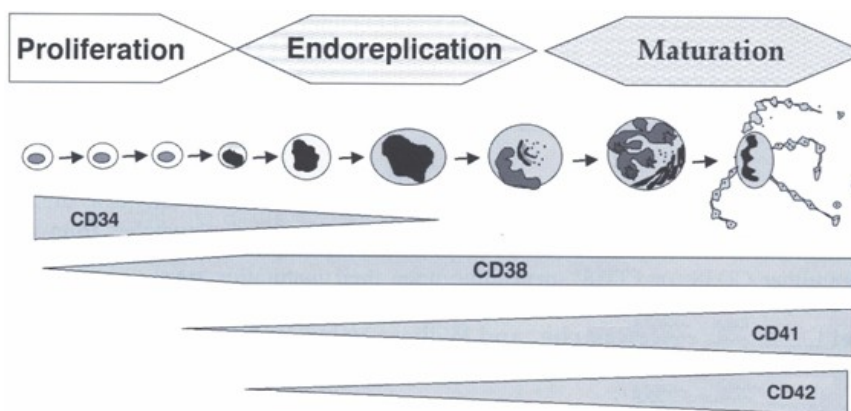
Figure 1.3: Expression of different markers during MK differentiation, adapted from[11].

1.2.2. Polyploidization

One of the most distinct features of MK development is polyploidization, in which the DNA is repeatedly replicated in the absence of cell division by a process called endomitosis. While a normal cell is diploid (2N), MKs undergo several rounds of polyploidization, where ploidy levels increase by a factor 2 with each round, and may vary from 4N to 256N[25,26]. Why MKs become polyploid is not totally understood. Increase in MK ploidy is associated with increase in MK volume (cytoplasm enlargement). It is therefore hypothesized that higher-ploidy cells could produce more platelets than lower-ploidy cells or that the platelet formation is more efficient from a single large MK cell than from several smaller ones[20].

The mechanisms regulating the MK polyploidization has been investigated by numerous researchers. It had been postulated that MK polyploidization is due to a skipping of mitosis after each round of DNA replication. For instance, Nagata et al. and Vitrat et al. have reported that during polyploidization, MK enters mitosis and progress through normal prophase, prometaphase, metaphase, and anaphase A, but not to anaphase B, telophase or cytokinesis[27,28] (Figure 1.4). Recently, Geddis et al. reported that endomitotic MKs undergo normal cell cycle progression up to the M phase, then proceeds through prophase, prometaphase, metaphase, anaphase and telophase but fail to complete cell division due to a

late interruption of cytokinesis at the cleavage furrow ingression stage[29]. Using time-lapse confocal microscopy, Lordier et al. recently confirmed that cleavage furrow ingression occurs in all of the sightings of diploid human MKs undergoing endomitosis (n = 11)[30]. These authors also provided strong evidences that furrow regression and cytokinesis failure was the results of a lack of an active actomyosin ring at the cleavage furrow site in the endomitotic MKs, due to a defect in non-muscle myosin IIA protein accumulation and a reduced activity of the Rho-ROCK pathway[30]. This and perhaps other abnormalities are thought to lead to furrow regression. Thus, it is not clear yet if interrupted cytokinesis is either a rare or a frequent phenomenon of MK development. Given the facts that cellular division is interrupted at such a late stage of mitosis, in this thesis it was hypothesized that, in some instances, polyploid MKs could complete cytokinesis and divide, although polyploid MK division has not yet been reported[18,19].
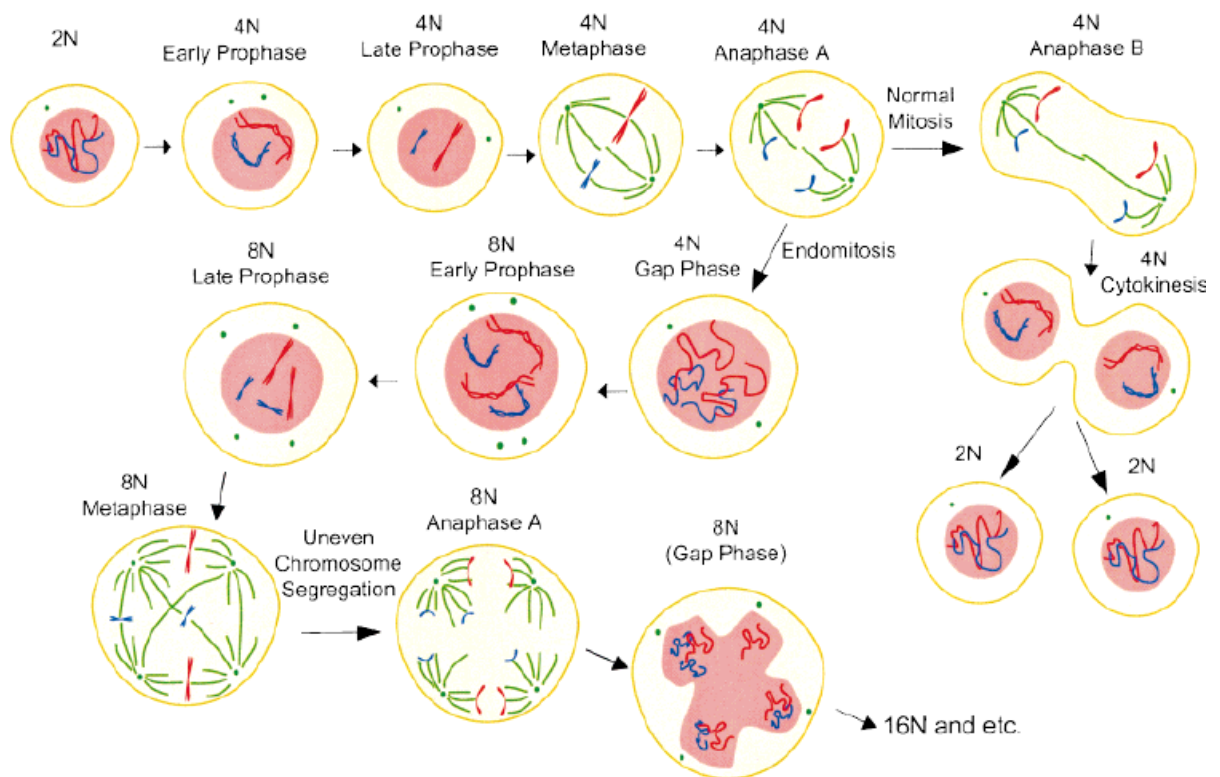
Figure 1.4: Polyploidization process during megakaryopoiesis[26].

It is often useful to calculate the mean ploidy of a given culture for comparison purposes. Mean ploidy can be calculated as follow[31]:

$$MeanPloidy = \frac{[2 \times 2N] + [4 \times 4N] + [8 \times 8N] + [6 \times 16N] + [2 \times 32N] + [4 \times 64N]}{[2N] + [4N] + [8N] + [16N] + [32N] + [64N]}$$

where [xN] is the cell concentration of the xN ploidy level.

1.2.3. MK Cytoplasmic Maturation

After completion of the polyploidization process, MK initiates a maturation stage. During this stage, platelet-specific proteins, organelles and membrane systems accumulate in the cell cytoplasm[1]. During the MK cytoplasmic maturation, the DMS is developed, a dense tubular system is assembled and granules are formed[1].

One of the remarkable features of a mature MK is its marked DMS. The DMS is a network of smooth narrow membrane channels, homogeneously distributed everywhere in the cytoplasm, and derived from multiple invaginations of the MK plasma membrane[32]. The DMS is observable in immature MKs, but becomes more evident in mature MK[1]. The membranes of the DMS at all stages of development is in contact with external environment and can be visualized with extracellular tracers, such as ruthenium red, lanthanum salts, and tannic acid[32-34]. The DMS function also has been studied by many researchers. It has been proposed that the DMS is derived from the plasma membrane invagination and function as a mechanism of cytoplasm fragmentation into platelet filaments (platelet territories formation in MK cytoplasm)[35]. Later studies suggest that the DMS acts primarily as a membrane reservoir for proplatelet formation[1].

MK has a dense tubular system, distinct from DMS, which is thought to be the place where prostaglandin (lipid compound derived enzymatically from fatty acids) in platelets is generated. The dense tubular system is not in contact with the external milieu since it does not stain with extracellular membrane tracers[1].

MK maturation is identified by the gradual formation and presence of granules. The most important are α-granules, which contains platelet adhesive proteins, coagulation factors, plasma proteins and a vast array of other soluble factors[36]. They have a diameter of 0.2 - 0.5 μm, a dark nucleoid core, and are spherical in shape[1]. These granules appear in early stage of MK differentiation and derived from the Golgi apparatus, where their dark central core

within budding vesicles becomes rapidly visible[1]. The α-granule membrane has several receptors that appear during MK maturation such as P-Selectin, GP IIb/IIIa, CD36, and CD9[18]. α-granules are unique organelles in which the protein contents are required by two distinguishable mechanisms of biosynthesis and plasma membrane endocytosis.
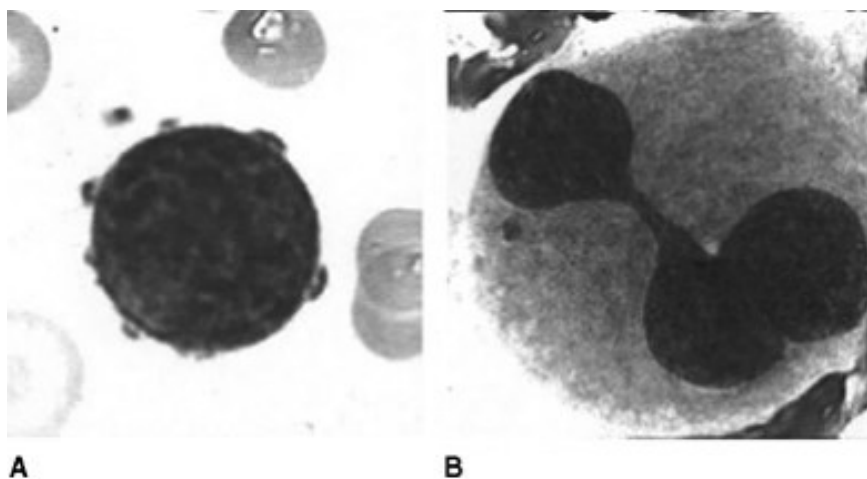
Figure 1.5: Different maturation steps of MK. A) Immature MK is characterized as small size, high nucleus/cytoplasm ratio and thin chromatin; B) mature MK appears as a large cell with a polylobulated nucleus and uniform granules (adapted from[18]).

1.2.4. Platelet Formation

Platelets, or thrombocytes, are tiny anuclear blood cells that circulate in the body. Their function is to participate in the clotting process. Low level (a condition known as thrombocytopenia) predisposes patients to bleeding, while high level, although asymptotic, may increase the risk of thrombosis (formation of clot inside a blood vessel causing the obstruction of the blood flow). The normal platelet count in human is 150,000 - 450,000 cells per microliter of blood. A platelet number below 50,000 cells/μL is called thrombocytopenia and involves a high risk of bleeding in the case of injury. About 2/3 of platelets circulate, while 1/3 are in the splenic pool or other extravascular locations. The platelets are renewed with a turnover time of 8-10 days in human and 4 days in rodents[37,38]. At steady state, when platelet production is equal to platelet destruction, daily production of platelet is in the range of 30,000 - 40,000/μL. Platelet production can be increased up to 8-fold if needed. Estimations for the platelet yield vary from 1,500 to 4,000 platelets per MKs *in vivo*[38], but is 2 to 3 order of magnitude lower *in vitro*. Thus, for an *in vitro* platelet

production process, it is highly important to improve platelet productivity to approach *in vivo* level. Estimating these parameters using mathematical modeling is a part of this thesis work.

It is universally agreed that platelets are derived from MKs. Platelets contain organelles such as mitochondrion, granules (especially α-granules), soluble macromolecules and messenger RNAs, all derived from the MK, but have no nucleus or DNA[39]. At the end of differentiation, mature MKs form and extend arm-like tentacles called proplatelets, from which platelets will be released. During this process, the platelet content, formed of about 400 molecules[40], will be synthesized and will migrate through the proplatelets. After their release into the blood circulation, platelets can survive up to 10 days[37,38].

Proplatelet formation occurs mainly in highly polyploid and terminally mature MKs and is followed by apoptosis, wherein most of the cytoplasm is converted into lengthy beaded extensions[39,41]. Time-lapse video microscopy of this phenomenon by Italiano et al. and Patel et al. reveals the unexpected dynamic nature of proplatelet morphogenesis[3,42]. These authors showed that proplatelet structures interconvert reversibly between spread and tubular forms. Although the MK maximum diameter size is of 150 μm[20], proplatelet can be as long as millimeters[42]. The proplatelet elongation rate has also been determined (by microscopy of cultured mouse MKs) and range from 0.30 to 1.59 μm/min (0.85 ± 0.24 μm/min, n = 77)[42]. During the last decade, *ex vivo* proplatelet formation has been viewed by some as an artefact caused by culture conditions[40,43,44]. Lately however, using multiphoton intravital fluorescent microscopy, it has been shown that identical processes were also taking place *in vivo*, putting this concern to rest[45]. Imaging in the mice marrow cavity, the authors have shown that MKs (labelled with yellow fluorescent protein) release large amount of proplatelets under flowing blood shear stress. However, it remains that the mechanisms that regulate proplatelet formation are not fully known, but the effects of some stimulators have been identified[46].

In addition to the above-mentioned complex processes of differentiation, maturation, and proplatelet formation, MK and platelets have some characteristics that provoke much curiosity and many of these remain unresolved to date. For instance, similarities and differences between MK and platelet features can be observed across species[47]. The

mammalian platelets possess no nucleus but non-mammalian (like vertebrates) platelets retain their nucleus. The platelet equivalent in fish is called a thrombocyte and is a circulating nucleated diploid cell[48,49] (Reviewed by Pang et al. 2005[50]). The purpose of platelet and erythroid anucleation in mammals is not clear at this moment. This phenomenon may reflect the evolutionary process by which platelet production became increasingly efficient, by allowing MKs to produce larger number of anucleated platelets[50].

1.2.5. Megakaryopoiesis Regulation

1.2.5.1. Effects of Cytokines

A cytokine is a small polypeptide, protein or glycoprotein secreted by cells that has a specific effect on the proliferation, differentiation and activity of cells that have the receptor for this cytokine. This chemical messenger controls the activity of cells particularly of the immune systems. Various cytokines stimulate megakaryopoiesis, which results in changes in proliferation or differentiation rates and levels of MK progenitors. In this section, the lessons from *in vivo* studies (animal models and clinical trials) are compared with the recorded results of *ex vivo* experiments to highlight their importance in the regulation of megakaryopoiesis.

1.2.5.1.1. Thrombopoietin

TPO is the principal growth factor regulating MK and platelet production. It has been called by different names: thrombopoietin[51], MK growth and development factor [39,52-55], MK colony stimulating factor[56-59], cloned-myeloproliferative leukemia virus oncogene (c-MPL) ligand[60-64] and megapoietin[65-67]. The primary site of TPO production is the liver. Lesser amounts are seen in the kidneys and brain. There is a strong inverse correlation between circulating TPO level and platelet amount in blood[68]. TPO has been shown in several studies to play a central role in the regulation of megakaryopoiesis and thrombopoiesis[69]. The TPO receptors, c-MPL, is found in a wide range of cells including mature MKs and platelets, CD34^{+} cells, and multipotent stem cells. Binding of TPO to c-MPL produces a number of effects: i) prevention of MK apoptosis[70], ii) increase in MK number, size and ploidy[65], and iii) increased rate of MK maturation[3]. Addition of TPO to CD34^{+} cell cultures

can actually result in the majority of cells becoming MKs and then shedding platelets[39]. In some instances however, platelet release may not require and actually may be inhibited by the presence of TPO[71].

Several important changes in platelet release response have been observed in animals and human treated daily with a recombinant form of TPO. Harker et al. reported, following the administration of TPO to baboons, that: i) during the first 4 days BM-MK ploidy increased to a maximum but there was no change in the platelet count[72]; ii) on day 5, the platelet count began to rise and did so in a dose-dependent manner; iii) there was an initial logarithmic relationship between the TPO dose and the plateau platelet count with a maximum six-fold increase in the rate of platelet production; and iv) at higher doses of TPO, the peak platelet count actually fell, probably due to the inhibitory effects of high dose of TPO on platelet shedding from MKs[73]. Choi et al. investigated the inhibitory effects of TPO on platelet production in mice (n = 5)[73], studied the range of TPO concentration from 0.1 to 630 μg/kg/d for 5 consecutive days and analyzed the platelet numbers at day 6. A maximal number of circulating platelets was observed at 6 - 60 μg/kg/d dose of TPO, about 5 - 6 times above normal platelet count.

Ex vivo studies with TPO showed that this cytokine supports the differentiation and proliferation of MK progenitor cells and has a major role for the maturation of MKs[39]. TPO also supports the formation and function of platelets *in vitro*[74]. When TPO is used alone in a cell culture, purified HSC population can survive[75]. TPO has also synergistic effects with many other cytokines and stimulating factors. When it is used in a combination with SCF or IL-3, it has shown a synergistic effect on the proliferation of MK progenitor[75]. *In vitro*, TPO promotes the proliferation and differentiation of immature MKs[63]. Adding IL-3 increased the ploidy level of MK produced in the presence of TPO. However, TPO is not uniquely specific to the MK lineage, as it also has a noticeable effect on the differentiation of HSC into the myeloid and erythroid lineages[76].

As explained above, TPO administration in vivo and in vitro results in a log increase in platelet production. Likewise, genetic elimination of TPO or its receptor in mouse[77,78] or in man by natural mutation[79] leads to a 85 - 90% (not 100%) reduction in platelet levels while other blood cells remain at normal levels. Platelets of patients with c-MPL gene mutation

shows no response to human TPO administration[79]. In a few cases, it has also been reported that MK culture could produce platelets ex vivo in the absence of TPO[46]. Thus, TPO can be considered as the primary regulator of megakaryopoiesis but not necessarily a crucial one.1.2. 5.1.2. Other important cytokines

Several other cytokines have been shown to stimulate megakaryopoiesis including FL, SCF, leukemia inhibitory factor (LIF), G-CSF, erythropoietin (EPO), IL-1, IL-3, IL-6, IL-9, and IL-11. The effects of the most effective cytokines are summarized below, together with some combinations that are known to be beneficial for megakaryopoiesis.

EPO

Synonyms[80]**:** Erythropoietin precursor, Epoietin.

Functions: Stimulates proliferation of megakaryocytic progenitors[81]; Also increases strongly total cell number (TCN) and non-MK cell expansion, and therefore reduces MK purity[82]; Principal regulator of erythropoiesis.

FL

Synonyms: Ligand for fetal liver; kinase 2 receptor;

Functions: Increases proliferation of MK progenitors[82], but not differentiation to immature and mature MKs[83].

G-CSF

Synonyms: Pluripoietin, CSFβ;

Functions: Does not improve MK production, but rather favours the myeloid lineage (increases the TCN)[84]; Enhances MK expansion if combined with TPO[85].

Granulocyte-macrophage colony-stimulating factor (GM-CSF)

Synonyms: Pluripoietin-α, CSFα.

Functions: Stimulates proliferation of megakaryocytic progenitors[81].

IL-1α

Synonyms: Hematopoietin-1, Lymphocyte-activating factor, Leukocyte endogenous mediator.

Functions: Appears to stimulate MK progenitors[86,87]; Modulates positively MK maturation and platelet release[88].

IL-3

Synonyms: Mast cell growth factor, Multi-colony stimulating factor.

Functions: Capable of supporting CFU-MK growth[89]; Stimulates proliferation of MK progenitors[81]; Does not increase the proplatelet formation[89]; Inhibits proplatelet formation when it is combined by IL-6 or TPO[89].

IL-6

Synonyms: Interferon β-2, B-cell stimulatory factor 2, Hybridoma growth factor, Hepatocyte stimulating factor, cytolytic T lymphocyte differentiation factor.

Functions: Stimulates proliferation of megakaryocytic progenitors[81]; Increases the MK numbers that form proplatelets after 2 days[89].

IL-9

Synonyms: not available.

Functions: Has a positive effect on MK expansion[81,90].

IL-11

Synonyms: Adipogenesis inhibitory factor, Oprelvekin (commercial), Neumega (commercial).

Functions: Stimulates the proliferation of megakaryocytic progenitors[81]; Has a direct effects on megakaryopoiesis[91]; Has a dose-dependent increasing effect on platelet levels in patients and monkeys[92,93].

IL-12

Synonyms: Natural killer stimulatory factor, cytotoxic lymphocyte maturation factor.

Functions: Stimulates the proliferation of megakaryocytic progenitors[81].

LIF

Synonyms: Melanoma-derived lipoprotein lipase inhibitor;

Functions: Modulates positively MK maturation and platelet release[94].

SCF

Synonyms: Kit Ligand, Steel Factor, Mast cell growth factor.

Functions: Reduces MK apoptosis in TPO-induced culture[95]; Increases polyploidization and MK maturation (with TPO)[95]; Promotes MK progenitors expansion from CB-CD34$^+$ cells[96] and has a positive effect on mature MK number[82].

LaIuppa et al., examined several cytokines affecting megakaryopoiesis including IL-3, IL-6, SCF, TPO, GM-CSF, and G-CSF and concluded that the minimum set of cytokines required for MK expansions is composed of TPO and G-CSF[85]. Shaw et al. compared the effect of different combination of TPO (50 ng/ml), IL-3 (100 ng/ml), FL (50 ng/ml), and SCF (50 ng/ml), with and without EPO (2 U/ml) and/or GM-CSF (10 ng/ml) on CB-CD34$^+$ cells and concluded that the addition of EPO and GM-CSF is not necessary for MK expansion[97]. Kie et al. showed that only SCF, among a large number of cytokines (FL, IL-3, IL-6, IL-11, LIF, G-CSF, and EPO), significantly reduced CB-MK apoptosis induced by TPO[95]. They also showed a significant increase in polyploidization of the CD41$^+$ cell fraction is achieved when SCF is used with TPO. By comparing the results of MK development in cultures containing FL with and without TPO for BM-CD34$^+$ cells, Sigurjonson et al. suggested that FL in synergy with TPO increased the MK progenitor numbers, but slowed down the MK differentiation which resulted in lower ploidy, and less mature MKs[83]. Cortin et al. and Pineault et al. also showed that FL had a positive effect only on MK progenitors expansion derived from CB- CD34$^+$ cells[82,96]. De Bruyn et al. concluded that the differentiation of CD34$^+$ cells to MK induced by TPO was neutralized by SCF for CB-cells, while FL had a similar effect for PB-cells[98]. The last stage of megakaryopoiesis is the extension of the cells' cytoplasm as proplatelet filaments. Focusing on this terminal step, Leven et al observed that IL-6 and TPO both increased the MK numbers that formed proplatelets after 2 days in culture[89].

There have been little systematic studies to investigate the effects of cytokine combinations on megakaryopoiesis. Systematic and multi-step statistical techniques were applied by Cortin and colleagues at Héma-Québec R&D department in collaboration with Dr Alain Garnier to efficiently address the interactive effects of a large number of cytokines on megakaryopoiesis starting from CB-CD34$^+$ cells[82]. Thirteen cytokines in the presence of TPO were screened by Placket-Burman designs and the most effective growth factors were further optimized by fractional and full factorial designs as well as composite central design. Their work showed that low concentration of SCF (ca. 1 ng/mL) stimulated MK proliferation and maturation, while higher concentration had a larger, but non-specific, impact on proliferation to the point of having a negative effect on mature MK purity. Moreover, they found that IL-6 and IL-9, in combination with TPO, had the most important

impact on MK expansion and maturation. The other available cytokine combinations in the literature were shown to have less or negative effects on megakaryopoiesis. Importantly MK numbers and purity as well as platelet production were well optimized by this research work. The optimum cocktail that was identified presented the highest expansion ratios of total cells from CB-HSC, increased the yields of MK and platelets using 66% less cytokines (compared to previous studies) and reaching MK purity above 90%. The proposed cytokine cocktail includes TPO (30 ng/ml), SCF (1 ng/ml), IL-6 (7.5 ng/ml) and IL-9 (13.5 ng/ml) and is known as BS1. The BS1 cocktail was used in this study for the detailed FACS monitoring of MK markers with the purpose of developing a mathematical model of megakaryopoiesis dynamics.

In summary, MK precursors' survival, proliferation and differentiation are coordinated and controlled by combinations of cytokines. TPO is the essential growth factor for adequate platelet production, but SCF, IL-3, IL-6, IL-9 and IL-11 all play important roles at different developmental stages.

1.2.5.2. Impacts of the HSC Sources on MK Properties

Characteristics of MK in cultures vary depending on the HSC source from which it is derived. For instance, comparative analyses of culture-derived MK have shown similar differentiation response in the presence of TPO, but different proliferation rate depending on the cell source (2 - 4 folds higher in CB-derived than in adult PB-derived cells)[99]. It is also known that different culture conditions can be required for various maturation stages. The effect of these culture conditions will also be cell source dependent. For instance, De Bruyn et al. have shown that TPO alone can induce MK differentiation in both CB- and PB-CD34$^+$ cells (42% of CD41$^+$ cells in CB vs. 59% in PB), but addition of SCF to TPO decreases CD41$^+$ percentage in CB- but not in PB-cells[98], demonstrating a different sensitivity of CB- and PB-cells to the synergy between TPO and SCF. Addition of FL, IL-6 and IL-11 to TPO increased the leukocytes expansion of CB- but not PB-cells, while the addition of SCF and FL, alone or together, to TPO increased the total leukocyte expansion of CB- and PB-cells. More precisely, while the addition of SCF or SCF+FL to TPO decreased significantly the CD41$^+$ percentage of CB-cells, it was rather the addition of FL or FL+SCF to TPO that had the same effect on PB-cells, suggesting that CD34$^+$ cell

differentiation into MK was reduced either by SCF for CB- or FL for PB-cells[98]. Else, it was also observed that high numbers of both immature and mature MK were obtained using a combination of TPO+IL-3 for CB- cells while TPO+IL-1 was a better cytokine combination with adult PB- or BM-cells[38].

Source of MK plays a significant role on the degree of polyploidization. In response to TPO, the majority of CB-MKs remain diploid (~ 85%) after 12 culture days, while more than half of the BM-MKs become polyploids[38,99-101]. The highest ploidy level reported so far for CB-MK was 18.5% of the cells displaying $\geq$ 8N ploidy when they were exposed to TPO (100 ng/ml), Flt3/Flk2 Ligand or FL (100 ng/ml), interleukin or IL-6 (10 ng/ml), and IL-11 (10 ng/ml)[98] and is similar to the regular ploidy distribution of BM-MK observed with 50 ng/mL TPO alone[99]. The maximum ploidy level achieved in CB-MK is typically of 16N and rarely of 32N, while it is 64N (and often 128N) in adult-derived MK[18,26,100,102]. Table 1.1 compares literature data on MK ploidy distribution for different cell sources and culture conditions.

Table 1.1: MK ploidy distribution (in %) for different cell sources and conditions.

Source	Cytokines (ng/ml)	day	2N	4N	8N	16N	32N	Ref.
CB	TPO (50)	12	81.7	7.6	10.7			99
PB			46	42	12			
BM	TPO (50-100)	12	73.5	10.7	10.2	5.7	0	103
FL[a]			79.2	20	0			
CB	TPO (10), IL-3 (10), SCF[b] (10)	7	62.9	31	5.9	0.2	0	101
BM			48.8	36.7	11.6	2.8	0.2	
CB	TPO (100)	7	87		13			104
CB	SCF (100), FL(100), IL-6 (20), IL-3 (20), G-CSF (20)	7	99		1			
CB	TPO (100)	12	83.9	13.5	2.6	0	0	100
PB			35.8	27.4	18.8	11.2	4.3	

[a]FL: fetal liver; [b]SCF: Stem Cell Factor. See abbreviations at page viii for further details.

Several studies have shown that CB-derived MKs do not display a full thrombopoietic potential[99], by observing that CB-MKs proliferate to a higher degree than adult cells in response to TPO. Platelet production is usually lower from CB-MKs than that from adult MKs (PB- or BM-derived). Mattia et al. showed that platelets are released after 12 to 14

days of culture with either PB- and CB-cells, but generated at a reduced level with CB-derived (35% in comparison to PB-cells), the later also yielding smaller platelets[100].

In brief, various HSC sources respond differently to cytokine stimulations in terms of expansion, differentiation and maturation, as well as platelet productivity. CB-MKs differ in several ways from adult BM-MKs; the former being smaller in size and reaching lower ploidy levels[105], but expanding much more[38]. The mechanisms responsible for such differences remain unclear at this point. However, it is thought to be one of the basis for the reduced thrombopoietic potential observed for CB-MKs *ex vivo*[99,100] and perhaps for the longer periods of thrombocytopenia experienced by patients transplanted with CB- rather than adult-MK[106].

1.2.5.3. Other Factors

Nicotinamide: Nicotinamide (NIC), also known as niacinamide and nicotinic acid amide, is the water-soluble vitamin B3 and has been shown to enhance MK polyploidization[107]. Giammona et al. showed the effect of NIC addition on human PB-derived MKs to be dose-dependent[107], where: i) 23%, 48%, and 64% of cells had high ploidy ($\geq$ 8N) when 0.0, 3.0 and 6.25 mM NIC were added to the culture, respectively; and ii) the cells were large, highly lobulated and reached ploidy levels of 16N, 32N and 64N when treated with 0, 3 and 6.25 mM NIC, respectively. In addition, it was found that NIC could also increase the ploidy level in primary murine MK and CHRF-288 cell line[107]. More recently, this research group using electron microscopy showed that addition of NIC did not alter MK ultrastructure under different culture conditions[108]. As discussed in *1.2.2 Polyploidization*, it can be advantageous to increase the ploidy level of MK, and therefore cell mass, to be able to enhance platelet yield, and therefore, in this context, a vitamin such as NIC could be very valuable to promote platelet production.

Incubation temperature: Beside biological factors and culture parameters shown to have a major effect on MK growth and development, incubation temperature has an important impact. Proulx et al. showed that incubation of CB-CD34$^+$ at 39ºC increased the number of MKs and MK progenitors expansion up to 10-fold compared to 37ºC[104]. This was also accompanied by an accelerated and increased MK maturation and proplatelet formation.

Very recently, Pineault et al. showed this mild hyperthermic condition increased the expansion of CD34$^+$ cells, but at the expense of slightly reduced viability in the early stages of culture, and also reduced mean ploidy level[109]. Effects of incubation temperature on megakaryopoiesis in the presence of the cytokine cocktail BS1 was addressed in this thesis, by applying mathematical model to culture dynamics in these different conditions, as discussed in *Chapter 4*.

1.3. Mathematical Modeling

The application of mathematical models and computational mathematics to biological processes provides important tools to quantify biological events. Different descriptive and mathematical models of stem cells (particularly HSCs) have already been constructed. This section reviews the comprehensive models on stem cells, HSCs, and explains the details of some *in vivo* and *ex vivo* models of megakaryopoiesis already developed.

1.3.1. Total Cell Numbers

To predict the cell population size by mathematical models, one of the most common models is the exponential growth equation:

$$N = V_0 \cdot 2^{\frac{t}{DT}} \tag{1.1}$$

According to this model, the number of cells (N) depends solely on the initial number of cells (N_0) and its division time (DT). The division time for a cell population growing according to this equation can be determined from the slope of linear plots of $Ln(N/N_0)$ versus time, since $Ln(\frac{N}{N_0}) = \frac{Ln2}{DT} \cdot t$. This model is based on the assumption that i) all cells in the studied population divide to give rise to two daughter cells that always divide and ii) there is no nutritional limitation. When a cell population does not follow this assumption, the exponential growth equation does not fit well to growth data. One of the non-exponential growth model is the James Sherley model[110]. In this model, the cell population number at any time (t) depends on division time and the mitotic fraction (α). In this model, "α" is the fraction of the cell population that can divide. Accordingly "*1-α*" is the part of

cell population that cannot divide. In other words, "*1-α*" shows the non-dividing fraction of a cell population, which includes quiescent, postmitotic differentiated, and/or dead cells. When α equals *1*, the Sherley model becomes the ideal exponential growth model. According to the Sherley model, cell growth can be described as:

$$N_1 = (1-\alpha)N_0 + \alpha N_0 \tag{1.2a}$$

$$N_2 = (1-\alpha)N_0 + (1-\alpha)(2\alpha N_0) + \alpha(2\alpha N_0) \tag{1.2b}$$

$$N_3 = (1-\alpha)N_0 + (1-\alpha)(2\alpha N_0) + (1-\alpha)(2\alpha \cdot 2\alpha N_0) + \alpha(2\alpha \cdot \alpha N_0) \tag{1.2c}$$

$$N_i = N_0[0.5 + 0.5\sum_{i=}^{i}\alpha] \tag{1.2d}$$

where *i* represents each generation and equals to *t/DT* and N_i is the number of cells at time *t*. By using series equation ($\sum_{i=0} = \frac{1-r^{n+1}}{1-r}$), the final model equation is derived as:

$$N = \frac{N_0}{2}\cdot\left(1 + \frac{1-(2\alpha)^{t/DT+1}}{1-2\alpha}\right) \tag{1.3a}$$

$$N = N_0 \cdot\left(1 + \frac{t}{2\times DT}\right) \qquad \text{when } \alpha = 0.5 \tag{1.3b}$$

According to this model, α range is between 0 and 1. Sherley[110] and Deasy et al.[111,112] assumed that α was time invariant and its value was determined by minimizing the residual sum of squares between the model and experimental data[110-114]. Certainly, the limit of this model is for cases, quite usual, where α and/or *DT* are not constant. In this case, α can be determined experimentally, by using Carboxyfluorescein Succinimidyl Ester (CFSE) staining[115-117] or live cell imaging for instance.

Another limit of the Sherley model is that it does not allow for any cell death count since the number of dead cells is lumped into the $(1-\alpha)\cdot N_i$ term and does not distinguish between populations of stem cells and differentiated cells, but rather counts total cell

number only. It therefore does not explicitly account for death kinetics. Furthermore, the Sherley model is not based on balances around infinitesimal time intervals, which ordinarily lead to a system of ordinary differential equations (ODE). By doing so, differentiating equation (1.3a) would give:

$$\frac{dN}{dt} = \frac{N_0}{2} \cdot \frac{-}{1-\alpha} \cdot \frac{1}{DT} \cdot (2\alpha^{\frac{t}{DT}^+} \cdot Ln(2\alpha \tag{1.4}$$

Assuming $Z = 2\alpha^{\frac{t}{DT}^+}$ leads to:

$$N = \frac{N_0}{2} \cdot \left(1 + \frac{1-Z}{1-2\alpha}\right) \tag{1.5}$$

$$Z = 2 - 2\alpha - \frac{2(1-2\alpha)}{N_0} \cdot N \tag{1.6}$$

Rearrangement of these equations gives:

$$\frac{dN}{dt} = \frac{\ln(2\alpha)}{DT} \cdot (N - \frac{1-\alpha}{1-\alpha} \cdot N_0) \tag{1.7}$$

In the exponential growth model, it was assumed (unrealistically) that resources for population growth were unlimited, that the effect of cytokines or the cell growth ability remained constant; subsequently the birth and death rates were assumed constant. Using alternatively the logistic growth model birth and death rates are rather assumed to depend on population size[118-121]:

$$\frac{dN}{dt} = \mu \cdot N \cdot \left(1 - \frac{N}{N_m}\right) \tag{1.8}$$

$$N = \frac{N_m}{1 + \frac{N_m - V_0}{N_0} e^{-\mu}} \tag{1.9}$$

where N_m is the maximum population size. The main properties of the logistic growth model are: i) the increase of population size over time follows a sigmoidal or S-shaped

curve; ii) the growth rate (dN/dt) increases with population size (N) to a peak rate of $\mu N_m/4$ when the population reaches half of the maximum size ($N_m/2$) and then reduces; and iii) The parameters can be obtained from the following linear form:

$$Ln\left(\frac{1}{N(t)} - \frac{1}{N_m}\right) = -\mu\ t + Ln\left(\frac{1}{N_0} - \frac{1}{N_m}\right)$$

(1.10)

A limitation of the logistic equation is that it cannot cover the decline phase (mortality after stationary phase). To overcome this problem a four-parameter empirical logistic model was proposed by Jolicoeur and Pointer[122] as:

$$N(t) = \frac{A}{e^{k_d \cdot} + Be^{-\mu}}$$

(1.11)

where k_d and μ represent the specific death and growth rates, respectively and A and B are non-negative parameters. In relation to the original logistic model shown (eq. 1.9), A and B represent N_m and $(N_m-N_0)/N_0$, respectively. In such a comparison (eq. 1.9 and 1.11), this 4-parametric model usually fits experimental data better, but its biological meaning is difficult to appreciate particularly when its differential form is used:

$$\frac{dN}{dt} = \mu\ N \cdot \left(1 - \frac{N}{N_m} \cdot (1 + \frac{k_d}{\mu}) \cdot e^{k_d \cdot t}\right)$$

(1.12)

For this reason, it is considered descriptive rather than explicative. This model was successfully applied to model mammalian cell batch and fed-batch kinetics by Goudar et al.[123].

The logistic growth model was also used to understand the interactions between two populations, for instance by Lotka (1925) and Volterra (1926) to interpret different types of interactions such as competition, predator-prey, mutualism and commensalisms as well as parasitism[124-126]. In these circumstances, the equations become:

$$\frac{dN_1}{dt} = \mu \cdot N_1 \cdot (1 - \frac{N_1 + \alpha \cdot N_2}{N_{m1}})$$

(1.13a)

$$\frac{dN_2}{dt} = \mu_\_ \cdot N_2 \cdot (1 - \frac{N_2 + \alpha_{\_\_} \cdot N_1}{N_{m2}}) \tag{1.13b}$$

where α_{12} represents the effect of population 2 on population 1 while the reversed effect is represented by α_{21}.

1.3.2. Stem Cell Model

From the biological point of view, a stem cell has four possible fates: proliferation, differentiation, death and quiescence. It is not always clear how these fates are controlled, mathematically however the choice between proliferation vs. differentiation has been described either as i) stochastic, ii) deterministic or iii) stochastic-deterministic[127,128]. Until the mechanisms of stem cell commitment are clarified, a deterministic model usually works and is simpler to use and identify. Different descriptive and mathematical models of stem cells and particularly HSC have been reported in an attempt to better explain cell proliferation or differentiation kinetics[128-137]. A common denominator among the large number of models for stem cells in both theoretical biology and biochemical engineering is the use of compartment model[128-137]. Peng et al. presented uni-lineage kinetic description of stem cell models[135]. Assuming that differentiated cells are unable to proliferate, a cell population balance on each compartment led to a set of dynamic equations that described the hematopoietic process. Hardly and Stark presented mathematical models of stem cells to investigate the different aspects of the balance between proliferation and apoptosis[133]. It was assumed that time evolves in steps corresponding to the length of the stem cell cycle. During each such time step, stem cells could divide, differentiate or die. The fraction of cells doing each of these was α_1, α_2 and α_3 respectively, so that

$$\alpha_\_ + \alpha_\_ + \alpha_\_ = \tag{1.14}$$

It was also assumed that differentiated cells did not divide, but a proportion (α_3) died in each time step. They discussed qualitatively the cell fates depending on these parameter values. A similar model was proposed by Prudhomme et al. by assuming that the growth rates of stem cells were time-independent[136].

The process of *ex vivo* HSC expansion and differentiation leading to mature blood cells by a series of steps or compartments (Figure 1.2) has been modeled by da Silva et al. using (bio)chemical reaction kinetics[131]. They provided a general balance equation as:

$$\frac{dN_i}{dt} = k_p \cdot \gamma \, N_i + k_m . N_{i-} - \sum k_{nj} N_i - k_d . N_i \tag{1.15}$$

where N_i represents the concentration of cultured HSC cells in a given i compartment; N_{i-1} shows the concentration of parent cell type (previous upstream compartment); k_p, k_{mj} and k_d are proliferation, differentiation and death rate coefficients respectively, for every compartment; j shows the next downstream compartments. If $j > 1$, it means that a parent cell can divide into more than one type of cells; and γ is a correction factor of proliferation rate and defined as $\gamma = \dfrac{N_m - \sum_i}{N_m}$ where N_m is the maximum concentration of total cells.

1.3.3. Megakaryopoiesis Model

While numerous attempts have been made to simulate the stem cell fates, the studies on megakaryopoiesis modeling are few. A dynamic model of TPO, platelets and MKs in human body was proposed by Bernstein and colleagues[129]. This study simulates the TPO production in patients with leukemia undergoing chemotherapy that is dominantly regulated by changes in platelet and MK levels in blood ([P] and [MK], respectively). In this model, the TPO concentration in the blood ([TPO]) is the result of constant production (k_{TPO}) and removal (k_{rmv}) rates through binding to platelet (n_{plt}) and MK (n_{MK}) according to:

$$\frac{d[TPO]}{dt} = k_{TPO} - k_{rmv} \cdot [TPO] \cdot (n_{MK} \cdot [MK] + n_{plt} \cdot [P]) \tag{1.16}$$

where the n_{plt} and n_{MK} were estimated to be 30 and 12,000, respectively from previous studies. The MK number evolution in BM ([MK]) was also modeled as the result of their production (at a constant rate, k_{MK}) from stem cells, conversion to platelets (first-order rate constant, k_{MK-Plt}), and loss due to chemotherapy (first order rate constant, k_{chm}):

$$\frac{d[MK]}{dt} = k_{MK} \cdot S_{TPO} - k_{MK-plt} \cdot [MK] \cdot S_{TPO}, \text{ for } t > T_c \tag{1.17}$$

$$\frac{d[MK]}{dt} = k_{MK} \cdot S_{TPO} - k_{chm} \cdot [MK], \text{ for } t \leq T_c \tag{1.18}$$

where T_c was defined as the time to achieve MK aplasia and was assumed to be 14 days since the fall in platelet counts is generally observed 14 days after the initiation of chemotherapy. S_{TPO} is a nonlinear function that shows stimulatory effects of TPO on the production of MK and platelets as

$$S_{TPO} = \frac{[TPO]}{EC_{50} + TPO]} \tag{1.19}$$

Where EC_{50} is the TPO concentration producing 50% of the maximum value of k_{MK} and k_{MK-Plt}, and its value was assumed to be 0.8 ng/ml, taken from the midrange TPO concentration in blood.

In addition, the platelet numbers in the blood ([P]) were also described as follows:

$$\frac{d[P]}{dt} = k_{Plt} \cdot Q_p \cdot S_{TPO} \cdot [MK] - k_{loss} \cdot [P] + k_{trnsf}, \text{ for } t > T_c \tag{1.20}$$

$$\frac{d[P]}{dt} = -k_{loss} \cdot [P], \text{ for } t \leq T_c \tag{1.21}$$

with a first-order rate constant for normal platelet loss (k_{loss}). $k_{plt} \cdot Q_p$ represents the specific platelet production rate (platelet number per MK number per day) in which the factor Q_p takes into account the fact that one MK cell sheds on average 3,000 platelets. The zero-order rate constant k_{trnsf} represents transfusions of platelets which occurred after chemotherapy was completed and prior to platelet recovery (= 0.5 x 10^9 platelets/L/day). Values of k_{loss} were obtained for individual patients by curve fitting. This model supports the hypothesis that circulating TPO amount is regulated by MK and platelets.

Regulation of platelet production *in vivo* was simulated through an age-structured model by Santillan et al.[138]. An age-structured model considers *N(t,a)* to be the number of cells at a

given time (t) and age (a) and assumes a cell can live to a maximum age A. As summarized in Figure 1.6, the model is composed of three major compartments: platelets, TPO and MK, where the MK compartment is divided into three different polyploidy compartments: $\leq$ 4N, 8N - 32N, and $\geq$ 64N. The negative feedback mechanism for the control of platelets by the TPO production was considered to operate following:

$$\frac{d[TPO]}{dt} = f([P]) - k \cdot [TPO] \qquad (1.22)$$

where the function f([P]) represents the production of TPO which is controlled by the total number of platelets in the blood ([P]) and assumed to follow a Hill-type equation:

$$f([P]) = \frac{a}{1 + K \cdot [P]^r} \qquad (1.23)$$

where K and r are constant parameters. The last term of equation 1.22 (-k.[TPO]) represents the removal rate of TPO, which is first order with respect to TPO concentration. To find the unknown parameters, the model was solved for steady state, and fitted to published results for sheep and mice such as the relationship between TPO concentration and platelet numbers[139], and values of TPO and platelet counts after an administration of TPO to patients[140], the maturation time of MKs[141], etc.

$$k_i(T) = \frac{\alpha_i T}{1 + \beta_i T}$$

$S_0(\text{TPO})$

Ploidy 2, 4

$$\frac{\partial m_0(t,\mu)}{\partial t} + \frac{\partial m_0(t,\mu)}{\partial \mu} = -k_0(TPO)m_0(t,\mu)$$

$$m_0(t,0) = S_0(TPO)$$

$k_0(\text{TPO})$

Ploidy 8, 16, 32

$$\frac{\partial m_1(t,\mu)}{\partial t} + \frac{\partial m_1(t,\mu)}{\partial \mu} = k_0(TPO)m_0(t,\mu) - k_1(TPO)m_1(t,\mu)$$

$$m_1(t,0) = 0$$

$k_1(\text{TPO})$

Ploidy 64, 128

$$\frac{\partial m_2(t,\mu)}{\partial t} + \frac{\partial m_2(t,\mu)}{\partial \mu} = k_1(TPO)m_1(t,\mu)$$

$$m_2(t,0) = 0$$

$$W_1 m_1(t,\mu_F) = p_1(t,0)$$

$$W_1 = \frac{N(p_8 + 2p_{16} + 4p_{32})}{(p_8 + p_{16} + p_{32})}$$

$$W_2 m_2(t,\mu_F) = p_2(t,0)$$

$$W_2 = \frac{N(8p_{64} + 16p_{128})}{(p_{64} + p_{128})}$$

TPO

$$\frac{d[TPO]}{dt} = f(P) - k[TPO]$$

$$f(P) = \frac{a}{1 + KP^r}$$

$$P(t) = \int_0^{v_F(t)} p(t,v)dv$$

Platelet

$$\frac{\partial p(t,v)}{\partial t} + \frac{\partial p(t,v)}{\partial v} = -\gamma p(t,v)$$

$$p(t,0) = W_1 m_1(t,\mu_F) + W_2 m_2(t,\mu_F)$$

$$(1 - \dot{v}_F)\, p(t, v_F(t)) = Q$$
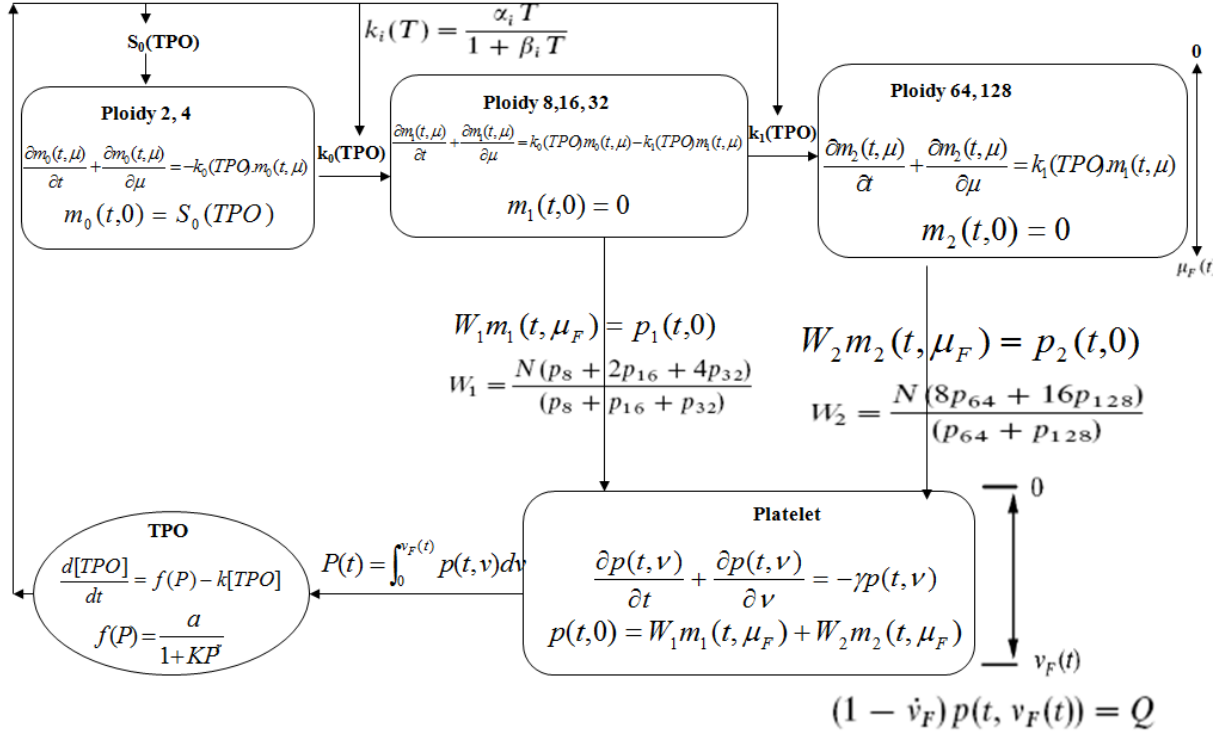
Figure 1.6: Schematic of the age-structured model for thrombopoiesis, proposed by Santillan et al.[138].

1.3.4. Cytokine Kinetics

Effect of cytokines on stem cell fates was also previously modeled. To make a correlation between environmental conditions and cell growth, a Monod-type equation is a good starting point to model the mean specific growth rate as a function of a single cytokine concentration:

$$\mu = \frac{\mu_{max} \cdot [C]}{K_C + C]} \tag{1.24}$$

where μ_{max} (h^{-1}) is the specific growth rate when the cytokine concentration approaches saturation; [C] is the concentration of cytokine (ng/ml), and K_C is the apparent half-saturation constant (ng/ml). Like other Michaelis-Menten approaches for enzyme activity study purposes, this nonlinear equation can easily be converted to a linear equation and the best values of the μ_{max} and K_C parameters can be obtained from one of these equations, the Lineweaver-Burk and the Hanes-Woolf transformations, respectively:

$$\frac{1}{\mu} = \frac{1}{\mu_{max}} + \frac{K_C}{\mu_{max}} \cdot \frac{1}{[C]} \tag{1.25a}$$

$$\frac{[C]}{\mu} = \frac{K_C}{\mu_{max}} + \frac{1}{\mu_{max}} \cdot [C] \tag{1.25b}$$

It has been reported that the Monod-type model shows a consistent and systematic lack of fit for the growth rates measured at intermediate and high cytokine concentrations[142]. Chaudhry et al. proposed a Hill-type function as following[142]:

$$\mu = \frac{\mu_{max} \cdot C^n}{K_C^n + C^n} \tag{1.26}$$

where n is the Hill's exponent and influences further the shape of the curve. When $n > 1$, the curve shows a sigmoidal behaviour, while $n > 5$ represents something close to a step change in response. Else, for $n < 1$, the curve shows a more gradual rise to the maximum value. This function becomes the Monod model when $n = 1$. These authors have also defined another model for the synergistic interaction effects among cytokines (C_1 and C_2 in the following equation). In this model, γ is an interaction parameter. The effect of the value of γ, for the cases where it is either positive or negative can be interpreted easily.

$$\mu = \frac{\mu_{max1} \cdot [C_1]^n}{K_{C_1}^n + C_1]^n} + \frac{\mu_{max2} \cdot [C_2]^m}{K_{C_2}^m + C_2]^m} + \gamma \times \frac{\mu_{max1} \cdot [C_1]^n}{K_{C_1}^n + C_1]^n} \times \frac{\mu_{max2} \cdot [C_2]^m}{K_{C_2}^m + C_2]^m} \tag{1.27}$$

To find the best values of the three parameters (μ_{max}, K_c and n), the authors applied a non-linear regression. Linear regression could also be employed according to the following procedure:

1. Assume $n = 1$ and find the best values of μ_{max} and K_C from either eq. 1.25a or 1.25b.

2. Obtain the best value of "n" by plotting $Ln\left(\frac{1}{\mu} - \frac{1}{\mu_{max}}\right)$ vs. $Ln([C])$ from

$$Ln\left(\frac{1}{\mu} - \frac{1}{\mu_{max}}\right) = Ln\left(\frac{K_C}{\mu_{max}}\right) - n \cdot Ln([C]) \tag{1.28}$$

3. Using new *n* value from (1.28), find new values for the μ_{max} and K_C parameters from one of these equations which gives better regression:

$$\frac{1}{\mu} = \frac{1}{\mu_{ax}} + \frac{K_C}{\mu_{ax}} \cdot \frac{1}{[C]^n} \qquad\qquad (1.29a)$$

$$\frac{[C]^n}{\mu} = \frac{K_C}{\mu_{ax}} + \frac{1}{\mu_{ax}} \cdot [C]^n \qquad\qquad (1.29b)$$

4. Repeat steps 2 and 3 until a minimum sum of squares of the residuals is obtained.

5. Apply parameter identifiability analysis, which is study of multiple-equation models in which the equations have common variables and analysis is performed based on how much the response of a model varies given the perturbation of a parameter value.

Linear regressions can be performed using the Microsoft Excel *linereg* function, while non-linear regression is performed using the Excel solver or the Matlab optimization toolbox.

1.4. Live Cell Imaging

A common feature of quantitative tools in cell biology is that they rely on experimental data that are averaged measurements from a large population of cells. Cell population average-based measurement gives an overall estimate of the frequency for a given cellular events but it does not provide measurements of the distribution of any given property. Furthermore, event single-cell based analysis methods, such as flow cytometry, although providing property distribution data, only permit to obtain a snapshot at a given moment of that distribution, not allowing cell fate tracking. Such limitation can be overcome by time-lapse video microscopy. This approach allows the collection of a large array of data from a single cell (or many in parallel), direct observation and measurement of cell heterogeneity. Another advantage of live cell imaging and one of its unique properties is that the time of observation of such event is accurately measured and this provides additional insights that can be used to understand the dynamics of cellular processes. As opposed to snapshot measurements, recording over time of cellular events allows to reconstruct the time-course of cellular events (that can be visualized) and to distinguish temporal cell-to-cell

variability[143]. Due to its many advantages, time-lapse video microscopy has attracted much interest over the past decade in cell biology[143,144].

Initial movie on cellular dynamics dates back to 1972 by Bajer and Bajer[145], in which a silver halide-based film was made which demonstrated dramatic cellular mortality (reviewed by Hinchcliffe[146]). Over the last four decades, analog video-capture system was replaced by digital computer-based imaging systems, photobiology/photochemistry have been coupled with imaging technology, e.g. development of sophisticated probes within living cells and a green fluorescent protein, therefore the field of cell biology has gained much benefits from these improvements[146].

Although the live cell imaging approach has several advantages, there are some limitations that must be considered[143]. For instance, cells can be damaged by extended exposure to light. Photobleaching in fluorescent microscopy is another concern. Thus, control experiments always need to be performed to be certain that cellular processes are not affected adversely or that the observed events are not an imaging artefact. Thanks to the many advances in microscopy technology and other fields in parallel, data collection is generally fast but sufficient sampling the cellular events is one of the important factors in experimental design. That dozens, hundreds or thousands of data need to be collected to be able to generalize the observed events from single cell to a big population is another challenge. Furthermore, analysis of the imaging data for many applications, i.e. cell tracking, might need a custom program or involve manual analysis which can be time consuming or may be a source of variation or error in regards to the measurements.

Most of the previous works in live cell imaging has focused on a short-term acquisition of the cellular events, e.g. minutes or hours. Long-term live cell imaging is attracting but has its own challenges. For instance, an environmental chamber to keep the cells in a physiological condition is a must and automated focus control to capture good images is required[143]. Several attempts have been made to keep the cells as happy as possible in *ex vivo* culture maintained in a regular incubator. Developing micro-well array system for 4-day imaging of HSC undergoing self-renewal[147] and using a microgrid fabrication for 6-day imaging without impact on the cell viability and proliferation of fetal liver cells[148] are two of the examples in this regard. Furthermore, recent progress on fluorescent semiconductor

nanocrystals, known as quantum dots or qdots, overcomes the photobleaching problems associated with long-term imaging and allows stable labelling of the cells over a week[149-151].

Time-lapse video microscopy has been used to study a wide range of cellular events, such as morphology changes during the attachment or migration[152], cell life span[153], growth[154], death[155], cell cycle phases[156], and etc. One of the most interesting cellular events is mitosis, which has been vastly studied in several organisms using time-lapse microscopy[146]. Staining of fixed cells revealed the mitotic spindle structure and organization[144]. Many key events that occur dynamically and transiently during mitosis are observed with the continuous imaging of living cells that ensures critical observations are not missed. In regards to megakaryopoiesis, time-lapse video microscopy has also been applied to visualize two important dynamic processes; proplatelet formation and endomitosis. In 1999, Italiano et al visualized and reported proplatelet formation *ex vivo* from murine BM-MK for the first time[3]. Using multiphoton intravital microscopy, it was shown that such a dynamic event can also occur *in vivo*[45]. Early studies in 1997 and 1998 on fixed-stained cells showed that polyploid MK undergoes endomitosis by skipping Anaphase A without completing cytokinesis[27,28], while recent studies using time-lapse fluorescent microscopy showed that this cell progresses further than Anaphase A, e.g. in which Anaphase B, cleavage furrow ingression followed by regression was also observed[29,30]. Giving such information that a polyploid MK can progress until the late stage of cytokinesis, it was a motivation to use a sophisticated imaging tool to determine whether polyploid MK can divide. Toward this, large-field, e.g. using tiling technique, and long-term approach was developed.

To perform a long-term imaging experiment, several important questions needed to be addressed to succeed: i) would the CB-CD34+ cells and derived MK be viable and healthy in the experimental set-up? ii) would the events associated with MK maturation be occurring under the long-term large-field set-up and can be followed?, and iii) at what frequency should images be taken? Hence, we attempted to create an environment suitable for the maintenance of the cells (survival, function) and keep these suspended cells under track while recording the dynamic cellular processes every few minutes.

2. Hypothesis and Study Objectives

The overall goal of this project was to make a quantitative examination of *in vitro* megakaryopoiesis. The main hypothesis of this thesis was that mathematical modeling together with a new long-term large-field live cell imaging approach could reveal new insights into the MK differentiation and maturation. In this thesis, two quantitative approaches were developed to analyze the fates of MK progenitors and MKs generated by *ex vivo* expansion of CB- or BM-CD34$^+$ cells (enriched in HSCs). For this purpose, a flow cytometry-based mathematical model and automated imaging system were used as tools to describe MK expansion and maturation and to improve the understanding of MK growth and development.

Chantal Proulx and colleagues at Héma-Québec R&D department showed that incubating CB-CD34$^+$ cells undergoing MK differentiation at 39ºC increased the overall expansion of MK progenitors and MKs up to 10-fold compared with cultures maintained at 37ºC[104]. This was accompanied by an accelerated and increased MK maturation and proplatelet formation. Furthermore, Dr. Nicolas Pineault and colleagues subsequently showed that this mild hyperthermic condition increased the expansion of CD34$^+$ cells and only slightly reduced viability in the early stages of culture[109]. In the first part of this study, the main objective was to develop a mathematical model to describe cellular events occur during *ex vivo* megakaryopoiesis. The hypothesis was that the change in incubation temperature (from 37 to 39ºC) should alter the proliferation, differentiation or death rates of HSC and progenitors, and platelet number and productivity and this alteration could be quantified. To test our hypothesis, a novel mathematical model based on three surface marker staining data was applied to predict the fates of HSC and progenitors grown in BS1 cytokine cocktail at 37 or 39°C during *ex vivo* megakaryopoiesis. Using a 3-D flow cytometry-based data set, the specific objectives of this part were: i) to develop a practical descriptive model for the differentiation, proliferation and death rates of CD34$^+$ cells undergoing differentiation into immature MK, mature MK and non-MK subpopulations all the way up to platelet production, as well as specific platelet production and death rates (Objective #1); ii) validate the developed model by assessing the parameter identifiability to investigate whether one or more parameters can be estimated (Objective #2); and iii) determine the

impact of the temperature of incubation on the various parameters of the model (Objective #3). For this purpose, ODE sets of compartment models were built and solved numerically. The model parameters were estimated using a hybrid stochastic optimizer and parameter estimability was subsequently analyzed using global and local sensitivity analyses and principal component analysis (PCA).

In the first part of this research, it was found to be difficult to identify model parameters based solely on flow cytometry data. For instance, it was impossible to be certain that expansion of a subpopulation was due to the differentiation from the previous subpopulation rather than its self-renewal. The motivation and objectives of the second part of this thesis were to obtain more detailed experimental information on MK dynamics by studying in continuous the process of MK differentiation at the single cell level. For this purpose and looking for an alternative approach, a long-term and large-field live cell imaging approach was developed. Surprisingly, the division of polyploid MK was observed using this system. Thus, a systematic study was designed to challenge the long-standing and universally accepted hypothesis that polyploid MKs are formed solely through aborted cytokinesis. The specific objectives of this research work were to: i) show that polyploid MK can divide and this phenomenon occurs frequently (Objective #4); ii) compare the polyploid MK division rate between different HSC cell sources (CB- vs. BM-cells) and ploidy class (Objective #5); iii) investigate whether the cells generated through polyploid MK mitosis are normal and are not an artefact of imaging (Objective #6); iv) determine if the proliferation of polyploid MKs has a significant impact on the origin of polyploid cells in MK cultures (Objective #7); v) check the effect of a few agents, such as nicotinamide, on the polyploid MK division rate (Objective #8); vi) construct MK cell lineage trees to identify any particular patterns that could be useful to understand megakaryopoiesis (Objective #9); vii) help the model parameter identifiability in the first part of this research, for instance distinguish whether immature MK expansion is due to differentiation of MK progenitors or proliferation of immature MK (Objective #10). Toward this, first an incubation chamber was developed for cell culture mounted on a microscope stage linked to a camera and computer programmed for time-lapse imaging of cells over long periods. Then, time-lapse video record of MK growth and development in the presence of TPO alone was obtained over a total of 10 days of culture. The cells were tracked and the

observed cellular events were recorded, classified into four groups (mitosis, endomitosis, proplatelet formation and death) and then analyzed. The correlation between cell fates and ploidy level as maturation step were investigated and discussed.

3. Materials and Methods

3.1. Cell Sources

3.1.1. Human CD34-Enriched Cells

Human CB- or BM-CD34^{+} cells were used in this research as an enriched source of HSC and multipotent progenitors to generate MK progenitors, MK and platelets *in vitro*. Human umbilical CB-mononuclear cells were collected as previously described[104,157] according to a protocol approved by the ethic committees of Héma-Québec and Hôpital St-Francois d'Assise[157]. CB-CD34^{+} cells were enriched by negative selection using an EasySep[(R)] human progenitor cells enrichment kit (StemCell Technologies, Vancouver, BC, Canada) following the manufacturer's guide to a purity ≥ 90%. Collected CB-CD34^{+} cells were aliquoted and cryopreserved as explained below. Cryopreserved human BM-CD34^{+} cells (purity ≥ 90%) were obtained from Lonza (Chicago, IL, USA).

3.1.2. Murine Marrow Cells

Murine BM-cells (wild-type female BALB/c mice) were gifts from Dr. Renée Bazin (R&D department of Héma-Québec) were treated like human BM-MKs, except the TPO concentration during the cell culture was 200 ng/ml.

3.1.3. Principal Steps for CD34^{+} Cryopreservation

1. Centrifuge the collected CB-CD34^{+} cells for 10 min at 514 g.
2. Resuspend the cell pellet in cryoprotective medium (40% fetal bovine serum (FBS, Invitrogen) and 10% dimethylsulfoxide (DMSO, Sigma-Aldrich) in Iscove's modified Dulbecco's medium (IMDM, Invitrogen) maintained at 4ºC, at a density of 500,000 cells/mL (or other desired concentrations). Prepare 1 mL aliquots of this suspension into cryotubes.
3. Place the cryotubes at -80ºC overnight, and then transfer to liquid nitrogen.

3.2. Cell Culture Preparation

3.2.1. Materials and Reagents

All of the following materials and reagents were prepared in aseptic condition according to previous protocols already developed either by Héma-Québec or Dr. Garnier's research group[109,158,159]. Culture reagents were stored at 4ºC except for cytokines that were stored at -35°C.

- Enriched CD34$^+$ cells.
- Iscove's modified Dulbecco's medium or IMDM (Invitrogen).
- Phosphate buffered saline or PBS (Gibco BRL).
- Bovine serum albumin, insulin and transferrin mixture or BIT (Stem Cell Technologies, Vancouver, BC, Canada).
- Bovine serum albumin (BSA): fraction V, 7.5% (w/v), (Invitrogen).
- PBS+1% BSA: to prepare a 10 mL solution follow this calculation: $C_1V_1=C_2V_2$ where C_1 and C_2 are the initial (stock) and final concentrations, respectively and V_1 and V_2 represent the volumes of the initial and final solutions respectively. $V_1 = C_2V_2/C_1 = (1\% \times 10 \text{ mL}) / 7.5\% = 1.33 \text{ mL}$; thus, add 1.33 mL of 7.5% BSA into 8.67 mL PBS.
- Low-density lipoprotein or LDL solution (Sigma-Aldrich).
- 2-Mercaptoethanol 50 mM (ME, Sigma-Aldrich). $C_1 = 14.3$ M (stock concentration); $C_2 = 50$ mM; $C_1V_1 = C_2V_2 \rightarrow V_1 = 0.050$ M $\times$ 14.3 mL / 14.3 mL = 0.05 mL; i.e. add 50 µL of the stock solution into 14.250 mL dH2O and filter (0.22 µm, Millipore, MA, USA).
- Basal Medium or Eave's base, prepared according to Table 3.1 formulation.

Table 3.1: Eave's basal medium formulation

	Initial Concentration (C_1)	Final Concentration (C_2, 1X)	10 mL (1X)	10 mL (2X)
2-ME	50 mM	50 µM	10 µL	20 µL
LDL	25 mg/ml	0.1 mg/mL	40 µL	80 µL
BIT	---	20%	2 mL	4 mL
IMDM	---	---	7.95 mL	5.9 mL

- Human recombinant cytokines such as TPO, SCF, IL-9, and IL-6 (PeproTech, Rocky Hill, NJ, USA). Reconstituted at 10 µg/mL with sterile PBS + 1% BSA and aliquoted to 100 µL. Keep at -35°C.

- MK culture medium: Eave's basal medium supplemented with selected cytokines. In this work, either TPO alone (100 ng/ml) or BS1 cytokine cocktail[82] was used. The BS1 cocktail contains the following cytokines at final concentrations: SCF (1 ng/mL), TPO (30 ng/mL), IL-9 (13.5 ng/mL), and IL-6 (7.5 ng/mL). Prepared according to Table 3.2 formulation and filter (0.22 µm).

Table 3.2: Cytokine cocktail preparation, **a)** TPO alone, **b)** BS1 cocktail.

a) TPO alone

	Stock Concentration	Final Concentration (1X)	10 ml (1X)	10 mL (2X)
TPO	10 µg/mL	100 ng/mL	100 µL	200 µL
Eaves	1X or 2X	1X or 2X	9.9 mL	9.8 mL

b) BS1 cocktail

	Stock Concentration	Final Concentration (1X)	10 ml (1X)	10 mL (2X)
TPO	10 µg/mL	30 ng/mL	30. µL	60.0 µL
SCF	10 µg/mL	1 ng/mL	1.0 µL	2.0 µL
IL-6	10 µg/mL	7.5 ng/mL	7.5 µL	15.0 µL
IL-9	10 µg/mL	13.5 ng/mL	13.5 µL	27.0 µL
Eaves	1X or 2X	1X or 2X	9.170 mL	8.340 mL

- PBS-glucose solution; $C_2 = 2$ g/l glucose and $C_2 = 5$ mg/L phenol red; add 0.2 g glucose and 0.5 g phenol red into 100 mL PBS and filter (0.22 µm).

- 0.4% Trypan blue solution (Invitrogen).

- Hematocytometer (Hausser Scientific, Horsham, PA, USA).

- Cell culture microplates (Costar, Corning Incorporated, Corning, NY, USA, or Beckton Dickinson Labware) such as 24- and 48-well plates.
- Polypropylene centrifuge tubes (Falcon, Beckton Dickinson Labware); 15 and 50 mL.
- Centrifuge (Beckman GS-6; Beckman Coulter, Montreal, QC, Canada).

3.2.2. Methods

The protocol used to produce MK and platelet *ex vivo* is based on those recently published by V. Cortin et al. [159]. The mathematical model of megakaryopoiesis (Chapter 4) was developed based on the analyses of MK and platelet development kinetics provided by Jean-François Boucher (MSc student under N. Pineault at Héma-Québec) following this protocol. In summary, MK cultures are performed in 24-well tissue culture plates in 1 mL volume (range: 0.5 - 2.0 mL). The cultures are filled into the central wells and the external wells are filled with PBS or water, to reduce the evaporation, especially when culturing cells at elevated temperatures (i.e. 39ºC). The cultures are also performed in 6-, 48-, 96-, 384-well plates or in T-flasks (Costar, Corning Incorporated, Corning, NY, USA) when required, by keeping the same culture volume to surface ratio as suggested in Table 3.3. The whole MK culture lasts a maximum of 14 days where the cells mainly proliferate and differentiate into MK progenitors during the first 6-8 days, while they mature and release platelets during the second week with a maximal platelet production around day 14. Cell number, viability and phenotype analyses (see below) are usually performed every 3 - 4 days to assess cell count, cell expansion, differentiation, and platelet production.

3.2.2.1. Principal Steps for MK and Platelet Production *Ex vivo*

1- Thaw the cryopreserved CD34$^+$ cells (-170ºC) in a 37ºC water bath, without mixing.
2- Transfer the cells in a 15 mL Falcon tube. Add gently pre-warmed PBS-glucose solution (37ºC) to the tube, particularly the first 5 mL very slowly.
3- Spin the cells for 10 min at 228 g or 1,500 rpm, without brake, at room temperature (RT). Discard the supernatant.
4- Suspend the cells in MK culture medium, with a final cell concentration around 300,000 – 600,000 cells/mL.

5- Take a sample (~50 µL) and measure the cell number and viability by haemocytometer and Trypan blue, at least three times.

6- Adjust the cell concentration to target value, e.g. 20,000 - 40,000 cells/mL in MK culture medium. Incubate at 37 or 39°C, 10% CO_2, in a humidified incubator. If analyses of the cultures are performed within the first few days of culture, higher cell density can be used.

7- On day 4 of the culture, mix slowly the well-plate contents, remove around half of the cell suspension volume, and add an equivalent volume of fresh pre-warmed MK culture medium or adjust it to the initial volume if the total volume reduced due to evaporation.

8- On day 7, measure the cell number; add fresh pre-warmed MK culture medium to have 200,000 cells/mL.

9- On day 10, follow step 8 and use final cell density of 200,000 – 250,000 cells/mL.

10- On day 14, do cell analysis and dispose the culture.

Table 3.3: Optimal culture volume range.

Flask/Well Plate	Min Volume	Max Volume
6-well plate	2 mL	4 mL
24-well plate	0.5 mL	2 mL
48-well plate	0.25	1 mL
96-well plate	0.125	0.5 mL
T-25 Flask	5 mL	12.5 mL
T-75 Flask	15 mL	37.5 mL

(Source: http://www.protocol-online.org/forums/topic/6418-maximal-and-minimal-volume-in-t75-and-t25-flask/)

3.2.2.2. Cell Culture Media Preparation for Live Cell Imaging

The required materials and principle of culture preparation for live cell imaging are the same as *3.2.3.Cell Culture Preparation*. The main differences are the lower cell density (around 10-fold) and the use of methylcellulose (MC, Sigma-Aldrich). Note: to have a better image quality of the culture, phenol red-free IMDM is recommended.

Principal Steps:

1- Prepare Eaves base (2X): i.e. every element concentration is doubled except IMDM according to Table 3.1.

2- Prepare cytokine cocktail (2X) as described in Table 3.2.

3- Prepare MC (2X); the final concentration of MC in the culture is 0.375% (w/v) or 3.75 g/l. First, prepare a 1% MC (as a stock solution) by adding 100 mg MC in 10 mL IMDM and mix at 4ºC for at least 6 hours or until all particles are dissolved. Filter the solution (0.22 μm) in aseptic condition. To avoid bacterial growth during the mixing, it is important to add 2% antibiotic into MC (2X), such as penicillin-streptomycin, which will be ~1% (final concentration) after culture preparation.

4- Prepare the culture for imaging as Table 3.4 formulation. Prepare also a culture medium without MC as a control to study the effect of MC addition.

Table 3.4: Imaging culture medium formulation.

	Stock Concentration	Final Concentration	1mL Culture (MC+)	1mL Culture (MC-)
TPO (2X) in Eaves (2X)	200 ng/ml	100 ng/mL	500 μL	500 μL
MC (1% in IMDM)	1%	0.375%	375 μL	---
IMDM	---	---	25 μL	400 μL
Cells (in IMDM)	40,000 cells/mL	4000 cells/mL	100 μL	100 μL

3.2.2.3. Nicotinamide or Rock Inhibitor Treatment

In some CB-cultures, 4.5 mM nicotinamide (NIC) was added at day 0 and day 4 (Sigma-Aldrich, St-Louis, MO, USA) or 50 μM Rho-associated kinase (Rock) inhibitor Y27632 (Calbiochem, Madison, WI, USA) at day 6 only. For the imaging experiments, cell cultures were supplemented with 3.75 g/L methylcellulose (Sigma-Aldrich) and 1% penicillin-streptomycin solution (Invitrogen, Carlsbad, CA, USA).

3.3. Flow Cytometry Analysis of *Ex Vivo* Produced MKs and Platelets

3.3.1. Overview

Flow cytometry was used to quantitatively characterize megakaryopoiesis. Phenotypic analysis is performed using fluorochrome-conjugated antibodies against specific MK

receptors. $CD34^+CD41a^-$, $CD41a^+$ and $CD41a^+CD42b^+$ immunostaining allowed the quantification of HSCs, total MKs and mature MKs, respectively. Platelets are recognised as $CD41a^+CD42b^+$ events with gating on bottom left region of SSC and FSC chart. MK ploidy levels can also be quantified by flow cytometry (see below). A flow cytometer with two or three-channels can be used to simultaneously measure MKs and platelets.

3.3.2. Preparation of Samples for Flow Cytometry Analysis

Samples from the imaged or non-imaged cultures were taken at different days, and analyzed by flow cytometry using a FACS-Calibur (Becton Dickinson Immunocytometry Systems, San Jose, CA) as previously described[157,109,158,159].

3.3.2.1. Materials and Reagents

- Bovine serum albumin (BSA): fraction V, 7.5% (w/v), (Invitrogen).
- Triton X-100 (Bio-Rad Laboratories, Life Science Research, Hercules, CA, USA); $C_2 = 10\%$ (v/v), dissolve 1 mL pure Triton X-100 in 9 mL PBS.
- MK washing buffer (10X): add 0.360 g theophylline 20 mM (Sigma-Aldrich) and 7.643 g sodium citrate (Bioshop Canada Inc) into 200 mL pre-warmed PBS at 37ºC, and filter (0.22 µm). This is stable for 3 months at 4ºC.
- Prepare MK buffer (1X): use 20 mL MK buffer (10X) and 26.8 mL BSA (7.5%) and fill with PBS to 200 mL. It is better to keep the MK buffer under sterile conditions although cytometry analysis does not require aseptic operations.
- Para formaldehyde or PFA (Sigma-Aldrich), $C_2 = 4\%$; dissolve 8 g PFA in 200 mL PBS by heating in a water bath at 55ºC, operate inside a chemical hood. Filter (0.45 µm), protect from light and store at 4ºC.
- DNase-free RNase A (Sigma-Aldrich), $C_2 = 2$ mg/mL; dissolve 10 mg RNase A in 5 mL deionised distilled sterile water. Aliquot and store at -20ºC.
- Fluorochrome human antibodies and murine isotypes (control) conjugated with fluorochroms: PE-coupled anti-CD34 (Immunotech, Beckman Coulter Co., Marseille, France), APC-coupled anti-CD41a, FITC-coupled anti-CD42b (Becton Dickinson), or PE-coupled anti-CD62 (Immunotech). Control isotypes were murine IgG1 conjugated to -APC, -PE, and -FITC.

- Rat anti-mouse CD41 conjugated with Fluorescein Isothiocyanate (catalogue # 553848, Becton Dickinson Immunocytometry Systems, San Jose, CA)

- Propidium iodide or PI (Sigma-Aldrich), $C_2 = 1$ mg/mL, add 0.025 g PI in 25 mL deionised distilled water, aliquot (to 1 mL) and store at -20ºC.

- DNA staining PI solution, $C_2 = 20$ µg/mL, Mix 2% PI solution (1 mg/mL), 1% Triton X-100 solution (10%) and 5% RNase A (2 mg/mL) into MK buffer (1X). For example, to make 1 mL of the solution, add 10 µl Triton X-100, 20 µl PI, 50 µl RNase A, to 9.92 mL MK buffer.

- Centrifuge (Biofuge Pico, Heraeus Instruments).

- FACS-Calibur flow cytometer (Becton Dickinson Immunocytometry Systems, San Jose, CA, USA).

- 1.5 mL homopolymer centrifuge microtubes (Axygen Scientific, Union City, CA, USA).

- 5-mL polystyrene FACS tubes (Bio-Rad Laboratories).

3.3.2.2. Methods

This protocol is designed for the analysis of the MKs only, but flow cytometry analysis of the cell and platelet fractions can be performed simultaneously[109,158,159]. Platelet analysis is done following the same protocol of the antibody staining and preparation for MK (see below) but with different flow cytometry software protocol that is described in "3.*3.3.1. Principal steps for flow cytometry set-up and sample analysis*".

1- Count the cell number and determine the cell viability using a haemocytometer and trypan blue.

2- Resuspend slowly the cell culture, take a 200 µL sample of cell suspension with total cell number of 100,000 - 500,000 cells, and put into two 5 mL FACS tubes.

3- Add monoclonal antibodies (CD34, CD41a, CD42b, etc) to each tube and incubate 30 min in the dark condition on ice. Each specific antibody staining should be accompanied by a control (isotopic control stain) in parallel at the same condition. All antibodies are diluted 1:40 or as supplier's guide, except the anti-CD41a which is 1:200. It is important to do dose-response analysis of all antibodies.

4- Wash the stained cells by adding 1 - 2 mL of MK buffer (1X), centrifuge at 1,000 g or 2,500 rpm for 5 min, at RT. Remove the supernatants, suspend the pellets in 0.3 - 0.5 mL MK buffer and add PI at a final concentration of 5 µg/mL.

5- Do flow cytometry analysis (see below) immediately, and acquire a minimum of 10,000 viable (PI-negative) cell events.

3.3.3. MK Differentiation Analysis

This is a summarized protocol of how to use flow cytometry to analyze the cellular and platelet events, and more details can be found in the literature[109,158,159]. Before performing flow cytometry experiment, be sure that a proper MK-platelet analysis acquisition template is available for the cytometer software in use (e.g. CellQuest[TM]). A representative acquisition strategy is shown in Figure 3.1. A hematopoietic or megakaryocytic cell line can be used to construct the set-up and acquisition template.

3.3.3.1. Principal Steps for Flow Cytometry Set-Up and Sample Analysis

1- Cell region R1: Draw the R1 region around the cells in a 2D dot-plot acquisition window of side scatter (SSC) on *y*-axis vs forward scatter (FSC) on *x*-axis, as shown in Figure 3.1A. Cellular events have increased FSC and SSC properties in comparison to platelets and debris and are recognized by gating on this region in next steps.

2- Platelet region R2: Draw the platelet region R2 in the same dot-plot windows of SSC vs. FSC in step 1, as shown in Figure 3.1A. Platelet events have lower FSC and SSC properties than that of cells and are recognized by gating on this region in next steps. The region is validated using normal platelets (data not shown) and long experience at Héma-Québec as described previously[109,158,159].

3- Propidium iodide (PI) cell region R3: create a dot-plot acquisition window on the PI or FL3 channel on *y*-axis vs FSC on *x*-axis plot. Draw the R3 region around the reduced PI cellular events (lower half) as shown in Figure 3.1B, and gate on R1 region in Figure 3.1A. This region is used in next steps as a gate to recognize viable cells.

4- Create a dot-plot acquisition window on the APC antibody or FL4 channel (like CD41a-APC) *y*-axis vs PE antibody or FL2 channel (for instance CD34-PE) *x*-axis plot. Draw a quadrant, gate on R3xR1 cells to analyze the viable cells. Every quadrant has four parts:

right hand and upper side of the quadrant show the positive expressions while the left hand and lower side show the negative expressions of the joint markers. MK progenitors will be in the top left quadrant (CD34$^+$41$^-$), as shown in Figure 3.1C.

5- Repeat step 4, but draw the APC antibody or FL4 channels (CD41a) *y*-axis vs FITC or FL1 channel (CD42b-FITC) *x*-axis plot to analyze immature (upper left, CD41$^+$42$^-$) and mature (upper right, CD41$^+$42$^+$) MK (Figure 3.1D).

6- Live platelet: repeat step 3 for platelet (R2 gate), as shown on Figure 3.1E. Live platelet will be PI negative (R4 region) while PI-positive events will most likely be cell debris and/or microvesicles.

7- To recognize the mature functional platelets, repeat step 5 on R2 x R4 events, as shown in Figure 3.1F. Top right quadrant of CD41$^+$CD42$^+$ represents mature functional platelets.

8- First, run the isotopic stained samples, like IgG-APC, IgG-PE and IgG-FITC, to make the cytometer settings. Then adjust the background levels. Next, run samples. Note: background adjustment can be done offline with CellQuest or other softwares.

9- Acquire viable cell events of minimum 10,000 (R1 x R3).

10- When the whole flow cytometry acquisition template and settings are done, they should be saved for future experiments that can be performed rapidly.
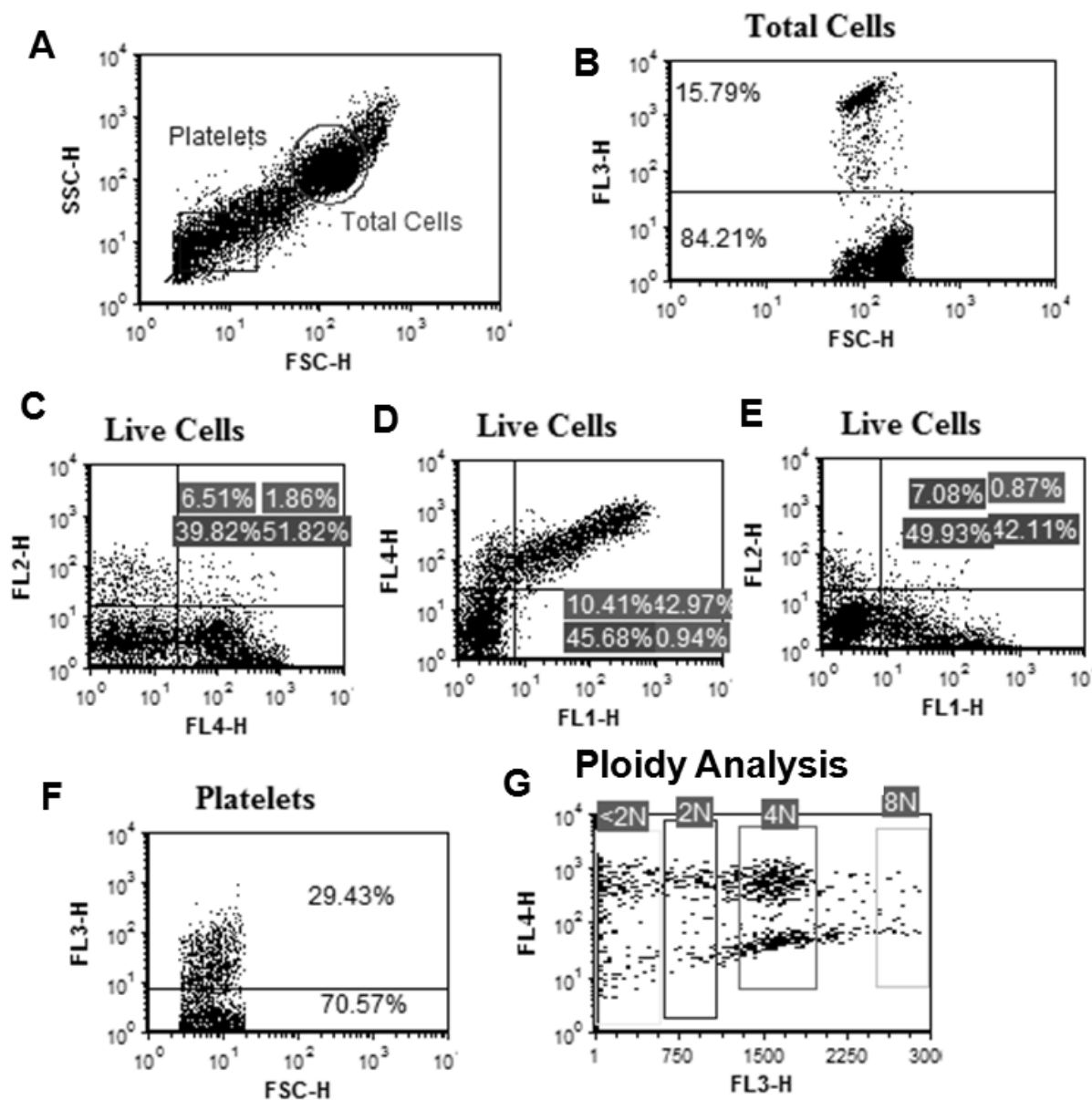
Figure 3.1: Flow cytometry analysis of CB- or BM-derived MK and platelets. **A)** Cellular (R1) and platelet (R2) events in a dot-plot of SSC (*y*-axis) vs FSC (*x*-axis); **B and E)** The viability analysis of the cellular (R1) and platelet (R2) events as shown by the PI-negative regions for the cells (R3) and platelets (R4) events, respectively; **C)** The CD34 and CD41a expressions of viable cells (R1 x R3) events; **D and F)** The CD41a and CD42b expressions of viable cells (R1 x R3) and platelet (R2 x R4) events. G) Ploidy analysis of CB-MK at day 10 is determined by a dot-plot CD41+ vs PI events in y- and x-axes, respectively.

3.3.4. Measurement of Platelet Number and Quality

Quantification of platelets (overviewed in Figure 3.1) was done by flow cytometry as described in part by Norol et al[160]. Briefly, platelets were enumerated as PI-negative $CD41a^+CD42b^+$ events with similar scatter properties as control platelets prepared from adult blood. Platelet produced per seeded cells was calculated as follows: platelets/cell ratio x percentage of $CD41a^+CD42b^+$-platelets x TNC (see above). The platelets/cell ratio was derived using cytometry data as follow; number of events belonging to the platelets region /number of events belonging to the cell region[104].

3.3.5. MK Ploidy Determination

This is a summarized protocol of how to use flow cytometry to analyze the MK ploidy distribution. More details can be found in the literature[109,158,159].

1- Mix slowly the culture sample and take 200 µL sample of cell suspension with total cell number of $1 – 5$ x 10^5 cells and put into two 5 mL FACS tubes.

2- Add 200 µL PFA 1% solution to each tube, and incubate 20 - 60 min at 4ºC.

3- Add 1 mL MK buffer (1X) and resuspend the cell pellets, spin at 2,380 g for 5 min. remove the supernatant and resuspend the cells in another 200 µl MK buffer (1X).

4- Add MK antibodies to each tube, like CD41a-APC and CD42-FITC. Incubate 30 min at 4ºC in the dark.

5- Resuspend the stained cells in 0.5 mL DNA marking PI solution, and incubate at least 30 min in the dark at RT.

6- Move the samples into FACS tubes to analyze by flow cytometry. Use the saved template or create according to the "*3.3.3. MK Differentiation Analysis*".

7- Create a 2D dot-plot of $CD41a^+$ (total MK) or $CD42b^+$ (mature MK) cell events on *y*-axis vs PI on *x*-axis, as shown in Figure 3.1G.

3.4. Time-lapse Video Microscopy

3.4.1. Overview

Live cell imaging was performed using a fully automated inverted microscope (IX81, Olympus, Canada) that was controlled using the QED software (Media Cybernetics, Bethesda, MD, USA). To improve the consistency of microscopic field positioning for long-term experiments, stage movements were controlled using servo- rather than stepper-motors. Bright field, phase-contrast and fluorescent images were acquired using a monochrome charge-coupled device (CCD) camera (Retiga 200R, QImaging). A Lambda LS 175-W Xenon lamp (Sutter Instruments, USA) was used as the fluorescence light source. A green filter was installed on the halogen light source for bright field imaging (Osram HLX 64625, 100W, 12V, GY 6,35). Automatic shutters (Olympus Japan, IX2-SHA) were used on both light sources to minimize detrimental effects of long exposure time.

3.4.2. Imaging Chambers and Set-Ups

As shown in Figure 3.2, two Plexiglas chambers were designed; 1) a large dark outer chamber encompassing the whole optical system which allowed temperature control ($37 \pm 0.1°C$) by hot air circulation, and 2) a small gas-tight chamber located on the microscope stage where humidified air mixture (10% CO_2/90% air) was fed. Cells were seeded at a density of 0.25 - 0.40 x 10^4 cells/ml in 24-well plates (1ml/well) and monitored for 5 days at 20X magnification. Bright field images were captured every 2.0 - 3.0 minutes. Imaging of $CD34^+$ cell cultures took place with an initial cell density of 0.25 - 0.4 x 10^4 cells/ml, from day 0 to day 5 or from day 5 to day 10 in which the initial cell density (at day 0 of culture) was set to 4 x 10^4 cells/ml.

The large fields of view used for cell tracking were obtained by tiling 5 x 5, 7 x 7 or 9 x 7 digital images with pixel resolution of 1,600 x 1,200 (pixel size of 7.4 μm at 1X, 12 bits/pixel). The captured area after tiling was therefore 2.96 x 2.22, 4.14 x 3.11, or 4.00 x 4.14 mm^2, respectively (at 20X magnification), i.e. 3.8, 7.5, and 9.63% of the total surface area of a 24-well plate, respectively. For each experiment, the area of culture captured by

the camera was adjusted to ensure that 2 - 4 cells were initially present within each field of view in tiled images. At least three independent experiments were performed for both CB- and BM-cell sources and for both time windows (days 0 to 5 or days 5 to 10). Cells difficult to track such as those leaving the field of view or those forming colonies were kept in the analysis only if they could be tracked individually for over 90% of the experiment duration. Only a marginal number of cells were left out (less than 1%).
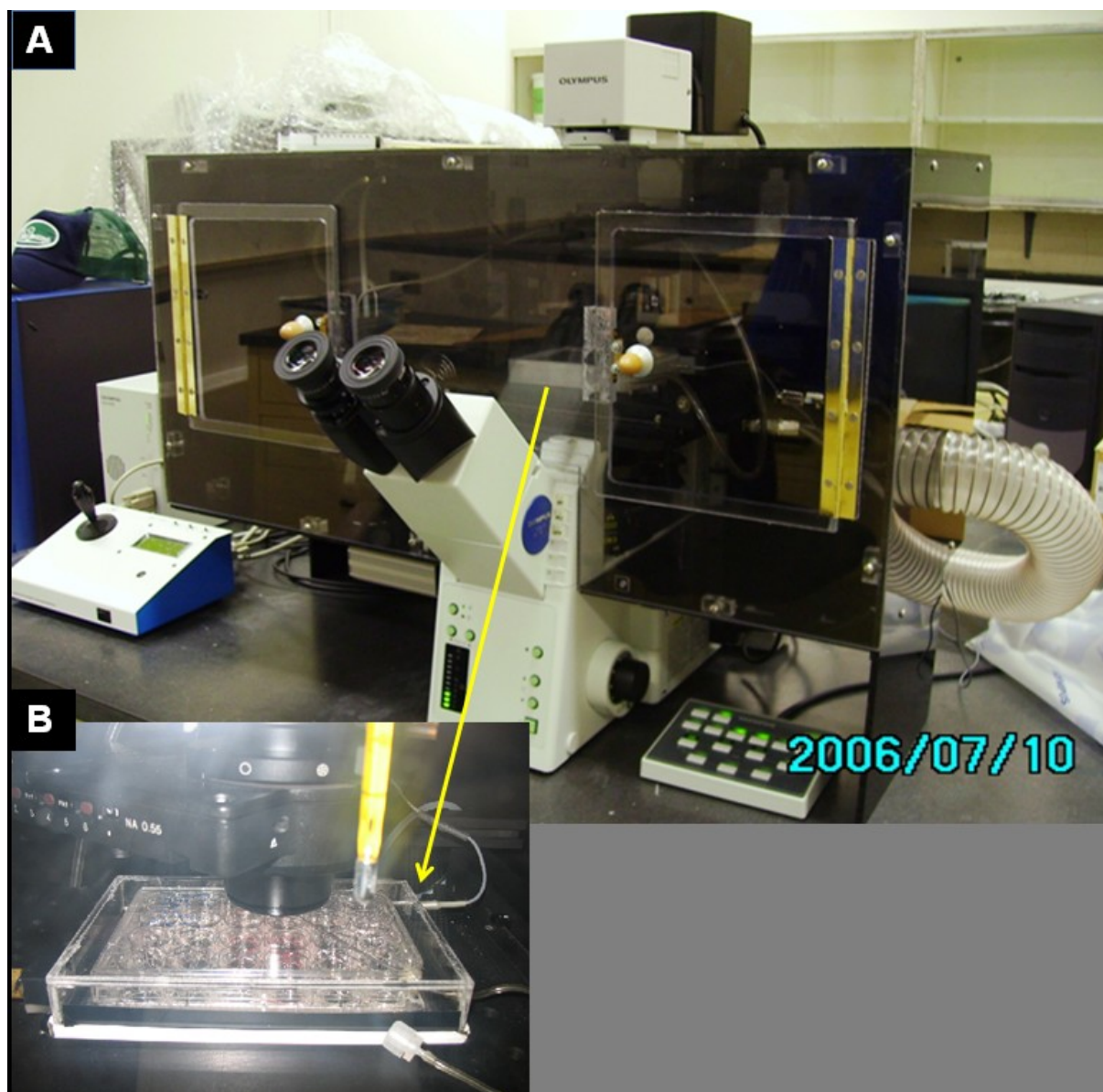
Figure 3.2: Live cell imaging chambers. **A)** a large, temperature controled dark chamber which encompasses the whole optical system, **B)** a small chamber mounted on the stage in which the cultured cells are kept in a controlled atmosphere (CO_2 and humidified).

3.4.3. Image Acquisition

This section is a summary of QED software manual (Media Cybernetics, Bethesda, MD, USA) and explains how to use this software for different imaging tasks. Combination of different steps is required to reach the experiment objective. The first 10 steps below are mandatory for any imaging experiment; the rest depends on the nature of the experiment and can be applied individually.

1- Install InVivo software, according to the user's guide, chapters 1 - 2[161].

   Note: the software is hardware locked and the hardware key (dongle) is included with the package.

2- Start the program by double clicking on the *InVivo* icon on the desktop.

3- Maintain the user name (Dr. Garnier's Lab) and configuration (config2), or use the menus to select another user name and configuration and click on continue. Microscope and camera setups are configured by the technician/expert and should not be changed during the experimentation.

4- The camera acquisition window starts as illustrated in Figure 3.3.
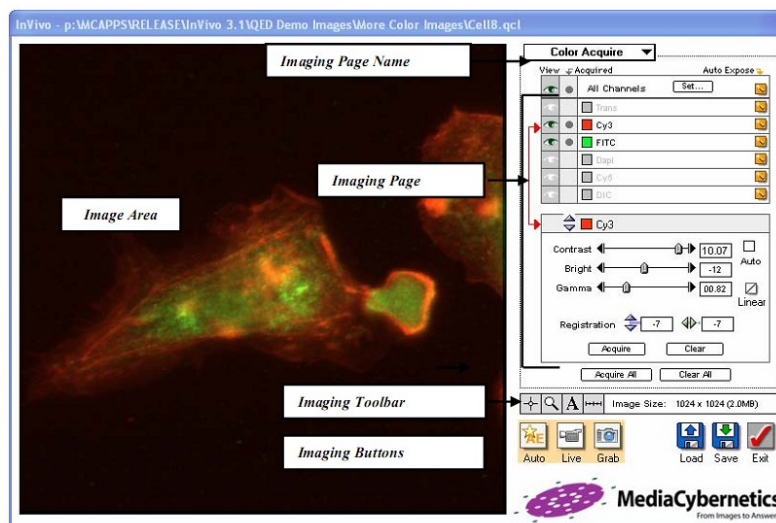
Figure 3.3: Camera acquisition window in QED InVivo software[161].

5- The toolbar appears in two rows as shown in Figure 3.4.
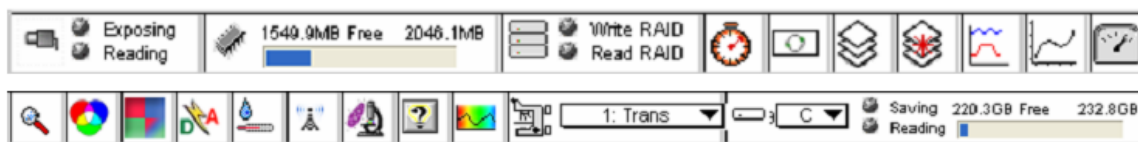
Figure 3.4: QED InVivo toolbar[161].

6- To access the *Microscope Control* window, follow these steps.

    a.   On the *InVivo* toolbar, click on *microscopy control* icon (see Figure 3.5).
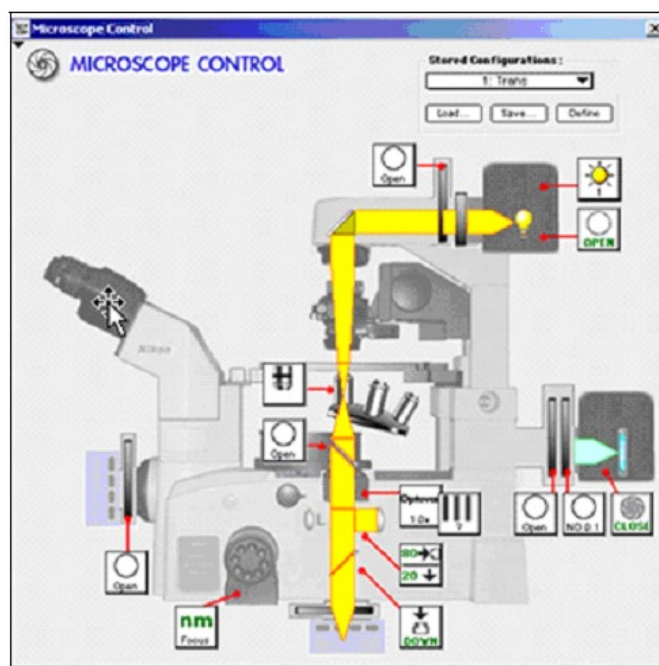
Figure 3.5: Microscopy control window in QED InVivo[161].

    b. Use a microscope configuration (i.e. start up default).

7- Click *Stage Navigation* icon on the InVivo toolbar, the Stage Navigation window appears as shown in Figure 3.6.
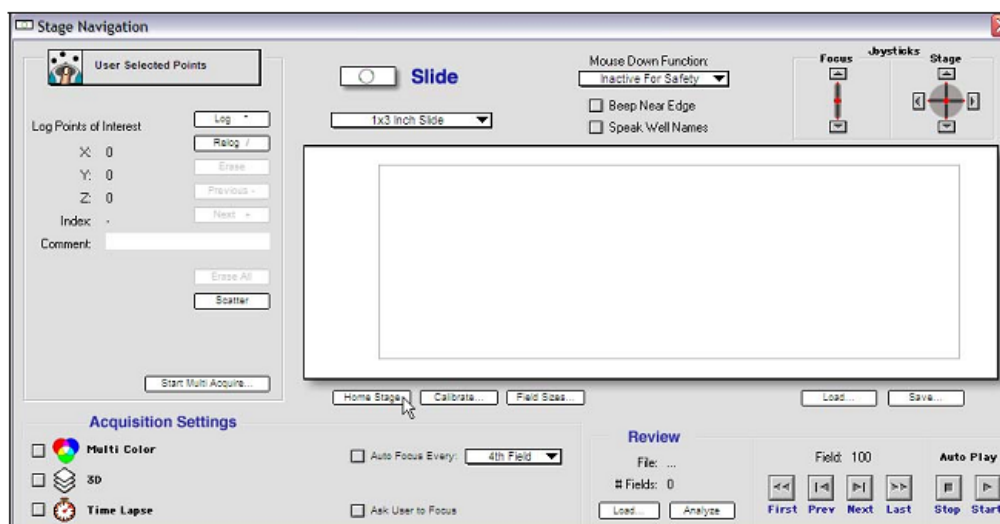
Figure 3.6: Stage navigation window in QED InVivo image acquisition[161].

8- Click [*Home Stage*] and do stage homing.

9- Click [*calibrate*] and calibrate it either as slide or well-plate depending on the sample type used in the experiment.

10- At the *Stage Navigation* window, click [*Field Sizes*] and check if the proper objective is selected. If it is wrong, click on the objective 1 (e.g. 10X), hit *set*. Next, move the objective to the working position (e.g. 20X) which is planned to use in the experiment.

Note: Be certain that you have successfully followed all previous steps. The next steps are optional and based on the aims of an experiment can be done individually or in a group together.

11- Acquire monochrome images:

a. Display a live preview by clicking *live view* icon on the Imaging toolbar.

b. To adjust the exposure, contrast and brightness automatically, click the *autoexposure*

 button on the Imaging toolbar.

c. Take a snapshot, save and check the image with another software if required, i.e. ImageJ or Matlab.

12- Acquire multiple channel (color) images:

a. Click *Imaging Modes* icon on the InVivo toolbar, the Imaging Modes window appears as Figure 3.7.
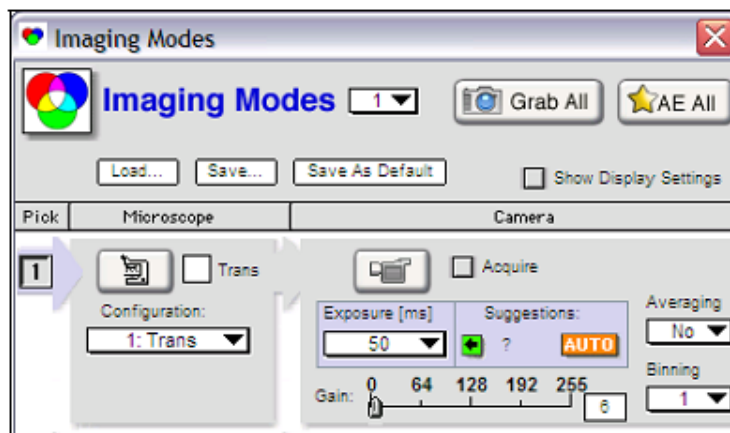
Figure 3.7: Imaging Mode window in QED InVivo software[161].

b. Drop down the *Number of Modes* menu and select *2*. The default setup for channel one is *Trans* and for channel two is *FITC*.

c. Click the *configuration* button for channel one or two.

d. Adjust binning (choose 1), gain (select no gain), brightness, contrast and gamma at the desired value from drop down menus.

e. For each channel, check the *Acquire box(s)* .

f. Take a snapshot (click **Grab All**), save and check the image with other softwares such as ImageJ.
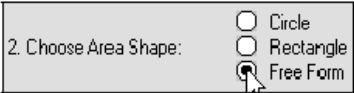
13- Acquire mosaic/tiled images:
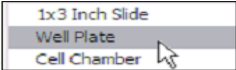
a. Do the calibration for **1x3 Slide** or be sure this step has been done during the start up. It is important to push the off focus button on the microscope body to avoid any damages on objectives by stage movement during the calibration.

b. At the *Stage Navigation* window, maintain the default **User Selected Points** to *Log Points of Interest*.
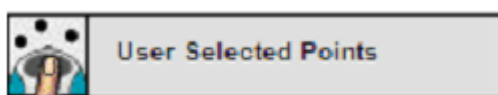
c. To select the *autoscan area*, drop down the menu and select **Autoscan: Ox Plowing**.

d. Select **rectangle** form from *Choose Area Shape* to create a shape around the points of interest.

e. Select **1x3 Inch Slide** → from the drop down menu.

f. Click on the *slide* to add a point to the shape, and then click **[Log]**. Repeat this for the second (end) point. Note: This software does not allow selection of more than two points. If you choose more than two points, the larger rectangular area will be selected.

g. Acquire images and then review the fields by clicking **[First Field]** and then **[Next Field]**.

14- Acquire well-plate:

   a. Calibrate the stage as well-plate.

   b. Follow stage 13b-e, and select **well plate**.

   c. To log select wells, click **[Select Wells]**. The Mouse Down Function changes to Select Well Area. Draw a shape around the wells to be acquired.

   d. Enter zero (or other values if it works) as offsets of X and Y.

   e. Enter the number of fields or images to acquire per well. This number can be 1, 4, 9, or 16, which means 1 x 1, 2 x 2, 3 x 3, or 4 x 4 mini-tiling of each well, respectively. This software does not currently support other combinations, like 2 x 3.

15- Acquire time-lapse images:

   a. To access the Time Lapse window, click on the InVivo toolbar, the Time Lapse window appears as Figure 3.8:
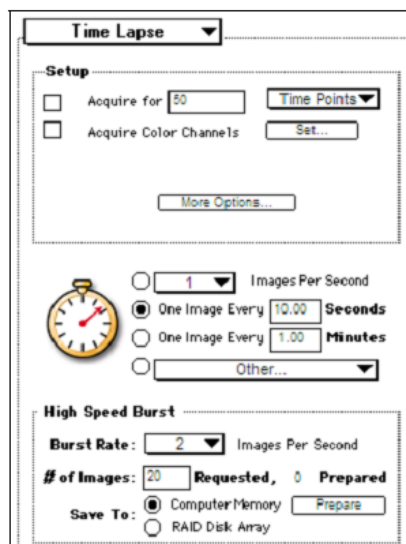
Figure 3.8: Time laps window in QED InVivo software[161].

b. Specify a number of images and time interval. For example, to run a 2-day experiment where one picture will be taken every 2.5 minutes, enter 2 x 24 x 60 / 2.5 = 1,152 time points and tick the option in the setup.

16- To do advanced acquisition:

a. Use multiple selections from **Acquisition Settings**, as shown in Figure 3.9.
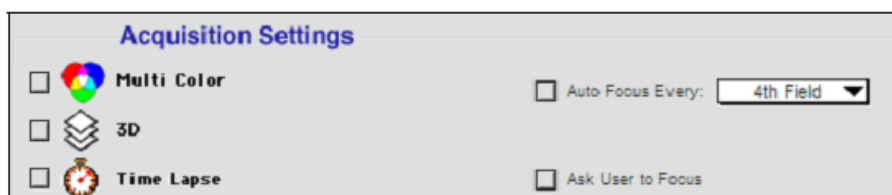
Figure 3.9: Acquisition Settings window in QED InVivo software[161].

b. Follow the above-mentioned steps one by one, and click on the relevant box at *Acquisition Settings*.

3.4.4. Image Processing and Analysis

When analyzing images, the frame number, unique cell identification (ID) number and time were recorded in a spreadsheet in which the following events occurred: cell division, cell polyploidization, proplatelet formation, cell death, elongation, colony formation, entrance or exit from the field of view. A set of custom Matlab R2008b (MathWork Inc.) scripts were developed to analyze the recorded data, construct cell lineage trees and compile

statistics. An integrated tool was also developed to extract regions of interest around predetermined sets of cells to prepare smaller videos of the most interesting and representative phenomena observed. Different steps were required to discriminate the cells from the background among acquired images[162]. Cell segmentation was performed by using a combination of mathematical and morphological operators[163-165] using the Matlab software. Once either the cell or its DNA was successfully segmented, several features were defined to characterize each segmented specimen. Some cell features were also quantified by manual segmentation using the ImageJ software (National Institute of Health).

3.4.5. Cell Lineage Trees

A representative cell lineage tree is shown in Figure 3.10. In the cell lineage trees, each horizontal line represents the life of a cell. The history of all generated daughter cells is written with a set of characters above the horizontal lines, for example 4DT10 = 14.87 in Figure 3.10. The first character (4 in this example) shows the cell generation number, starting with 1 for the first generation. The second and third characters are two letters corresponding to the following abbreviations. DT: division time (mitosis cycling time); PT: ploidy time (endomitosis cycling time); LT: life time. The last character is another number (10 in this example) corresponding to a unique cell ID for a given experiment. Finally, the computed life span of the cell in hours is provided after the equal sign (i.e. 14.87 hours in the example). Furthermore, each initial individual cell is given a name based on its location in a field (a two-digit number after "F") from a large tiled image. Each horizontal line width is proportional to each cell ploidy level, as determined by the observed past events (division or endomitosis) leading to it. The color of each line represents a cell fate: diploid cells undergoing mitosis: black; a cell undergoing endomitosis: red; proplatelet formation: green. For cell death or a cell leaving the field of view (i.e. lost cell), these events were written at the end of the line corresponding to that cell. Cell division or endomitosis is indicated by vertical lines. When a parent cell divides into two separate cells with clear boundaries, or becomes a single cell with a regular round shape, that time point (or frame number) is the end of the connecting line and the beginning of the next daughter(s) cell life. The cells undergo endomitosis, the horizontal line shifts up to show the ploidy level is increased, while it is shown in red and the line width is enlarged.
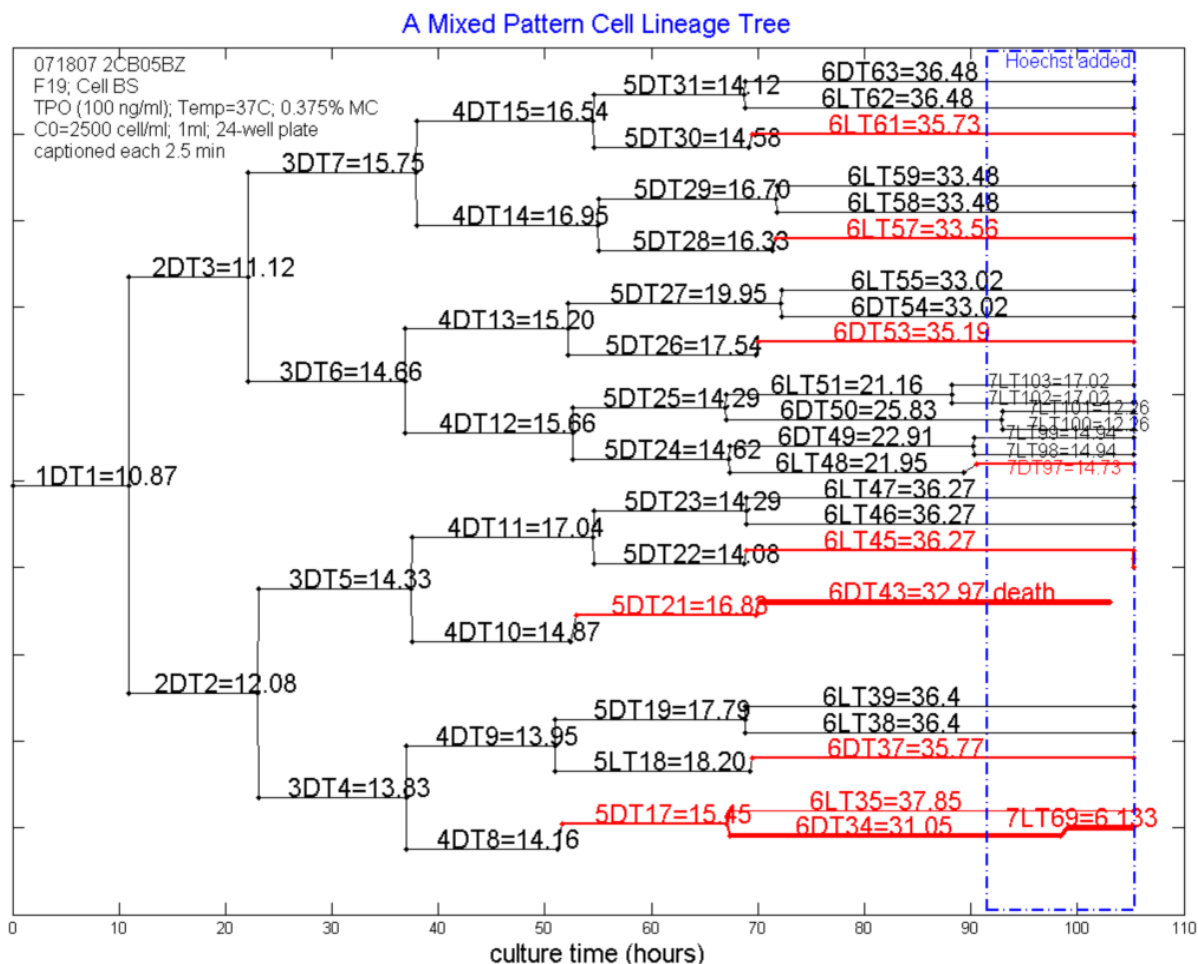
Figure 3.10: Representative CB-MK cell lineage tree pattern.

3.4.6. Cell Size Measurements

Cells were first identified by image segmentation as described in 3.*4.6. Image Processing and Analysis* and then their sizes were quantified by measurements of the projected cell surface area (*A*). Cell volume (*V*) and diameter (*D*) were then estimated based on spherical assumption of cell shape ($V \propto A^{3/2}$ and $D \propto A^{1/2}$). The relative cell volume for each cell was computed and normalized, dividing by the initial cell volume (immediately after mitosis or endomitosis). Cell sizes were quantified by calculating the volume (average of 2-5 frames) of the parental cells just before starting cleavage furrow and that of the daughter cells right after birth.

3.4.7. Hoechst 33342 DNA Staining

The cells were tracked as described in *Image Acquisition* and at the end of imaging, Hoechst 33342 (Invitrogen, Molecular Probes) was added (final concentration of 0.25 µg/ml) directly and gently into the culture through a sterilized stainless-steel tube running inside the microplate. This technique allowed to continue the imaging without disturbing the cells and to confirm the DNA content of the polyploid MK as the dye diffused. The fluorescent images of the cells were captured using a wide UV filter cube (Olympus Japan) with the following specifications: 360/40 nm excitation filter and a 460/50 nm emission filter. The fluorescence and bright field images were captured with a gain level of 1, without binning and with averaging and exposure times of 300 and 35 ms, respectively.

3.4.8. Sorting and Staining of Polyploid MKs for Confocal Microscopy

Hoechst 33342 (10µg/mL; Molecular Probes, Invitrogen) was added to the culture at day 10 for 2h at 37°C. Cells were then stained with anti-CD41 APC-conjugated MAb (Pharmingen) for 30 min at 4°C. Cell sorting procedure; nucleated cells were gated on a SSC-FCS dot-plot profile, then CD41$^+$ cells were gated on a histogram profile window, then CD41$^+$ non-doublet cells were gated in a Hoechst-Width vs Hoechst-Area dot-plot window, then cells with DNA contents equal or greater than 4N (Hoechst-A histogram) were sorted using a Epics Elite ESP FACS (Beckman-Coulter, Mississauga, ON, Canada). Isolated cells were plated on poly-L-lysine (10µg/ml) coated slides and then fixed in PTEMF (20mM Pipes pH 6.8, 0.2% Triton X-100, 10mM EGTA, 1mM MgCl$_2$, 3.7% formaldehyde) for 10 min at room temperature. Rabbit anti-γ tubulin (1:3000, Abcam) and phalloidin ALEXA 488 (1:50, Lonza) were used to stain centrosomes and actin-F. Stacks of confocal slices were collected with a FV1000 point scanning confocal microscope (Olympus) using FluoView software version 2.0.3 with a 60X 1.42 NA oil objective.

3.5. Statistical Analysis

Comparisons were analyzed using the Student t-test. Results were regarded as significant when p-values were below 0.05. When appropriate and available, experimental results were presented as mean plus or minus standard deviation or mean with range (min-max).

4. Flow Cytometry-Based Kinetic Modeling of *Ex Vivo* Megakaryopoiesis[$]

Younes Leysi-Derilou[1,2], Nicolas Pineault[2], Carl Duchesne[1*], and Alain Garnier[1*]

[1]Department of Chemical Engineering, Laval University, Québec, QC, Canada G1V 0A6;

[2]R&D Department, Héma-Québec, Québec, QC, Canada G1V 5C3

*Correspondence and Reprint Requests:

Drs. Alain Garnier and Carl Duchesne

Department of Chemical Engineering, Laval University, Québec, QC, Canada G1V 0A6

Telephones: (418) 656-3106 and (418) 656-5184. Fax: (418) 656-3993

E-Mails: alain.garnier@gch.ulaval.ca and carl.duchesne@gch.ulaval.ca;

4.1. Abstract/Résumé

As the understanding of hematopoietic stem cell (HSC) behaviour grows, and better control of cell decision processes is desired, it becomes increasingly complex to integrate such detailed knowledge into a meaningful and usable model. In this context, a new mathematical model was developed to describe *ex vivo* megakaryopoiesis, using a 3-dimensional flow cytometry-based kinetic modelling approach. Cord blood CD34$^+$ cells were cultured in the presence of a cytokine cocktail optimized for MK differentiation at two different incubation temperatures (37°C vs. 39°C). A set of differential equations was applied to analyze the proliferation, differentiation and death rates of HSC, immature and mature megakaryocytes (MK), and non-MK cells, together with platelet production and decay rates. The non-linear regression results were validated by assessing the parameter identifiability using global and local sensitivity analyses, and principal component analysis to reveal dependencies among the parameters and to simplify the MK differentiation pathway model. The proposed model describes the increase in platelet productivity, platelet death rate, MK maturation, and growth reduction of HSC and non-MK populations due to the elevated temperature. The model provides insight into phenomena that would otherwise be difficult to interpret.

Comme la compréhension du comportement des cellules souches hématopoïétiques (HSC) s'améliore année après année et qu'un meilleur contrôle des processus de décision cellulaire est désiré, il devient de plus en plus difficile d'intégrer ces connaissances de pointe dans un modèle cohérent et utilisable. Dans ce contexte, nous avons développé un nouveau modèle mathématique pour décrire le processus de la mégakaryopoïèse *ex vivo,* en utilisant un modèle cinétique 3-D basé sur des donnés provenant de la cytométrie. Des cellules CD34$^+$ de sang de cordon ont été cultivées en présence d'un cocktail de cytokines optimisé pour la différenciation en mégacaryocytes (MK) à deux températures différentes d'incubation (37°C et 39°C). Un ensemble d'équations différentielles a été utilisé pour analyser la prolifération, la différenciation et les taux de mortalité des HSC, des MK immatures et matures et des cellules non-MK, ainsi que la productivité en plaquettes et le taux de perte de plaquettes. Les résultats de la régression non linéaire ont été validés par l'évaluation des paramètres en utilisant des analyses de sensibilité globales et locales, et en

utilisant l'analyse en composantes principales afin de révéler la dépendance entre les paramètres et de réduire le modèle. Le modèle proposé décrit l'augmentation de la productivité des plaquettes, le taux de mortalité des plaquettes, la maturation des MK, et la réduction de la croissance des populations des HSC et autres que les MK en raison de la température plus élevée. Le modèle permet de mieux comprendre des phénomènes qui seraient difficiles à interpréter par d'autres moyens.

4.2. Introduction

Megakaryopoiesis is a complex process by which hematopoietic stem cells (HSC) progressively differentiate into megakaryocytes (MK), which then undergo a number of development steps leading to the release of platelets by the MKs into blood circulation[1]. Platelets play an essential role in hemostasis.

Differentiation along the MK lineage can be monitored by the appearance and disappearance of specific cell surface markers. Thus, MK progenitors are enriched in the $CD34^+CD41a^+$ fractions, while immature and mature MKs are usually recognized as $CD41a^+CD42b$- and $CD41a^+CD42b^+$ cells, respectively[2] and *ex vivo* produced platelets that are functional co-express $CD41a^+CD42b^{+3}$. Unlike most cells, MKs undergo polyploidization during their normal development through a process known as endomitosis, in which the DNA content of a cell increases from 4N up to 128N[4]. Highly polyploid MKs then go through a series of morphological changes to form long filaments called proplatelets. Platelets are then released in the marrow sinusoids from the fragmentation of the proplatelets which is regulated in part by shear stress[5].

A combination of cytokines and physical factors coordinates megakaryopoiesis. We have previously reported a new cytokine cocktail BS1, optimized for the maturation of cord blood (CB) derived MK, developed by a statistical design of experiment approach[6]. This cocktail, composed of thrombopoietin (TPO), stem cell factor (SCF), and two interleukins (IL-6 and IL-9), was also shown to efficiently induce MK differentiation of CB-derived $CD34^+$ cells and to produce MKs and platelets of high purity ($\geq$ 90% $CD41^+$)[7]. Among physical factors, the temperature of incubation was previously shown to have a strong effect on megakaryopoiesis[8]. It has been shown that CB-$CD34^+$ cultures maintained under mild hyperthermia (39^oC) produced more MKs and more platelets than cultures maintained at $37°C$[8]. It was also demonstrated that the differentiation and proliferation processes are significantly accelerated at 39^oC[7,9].

More precise understanding of the cells and cell population dynamics can be provided through mathematical modeling of complex processes such as *ex vivo* megakaryopoiesis. In general, stem cells placed in *ex vivo* cultures can have four fates: proliferation,

differentiation, death or quiescence. Different mathematical models of stem cells and particularly HSC have been reported in an attempt to better describe cell proliferation or differentiation kinetics[10-19]. A common denominator among the large number of models for stem cells in both theoretical biology and biochemical engineering is the use of subpopulation compartments. While numerous attempts have been made to simulate stem cell fates of other cellular systems, few quantitative studies are currently available on megakaryopoiesis. An initial mathematical model of megakaryopoiesis for healthy rats was published which included a total of four compartments for the stem cells, MKs, platelets and TPO[20]. According to this model, the multipotent cells and committed precursors were identified as the first compartment for which the proliferation rate depended on the TPO concentration, the relative number of stem cells, the mass of MKs and the number of platelets. A dynamic model of MKs, platelets and TPO counts in leukemic patients undergoing chemotherapy was also proposed[10]. In this model, TPO production was regulated by changes in platelet and MK mass, while TPO concentration in the blood was assumed to be the result of a balance between production and removal via binding of TPO to platelets and MKs. The number of MKs in bone marrow (BM) was also modeled as the result of MK production from stem cells, conversion to platelets, and loss due to chemotherapy. Similar compartmental dynamic models were applied by other research groups[15,21]. Regulation of *in vivo* platelet production was also simulated through an age-structured model[22], which considered three classes of MK ploidy ($\leq$ 4N, 8N to 32N and $\geq$ 64N), platelet and TPO compartments where TPO controlled the differentiation rates of MKs while its production was controlled by platelet number through a negative feedback. Other age-structured models of megakaryopoiesis[23] and erythropoiesis in conjunction with thrombopoiesis[11] were also published. To find the unknown parameters, these models were generally solved for the steady state and usually exploited previously published results and experimental data from animal models.

The main goal of this work was to develop a practical descriptive dynamic model for the differentiation, proliferation and death rates of CB-CD34$^+$ cells undergoing differentiation into immature and mature MKs all the way up to platelet production *in vitro*, to represent the case where MKs are produced in laboratory conditions. It was hypothesized that the change in incubation temperature (from 37ºC to 39ºC) should alter the proliferation,

differentiation or death rates of initial HSC, immature and mature MK, and non-MK populations, and specific production and death rates of platelet, and this alteration could be quantified. To our knowledge, this is the first flow cytometry-based model that is applied to quantify megakaryocytic cell fates *ex vivo*. Parameter estimability analysis, using both local and global sensitivity analyses was performed to assess parameter identifiability. Using principal component analysis (PCA), it was also shown that certain combinations of the model parameters were highly correlated to each other in terms of their effects on multiple responses, which led to model simplification. The model and analysis framework described here provides an efficient multi-step approach for better understanding the complex stem cell differentiation dynamic.

4.3. Materials and Methods

Culture of CD34^{+} Cells

Human umbilical CB cells were collected with institutional review board approval and maternal consent and cryopreserved as previously described[24]. HSC were enriched by negative selection on StemSep Cell Separation System using the Human Progenitor Enrichment Cocktail (StemCell Technologies, Vancouver, Canada). CD34-enriched CB cells (70 - 80 %) were plated at 4×10^4 cells/ml at day 0 in serum free medium complemented with the cytokine cocktail BS1: SCF (1 ng/ml), TPO (30 ng/ml), IL-9 (13.5 ng/ml) and IL-6 (7.5 ng/ml) as previously described[6]. Cell cultures were diluted on day 4, 7 and 10 by replacing 1/3 or 1/4 of the spent medium with fresh. Cultures were maintained at 10% CO_2 in humidified air at 37^oC or 39^oC. Viability and total cell number (TCN) were measured from day 3 to 14 by cell count with trypan blue exclusion (0.4% Gibco BRL) using a hematocytometer. Each culture condition was done in duplicate, and a total of two independent experiments were done.

Flow Cytometry Analysis

Samples from the cultures were taken every other day between day 3 and 14 and analyzed by flow cytometry using a FACS-Calibur (Becton Dickinson Immunocytometry Systems,

San Jose, CA) as previously described[7,9]. Quantification of MK surface marker expression and platelets was done by cytometry as previously described[7,9,25].

General Model Formulation

The megakaryopoiesis process can be divided into discrete compartments where each compartment represents a specific lineage subpopulation, from multipotent HSC to platelets. The concentration balance of each cell population or compartment (*i*) can be written as follows: the cell concentration (X_i) depends on the cell concentration from the upstream compartment (X_{i-1}), the cell proliferation rate ($k_{i,i}$), the death rate (k_{di}), and the differentiation rates from the previous upstream compartment ($k_{i-1,i}$) or to the next downstream compartment ($k_{i,i+1}$), as well as the degrees of symmetrical differentiation ($S_{i-1,i}$ and $S_{i,i+1}$ which varies between 0 and 1 for complete asymmetrical and symmetrical differentiation, respectively):

$$\frac{dX_i}{dt} = k_{i-1,i} \cdot (1 + S_{i-1,i}) \cdot X_{i-1} + (k_{ii} - k_{i,i+1} \cdot S_{i,i+1} - k_{di}) \cdot X_i \tag{4.1}$$

for *i* = [*A, B, ..., P*] compartments

A system of ordinary differential equations (ODEs), each representing a cell balance for a given compartment, was constructed for a total of *n* compartments.

Model Assumptions

For each subpopulation, a Monod-type cell growth model was used to consider the effect of a limiting substrate concentration on the specific growth rate (μ_i), irrespective of whether the cells were going to proliferate or differentiate:

$$\mu_i = \frac{\mu_{max,i} \cdot [L]}{K_L + L]} \tag{4.2}$$

where [*L*] is the limiting substrate concentration (e.g. a carbon source such as glucose), μ_{max} is the maximum specific cell growth rate and K_L is the Monod affinity constant.

Furthermore, the following equation was used to describe the relationship between substrate consumption and the total cell concentration (X_T):

$$[L] = \frac{X_{T,\max} - Y_T}{Y_{X/L}}$$ (4.3)

where $X_{T,max}$ is the maximum total cell concentration, $Y_{X/L}$ is the yield of substrate conversion to cell mass, irrespective of the cell type, and X_T is the total cell concentration, sum of cell concentrations of all compartments except P ($i=[A, B,..., P]$ compartment):

$$X_T = \sum_{i=A}^{Z} X_i$$ (4.4)

Rearranging equations (4.2) and (4.3) leads to:

$$\mu_{.} = \frac{\mu_{...ax,i} \cdot (X_{T,\max} - Y_T)}{K_L \cdot Y_{X/L} + X_{T,\max} - Y_T)}$$ (4.5)

where the specific growth rate is not related directly to the limiting substrate concentration and can therefore be used without immediate knowledge of [L]. Based on the rational that every cell subpopulation had different capacity to grow up to a maximum specific growth rate but had similar sensitivity to the limiting substrate composition, it was assumed that each subpopulation had distinct $\mu_{....}$ (μ_i) but similar values of K_L and $Y_{X/L}$. To distinguish between dividing cells that would contribute to their own population generation (self-renewal) from those that would differentiate, μ_i was modulated by a differentiation factor, d_i, in which $k_{ii} = \mu_{.} \cdot (1 - l_i)$ and $k_{ij} = \mu_{.} \cdot d_i$ represents proliferation and differentiation rates, respectively. The differentiation factor (d_i) is assumed to follow a sigmoidal function:

$$d_i = \frac{1}{1 + \;^{-\,_{i}\,'\,t-\;)}}$$ (4.6)

where r_i and t_i are rate and time constants in the sigmoidal differentiation function and are specific to each subpopulation. The sigmoidal function was used based on the empirical observations that the differentiation seemed to start after a certain time in the culture and

occurred in a progressive manner. Obviously, d_i values vary between 0 and 1 following a sigmoidal function. In the case where a compartment differentiates into several compartments, the proportion of cells differentiating into each downstream compartment was determined by a constant ratio (y_{ij}):

$$\sum_{j=B}^{P} y_{ij} = 1 \tag{4.7}$$

Therefore, the proliferation rate of a subpopulation i (k_{ii}) is defined as:

$$k_{ii} = \mu \cdot (1 - d_i) = \frac{\mu_{ax,i} \cdot (X_{max,T} - X_T)}{K_L \cdot Y_{X/L} + (X_{max,T} - X_T)} \cdot \left(1 - \frac{1}{1 + e^{-r_i \cdot (t - t_i)}}\right) \tag{4.8a}$$

While the differentiation rate of a subpopulation i into a single subpopulation j is defined as:

$$k_{ij} = \mu \cdot d_i = \frac{\mu_{ax,i} \cdot (X_{max,T} - Y_T)}{K_L \cdot Y_{X/L} + (X_{max,T} - Y_T)} \cdot \frac{1}{1 + e^{-r_i \cdot (t -)}} \cdot y_{ij} \tag{4.8b}$$

Another interesting feature of stem cells is their capacity to differentiate either symmetrically, into two differentiated cells, or asymmetrically, yielding only one differentiated cell and one stem cell. If a single "A" cell differentiates asymmetrically to give rise to one A and one B cell, accumulation rates of A and B cells are respectively:

$$\frac{dA}{dt} = \tag{4.9a}$$

$$\frac{dB}{dt} = \quad \cdot \tag{4.9b}$$

where k_{AB} is the differentiation rate of A to B. Otherwise, in the case of symmetrical differentiation, these equations become:

$$\frac{dA}{dt} = - \quad \overline{} \cdot$$ 　　　　　　　　　　　(4.9c)

$$\frac{dB}{dt} = \quad \cdot \quad \overline{} \cdot$$ 　　　　　　　　　　　(4.9d)

To consider this phenomenon in the model, a time invariant symmetrical differentiation factor, S_{ij} is introduced and takes values from zero, for complete asymmetrical differentiation, and one for complete symmetrical differentiation. Given these values and considering the above mentioned example (eq. 4.9a-d), balance equations incorporating the symmetrical differentiation factors S_{ij} can be written as:

$$\frac{dA}{dt} = - \quad \overline{} \cdot \quad \overline{} \cdot$$ 　　　　　　　　　　　(4.9e)

$$\frac{dB}{dt} = \quad + \quad \cdot \quad \cdot$$ 　　　　　　　　　　　(4.9f).

Finally, the death rate (k_{di}) was assumed time invariant for each subpopulation.

Parameter Estimation

The Runge-Kutta fourth-order method was used for solving the system of ODE within the Matlab environment (i.e. function *ode45*). Parameters were estimated by non-linear weighted least squares regression using the following objective function:

$$SS = \sum_{i=A}\sum_{m=1} w_i \cdot (X_{i,m}^{obs} - X_{i,m}^{model})^2$$ 　　　　　　　　　　　(4.10)

where $X_{i,m}^{obs}$ and $X_{i,m}^{model}$ are the measured and simulated responses for compartment i at time point m. Two model structures were considered, a more detailed model involving 7 responses and a reduced model based on 5 compartments. Measurements were available at 10 time points in all cases. The values of the scaling weights (w_i) were selected in order to normalize the effect of differences in range of cell concentrations between the compartments:

$$w_i = \frac{1}{\max(X_{i,m}) - \operatorname{nin}(X_{i,m})}$$

(4.11)

The models require estimating 35 and 20 parameters for the 7- and 5-compartment models, respectively.

Multiple local minima were encountered when minimizing SS, as it is typically the case in parameter estimation for non-linear models. To avoid being trapped into a local optimum a good coverage of the solution space is necessary. This was achieved by using a hybrid constrained stochastic optimization approach for parameter estimation. Lower and upper bounds for each parameters were established in order to maintain physical significance (e.g. non-negativity constraints) and based on some literature values, common knowledge in the field, and *a priori* experience with the model. These bounds are shown in (Table 4.1). Next, Matlab's gradient-based minimization with constraints algorithm (*fmincon* function) was used to find the set of parameter estimates that minimizes the objective function (eq. 4.10). This was achieved first by generating a set of about 3,000 vectors of parameter initial guesses. These were obtained by randomly selecting their values between their respective lower and upper bounds. A good coverage of the parameter space was therefore obtained. Then, each vector of initial guesses was used by the optimizer to find a solution. These solutions were re-optimized again using the last estimates as new initial guesses until no further improvement was obtained. In the case, the *fmincon* function did not converge, which happened rarely for 7-C model case, the program was relaunched by a new random initial guess. This procedure led to approximately 11,000 different solutions for the parameters, of which the solution with the smallest SS (eq. 4.10) was chosen as the most likely global minimum solution.

Sensitivity Analysis

Parameter sensitivity is defined as the partial derivative of a model response $X_i(t,\theta_r)$ at time point t with respect to a parameter θ_r, i.e. $\dfrac{\partial_i(t,\theta_r)}{\partial_r}$. In the literature, sensitivity coefficients are commonly used in a scaled form s_{ip}[26,27] to remove the effect of differences in the unit scales:

$$s_{ip} = \frac{\theta_r}{X_i(t,\theta_r)} \frac{\partial \acute{}_i(t,\theta_r)}{\partial \acute{}_r} = \frac{\partial \ln[X_i(t,\theta_r)]}{\partial \ln(\theta_r)} \tag{4.12}$$

Quantitative identifiability of the parameters was performed by evaluating the derivative in eq. 4.12 numerically for each model response. A small perturbation (i.e. 1%) was applied on each parameter, one at a time, around their optimal value while all other parameters were fixed at their optimal value. The parameter sensitivity matrix (Z), composed of p columns (parameters) and $m \times \iota$ rows (m = *9* time points and n = *5 or 7* responses), was obtained and organized as follows:

$$Z = \begin{bmatrix} \dfrac{\partial \ln(X_1(t_1,\theta_-))}{\partial \ln(\theta_\iota)} & \cdots & \dfrac{\partial \ln(X_1(t_1,\theta_r))}{\partial \ln(\theta_r)} \\ \vdots & \ddots & \vdots \\ \dfrac{\partial \ln(X_n(t_1,\theta_-))}{\partial \ln(\theta_\iota)} & \cdots & \dfrac{\partial \ln(X_n(t_1,\theta_r))}{\partial \ln(\theta_r)} \\ \dfrac{\partial \ln(X_1(t_2,\theta_-))}{\partial \ln(\theta_-)} & \cdots & \dfrac{\partial \ln(X_1(t_2,\theta_r))}{\partial \ln(\theta_r)} \\ \vdots & \ddots & \vdots \\ \dfrac{\partial \ln(X_n(t_m,\theta_-))}{\partial \ln(\theta_-)} & \cdots & \dfrac{\partial \ln(X_n(t_m,\theta_r))}{\partial \ln(\theta_r)} \end{bmatrix} \tag{4.13}$$

The Z matrix was analyzed following the approach proposed by Yao et al.[26], which consists of the following steps: i) the sum of squares of the elements in each column of Z (corresponding to a given parameter) is first computed, ii) the column with the highest magnitude of sum of squares was identified as the most estimable parameter and stored as the first column of matrix (Y_L), iii) the Z matrix was then regressed onto Y_L and the residuals were computed: $R = \mathcal{Z} - \acute{}_L \cdot (Y_L^T Y_L)^{-1} \cdot Y_L^T \cdot Z$, and iv) the procedure is then repeated starting with step (i) but replacing the original sensitivity matrix by the matrix of residuals (R). The procedure ends when all columns (i.e. parameters) in Z have been used. This yields a ranking of the parameter based on their estimability, from the most estimable to the least. A user defined threshold is applied to define the estimability in which the parameters with above the threshold considered as estimable parameters[26].

4.4. Results

A 3-D Flow Cytometry-Based Megakaryopoiesis Model

The megakaryopoiesis process can be divided into a series of discrete cellular stages, from multipotent HSC to fully mature MK and platelets. Each of these stages can be viewed as a compartment. Getting the benefits of differentiation-associated *in vitro* assays with flow cytometry, megakaryopoiesis is generally recognized phenotypically based on the expression (+) or lack of expression (-) of MK lineage and progenitor-associated cell surface antigens such as CD34, CD41, and CD42. Changes in cell expression during the MK growth and development as a function of time and incubation temperature were measured by flow cytometry as shown in Figure 4.1. In this figure, it is clear that expression of $CD34^+$ decreased over time, while that of the MK markers ($CD41^+$ and $CD42^+$) increased. Based on these data, a 3-D model with 7-compartments (7-C) was established, in which compartments were divided according to the absence or presence of the three principal cell surface markers (CD34, CD41, and CD42) as shown in Figure 4.2A. The fraction of each subpopulation or compartment in the 3-D model with respect to the total population was computed from the combined 2-D dot-plots shown in Figure 4.1. The cell concentration of each subpopulation or compartment in Figure 4.2 was obtained by multiplying these fractions by the total cell concentration as described in the *Appendix* (Figure 4.A1).

It is well established that HSC in culture can have four fates: proliferation (with a specific rate of k_{ii}), differentiation (k_{ij}), death (k_{di}) or quiescence. In the 3-D model presented in Figure 4.2A, the initial compartment was the enriched CB-derived $CD34^+41^-42^-$ HSCs (compartment *A*). These multipotent cells may self-renew, differentiate or die. If differentiation occurs, the cell moves to the next downstream compartment(s); otherwise, it remains in *A*. To reduce the number of parameters, quiescence is not considered explicitly in the model. The $CD41^+42^-$ cells (*B:* $CD34^+41^+42^-$ or *C:* $CD34^-41^+42^-$ compartments) represented immature MK and were able to proliferate, differentiate or die. The $CD41^+42^+$ subpopulations (i.e. *D:* $CD34^-41^+42^+$ or *F:* $CD34^+41^+42^+$ compartments) were comprised of mature MKs. Mature MKs underwent polyploidization, formed proplatelets and released

platelets, at a specific rate of Q_p, in which they ultimately underwent apoptosis[28]. The last compartment (P: CD41$^+$42$^+$) shows the functional platelet numbers shed from mature MKs and subjected to a limited duration ($k_{dP} > 0$) before they lose their functionality[3]. The non-megakaryocyte population is identified by the E compartment (CD34$^-$41$^-$42$^-$) and had no capability to differentiate into MK, i.e. $k_{EC} = 0$. The CD34$^+$41$^-$42$^+$ and CD34$^-$41$^-$42$^+$ subpopulations were considered negligible based on the available experimental data and the culture conditions used over 14 culture days ($\leq 0.05\%$). A simplified version of the model with a reduced number of parameters, 5-compartments (5-C) model, is shown in Figure 4.2B following the same approach. Compartments B and C as well as compartments F and D in the 7-C model were combined to form compartments I (immature MK) and M (mature MK) in 5-C model, respectively. It is important to note that in the 7-C model it was assumed that the F compartment could proliferate ($k_{FF} \geq 0$) but not the D compartment ($k_{DD} = 0$). Therefore, it was assumed that cells in the M compartment in the 5-C model, which was composed by the combination of F and D compartments in the 7-C model, were able to proliferate. This proliferation of M cells is supported by our recent finding that polyploid mature MK can complete cytokinesis and therefore divide[29]. Balance ODEs for both 5-C and 7-C models are shown in the *Appendix*.

Parameter Estimation Using Constrained Optimisation

To facilitate the model identification, a few parameters were estimated independently using the available data (i.e. not based on the model). These parameters include the specific death rates of each compartment (A to P) and the specific platelet production rate (Q_P). These were determined by monitoring distinctly both live and dead cells on each 2-D histograms shown in Figure 4.1 by gating propidium iodide (PI)-positive and PI-negative cellular events that represented live and dead cells, respectively. As shown in Figure 4.3A, total cell viability decreased significantly and linearly as indicated by $R^2 = 0.84$ and 0.72 for 37 and 39ºC, respectively. Thus, it was assumed that the rate of dying cells or $dN_d(t)/dt$ was proportional to number of viable cells $N_v(t)$ over time (t):

$$\frac{dN_d(t)}{dt} = k_d \cdot N_v(t) \qquad (4.14a)$$

$$N_d(t) = \tau_d \cdot \int\limits_{t_0}^{t} N_v(t) \cdot dt + V_d(t_0) \tag{4.14b}$$

Therefore, the specific death rates (k_{di}) were computed from the slope of the number of dead cells in each population or subpopulation, $N_d(t)$, against the integrated number of viable cells over time ($\int\limits_{t=0}^{t} N_v(t).dt$) plots. As presented in Figure 4.3B-C, results showed a very good regression to estimate these specific death rates for total cells or immature MK, k_{dX} and k_{dI}, at both incubation temperatures (R^2 = 0.99), but lower regression coefficients were obtained for M, A or E compartments (data not shown). Looking at the plot of the M compartment, it was seen that the data followed two distinct slopes, one between days 0 – 7 and the other between days 8 – 14. Therefore, the specific death rates of M compartment was considered time-dependent and split into two time-windows as shown in Figures 4.3D1-D2 and Table 4.2A. The specific death rates of total cells (k_{dX}) was used as an estimation for that of A and E compartments (Figure 4.3B and Table 4.2A).

Next, the specific platelet death rate (k_{dp}) was estimated. It is important to note that PI-positive vs. platelet-like size events cannot specifically be attributed to dead platelets. The reason for this is that PI in fact stains the DNA but platelets are devoid of DNA. The precise composition of these events is not well understood, that might be composed mainly of MK debris. Nonetheless, using such events to estimate k_{dp} showed weak regression (R^2 = 0.54 and 0.69 at 37 and 39ºC, respectively). It was recently demonstrated that functional platelets produced *ex vivo* are CD41$^+$CD42^{+}[3]. The platelet size events that fail to express CD42 were metabolically inactive and unable to be activated or undergo shape changes[3]. Hence, the proportion of CD41$^+$CD42$^-$ events (gated on platelet-like size region)[25] were used as dead platelets[3]. Thus, the data for platelets using CD41$^+$CD42$^+$ and CD41$^+$CD42$^-$ events were analyzed as live and dead platelets, respectively and estimated the specific death rate like that of MK in which R^2 was 0.85 and 0.98 at 37 and 39ºC, respectively (Figure 4.3E).

Finally, the specific platelet production rate (Q_p) was determined by the slope of viable platelets ($CD41^+42^+$ events) against integrated mature MK or $\int_{t=0}^{t} M(t) \cdot dt$ (Figure 4.3F, $R^2 =$ 0.88).

Model Structure Reduction

An important step in mathematical modeling is to evaluate the estimability of the parameters within each model. In this step, it is critical to find if a solution exists within a reasonably limited confidence space and the parameters to be estimated without large uncertainty limits. The 7-C model shown in Figure 4.2A had 35 parameters of which 8 were estimated independently and the rest to be estimated (Table 4.1). Sensitivity analysis was then performed to determine parameter estimability. Sensitivity analysis around the global optimum, according to Yao et al.[26], revealed that only 13 parameters out of 27 could be estimated considering the model structure and the available data. Non-estimable parameters included the differentiation-related parameters among the intermediate stages (*B, C* and *F*) which included S_{CD}, S_{AC}, y_{BD}, S_{BD}, S_{AB}, S_{BC}, y_{AB}, t_C, t_F, and S_{BF}. Therefore, a simplified version of the model with a reduced number of parameters was developed by simplifying the model structure. To do so, compartments *B and C* as well as compartments *F* and *D* in the 7-C model were merged to form compartments *I* and *M* in 5-C model respectively. This resulted in reduction of the number of compartments/responses from 7 to 5 (Figure 4.2B) and parameters from 35 to 20 (Table 4.1).

Global Parameter Estimability

Finding the global minimum among several local minima is a challenging task, particularly when the number of parameters is large and the model is non-linear. To estimate the parameter values, a hybrid stochastic optimization method was developed as explained in *Parameter Estimation*. The result of applying this estimation method together with independent parameter estimation in 5-C model is summarized in Table 4.2 for both incubation temperatures of 37 and 39°C. Most importantly, the proposed model fitted reasonably well to the experimental data as an average R^2 of the 5 different responses were

0.91 with a range of [0.86 - 0.98] and 0.75 [0.65 - 0.95] for 37 and 39°C, respectively (Figure 4.4).

To better describe a parameter uncertainty space, a 95% confidence region (a linear approximate for a non-linear model) was defined by calculating a value of SS that would still lead to a reasonably good fit[30]:

$$SS = SS_{min} \cdot \left(1 + \frac{p}{n-p} \cdot F_{\alpha\ p,n-p} \right) \tag{4.15}$$

where p is the number of estimated parameters, n shows the number of experimental data points, and $F_{\alpha,p,n-p}$ is the critical value of Fisher F-distribution at a probability level (α) of 0.05. Assuming a normal and independent distribution for the errors, the value of SS/SS_{min} for the 5-C model was 1.77. Such a limit is rigorously exact for a linear system, but only an approximation for a non-linear model, such as in our case. Of around 11,000 solution sets obtained using the hybrid stochastic optimization method, 7,500 sets had SS/SS_{min} value below 1.77. The response simulations obtained using these 7,500 response sets were drawn in light gray in Figure 4.4. It can be observed that this represented a range of responses that was too large and did not fit well the experimental data. Therefore a lower value of SS/SS_{min} was searched in which parameter sets would generate response simulations that would fit reasonably well the experimental data. Performing the similar approach based on single response, it was found that parameter sets generating SS/SS_{min} values below 1.2 would do so in multi-response system (simulation curves in dark gray, Figure 4.4). Therefore such a threshold of $SS/SS_{min} \leq 1.2$ was considered as the limit of the empirical confidence space or interval for this model.

The possible correlation among parameters was addressed by applying PCA on solution matrix W, 1,200 rows and 14 columns (parameters), and its transpose W^T whose elements were parameter sets with $SS/SS_{min} \leq 1.2$. The matrix $W^T W$ could be decomposed using its eigenvalues and eigenvectors as $W^T W = UVU^T$ where V represented a diagonal matrix containing the eigenvalues and U contained the uncorrelated and orthogonal eigenvectors or principal components (PC). The methodology of numerical simulation and application of PCA is available in the literature[31-33]. Useful information can be gained using PCA, based

on the magnitudes of eigenvalues and eigenvectors. Table 4.3A shows the obtained eigenvalues, their relative importance and cumulative sum. Eigenvectors of the first 9 columns with magnitude above 0.2 are shown in Table 4.3B. The largest effect on responses (*PC1*) was brought about by a simultaneous change in the parameters μ_{maxA}, μ_{maxI}, S_{AE}, y_{AI}, μ_{maxE}, t_A and μ_{maxM} along the vector U_1. Therefore, simultaneous changes of these parameters played much important role in megakaryopoiesis, which accounted for 33%. The second most important effect (*PC2* and *PC3* together) was brought by a parameter group of $K_L Y_{X/L}$, t_I, μ_{maxM}, μ_{maxI}, μ_{maxA}, t_A, S_{AE} and X_{max} and their combinations played 38% of the role.

To better understand the individual role of each parameter in creation of the solution space, PCA results were further analyzed. To compute the contribution of each parameter within the principal components, the eigenvectors of each parameter at Table 4.3B was multiplied to the relevant importance (%) of that principal component (Table 4.3A, the second column). Like Morris methods in global sensitivity analysis[34], two measures were proposed for each parameter: *m'*, an estimate of the mean of each parameter contribution (%) in all principal components, and σ, an estimate of the standard deviation of each parameter contribution (%). These two measures were used as indicators of which parameters could be considered important individually or in a combination with others. A large value of *m'* indicates a parameter with an important overall role in the solution matrix (*W*), while a large value of σ indicates a parameter whose influence is highly dependent on the values of other parameters and/or whose effect is highly non-linear. Thus, *m'* and σ were computed and plotted against each other (Figure 4.5). It is noteworthy that the relationship between *m*□ and σ is approximately linear. This is true and a common characteristic for most of the global sensitivity analysis using the Morris method since the majority of the models in cell biology are highly nonlinear[35]. Thus, a parameter that is important in the model is usually more involved in non-linear or interactive effects and vice versa. This result showed that two parameters, μ_{maxI} and μ_{maxA}, had the highest contribution and the most curvature or interactive effects with other parameters. In contrast, S_{AI} and most likely S_{IM}, the closest parameters to the origin, had the lowest roles and the least interactive correlations with other parameters to create the parameter space.

Global and Local Sensitivity Analyses

To systematically explore the multidimensional parameter space, parameter estimability of the 5-C model was analyzed by sensitivity analysis. Sensitivity coefficients were obtained by varying one parameter at a time with ± 1% perturbation around their most likely optimal values (absolute values) shown in Table 4.2B. The normalized sensitivity matrix Z (i.e. eqn. 13) was calculated, and then the parameter estimability analysis proposed by Yao et al.[26] was applied to get the ranking of the parameters can be estimated locally. As shown in Table 4.4, the first two most estimable parameters found by this approach were parameters μ_{maxI} and t_A. The number of estimable parameters depended on the custom-defined cut-off value[26]. Two cut-off values of 0.1% and 0.0001% were defined as thresholds wherein a parameter could show influence on one of the responses[26]. The cut-off value of 0.0001% was equal to choosing 0.04 for SS_R (sum of squares of the residual matrix R) in Yao et al. method[26] as it can be seen in Table 4.4, e.g. having at least 2% change in one of the responses if a maximum 10% perturbation applies to a parameter value. These thresholds were used to classify the 14 parameters into three groups of: i) 6 estimable parameters (μ_{maxI}, t_A, μ_{maxA}, t_I, r_A and X_{max}), ii) 4 less-estimable parameters (r_I, S_{AE}, μ_{maxE} and μ_{maxM}) and iii) 4 parameters that, most likely, could not be estimated from the available experimental data ($K_L Y_{X/L}$, S_{IM}, y_{AI}, and S_{AI}). In other words, the first 6 parameters have a great influence on the model responses around their optimal values and can therefore be evaluated precisely. Accordingly, the analysis showed that the model responses had less sensitivity to the second (ii) and the third (iii) series of parameters that are shown by light gray and dark gray colors in Table 4.4. The results of this approach are in agreement with what was found by applying PCA and comparison of each parameter's contribution in solution matrix W ($m\square$ and σ measures).

The Yao et al parameter estimability approach[26] was also performed at several local minima that allowed to investigate which parameters were always estimable, e.g. globally identifiable, and those that could only be estimated locally around few local minima. This analysis was applied on sets of parameter solutions which had SS/SS_{min} values of 1.01, 1.05, 1.10, 1.18, 1.50 and 1.77, therefore within the approximate 95% confidence region (~7500 solution sets)[30]. Furthermore, 6 sets of parameter values chosen in which one of the

responses had the highest R^2 value together with some randomly chosen data sets among ~95% confidence regions and then the sensitivity analysis using Yao et al.[26] was performed around these local minima. Results of this analysis corroborated the ranking obtained in the vicinity of the most likely global minimum and showed that some of the non- and less-estimable parameters (series iii and ii) now appeared as less estimable and even estimable (data not shown). In brief, applying global and local sensitivity analyses revealed that: i) six parameters of μ_{maxI}, t_A, μ_{maxA}, t_I, r_A and X_{max} can be estimated locally (at the most likely global minimum), ii) three parameters of r_I, μ_{maxE} and μ_{maxM} can be estimated locally but might be globally, iii) S_{AE}, $K_L Y_{X/L}$ and y_{AI} might be estimated globally, and iv) two parameters of S_{IM} and S_{AI} could not be estimated considering the model structure and the available experimental data.

Model Dimension Reduction

To reduce the 5-C model dimension even further, which was of 14 parameters, estimability was evaluated by a last approach. Starting from the most estimable parameter (μ_{maxI}) while the other (13 or less) parameters were kept constant at the obtained optimal values, the best SS value (eq. 4.10) was searched and this was continued until the combinations of the all 14 parameters were tested. As shown in Figure 4.6, searching to optimize 1 to 9 parameters could lead in slight improvement in the SS_{min} value, while any addition of parameters above 9 did not allow further improvement in SS_{min} value. This analysis showed that the number of parameters or model dimension could be reduced to 9, which contained the parameters of μ_{maxI}, t_A, μ_{maxA}, t_I, r_A, X_{max}, r_I, S_{AE} and μ_{maxE} forming the basic part of the model, called "megakaryopoiesis kernel". Therefore, a combination of the proliferation rates of A, I and E but not M, and differentiation time and rate of initial population (A: CD34$^+$41$^-$42$^-$) to immature MK (I: CD41$^+$42$^-$) then to mature MK (M: CD41$^+$42$^+$), as well as maximum cell density of all compartments (X_{max}) but not Monod affinity constant ($K_L Y_{X/L}$) formed the most influential part of the process. This analysis revealed that such a MK mechanism kernel in fact came from the important role of the intermediate compartment of immature MK (I) stage.

Insights Provided by 5-Compartment Megakaryopoiesis Model

Previous studies demonstrated that incubation of CB-CD34$^+$ cells at 39°C resulted in accelerated MK differentiation and maturation, as well as increase MK and platelet outputs[8,9]. The proposed model and its parameters are consistent in large part with these studies (Table 4.2 and Figure 4.4). Indeed, the simulated culture dynamic presented in Figure 4.4 and the results of comparison of parameter values at both incubation temperatures presented in Table 4.2 show clearly that MK differentiation is promoted by mild hyperthermia during the first 10 days of the culture since the growth of the compartments A (HSC) and E (non-MK) were significantly reduced at 39°C, while the growth of compartment I was slightly greater. In addition, during the late phase of culture (day 10 - 14), growth of immature and mature MK (I and M, respectively) and platelet production (P) and total cell expansion were significantly higher at 39°C than 37°C. Hence, the model appropriately simulated the growth response of the various compartments for both incubation temperatures.

As presented in Table 4.2, comparison of the optimal value of parameters at two incubation temperatures showed that maximum total cell concentration (X_{max}), maximum specific growth rates of A and I (μ_{maxA} and μ_{maxI}), selective differentiation rate of A to I (y_{AI}), symmetrical differentiations of I to M (S_{IM}), death rates of all compartments (k_{dX}, k_{dI}, k_{dM}, and k_{dP}) except that of M during the second week (k_{dM}), and specific platelet production rate (Q_p) increased with temperature elevation, while the others showed an opposite response. However, considering the large range of the parameter values (Figure 4.4 and Table 4.2), such differences in parameter values between two temperatures should be compared with caution. Applying global parameter estimability showed some parameters had overlapping values at two temperatures, which included t_I and k_{dM} (at days 8 − 14). This could be interpreted as temperature having a non-significant effect on these parameters, or as the model resolution being too low to distinguish the effects of the temperature shift.

The specific platelet production rate (Q_p) was predicted by direct estimation of this parameter at both incubation temperatures (Figure 4.3E-F). The result showed 1.2-fold higher platelet production at 39°C. This increase was consistent with previous reports on the effect of elevated temperature on the number of platelets generated *ex vivo*[8,9]. Further

analysis showed that platelets disappeared at the same rate of production (Q_p) since k_{dP} was found 1.3-fold higher at 39°C. It is important to note that the proportion of CD41$^+$CD42$^-$ vs platelet-like size events were used as representative of dead (non-functional) platelets, which in itself was not really precise estimation of k_{dp} because MK debris without nucleus could represent a large portion of that population. However, this increased platelet death rate at 39°C makes sense and is consistent with the accelerated and increased production of platelets at 39°C given that programmed cell death is initiated during the release of platelets from MKs[28].

To highlight the dynamic nature of some parameters, their variations were computed from the optimal values of time-independent parameters and plotted within the empirical confidence regions in 5-C model at 37°C and presented in Figure 4.7. Comparison of alterations of these parameters over culture period shows that the specific growth rate of I (μ_I) had the highest magnitude among the all four growing subpopulations, while that of M and E was lower than that of I or A during 14 culture days. In all cases, this term showed gradually small reduction over time. Subsequently, this resulted in the higher values of proliferation rates of I (the largest value over the whole culture period) and A compartments than E and M, i.e. $k_{II} > k_{AA} > k_{EE} \geq k_{MM}$. Interestingly, the proliferation rate of compartment A (k_{AA}) became negligible after day 4 and showed the highest slope of reduction over time, that of I (k_{II}) started hitting zero at day 4.5 while k_{EE} and k_{MM} showed slight reduction during the culture period that also indicated activity of these populations. In contrast, dynamic behaviour of the differentiation rates showed a sharp increase during the first 2 - 4 days followed by a slight reduction until the end of the culture. This might be explained by the sigmoidal function imposed to the differentiation coefficients (d), among which the differentiation coefficient of subpopulation A (d_A) reached maximum (1) during the first 2 - 3 days while that of I (d_I) occurred during days 4 - 14.

4.5. Discussion

The approach of multi-dimensional, multi-compartmental kinetic modeling is applicable for every stem cell population balance in general and was designed in this study for megakaryopoiesis. The model was based on three cell surface marker data collected by flow

cytometry and considered the five major compartments of HSC, immature MK, mature MK, non-MK and platelets. The developed mathematical model allowed a deeper understanding of the differentiation and proliferation pathways and estimation of their rates. By doing so, parameters of the regulatory system, which cannot be measured directly or experimentally, may be indirectly inferred, depending on the diversity and quality of experimental data. The simulations made using the proposed model fitted the data adequately. The variation of experimental data was high, even when duplicate or triplicate samples were taken. This was especially apparent at the end of cultures ($\pm$ 10%) and between different lots of cord blood cell ($\pm$ 20%).

The proposed model structure was based on proliferation, differentiation and death fates as well as symmetrical differentiation coefficients. This compartment model did not consider a fate such as quiescence in its structure to save the number of parameters to be estimated. Using imaging study it has been shown that quiescent HSC enters rapidly into cell cycle or self-renewal in response to G-CSF stimulation[36]. Therefore, neglecting this phenomenon might have had a minimal impact on the results of parameter estimation. On the other hand, using PCA and estimability analysis it was found that two parameters of S_{AI} and S_{IM} (asymmetrical differentiation of A to I and I to M, respectively) had minimal impacts on creation of the solution space either individually or in a combination with the other parameters as they were analyzed as non-estimable. Thus, the asymmetrical coefficient parameters might be removed from the model structure, which would allow reducing the number of parameters and further simplification.

Sensitivity analysis is essential for understanding how model parameters influence the model responses and to validate the model. Here advantages of applying local and global sensitivity analyses were shown to be certain of parameter estimability that also brings additional information. However, the large uncertainty regions of some parameter could mean that the model is non-identifiable parametrically which is a common feature of this sort of model[37]. The parameter estimation is sufficiently robust to evaluate the order of magnitude of the rates and the relative importance of the different steps in biological processes occurring in megakaryopoiesis.

To test our model, the number of conditions was limited to two incubation temperatures. Other incubation temperatures were not found physiologically important. For instance 33°C was reported as less effective on MK differentiation, while 41°C (extreme hyperthermia) caused deactivation of produced platelets. Therefore, the model built here remains descriptive rather than predictive or mechanistic. Neither this model as quantitative tool nor other quantitative or qualitative tools as previously reported by other researchers could explain why 39°C appeared better than 37°C in MK development. On the other hand, the data set for every condition was duplicated. One might try to validate the model parameters using one set of data among the duplicates, and then use the other one for parameter estimation. Alternatively, pseudo-experimental data strategy, generating artificial experimental data by simulation, might be used to validate the model and parameters [27,37].

The use of variable differentiation rate is a common approach in stem cell differentiation modeling. The transfer rate from a compartment to the next is generally correlated with cytokine concentration. For instance, Santillan et al.[22] used a negative feedback from TPO concentration to simulate the differentiation of lower- to higher ploidy class of MK, where in turn TPO concentration was controlled by the total number of platelets in the blood, following:

$$\frac{dTPO}{dt} = \frac{a}{1 + bP^n} - k \cdot TPO \tag{4.16}$$

where *a, b, n,* and *k* were constants. Comparatively, in our approach it was assumed that the concentrations of TPO and all other cytokines together with other growth factors in the medium ([L]) were controlled by the total cells (X_T) that existed in the culture, shown by eq. 4.2 – 4.5. In this study, medium was refreshed frequently to insure proper maintenance of cytokine concentrations during the experiments. At this point, the inclusion of relevant cytokine effects on megakaryopoiesis was not considered, but it would certainly be interesting to include these in future models, particularly for TPO concentration and utilization rate.

In summary, the non-linear 3D formulation shown provides a general framework of system dynamic for the purpose of quantifying rates of proliferation, differentiation and death of

megakaryopoiesis subpopulations. Due to the non-linear characteristics of this sort of ODE systems, the estimated values of parameters were analyzed in different ways such as model structure simplification, model dimension reduction, PCA and parameter estimability evaluation on both local and global scales as well as introducing empirical confidence regions of parameters. This provided an efficient and confident estimation of HSC and MK cellular proliferation, differentiation and death rates. Analyses presented here may provide reliable new insight into the cell decision and differentiation mechanisms.

Acknowledgements

Abbreviations

BM	Bone Marrow
CB	Cord Blood
HSC	Hematopoietic Stem Cell
IL	Interleukin
MK	Megakaryocyte
ODE	Ordinary Differential Equation
PC	Principal Component
PCA	Principal Component Analysis
TCN	Total Cell Number
TPO	Thrombopoietin
SCF	Stem Cell Factor

4.6. Appendix

1) Balance equations of 7-C model:

$$\frac{dA}{dt} = \mu_{AA} - \left(\mu_{AB} \cdot S_{AB} + \mu_{AC} \cdot S_{AC} + \mu_{AE} \cdot S_{AE} + \mu_{dA} \right) \cdot A \qquad (4.A1)$$

$$\frac{dB}{dt} = k_{AB} \cdot A + k_{AB} \cdot A + k_{BB} - k_{BC} \cdot S_{BC} + k_{BD} \cdot S_{BD} + k_{BF} \cdot S_{BF} + k_{dB} \cdot B \quad (4.A2)$$

$$\frac{dC}{dt} = k_{AC} \cdot A + k_{AC} \cdot A + k_{BC} \cdot B + k_{BC} \cdot B + k_{CC} - k_{CD} \cdot S_{CD} + k_{dC} \cdot C \quad (4.A3)$$

$$\frac{dD}{dt} = k_{BD} \cdot B + k_{BD} \cdot B + k_{CD} \cdot C + k_{CD} \cdot C + k_{FD} \cdot F - k_{dD} \cdot D \quad (4.A4)$$

$$\frac{dE}{dt} = k_{AE} \cdot A + k_{AE} \cdot A + k_{EE} - k_{dE} \cdot E \quad (4.A5)$$

$$\frac{dF}{dt} = k_{BF} \cdot B + k_{BF} \cdot B - k_{FD} + k_{dF} \cdot F \quad (4.A6)$$

$$\frac{dP}{dt} = Q_P \cdot D - k_{dp} \cdot P \quad (4.A7)$$

$$X = A + B + C + D + E + F \quad (4.A8)$$

where:

$$k_{AA} = \frac{\mu_{\max,A} \cdot (X_{\max} - X)}{K_L \cdot Y_{X/L} + (X_{\max} - X)} \cdot \left(1 - \frac{1}{1 + e^{-r_A(t-t_A)}}\right) \quad (4.A9)$$

$$k_{AB} = \frac{\mu_{\max,A} \cdot (X_{\max} - X)}{K_L \cdot Y_{X/L} + (X_{\max} - X)} \cdot \frac{1}{1 + e^{-r_A(t-t_A)}} \cdot y_{AB} \quad (4.A10)$$

$$k_{AC} = \frac{\mu_{\max,A} \cdot (X_{\max} - X)}{K_L \cdot Y_{X/L} + (X_{\max} - X)} \cdot \frac{1}{1 + e^{-r_A(t-t_A)}} \cdot y_{AC} \quad (4.A11)$$

$$k_{AE} = \frac{\mu_{\max,A} \cdot (X_{\max} - X)}{K_L \cdot Y_{X/L} + (X_{\max} - X)} \cdot \frac{1}{1 + e^{-r_A(t-t_A)}} \cdot (1 - y_{AB} - y_{AC}) \quad (4.A12)$$

$$k_{BB} = \frac{\mu_{\max,B} \cdot (X_{\max} - X)}{K_L \cdot Y_{X/L} + (X_{\max} - X)} \cdot \left(1 - \frac{1}{1 + e^{-r_B(t-t_B)}}\right) \quad (4.A13)$$

$$k_{BC} = \frac{\mu_{ax,B} \cdot (X_{max} - Y)}{K_L \cdot Y_{X/L} + (X_{max} - Y)} \cdot \frac{1}{1 + e^{-r_B(t-t_B)}} \cdot y_{BC} \qquad (4.A14)$$

$$k_{BD} = \frac{\mu_{ax,B} \cdot (X_{max} - Y)}{K_L \cdot Y_{X/L} + (X_{max} - Y)} \cdot \frac{1}{1 + e^{-r_B(t-t_B)}} \cdot y_{BD} \qquad (4.A15)$$

$$k_{BF} = \frac{\mu_{ax,B} \cdot (X_{max} - Y)}{K_L \cdot Y_{X/L} + X_{max} - Y)} \cdot \frac{1}{1 + e^{-r_B(t-t_B)}} \cdot (1 - y_{BC} - y_{BD}) \qquad (4.A16)$$

$$k_{CC} = \frac{\mu_{ax,C} \cdot (X_{max} - X)}{K_L \cdot Y_{X/L} + (X_{max} - X)} \cdot \left(1 - \frac{1}{1 + e^{-r_C(t-t_C)}}\right) \qquad (4.A17)$$

$$k_{CD} = \frac{\mu_{ax,C} \cdot (X_{max} - Y)}{K_L \cdot Y_{X/L} + X_{max} - Y)} \cdot \frac{1}{1 + e^{-r_C(t-t_C)}} \qquad (4.A18)$$

$$k_{EE} = \frac{\mu_{ax,E} \cdot (X_{max} - Y)}{K_L \cdot Y_{X/L} + X_{max} - Y)} \qquad (4.A19)$$

$$k_{FF} = \frac{\mu_{ax,F} \cdot (X_{max} - X)}{K_L \cdot Y_{X/L} + (X_{max} - X)} \cdot \left(1 - \frac{1}{1 + e^{-r_F(t-t_F)}}\right) \qquad (4.A20)$$

$$k_{FD} = \frac{\mu_{ax,F} \cdot (X_{max} - Y)}{K_L \cdot Y_{X/L} + X_{max} - Y)} \cdot \frac{1}{1 + e^{-r_F(t-t_F)}} \qquad (4.A21)$$

2) Balance equations of 5-C model:

$$\frac{dA}{dt} = k_{AA} - k_{AI} \cdot S_{AI} + k_{AE} \cdot S_{AE} + k_{dA} \cdot A \qquad (4.A22)$$

$$\frac{dI}{dt} = k_{AI} \cdot + S_{AI} \cdot A + (k_{II} - k_{IM} - k_{dI}) \cdot I \qquad (4.A23)$$

$$\frac{dM}{dt} = k_{IM} \cdot + S_{IM} \cdot I + (k_{MM} - k_{dM}) \cdot C \qquad (4.A24)$$

$$\frac{dP}{dt} = 2_P \cdot M - k_{dp} \cdot P \tag{4.A25}$$

$$X = A + I + M + E \tag{4.A26}$$

where

$$k_{AA} = \frac{\mu_{ax,A} \cdot (X_{max} - X)}{K_L \cdot Y_{X/L} + (X_{max} - X)} \cdot \left(1 - \frac{1}{1 + e^{-r_A(t-t_A)}} \right) \tag{4.A27}$$

$$k_{AI} = \frac{\mu_{ax,A} \cdot (X_{max} - Y)}{K_L \cdot Y_{X/L} + (X_{max} - Y)} \cdot \frac{1}{1 + e^{-r_A(t-t_A)}} \cdot y_{AI} \tag{4.A28}$$

$$k_{AE} = \frac{\mu_{ax,A} \cdot (X_{max} - Y)}{K_L \cdot Y_{X/L} + X_{max} - Y)} \cdot \frac{1}{1 + e^{-r_A(t-t_A)}} \cdot (1 - y_{AI}) \tag{4.A29}$$

$$k_{EE} = \frac{\mu_{ax,E} \cdot (X_{max} - Y)}{K_L \cdot Y_{X/L} + X_{max} - Y)} \tag{4.A30}$$

$$k_{II} = \frac{\mu_{ax,I} \cdot (X_{max} - X)}{K_L \cdot Y_{X/L} + (X_{max} - X)} \cdot \left(1 - \frac{1}{1 + e^{-r_I(t-t_I)}} \right) \tag{4.A31}$$

$$k_{MM} = \frac{\mu_{ax,M} \cdot (X_{max} - Y)}{K_L \cdot Y_{X/L} + X_{max} - Y)} \tag{4.A32}$$
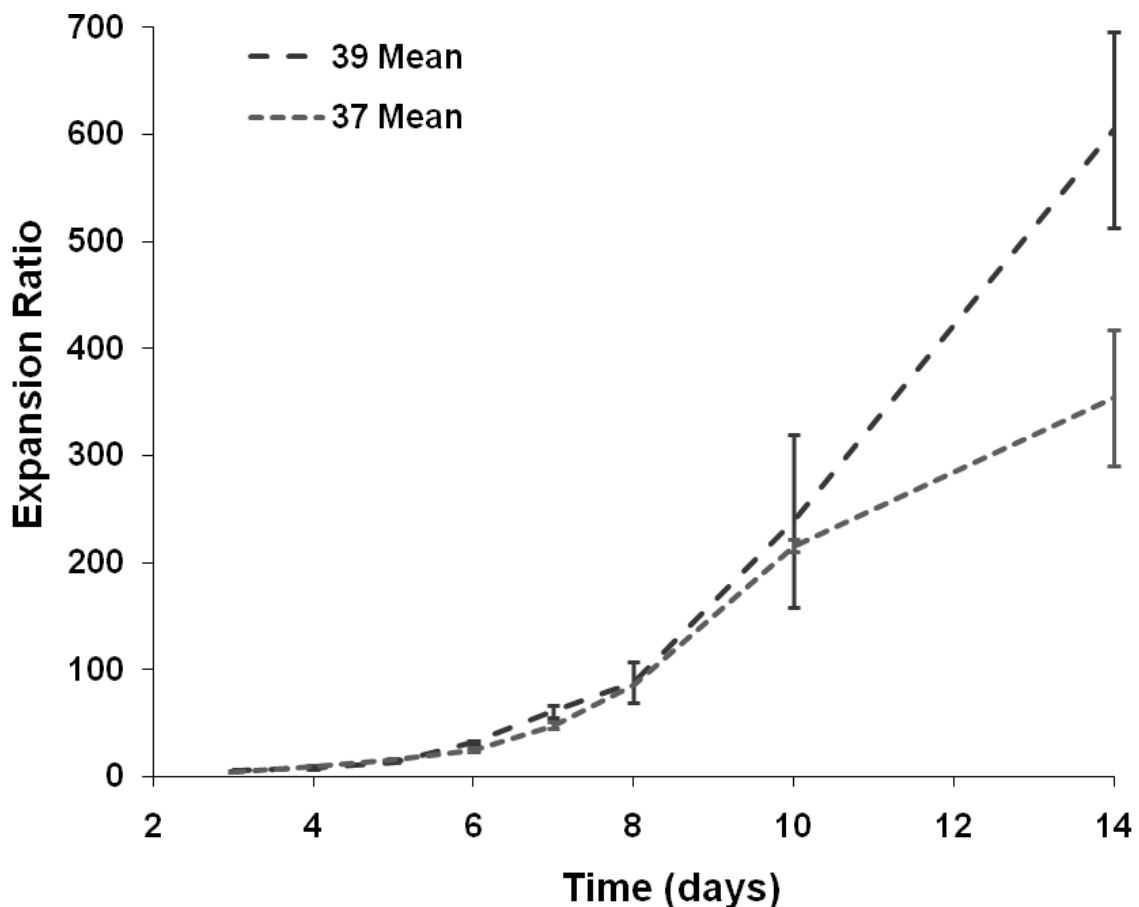
Figure 4.A1: Total cell expansion kinetics of cord blood CD34^{+} cells cultured with BS1 cocktail[6] at two incubation temperatures of 37 and 39°C during two weeks. The number of Trypan blue negative cells was counted (n ≥ 4) at each time point, and divided by the number of seeded cells at day 0 (4 x 10^5 cells/ml). Cultures were refreshed at days 4, 7 and 10. Mean result of two independent experiments shown.

4.7. References

1. Battinelli EM, Hartwig JH, Italiano JE, Jr. Delivering new insight into the biology of megakaryopoiesis and thrombopoiesis. Curr Opin Hematol. 2007;14:419-426.
2. Cramer EM, Vainchenker W. Chapter 25. Platelet Production: Cellular and Molecular Regulation (ed 5th). Philadelphia, PA: Lippincott Williams & Wilkins; 2006.
3. Robert A, Boyer L, Pineault N. Glycoprotein Ibα Receptor Instability Is Associated with Loss of Quality in Platelets Produced in Culture. Stem Cells and Development. 2010;Epub ahead of print.
4. Ravid K, Lu J, Zimmet JM, Jones MR. Roads to polyploidy: the megakaryocyte example. J Cell Physiol. 2002;190:7-20.

5. Junt T, Schulze H, Chen Z, et al. Dynamic visualization of thrombopoiesis within bone marrow. Science. 2007;317:1767-1770.

6. Cortin V, Garnier A, Pineault N, Lemieux R, Boyer L, Proulx C. Efficient in vitro megakaryocyte maturation using cytokine cocktails optimized by statistical experimental design. Exp Hematol. 2005;33:1182-1191.

7. Boyer L, Robert A, Proulx C, Pineault N. Increased production of megakaryocytes near purity from cord blood CD34+ cells using a short two-phase culture system. J Immunol Methods. 2008;332:82-91.

8. Proulx C, Dupuis N, St-Amour I, Boyer L, Lemieux R. Increased megakaryopoiesis in cultures of CD34-enriched cord blood cells maintained at 39 degrees C. Biotechnol Bioeng. 2004;88:675-680.

9. Pineault N, Boucher JF, Cayer MP, et al. Characterization of the effects and potential mechanisms leading to increased megakaryocytic differentiation under mild hyperthermia. Stem Cells Dev. 2008;17:483-493.

10. Bernstein SH, Jusko WJ, Krzyzanski W, Nichol J, Wetzler M. Pharmacodynamic modeling of thrombopoietin, platelet, and megakaryocyte dynamics in patients with acute myeloid leukemia undergoing dose intensive chemotherapy. J Clin Pharmacol. 2002;42:501-511.

11. Colijn C, Mackey MC. A mathematical model of hematopoiesis--I. Periodic chronic myelogenous leukemia. J Theor Biol. 2005;237:117-132.

12. da Silva CL, Goncalves R, Lemos F, et al. Modelling of ex vivo expansion/maintenance of hematopoietic stem cells. Bioprocess Biosyst Eng. 2003;25:365-369.

13. Goncalves R, da Silva CL, Ferreira BS, et al. Kinetic analysis of the ex vivo expansion of human hematopoietic stem/progenitor cells. Biotechnol Lett. 2006;28:335-340.

14. Hardy K, Stark J. Mathematical models of the balance between apoptosis and proliferation. Apoptosis. 2002;7:373-381.

15. Jin F, Krzyzanski W. Pharmacokinetic model of target-mediated disposition of thrombopoietin. AAPS PharmSci. 2004;6:E9.

16. Nielsen LK, Papoutsakis ET, Miller aWM. Modeling ex vivo hematopoiesis using chemical engineering metaphors. Chem Eng Sci. 1998;53:1913-1925.

17. Peng C-A, Koller MR, Palson aBO. Unilineage model of hematopoiesis predicts self-renewal of stem and progenitors cells based on ex vivo growth data. Biotechnol Bioeng. 1996;52:24-33.

18. Prudhomme WA, Duggar KH, Lauffenburger DA. Cell population dynamics model for deconvolution of murine embryonic stem cell self-renewal and differentiation responses to cytokines and extracellular matrix. Biotechnol Bioeng. 2004;88:264-272.

19. Viswanathan S, Zandstra PW. Towards predictive models of stem cell fate. Cytotechnology. 2003;41:75-92.

20. Wichmann HE, Gerhardts MD, Spechtmeyer H, Gross R. A mathematical model of thrombopoiesis in rats. Cell Tissue Kinet. 1979;12:551-567.

21. Harker LA, Roskos LK, Marzec UM, et al. Effects of megakaryocyte growth and development factor on platelet production, platelet life span, and platelet function in healthy human volunteers. Blood. 2000;95:2514-2522.

22. Santillan M, Mahaffy JM, Belair J, Mackey MC. Regulation of platelet production: the normal response to perturbation and cyclical platelet disease. J Theor Biol. 2000;206:585-603.

23. Skomorovski K, Harpak H, Ianovski A, et al. New TPO treatment schedules of increased safety and efficacy: pre-clinical validation of a thrombopoiesis simulation model. Br J Haematol. 2003;123:683-691.
24. Proulx C, Boyer L, Hurnanen DR, Lemieux R. Preferential ex vivo expansion of megakaryocytes from human cord blood CD34+-enriched cells in the presence of thrombopoietin and limiting amounts of stem cell factor and Flt-3 ligand. J Hematother Stem Cell Res. 2003;12:179-188.
25. Cortin V, Pineault N, Garnier A. Ex vivo megakaryocyte expansion and platelet production from human cord blood stem cells. Methods Mol Biol. 2009;482:109-126.
26. Yao KZ, Shaw BM, Kou B, McAuley KB, Bacon aDW. Modeling Ethylene/Butene Copolymerization with Multi-site Catalysts: Parameter Estimability and Experimental Design Polymer reaction Engineering. 2003;11:563-588.
27. Yue H, Brown M, Knowles J, Wang H, Broomhead DS, Kell DB. Insights into the behaviour of systems biology models from dynamic sensitivity and identifiability analysis: a case study of an NF-kappaB signalling pathway. Mol Biosyst. 2006;2:640-649.
28. Clarke MC, Savill J, Jones DB, Noble BS, Brown SB. Compartmentalized megakaryocyte death generates functional platelets committed to caspase-independent death. J Cell Biol. 2003;160:577-587.
29. Leysi-Derilou Y, Robert A, Duchesne C, Garnier A, Boyer L, Pineault N. Polyploid megakaryocytes can complete cytokinesis. Cell Cycle. 2010;9: 2587-2597.
30. Bates DM, Watts DG. Nonlinear regression analysis and its applications. New York ; Toronto: Wiley; 1988.
31. Blanco M, Coello J, Iturriaga H, Maspoch S, Riba J, Rovira E. Kinetic spectrophotometric determination of Ga(III)-Al(III) mixtures by stopped-flow injection analysis using principal component regression. Talanta. 1993;40:261-267.
32. Chester VL, Wrigley AT. The identification of age-related differences in kinetic gait parameters using principal component analysis. Clin Biomech (Bristol, Avon). 2008;23:212-220.
33. Vajda S, Valko P, TURANYI T. Principal Component Analysis of Kinetic Models International Journal of Chemical Kinetics. 1985;17:55-81.
34. Morris MD. Factorial sampling plans for preliminary computational experiments. Technometrics. 1991;33:161-174.
35. Saltelli A, Ratto M, Tarantola S, Campolongo F. Sensitivity analysis for chemical models. Chem Rev. 2005;105:2811-2828.
36. Wilson A, Laurenti E, Oser G, et al. Hematopoietic stem cells reversibly switch from dormancy to self-renewal during homeostasis and repair. Cell. 2008;135:1118-1129.
37. Kirouac DC, Madlambayan GJ, Yu M, Sykes EA, Ito C, Zandstra PW. Cell-cell interaction networks regulate blood stem and progenitor cell fate. Mol Syst Biol. 2009;5:293.

4.8. Tables and Figures

4.8.1. Tables

Table 4.1: List of parameters, constraints and numbers for the 3-D *ex vivo* 5- and 7-compartment megakaryopoiesis models.

Name	Units	LB[a]	UB[b]	Parameter Description	7-C[c]	5-C[d]
μ_{maxA}	day^{-1}	0	10	Maximum specific growth rate of A	3	3
μ_{maxB}	day^{-1}	0	10	Maximum specific growth rate of B	4	-
μ_{maxC}	day^{-1}	0	10	Maximum specific growth rate of C	5	-
μ_{maxE}	day^{-1}	0	10	Maximum specific growth rate of E	7	6
μ_{maxF}	day^{-1}	0	10	Maximum specific growth rate of F	8	-
μ_{maxI}	day^{-1}	0	10	Maximum specific growth rate of I	6	4
μ_{maxM}	day^{-1}	0	10	Maximum specific growth rate of M	-	5
k_d	day^{-1}	0	5	Specific disappearance rate	28-34	15-19
$K_L Y_{X/L}$	$Cells/ml$	0	500	Monod affinity constant	2	2
Q_P	$Plts/Cells/day$	1	5,000	Specific platelet production rate	35	20
r_A	day^{-1}	0	10	Rate constant in sigmoidal differentiation function of A	13	9
r_B	day^{-1}	0	10	Rate constant in sigmoidal differentiation function of B	14	-
r_C	day^{-1}	0	10	Rate constant in sigmoidal differentiation function of C	15	-
r_F	day^{-1}	0	10	Rate constant in sigmoidal differentiation function of F	16	-
r_I	day^{-1}	0	10	Rate constant in sigmoidal differentiation function of I	-	10
S_{AB}	---	0	1	Symmetrical differentiation coefficient of A to B	21	-
S_{AC}	---	0	1	Symmetrical differentiation coefficient of A to C	22	-
S_{AE}	---	0	1	Symmetrical differentiation coefficient of A to E	23	13
S_{AI}	---	0	1	Symmetrical differentiation coefficient of A to I	-	12
S_{BC}	---	0	1	Symmetrical differentiation coefficient of B to C	24	-
S_{BD}	---	0	1	Symmetrical differentiation coefficient of B to D	25	-
S_{BF}	---	0	1	Symmetrical differentiation coefficient of B to F	26	-
S_{FD}	---	0	1	Symmetrical differentiation coefficient of F to D	27	-
S_{IM}	---	0	1	Symmetrical differentiation coefficient of I to M	-	14
t_A	day	0	14	Time constant in sigmoidal differentiation function of A	9	7
t_B	day	0	14	Time constant in sigmoidal differentiation function of B	10	-
t_C	day	0	14	Time constant in sigmoidal differentiation function of C	11	-
t_F	day	0	14	Time constant in sigmoidal differentiation function of F	12	-
t_I	day	0	14	Time constant in sigmoidal differentiation function of I	-	8
X_{max}	$Cells$	100	1,000	Maximum total cell concentration	1	1
y_{AB}	---	0	1	Selective differentiation rate of A to B	17	-
y_{AC}	---	0	1	Selective differentiation rate of A to C	18	-
y_{AI}	---	0	1	Selective differentiation rate of A to I	-	11
y_{BC}	---	0	1	Selective differentiation rate of B to C	19	-
y_{BD}	---	0	1	Selective differentiation rate of B to D	20	-

a) LB: lower bound; b) UB: upper bound; c) 7-C: 7-compartment model; d) 5-C: 5-compartment model.

Table 4.2: Optimal values of 5-C model parameters at two incubation temperatures. **A)** Estimated independently and individually. **B)** Estimated by the hybrid stochastic optimization method.

A. Estimated independently and individually.

Parameter	Time (day)	37ºC Estimated value	R^2	39ºC Estimated value	R^2	Ratio[a]
k_{dA}, k_{dE}, k_{dX}	0 – 14	0.1561	0.9903	0.2272	0.9965	1.46
k_{dI}	0 – 14	0.6543	0.9986	1.2190	0.9985	1.86
k_{dM}	0 – 7	0.0373	0.9055	0.0489	0.9739	1.31
	8 – 14	0.0131	0.8687	0.0129	0.9370	0.98
k_{dP}	0 – 14	0.4444	0.8516	0.5645	0.9779	1.27
Q_p	0 – 14	0.1453	0.8831	0.1704	0.8795	1.17

a) ratio of the optimized value of the parameters at 39ºC to that at 37ºC.

B. Estimated by the hybrid stochastic optimization method.

No.	Parameter	37ºC	39ºC	Ratio
1	X_{max}	333.26[a] ± 154.62[b] [211[c] - 583[d]]	377.21 ± 135.50 [200 - 800]	1.13[e]
2	$K_L Y_{X/L}$	85.23 ± 120.29 [0 - 412]	1.11E-4 ± 104.09 [0 - 398]	1.3E-6
3	μ_{maxA}	1.1908 ± 0.3249 [0.72 - 3.25]	1.6781 ± 0.5791 [0.90 - 6.68]	1.41
4	μ_{maxI}	2.0960 ± 0.4780 [0.93 - 6.25]	2.5967± 0.4392 [1.52 - 3.55]	1.24
5	μ_{maxM}	0.1852 ± 0.5395 [0.01 - 2.1]	0.0726 ± 0.3974 [0.01 - 1.38]	0.39
6	μ_{maxE}	0.1110 ± 0.0956 [0.01 - 0.68]	0.0100± 0.1140 [0.01 - 0.68]	0.10
7	t_A	6.9163 ± 1.1181 [1.59 - 8.36]	3.15E-4 ± 2.1647[0 - 14]	4.5E-5
8	t_I	14 ± 3.3276 [0 - 14]	14 ± 2.8151 [0.01 - 14]	1
9	r_A	0.3869 ± 0.1930 [0.11 - 2.0]	0.2369 ± 0.1199 [0 - 2.0]	0.61
10	r_I	0.0957 ±0.6108 [0 - 2.0]	0.0503 ± 0.7811 [0 – 2.0]	0.53
11	y_{AI}	1.45E-12 ± 0.1279 [0 - 0.61]	0.0689 ± 0.1848 [0 - 0.76]	4.7E10
12	S_{AI}	0.1139 ± 0.3847 [0 - 1.0]	1.46E-6 ± 0.2980[0 - 1.0]	1.3E-5
13	S_{AE}	1.0 ± 0.3031 [0 - 1.0]	0 ± 0.1915 [0 - 1.0]	0
14	S_{IM}	2.13E-5 ± 0.0753[0 - 0.99]	2.64E-5 ± 0.0711[0 - 0.99]	1.24

a) Optimum values of the parameters found based on the objective function according to eq. 4.10; b) standard deviation; c) minimum and d) maximum values of the parameters within approximate 95% confidence intervals, achieved in multi-dimensional space rather than individual space; and e) ratio of the optimized value of the parameters at 39ºC to that at 37ºC.

Table 4.3: PCA of the solution matrix (*W*) within the empirical confidence interval for the 5-C model for T = 37ºC data set. **A)** Eigenvalues and their relative importance; **B)** Values of eigenvectors. The solution matrix (*W: 1200 rows x 14column*) was composed of 1,200 parameter sets that generated $SS/SS_{min} \leq 1.2$.

A. Eigenvalues and their relative importance.

	EigenValues	Importance (%)	Cumulative Sum
1	5,610	32.58	32.58
2	3,364	19.53	52.11
3	3,152	18.30	70.42

4	1,827	10.61	81.02
5	1,325	7.69	88.72
6	792	4.60	93.32
7	487	2.83	96.15
8	415	2.41	98.56
9	133	0.770	99.33
10	63	0.364	99.69
11	23	0.135	99.83
12	14	0.081	99.91
13	13	0.074	99.98
14	2.74	0.016	100

B) Values of eigenvectors.

	1	2	3	4	5	6	7	8	9
1[a]	μ_{maxA} 0.6101[b]	μ_{maxI} 0.5894	S_{AE} 0.2449	y_{AI} 0.2422	μ_{maxE} 0.2338	t_A 0.2220	μ_{maxM} 0.2119		
2	$K_LY_{X/L}$ 0.4540	t_I 0.4476	μ_{maxM} 0.4181	r_I 0.4077	μ_{maxI} 0.2653	μ_{maxA} 0.2618			
3	$K_LY_{X/L}$ 0.6593	μ_{maxM} 0.3669	μ_{maxI} 0.3005	S_{AE} 0.2760	t_A 0.2657	X_{max} 0.2511	t_I 0.2278		
4	t_A 0.5646	S_{AE} 0.5517	t_I 0.3150	$K_LY_{X/L}$ 0.2375	μ_{maxM} 0.2281	μ_{maxA} 0.2212	μ_{maxI} 0.2058		
5	r_A 0.6391	μ_{maxE} 0.5954	μ_{maxA} 0.2729	y_{AI} 0.2685	t_A 0.2059				
6	X_{max} 0.7250	S_{IM} 0.3684	μ_{maxI} 0.3471	t_I 0.3213	r_I 0.2189	μ_{maxA} 0.2044			
7	y_{AI} 0.4285	μ_{maxM} 0.4196	t_I 0.3652	t_A 0.3443	r_A 0.2929	S_{IM} 0.2764	μ_{maxI} 0.2634	S_{AE} 0.2116	r_I 0.1990
8	μ_{maxE} 0.5149	r_I 0.4059	r_A 0.4032	S_{AE} 0.3697	y_{AI} 0.2688	μ_{maxA} 0.2541	μ_{maxM} 0.2304		
9	S_{AI} 0.8629	S_{IM} 0.3297							
10	S_{IM} 0.6287	r_I 0.4511	S_{AI} 0.3520	t_I 0.3382	μ_{maxM} 0.2860				
11	y_{AI} 0.7432	r_I 0.3565	S_{IM} 0.2510	μ_{maxM} 0.2320	t_I 0.2313	μ_{maxE} 0.2103			
12	X_{max} 0.4961	r_I 0.3554	r_A 0.3370	S_{IM} 0.3085	S_{AI} 0.2752	$K_LY_{X/L}$ 0.2659	μ_{maxA} 0.2530	t_I 0.2357	S_{AE} 0.2220
13	t_A 0.5177	S_{AE} 0.4684	r_A 0.3547	t_I 0.3392	μ_{maxM} 0.3185	X_{max} 0.2720	S_{IM} 0.2032		
14	μ_{maxI} 0.4448	$K_LY_{X/L}$ 0.4117	μ_{maxA} 0.3875	μ_{maxE} 0.3847	μ_{maxM} 0.3132	t_I 0.2447	r_A 0.2054		

a) Principal component number; b) eigenvector values.

Table 4.4: Parameter estimability of the 5-C model through sensitivity analyses on global minima. Parameters were ranked from the most to the least estimable, in which a ± 1% perturbation was applied.

	Parameter	$SS_R{}^a$	%Estimability[b]
1	μ_{maxI}	7,653.01	100.00%
2	t_A	1,353.78	17.69%
3	μ_{maxA}	317.148	4.40%
4	t_I	129.081	1.69%
5	r_A	45.7321	0.60%
6	X_{max}	13.5454	0.18%
7	r_I	7.0967	0.09%
8	S_{AE}	2.8266	0.04%
9	μ_{maxE}	1.1334	0.01%
10	μ_{maxM}	0.0251	0.0003%
11	$K_L Y_{X/L}$	1.8E-10	2.3E-12%
12	S_{IM}	3.6E-18	4.7E-20%
13	y_{AI}	4.5E-22	5.9E-24%
14	S_{AI}	5.0E-24	6.5E-26%

a) The sum of squares of the residuals matrix (R) in Yao et al. method in *Sensitivity Analysis*; b) %Estimability was defined as 100% for the parameter with the highest SS_R value. White, light gray and dark gray regions represent the estimable, less-estimable, and non-estimable parameters, respectively. Two cut-off values of 0.1% and 0.0001% estimability were defined for this classification.

4.8.2: Figures
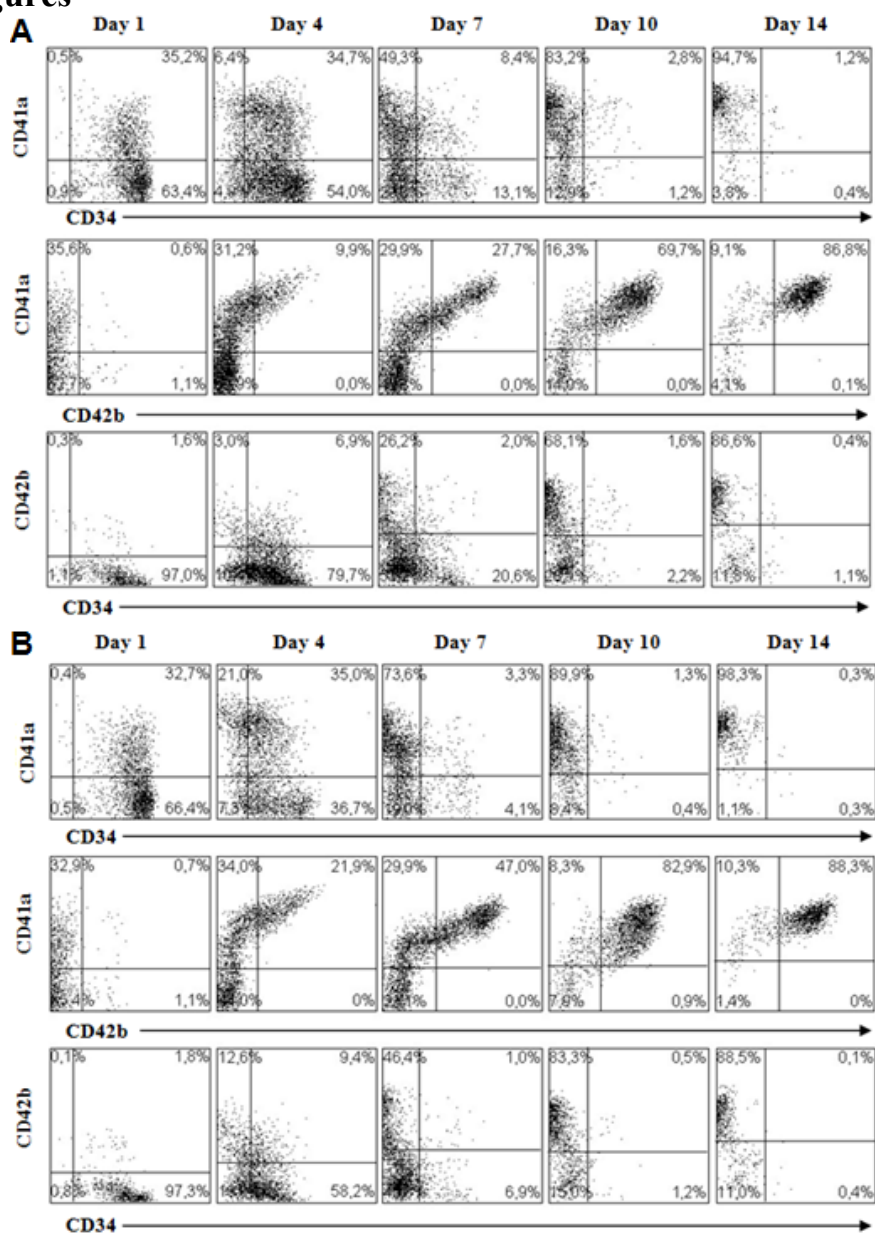
Figure 4.1: Dynamics of flow cytometry pattern changes during the 14-day culture of CB-derived MK development at 37 **(A)** and 39°C **(B)**. Viable cells were analyzed for CD34$^+$, CD41$^+$, and CD42$^+$ expression. The percentages of CD34/41, CD41/42 and CD34/42 events are marked in the respective 2-D quadrants. A representative experiment shown (r = 2).
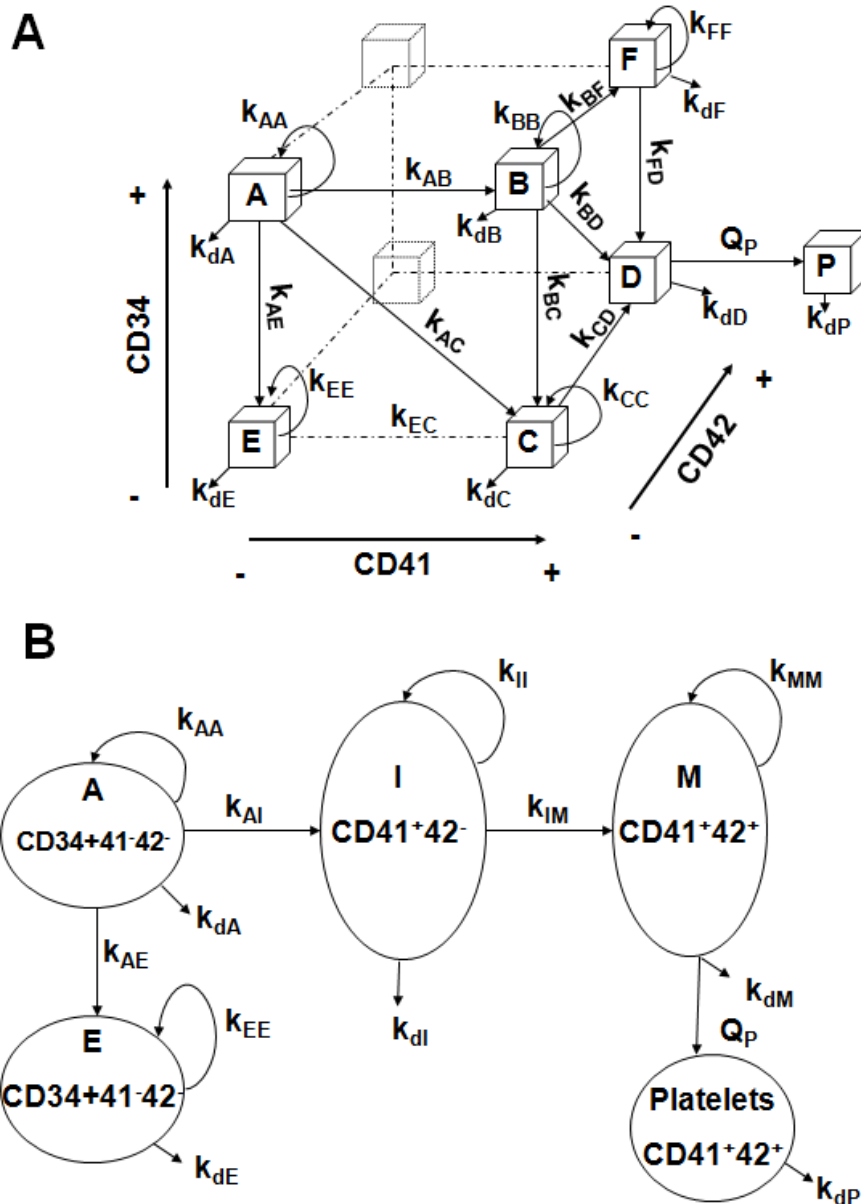
Figure 4.2: 3-D model of megakaryocyte and platelet developments based on flow cytometry data of 3 markers (CD34, CD41 and CD42). See section "*A 3D flow cytometry-based megakaryopoiesis model*" for further details. **A)** a 7-compartment (7-C) model with 35 parameters in which 8 parameters are evaluated independently, **B)** a 5-compartment (5-C) model with 20 parameters in which 6 parameters are evaluated independently. "*A*" is the starting HSC population (CD34$^+$41$^-$42$^-$). "*B*" and "*C*" represent immature MKs that are CD34$^+$41$^+$42$^-$ and CD34$^-$41$^+$42$^-$, respectively. "*D*" and "*F*" show mature MK which are CD34$^-$41$^+$42$^+$ and CD34$^+$41$^+$42$^+$, respectively. "*E*" is CD34$^-$41$^-$42$^-$ and represents a non-MK population. "*P*" represents platelets (CD41$^+$42$^+$). In panel **B**, *I=B+C* and *M=D+F* represent immature (CD41$^+$42$^-$) and mature MK (CD41$^+$42$^+$), respectively.
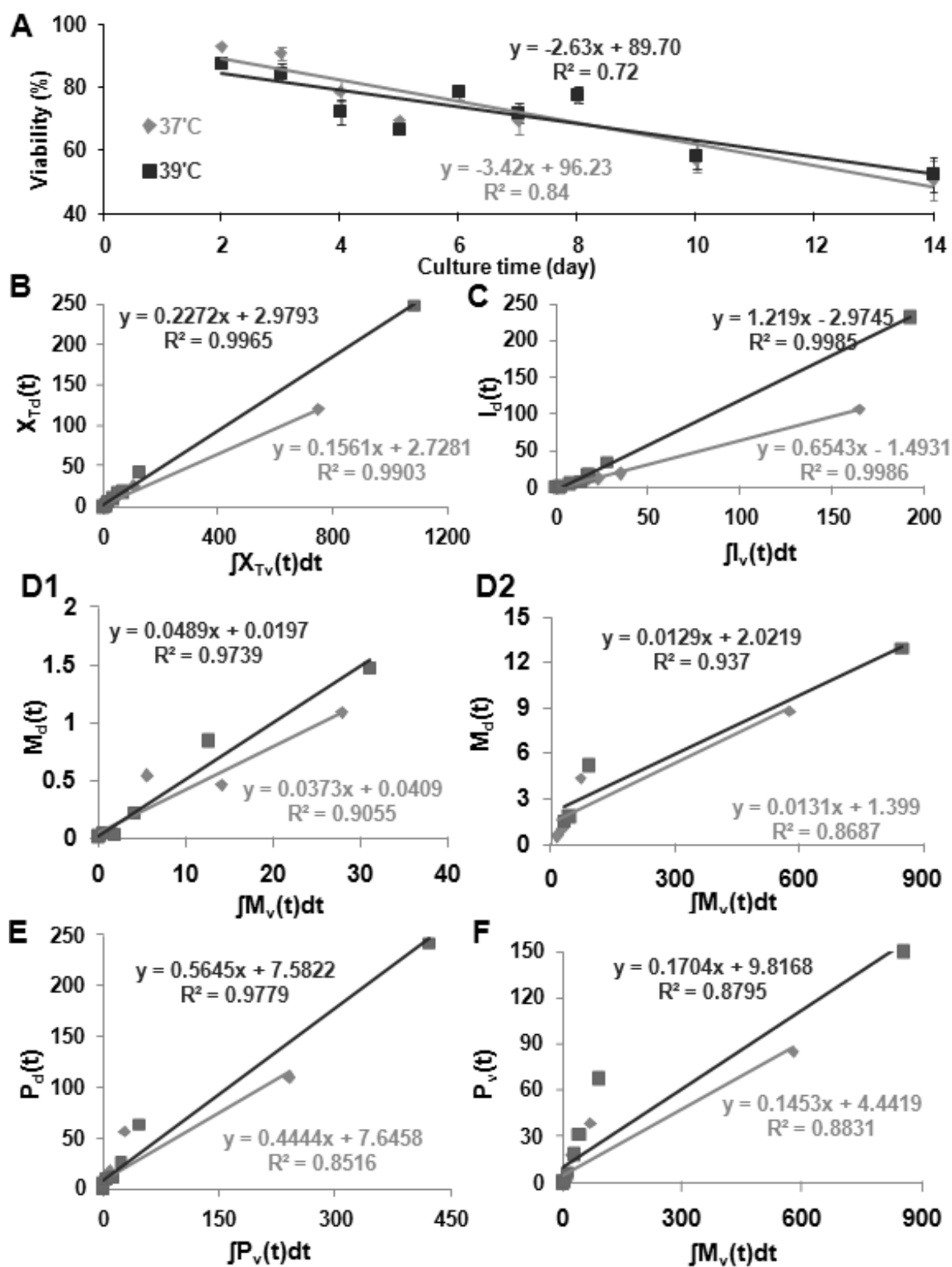
Figure 4.3: Independent estimation of some parameters for two incubation temperatures of 37 and 39°C. **A)** kinetics of cell viability. **B-E)** death rates of compartments are estimated by plotting dead cells or $N_d(t)$ against integrated number of viable cells over time (t) or

$\int\limits_{t=0}^{t} N_v(t) \cdot dt$. **F)** specific platelet production rate (Q_p) is estimated by plotting the viable

platelet number or $P_v(t)$ against integrated viable mature MK or $\int\limits_{t=0}^{t} M_v(t) \cdot dt$. Viable and

dead cell numbers over 14 culture days were used for all plots except panel **D**, in which two time frames of 0 - 7 **(D1)** and 8 - 14 **(D2)** culture days were considered. Gray diamond dots and line is 37°C data, and black square dots and line is 39°C.
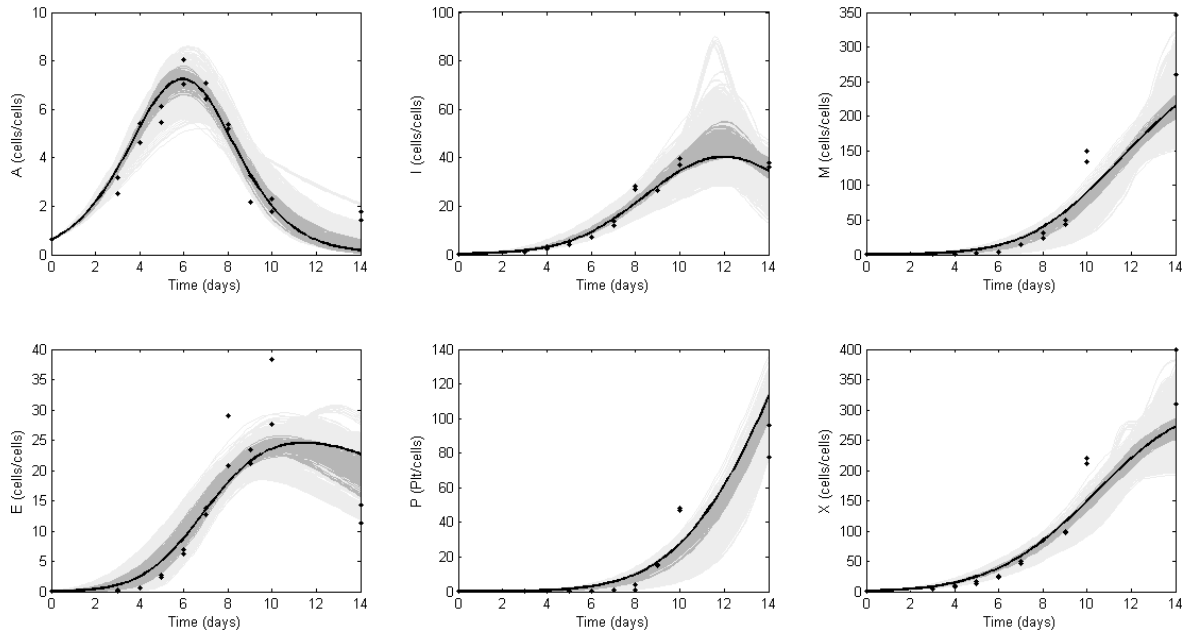
Figure 4.4: Confidence regions of fourteen-day culture responses of 5-compartment model simulated at 37°C. A 95% confidence region was defined when the value of SS/SS_{min} was below 1.77. Considering each individual response (i) should also have $SS_i/SS_{min,i}$ value below 1.77, it was found that parameter sets generating SS/SS_{min} values below 1.2 would fit reasonably well the experimental data. Dark and light gray regions include 7,500 and 1,200 parameter sets with SS/SS_{min} values below 1.77 and 1.18, respectively. Experimental and simulated data are presented with dots and solid lines, respectively.
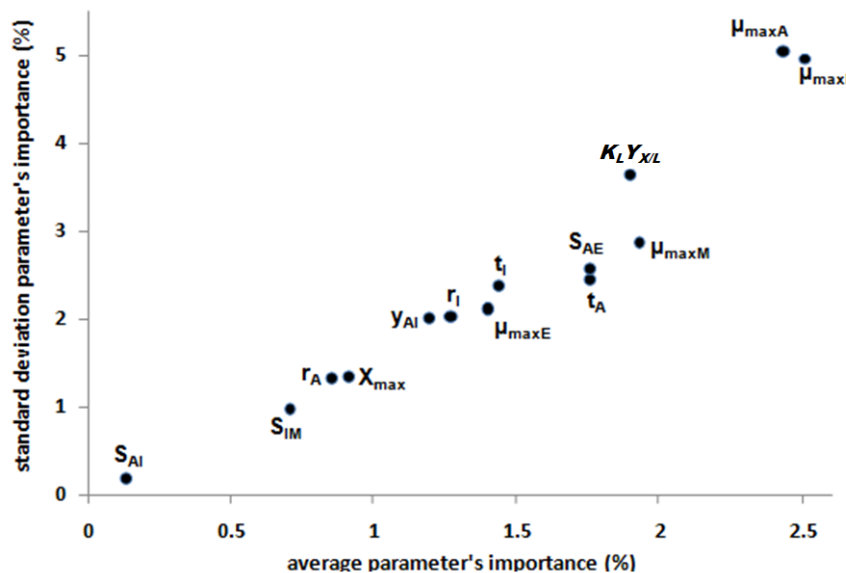
Figure 4.5: Global parameter identifiability using PCA on solution matrix (W). Individual parameter's importance (%) was defined by multiplying the importance (%) of each PC (shown in Table 4.3A) to the absolute value of coefficients (loadings) of the PC (shown in Table 4.3B). The solution matrix (W) composed of 1,200 parameter sets within empirical confidence. Mean (m') against the standard deviation (δ) of the parameter importance (%) is plotted.
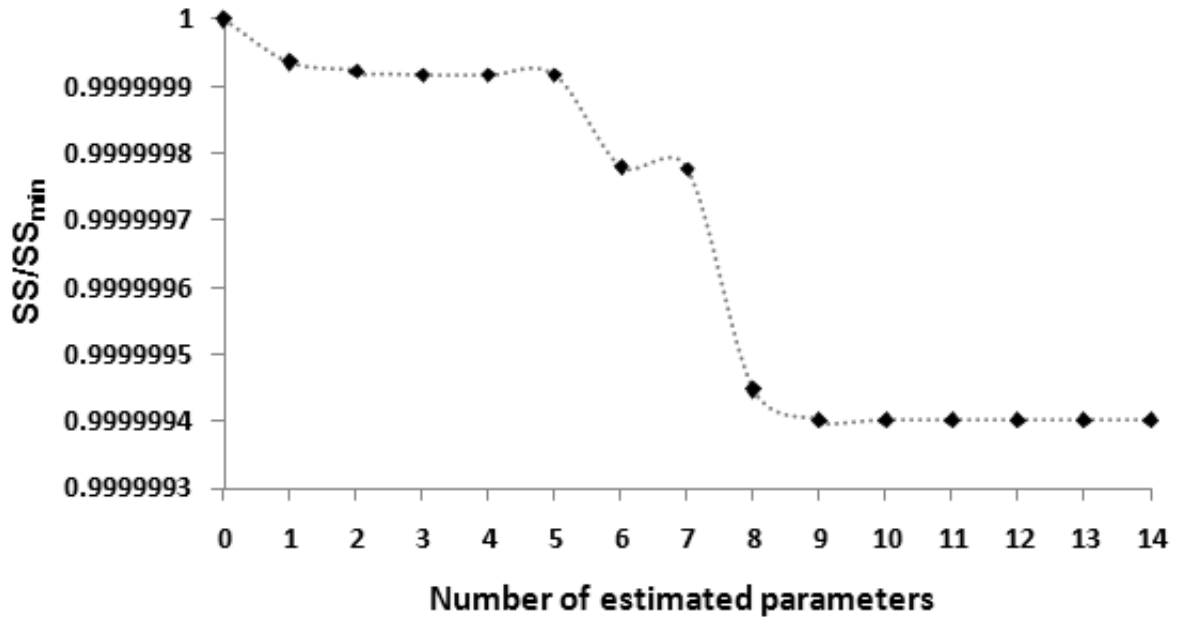
Figure 4.6: Parameter sensitivity analysis reveals the critical roles of parameters in model dimension, investigated by studying the effects of number of estimated parameters on minimizing the cost function. X-axis shows the number of estimated parameters which was estimated starting from the most estimable parameters at Table 4.4 (column 1) until all 14 parameters was combined together. Y-axis shows the best SS/SS_{min} value gained by searching at the limited number of parameters while the rest were fixed. SS_{min} was the lowest SS value (eq. 4.10) which was found when the optimum value of all 14 parameters was searched together.
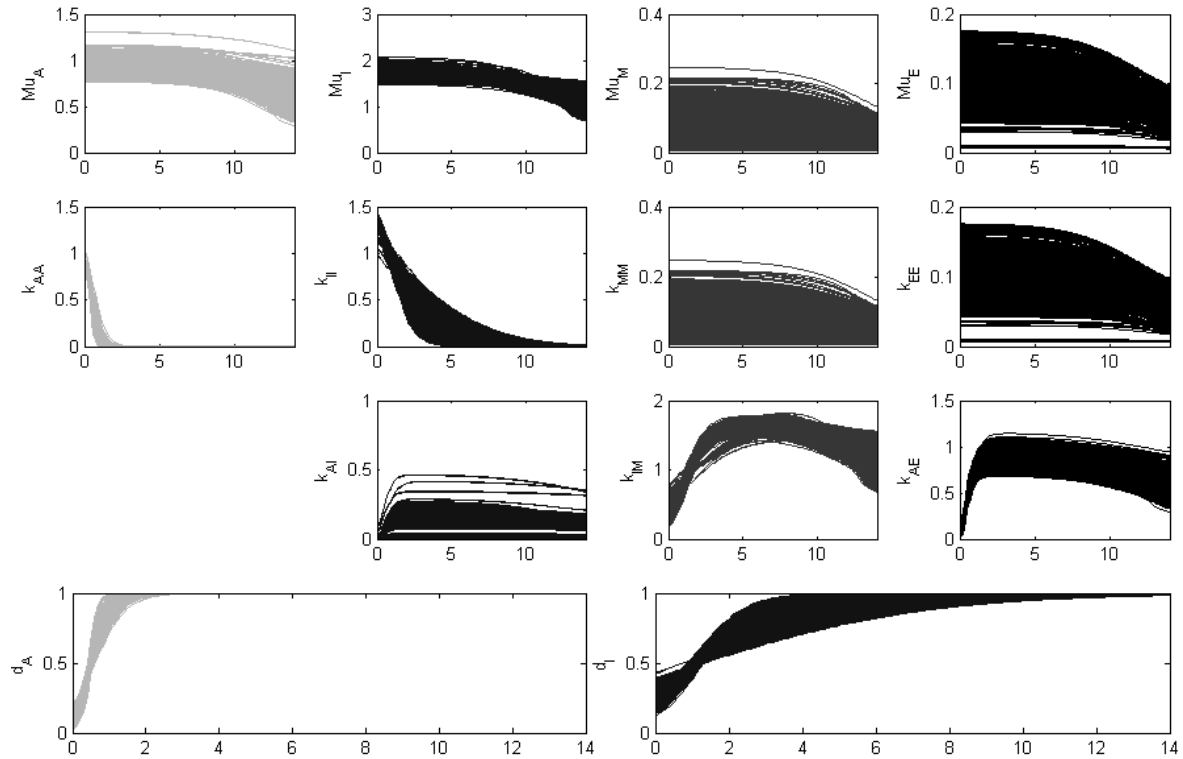
Figure 4.7: Variable dynamic parameter space of 5-C model at 37°C within empirical confidence intervals. The presented results included 1200 parameter c with *SS/SS$_{min}$* values below 1.18. Y-axis shows each parameter value and X-axis shows the culture time (days). Parameter units and constraints are described in Table 4.1.

5. Polyploid Megakaryocytes Can Complete Cytokinesis[$]

Younes Leysi-Derilou[1,2], Amélie Robert[2], Carl Duchesne[1], Alain Garnier[1], Lucie Boyer[2], and Nicolas Pineault[2*]

[1]Department of Chemical Engineering, Laval University, Québec, QC, Canada G1V 0A6
[2]R&D Department, Héma-Québec, Québec, QC, Canada G1V 5C3

*Correspondence and Reprint Requests: Dr. Nicolas Pineault
Héma-Québec, Research and Development Department, Laval University, Québec, QC
Canada G1V 5C3; Telephones: (418) 780-4362 x 3253; Fax: (418) 780-2091
E-Mails: nicolas.pineault@hema-quebec.qc.ca

5.1. Abstract/ Résumé

Megakaryocytes (MK) undergo polyploidization through endomitosis, a mitotic process that ends prematurely due to aborted cytokinesis. To better understand this and other events associated with MK differentiation, we performed long-term and large-field live cell imaging of human MKs derived in cord blood (CB)- and bone marrow (BM)-CD34$^+$ cell cultures. Polyploid level of imaged cells was evaluated using three complementary approaches; cell history, cell size and ploidy correlation and nuclei staining. This system and strategy enabled the direct observation of the development of a large number of MKs (n = 4,865) and to quantify their fates. The most significant finding of this study is that a considerable proportion of polyploid MKs could complete cytokinesis. This unexpected process gave rise to polyploid daughter cell(s) with normal fates and contributed significantly to the expansion of polyploid MKs. Further analyses revealed that the proliferation rate amongst polyploid MKs was inversely correlated to their ploidy level, and that this phenomenon was much more frequent in CB- than BM-derived MKs. Accordingly, endomitosis was identified as the dominant fate of polyploid BM-MKs, while this was less accentuated for polyploid CB-MKs. These findings explain partially why CB-derived MKs remain in lower ploidy class. In conclusion, this study demonstrates that the development of polyploid MK results from the failure and/or success of cytokinesis and brings a new paradigm to the field of megakaryopoiesis.

Les mégacaryocytes (MK) deviennent polyploïdes par l'entremise de l'endomitose, un processus mitotique qui se termine prématurément en raison de l'interruption de la cytocinèse. Pour mieux comprendre ce processus et d'autres événements liés à la différenciation des MK, nous avons imagé sur de longues périodes de temps le développement de MKs dérivées de cellules CD34$^+$ de sang de cordon (CB) et de moelle osseuse (BM). Le niveau de polyploïdie des cellules imagées a été évalué en utilisant trois approches complémentaires: l'historique des cellules, la corrélation entre la taille des cellules et la ploïdie et la coloration des noyaux. Ce système et cette stratégie ont permis d'observer directement la génèse d'un grand nombre de MK (n = 4,865) et de suivre leur

destin. Le résultat le plus significatif de cette étude est qu'une proportion considérable de MKs polyploïdes pourrait compléter la cytocinèse. Ce processus inattendu a donné lieu à des cellules polyploïdes filles dont le sort est normal et a contribué de manière significative à l'expansion des MK polyploïdes. D'autres analyses ont révélé que le taux de prolifération parmi les MK polyploïdes est inversement corrélé à leur niveau de ploïdie, et que ce phénomène était beaucoup plus fréquent chez les MKs de dérivés de CB. En conséquence, l'endomitose a été identifiée comme le sort dominant MKs-BM polyploïdes, alors que cela était moins accentué pour ceux issus de CB. Ces résultats expliquent en partie pourquoi les MKs-CB atteignent un niveau plus faible de ploidie que les MK-BM. En conclusion, cette étude démontre que le développement des MK polyploïdes résulte de l'échec et/ou du succès de la cytocinèse, et pose donc un nouveau paradigme dans le domaine de la mégakaryopoïèse.

5.2. Introduction

Megakaryopoiesis is initiated in the marrow with the proliferation of hematopoietic stem cells (HSC) followed by their gradual commitment and differentiation along the MK lineage. Immature MKs then undergo a series of maturation processes, namely endomitosis and cytoplasmic maturation which ends with the formation of proplatelets and the release of platelets into blood circulation[1,2].

Ex vivo culture of CD34^{+} cells in thrombopoietin (TPO) containing medium is a well established model to study megakaryopoiesis for different CD34^{+} cell sources[3-5]. For instance, it has recently been shown that MK proplatelet formation, frequently observed *in vitro*, was indeed a genuine *in vivo* phenomenon[2]. Another important *ex vivo* finding corroborated by *in vivo* observations[6,7] is that cord blood-derived MKs (CB-MK) differ in several ways from adult bone marrow-derived MKs (BM-MK); the former being smaller in size and reaching lower ploidy levels[6] but expanding much more[5]. Indeed, the vast majority of CB-MKs remain diploid, while more than half of the BM-MKs become polyploids[3,5,8,9]. The mechanisms responsible for such differences remain unclear at this point.

Polyploidization is an important step in the maturation process of MKs. First thought to be entirely distinct from mitosis, endomitosis, the process by which MKs become polyploid, follow for most part the same sequence of events. Hence, endomitotic MKs undergo normal cell cycle progression up to the M phase, then proceed through prophase, prometaphase, metaphase, anaphase and telophase but fail to complete cell division due to a late interruption of cytokinesis at the cleavage furrow ingression stage[10]. Using time-lapse confocal microscopy, Lordier et al. recently confirmed that cleavage furrow ingression occurs in all of the sightings of diploid (2N) human MKs undergoing endomitosis[11]. They also provided strong evidences that furrow regression and cytokinesis failure was the results of a lack of an active actomyosin ring at the cleavage furrow site in the endomitotic MKs due to a defect in non muscle myosin IIA protein accumulation and reduced activity of the Rho-Rock pathway[11]. Interestingly, 3D immunofluorescence analyses of over 900 fixed CD41^{+} tetraploid (4N) MKs also revealed that a large proportion of tetraploid MKs (20 - 45%) successfully completed nuclear division and displayed two separated nuclei[11]. Given

that cellular division is interrupted at such a late stage of mitosis, it could be anticipated that in some instances polyploid MKs could complete cytokinesis and divide, though this has not been reported. Division of polyploid cells is not in itself a novel concept since it has been observed to a different extent in the context of hepatocyte[12] and tumour developments[7,13]. On the other hand, Schwertz et al. just recently reported that blood platelets can also undergo division and produce functional platelet progeny, through a process that resembles extension of proplatelet evolution[14].

To further investigate the processes of MK differentiation and maturation, a long-term and large-field *in vitro* live cell imaging system was developed capable of maintaining and observing cell cultures over periods of up to 5 days. Hundreds of CB- or BM-enriched CD34^{+} cells were tracked as they proliferated and differentiated into mature MKs. Overall, the fates of around 5,000 individual cells were quantified based on recorded cellular morphological changes. This investigation revealed for the first time that polyploid MKs can still complete cell division, and that this process is more prominent for CB-MKs.

5.3. Results

Live Cell Imaging of MK Cultures

Long-term and large-field time lapse video microscopy was first performed on CB-CD34^{+}-enriched cells (≥ 90% purity) induced to undergo specific megakaryocytic differentiation with the addition of TPO (100 ng/ml). Bright field (20X) images of the cultures were captured every 2.0 - 3.0 minutes during two time windows: i) from day 0 to day 5 to study megakaryocytic differentiation and the onset of polyploidization, or ii) from day 5 to day 10 to study MK maturation. Methylcellulose was added to the cultures at low concentration (3.75 g/L) to slow down cell movements. This made possible the tracking of cells up to 10 generations. Preliminary control experiments revealed no significant differences in cell expansion, viability and in the CD41 and CD42 expression profiles between MK cultures maintained in a regular incubator or in the microscope incubating chamber submitted or not to light exposition and methylcellulose (Figure 5.S1). MK differentiation and MK purity (%CD41^{+} cells) were also confirmed for all cultures by cytometry at days 5 (44 ± 3%), 10 (87 ± 5%) and 14 (95± 3%). Evidently, not all diploid cells tracked early in culture (day 0 -

5) belonged to the MK lineage. To circumvent this limitation and to favour the tracking of cells undergoing MKs differentiation, we focused our attention to diploid cells that produced polyploid progeny since this is a unique hallmark of MK. This approach allowed us to investigate and measure the fates of a very large number of cells (n = 5,000) undergoing normal MK differentiation and maturation events, such as endomitosis and proplatelet formation.

Based on observations cross-validated with the relevant literature[10,11,15-17], four main types of cellular events were defined. These were: i) *mitosis* (Figure 5.S2A), indicated by complete division of a cell to two individual daughter cells; ii) *endomitosis*, characterized by the failure of cytokinesis leading to the formation of a polyploid cell, (Figure 5.S2B); iii) *proplatelet formation*, characterized by a sequence of profound morphological changes culminating into the projection of a series of long arm-like branched filaments (Figure 5.S2C); and iv) *cell death*, recognized by a series of events such as absence of cell movement, cell shrinkage or blebbing, and loss of cell refractive index (Figure 5.S2D). Cell death resulting from either necrosis or apoptosis was grouped together and reported as one group.

Ploidy Levels of Cells in Culture Were Determined by Three Complementary Methods

Ploidy level analysis of MK cultures is typically done by flow cytometry[18]. However, this technique has limitations since it cannot be used in the context of live cell imaging. One of the strength of live cell imaging is that it provides an accurate measurement of individual cell size from the initial minutes of birth up to the next cell cycle, while flow cytometry provides an average size for an asynchronous cell population. Within the limiting framework of live cell imaging with genetically unmodified human cells, endomitosis and ploidy levels were assessed using three complementary methods to ensure correct ploidy level determination. The first was based on the direct visualization of the dynamic morphological changes that occur during mitosis or endomitosis[10,11,16]. In this context, the ploidy level was determined based on the complete analysis of the history of the cell and its ancestors. A case in point is presented in Figure 5.1A. The second approach was based on Hoechst DNA staining of the undisturbed cells at the end of each culture, which provided a

direct assessment of the nuclear lobes[19,20]. Hoechst staining analyses of video clips as opposed to single images were used to complement the ploidy assessment based on cell history and/or cell size (Figure 5.1B-C). For instance, Figure 5.1B and supplemental video 5.1B show the ploidy classes of the tracked cells presented in Figure 5.1A, with one, two and four lobes. The last approach used cell size to indirectly infer ploidy level. Global correlation between ploidy level and average cell size was previously established[18,19,21,22]. A strong linear relationship between cell size and ploidy level was demonstrated when cell size is accurately measured ($R^2 = 0.97$)[22]. Herein, we also observed a robust linear correlation ($R^2 = 0.9969$) between cell size (volume) immediately following mitosis or endomitosis and ploidy level evaluated by method 1 or 2 (Figure 5.1D, see Supplementary Text B for further details). Taken together, these methods provided coherent and complementary assessment of the ploidy level of the cells that were tracked and therefore inter-validated themselves (n = 996).

Polyploid MK Undergoing Cleavage Furrow Ingression Can Complete Cytokinesis

In line with other studies[3,5,8,9], the majority of the tracked MKs derived from CB-CD34$^+$ cells remained diploids (mean of 71%, r = 5) or in low polyploid classes such as 4N (16%), 8N (7%) and 16N (3%). Direct visualisation of the dynamic morphological changes of an extremely large number of CB-MKs undergoing endomitosis (n = 918) confirmed that all these cells showed a clear sign of cleavage furrow ingression (Figure 5.S2B, frames 3 - 4)[10,11]. The duration of this failed cytokinesis process was 33.5 ± 28.7 minutes (n = 50) and 28.1 ± 21.6 minutes (n = 30) for 2N to 4N and 4N to 8N, respectively. In practice, endomitosis was found to be a very dynamic process; for example, tetraploid cells (Figure 5.2A, frames 2 - 4) initiating cytokinesis frequently entered a transient state in which four joint pseudo daughter cells appeared. These pseudo daughter cells then regressed partially and transiently to either one 4N and two 2Ns, or two pairs of 4N or one 6N and one 2N pseudo daughter cells (Figure 5.2). As recently reported[11], all pseudo daughter cells then regressed to form a single 8N cell when endomitosis was successfully completed (Figure 5.2A and supplemental video 5.2A).

It is generally accepted that polyploid MK cease to undergo mitosis. Contrary to such expectation, CB-polyploid MKs (4N - 16N) were frequently observed to fully complete

mitosis following completion of cytokinesis and cell abscission, and depending on the pattern of cleavage furrow regression and cell abscission, division of polyploid CB-MKs occurred symmetrically and asymmetrically. The most common occurrence of symmetric (Figure 5.2B and supplemental video 5.2B) and asymmetric (Figure 5.2C and supplemental video 5.2C) divisions were observed with tetraploids. In all cases, events prior to cell abscission were indistinguishable from those of other tetraploids undergoing endomitosis (Figure 5.2A); during cytokinesis, these cells formed four pseudo daughter cells that fused back together asynchronously (frames 5 - 8, Figure 5.2B-C). However, these pseudo daughter cells failed to regressed into a single 8N cell since the cell successfully completed cytokinesis and cell abscission (frame 9, Figure 5.2B-C); giving rise either to two tetraploid cells of similar size significantly smaller than the parent cell (~79% of the diameter of the parent cell, Figure 5.2B, frame 9 vs. frame 3, Table 5.S1), or two daughter cells of different sizes (~63% and ~91% diameters of the parent cell, Figure 5.2C frames 9 vs. frame 3, Table 5.S1). Based on cell size and ploidy correlation, the smaller cell was deemed diploid and the bigger one hexaploid (6N) (frames 9 - 10, Figure 5.2C). Hoechst staining of a representative hexaploid cells harbouring 3 nuclear lobes is shown in Figure 5.1C. Finally, division of tetraploids to more than two daughter cells also occurred following similar sequence of events (Figure 5.6B, frames 3 - 8, supplemental video 5.6B). Importantly, tracking of the daughter cells originating from polyploid MKs confirmed that these remained permanently separated and independent from each other as they sometime showed different fates (see below). Mitosis of polyploid MKs was also observed between day 10 - 14 of culture, though proplatelet formation was the dominant fate in this culture period (data not shown).

To confirm that this new phenomenon was not an artefact of the long term imaging conditions, confocal microscopy was used to address whether tri-lobular MKs could be observed as an indicator of tetraploid cell division in regular TPO cultures. CB-CD34+ cells were cultured for 10 days using the same medium without methylcellulose, then CD41+ cells with ploidy levels equal or greater than 4N were sorted by cytometry. Observation of fixed cells stained with phalloidin to delineate cell cortex and Hoechst confirmed the presence of 4N, 8N and 6N cells in cultures (Figure 5.3A). Z-series stack of confocal slices clearly demonstrates the presence of three well defined nuclear lobes of similar size

contained into the same cell (tri-lobular MK, supplemental video 5.3A-B). Cells were also stained with an anti-gamma tubulin to visualize their centrioles to complement the ploidy level analysis of the stained polyploid cells (Figure 5.3B). Non cycling 2N, 4N and 8N cells have 1, 2 and 4 centrosomes respectively, with each centrosome composed of 2 centrioles arranged perpendicularly[23]. While it was not possible to accurately count the number of centriole per cells, the overall size of the centrosome in the 6N cells (see insets in Figure 5.3B, supplemental video 5.3B) indicated the presence of multiple centrosomes within these cells, which appear to be in greater numbers than those observed in tetraploids but lower than that of octaploids.

Cell Division of Polyploid CB-Derived MK Occurs Frequently in Culture

To better characterize the new phenomenon of polyploid cell division, the fates of diploid, tetraploid, octaploid (8N) MKs and that of their progenies were quantified (Table 5.1). Overall, a total of 2,450 CB-MKs (1,772 x 2N, 340 x 4N, 33 x 6N, 208 x 8N, 10 x 12N and 87 x 16N) were tracked and included in our analyses. As expected based on the predominance of diploid cells in CB-MK cultures, mitosis was the dominant fate of diploids MKs (mean of 75.1%). The readers should however note that based on the low MK purity in the first 5 days of culture (commitment phase), the frequency of diploid MK undergoing endomitosis and proplatelet formation presented in Table 5.1 may be underestimated. Consistent with our previous observation, an important proportion of the 340 tracked tetraploids completed cytokinesis (27.35%), which resulted in the formation of either two tetraploids (18.82%), one diploid and one hexaploid cell (9.71%) or one tetraploid and two diploids (2.35%). Division of tetraploids to four diploids was not observed. Similarly, fate analyses of a total of 208 octaploids were followed: 8.17% were found to complete mitosis (Table 5.1). This included the divisions into two 8Ns (3.85%), one 4N and one 12N (4.81%), or two 4Ns and one 8N (1.44%, Figure 5.2D and supplemental video 5.2D). Division of 16N CB-MK was observed only once out of 87 tracked cells from 5 independent experiments (data not shown). In contrast to mitosis, the rate of endomitosis generally increased with the ploidy level. Hence, endomitosis occurred at a moderate frequency (12.5%) in diploid CB-MKs but its frequency increased by up to 4-fold after one or two rounds of endomitosis (Table 5.1).

Adult BM-Derived Polyploid MKs Can Also Complete Cytokinesis in Culture

Given the well established low propensity of CB-MK to become highly polyploid[3,9], we investigated whether division of polyploid MKs was exclusive to CB-MKs by performing similar experiments with adult human BM-CD34^{+} cells. In contrast to CB-MKs, the majority of the 1,670 tracked BM-MKs became polyploids and often completed several round of endomitosis (567 x 2N, 407 x 4N, 6 x 6N, 240 x 8N, 188 x 16N, 147 x 32N, and 115 x 64N). Despite this, BM-derived tetraploid MKs were also found to undergo mitosis (Figure 5.S3 and supplemental videos 5.S3A-B) at a significant level (6.63%, Table 5.1), producing either two 4Ns (5.16%) or one 2N and one 6N (1.47%), while division to more than two cells was not observed. Octaploid BM-MKs were also found capable of completing cytokinesis (1.25%), dividing into two octaploids, while mitosis was never observed for BM-MKs of greater ploidy despite following 188 x 16N and 147 x 32N cells. The frequency of endomitosis in diploid BM-MKs was found slightly higher than that of CB-cells, though this difference was not statistically significant ($p < 0.14$). This difference would have been certainly significant if we had measured the fate of all the diploid cells early in the CB-cultures but this was not the objective of this work. However, in contrast to the former, endomitosis clearly became the dominant fate in tetra- ($p < 0.0001$) and octaploid BM-MKs ($p < 0.0001$).

The Mitotic Potential of Polyploid MKs Varies as a Function of the Ploidy Level and Ontogeny

To better compare MK decision to complete or not cell division as a function of the stem cell source and ploidy level, a mitotic completion index was defined as the ratio of cells that completed cytokinesis to the total number of cells that entered mitosis. As shown in Figure 5.4, the mitotic potential index was found to vary as a function of ploidy level and ontogeny. This analysis showed that 4N and 8N MKs had roughly a 5-fold ($p < 0.001$) and 12-fold ($p < 0.0001$) greater chance to complete cell division if these were derived from CB- instead of BM-CD34^{+} cells, respectively. In addition, the mitotic potential index of MKs decreased as a function of their ploidy level independently of the cell source (Figure 5.4); the index for tetraploids and octaploids were found 2.2- and 4.4-, and 10.1- and 51.1-fold lower than that of diploids for CB- and BM-cells, respectively ($p < 0.0001$). Hence,

these results show that the frequency of cell division amongst polyploid MKs is inversely correlated to their ploidy level, and that this phenomenon is much more frequent in CB-MKs.

Polyploid MKs Generated through Division of Polyploid MKs Have Normal Fates and Cell Size

Next, we investigated whether polyploid MKs formed following mitosis of polyploid MKs had a development program comparable to those produced through endomitosis. For this, the fates of those two groups were compared. The sources and subsequent fates of the 107-tracked CB-tetraploids produced by mitosis are shown in Figure 5.5A. These cells were generally found to have behaviours indistinguishable to those formed through endomitosis; they could undergo endomitosis (Figure 5.6A and supplemental video 5.6A) up to 16N, complete mitosis (Figure 5.6B and supplemental video 5.6B) up to four consecutive times, form proplatelet (Figure 5.6C and supplemental video 5.6C) or undergo cell death (data not shown). In addition, 41 of these tetraploids had unknown fate, since they initiated but did not complete cell cycle before the end of the imaging period. The frequencies of these events were similar to those shown in Table 5.1, and random comparison of the CB-tetraploid cells originating from mitosis to that of endomitosis showed no significant difference in cell size ($p < 0.001$, $n = 20$).

The fates of 35 CB-diploids originating from asymmetrical divisions of polyploid MKs were also investigated. However, these fates were found quite different from other diploids (Figure 5.5B). Essentially, the majority failed to thrive as 26 died, two succeeded to divide, while 7 remained alive (4 - 30 hours) but had unknown fate. In contrast, the majority of hexaploid cells formed following the same cell division survived and underwent either mitosis ($n = 2$, Figure 5.S4 and supplemental video 5.S4) or endomitosis ($n = 20$). Consistent with the results obtained with CB-MKs, polyploid BM-MKs formed through mitosis showed normal development, predominantly undergoing endomitosis if they neither formed proplatelets (Figure 5.6C) nor died (data not shown). Fate analyses of the 12N cells indicated that these could undergo endomitosis ($n = 5$) or cell division ($n = 2$), while others died ($n = 7$) or had unknown fate ($n = 7$). Thus, these observations suggest that polyploid

MK mitosis did not result in any abnormal fates for the newly derived polyploid daughter cells, while the resulting diploid cells were for the most part non viable.

Division of Polyploid MKs Represents a Second Significant Source of Polyploid Cells in MK Culture

We then investigated whether the proliferation of polyploid MKs had a significant impact on the origin of polyploid cells in MK cultures. The contribution of various cell sources on the tetraploid cell population was first studied. A total of four sources were distinguished: 1) endomitosis of 2N cells, 2) symmetric division of 4N cells, 3) asymmetric divisions of 8N cells, and 4) division of other classes of polyploid cells such as 6N, 12N, and 16N. The first represents the conventional source, while the others are dependent on the division of pre-established polyploid cells. This analysis showed that endomitosis produced 67% of CB- and 87% of BM-tetraploid MKs (Figure 5.S5), while polyploid cell division accounted for 33% and 13% of the 4Ns, and 3% and 0% of the >4N CB- and BM-MKs, respectively. Hence, these results demonstrate that division of polyploid MKs represents a new and significant source of polyploid MKs, though endomitosis remains the principal source.

5.4. Discussion

In this work, long-term and large-field live cell imaging was used to study megakaryopoiesis, from the initial event of lineage commitment throughout the multi-steps of MK maturation. Careful estimation of ploidy level of tracked cells was achieved by combining three complementary approaches; cell history, cell size-ploidy correlation and Hoechst nuclei staining. This provided the opportunity to record the formation and for the first time the fates of a large number of polyploid MKs (n = 2,069).

The main discovery of this work is that a significant proportion of polyploid MKs can complete cytokinesis and undergo cell division. This phenomenon was unexpected given the general belief that MKs undergoing polyploidization cease to divide. However, our results clearly demonstrate that polyploid MKs can complete cytokinesis and cell abscission in culture (n = 156). While this has not yet been corroborated *in vivo*, several lines of evidence suggest that this is not a culture artefact due to cell stress owing to light exposure

or to the low concentration of methylcellulose since the 5-day long imaging protocol had little impact on the viability, differentiation and growth kinetics of MKs. In support of this, endomitosis and proplatelet formation occurred normally, and mitosis of polyploid MKs was also observed in methylcellulose-free cultures. In addition, cell division of polyploid MKs was not found dependent on the length of time in culture or on long term imaging (i.e. cumulative light exposition), as it was observed as early as 10 hours into imaging with previously non-imaged cultures or within 2 hours with gradient purified MKs (data not show).

The molecular cues responsible for cell fate decision in polyploid MKs remains unclear. However, addition of the Rock inhibitor Y27632 completely blocked mitosis of polyploid and diploid cells for both BM- (n = 309) and CB- (n = 436) MKs (unpublished data). The Rho/Rock pathway is responsible among other things for the activation of the actomyosin contractile ring. This result demonstrates that mitosis of polyploid MKs is as for diploids dependent on the Rho/Rock pathway.

Given that CB-MK do not become as highly polyploid as their BM-counterpart[3,9], we investigated whether this property was unique to the neonate-derived MKs that could perhaps explain this profound difference. This was however quickly refuted, though polyploid MK division occurred at a much lower rate in BM-MKs. Consistent with this, CB- and BM-MKs also diverged significantly in their capacity to undergo endomitosis, since the latter was clearly the dominant fate (> 75%) for polyploid BM-MKs while this was less accentuated for CB-MKs (~45%). These findings together with the increased mitotic activity of CB-cells[5,8] partially explain why CB-derived MKs remain either diploid or in low polyploid class[6,9,24].

MK polyploidy typically occurs in a doubling series of 4N, 8N, 16N and so forth. However, MKs with ploidy level estimated to be of 6N and 12N were observed in culture following the asymmetric division of tetraploid and octaploid MKs, respectively. Whether 6N and 12N MKs really exist *in vivo* or whether these cells arose due to culture artefact remains unanswered at this time. This question is certainly difficult to address given the low frequency of MKs in the marrow and to the low apparent frequency of these cells in culture (< 0.8%). However, the existence of tri-lobular MKs was confirmed by confocal

microscopy in regular TPO cultures, which corroborates our live cell imaging observations and argues against imaging artefacts. Furthermore, the existence of 6N cells may explain the small intermediate peak observed sometimes between 4N and 8N cells in cytometry DNA histogram analyses of CB- and BM-MK cultures apparent in several reports[8,11,22,25]. Polyploid cells with non-doubling series have also been reported in liver sections, though these cells undergo polyploidization through a different process[26]. These 6N cells were found viable and appeared to have normal fates such as endomitosis or mitosis in which these cells returned to the regular doubling ploidy series (2N, 4N …). On the other hand, the majority of the sister diploid cells were found non viable suggesting perhaps that these were aneuploids (< 2N), since such cells are under greater pressure to undergo apoptosis than larger polyploid cells[27]. Perhaps, aneuploidy in these cells results from the asymmetrical segregation of chromosomes, which has previously been reported to occur in some polyploid MKs due to the formation of multipolar complex spindle[28]. The latter, could also be responsible for the decrease in the frequency of cell division in MKs of increasing ploidy. Clearly, future experiments using techniques with greater resolution, such as fluorescent in situ hybridization will be required to firmly confirm the ploidy level and karyotype of these cells and to establish whether such cells exist in the marrow.

The capacity of polyploid MKs to undergo division was not constant during MK maturation as it was found to be inversely related to the degree of ploidy. This decline is consistent with the recent study of Geddis et al., who showed a significant reduction in furrow ingression in polyploid MKs[10]. Though little is known at this time on the division of polyploid MKs and its regulation, one legitimate hypothesis is that may occur in immature MKs that have not yet properly down regulated their mitotic program. In support of this, morphological examination of 4N and 8N MKs demonstrated that these cells are not yet fully mature[21]. Furthermore, division of polyploid MKs was observed much more frequently in CB-cell cultures, which contained a greater proportion of immature MKs, as judged by their reduced size and increased mitotic activity[3,5,9,29]. The molecular mechanisms responsible for these differences remain elusive but differences in the expression profile of cell cycle regulating proteins[3,8] may contribute to these divergence.

Live cell imaging has proved to be a powerful tool to study complex cellular processes such as endomitosis. Two such studies recently reported new insights into this process. Our results confirm their results that partial cleavage furrow ingression followed by regression and cytokinesis failure is an unambiguous hallmark of MK endomitosis. However, none of these two studies reported sightings of polyploid MKs completing cytokinesis. The latter could be the consequence of major differences in experimental designs; i) the previous studies used exclusively BM-MKs for which polyploid cell division occurs at reduced frequency and (ii), focused much of their efforts on the first round of endomitosis (2N to 4N) for which polyploid cell division does not apply, iii) we used long-term instead of short-term time lapse video microscopy. This enabled us to visualise the development of a much greater number of polyploid MKs (1,074 4Ns and 563 8Ns total) up to 5 days. In contrast, the other studies followed far fewer polyploid MKs (50 and ~20) over a shorter period of time (6 - 24 hours)[10,11] and finally, iv) one of these studies used exclusively murine MKs[10], thus species-related differences could also be involved. For instance, murine BM-MKs appear to have an increased propensity to undergo endomitosis in cultures since a significant proportion of murine MKs readily reaches ploidy level of 64 and 128N[30,31], while this is rarely observed with human MKs[3,9,32].

5.5. Summary

A large body of evidences presented in this study demonstrates that polyploid MKs can undergo cell division following successful completion of cytokinesis and give rise to polyploid daughter cell(s) with normal fates. Consequently, this study brings a new paradigm to the field of megakaryopoiesis as it challenges the concept that polyploid MKs are derived solely from cells undergoing endomitosis. Our results support the notion that endomitosis is the exclusive mechanism by which polyploidization is initiated and by which MKs increase their ploidy levels, while division of polyploid MKs could perhaps represent a mechanism responsible for the propagation of low ploidy MKs. Whether this occurs *in vivo* remains to be addressed in future studies, although many processes observed *in vitro* were subsequently confirmed *in vivo*[2,6,8,17].

Acknowledgments

5.6. Materials and Methods

CD34-Enriched CB- and BM-Cell Cultures

Human umbilical CB-cells were collected with informed consent and cryopreserved as described previously[33]. CD34^{+} cells were enriched by negative selection to a purity $\geq$ 90% (EasySep[(R)], human progenitor cell enrichment kit, StemCell Technologies, Vancouver, BC, Canada). Cryopreserved human BM-CD34^{+} cells (purity $\geq$ 90%) were obtained from Lonza Walker (Chicago, IL, USA). CD34^{+} cells were cultured in a serum free medium[33] supplemented with 100 ng/ml TPO cytokine (Peprotech, Rocky Hill, NJ). Cells were diluted with fresh medium at day 5. Cell cultures for imaging were supplemented with 3.75 g/L methylcellulose (Sigma) and 1% penicillin-streptomycin solution (Invitrogen, Carlsbad, CA, USA). All cultures were maintained in a humidified incubator at 37°C with 10% CO_2. Viable nucleated cells in control cultures were counted with a hematocytometer (0.4 % trypan blue, Invitrogen).

Flow Cytometry Analysis

Cells were analysed for the expression of CD41a/GPIIb (anti-CD41a-allophycocyanine) and CD42b/GPIbα (anti-CD42b (GPIbα, BD)-fluoresceine isothiocyanate) by flow cytometry (FACS-Calibur, Becton Dickinson, San Jose, CA) as described in[33,34].

Time-Lapse Video Microscopy

Live cell imaging was performed using a fully automated inverted microscope (IX81, Olympus, Canada) that was controlled using the QED software (Media Cybernetics). To improve the consistency of microscopic field positioning for long-term experiments, stage

movements were controlled using servo- rather than stepper-motors. Bright field, phase-contrast and fluorescent images were acquired by a monochrome charge-coupled device (CCD) camera (Retiga 200R, QImaging). A Lambda LS 175-W Xenon lamp (Sutter Instruments, USA) was used as the fluorescence light source. A green filter was installed on the halogen light source for bright field imaging (Osram HLX 64625, 100W, 12V, GY 6,35). Automatic shutters (Olympus Japan, IX2-SHA) were used on both light sources to minimize detrimental effects of long exposure time. More details are available in the supplementary material (Text A).

Sorting and Staining of Polyploid MKs for Confocal Microscopy

Hoechst 33342 (10μg/mL; Molecular Probes, Invitrogen) was added to the culture at day 10 for 2h at 37°C. Cells were then stained with anti-CD41 APC-conjugated MAb (Pharmingen) for 30 min at 4°C. Cell sorting procedure; nucleated cells were gated on a SSC-FCS dot-plot profile, then CD41$^+$ cells were gated on a histogram profile window, then CD41$^+$ non-doublet cells were gated in a Hoechst-Width vs Hoechst-Area dot-plot window, then cells with DNA contents equal or greater than 4N (Hoechst-A histogram) were sorted using a Epics Elite ESP FACS (Beckman-Coulter, Mississauga, ON, Canada). Isolated cells were plated on poly-L-lysine (10μg/ml) coated slides and then fixed in PTEMF (20mM Pipes pH 6.8, 0.2% Triton X-100, 10mM EGTA, 1mM MgCl$_2$, 3.7% formaldehyde) for 10min at room temperature. Rabbit anti-γ tubulin (1:3000, Abcam) and phalloidin ALEXA 488 (1:50, Lonza) were used to stain centrosomes and actin-F. Stacks of confocal slices were collected with a FV1000 point scanning confocal microscope (Olympus) using FluoView software version 2.0.3 with a 60X 1.42 NA oil objective.

DNA Staining

Hoechst 33342 (0.25 μg/ml) was added directly at the last day of culture. Fluorescent images, taken every 6-8 minutes, were captured using a wide UV filter cube (Olympus, Japan) with the following specifications: 330-385 nm excitation filter, 420 nm emission filter, and 400 nm dichromatic filter. The fluorescence and bright field images were captured with a gain level of 1, without binning and averaging and with exposure times of 300 and 35 ms, respectively.

Statistical Analysis

Comparisons were analyzed using the Student t-test. Results were regarded as significant when p-values were below 0.05.

Supplementary Materials

Supplementary materials include two texts, five figures and thirteen movies and can be found online at http://www.landesbioscience.com/.

5.7. References

1. Battinelli EM, Hartwig JH, Italiano JE, Jr. Delivering new insight into the biology of megakaryopoiesis and thrombopoiesis. Curr Opin Hematol. 2007;14:419-426.
2. Junt T, Schulze H, Chen Z, et al. Dynamic visualization of thrombopoiesis within bone marrow. Science. 2007;317:1767-1770.
3. Mattia G, Vulcano F, Milazzo L, et al. Different ploidy levels of megakaryocytes generated from peripheral or cord blood CD34+ cells are correlated with different levels of platelet release. Blood. 2002;99:888-897.
4. Norol F, Vitrat N, Cramer E, et al. Effects of cytokines on platelet production from blood and marrow CD34+ cells. Blood. 1998;91:830-843.
5. van den Oudenrijn S, von dem Borne AE, de Haas M. Differences in megakaryocyte expansion potential between CD34(+) stem cells derived from cord blood, peripheral blood, and bone marrow from adults and children. Exp Hematol. 2000;28:1054-1061.
6. Hegyi E, Nakazawa M, Debili N, et al. Developmental changes in human megakaryocyte ploidy. Exp Hematol. 1991;19:87-94.
7. Galipeau PC, Cowan DS, Sanchez CA, et al. 17p (p53) allelic losses, 4N (G2/tetraploid) populations, and progression to aneuploidy in Barrett's esophagus. Proc Natl Acad Sci U S A. 1996;93:7081-7084.
8. Bornstein R, Garcia-Vela J, Gilsanz F, Auray C, Cales C. Cord blood megakaryocytes do not complete maturation, as indicated by impaired establishment of endomitosis and low expression of G1/S cyclins upon thrombopoietin-induced differentiation. Br J Haematol. 2001;114:458-465.
9. Miyazaki R, Ogata H, Iguchi T, et al. Comparative analyses of megakaryocytes derived from cord blood and bone marrow. Br J Haematol. 2000;108:602-609.
10. Geddis AE, Fox NE, Tkachenko E, Kaushansky K. Endomitotic megakaryocytes that form a bipolar spindle exhibit cleavage furrow ingression followed by furrow regression. Cell Cycle. 2007;6:455-460.
11. Lordier L, Jalil A, Aurade F, et al. Megakaryocyte endomitosis is a failure of late cytokinesis related to defects in the contractile ring and Rho/Rock signaling. Blood. 2008;112:3164-3174.
12. Guidotti JE, Bregerie O, Robert A, Debey P, Brechot C, Desdouets C. Liver cell polyploidization: a pivotal role for binuclear hepatocytes. J Biol Chem. 2003;278:19095-19101.
13. Otto SP. The evolutionary consequences of polyploidy. Cell. 2007;131:452-462.
14. Schwertz H, Koster S, Kahr WH, et al. Anucleate platelets generate progeny. Blood. 2010.
15. Chu K, Teele N, Dewey MW, Albright N, Dewey WC. Computerized video time lapse study of cell cycle delay and arrest, mitotic catastrophe, apoptosis and clonogenic survival in irradiated 14-3-3sigma and CDKN1A (p21) knockout cell lines. Radiat Res. 2004;162:270-286.
16. Geddis AE, Kaushansky K. Endomitotic megakaryocytes form a midzone in anaphase but have a deficiency in cleavage furrow formation. Cell Cycle. 2006;5:538-545.
17. Italiano JE, Jr., Lecine P, Shivdasani RA, Hartwig JH. Blood platelets are assembled principally at the ends of proplatelet processes produced by differentiated megakaryocytes. J Cell Biol. 1999;147:1299-1312.

18. Tomer A, Harker LA, Burstein SA. Flow cytometric analysis of normal human megakaryocytes. Blood. 1988;71:1244-1252.
19. Worthington RE, Nakeff A, Micko S. Flow cytometric analysis of megakaryocyte differentiation. Cytometry. 1984;5:501-508.
20. Zhang Y, Nagata Y, Yu G, et al. Aberrant quantity and localization of Aurora-B/AIM-1 and survivin during megakaryocyte polyploidization and the consequences of Aurora-B/AIM-1-deregulated expression. Blood. 2004;103:3717-3726.
21. Levine RF, Hazzard KC, Lamberg JD. The significance of megakaryocyte size. Blood. 1982;60:1122-1131.
22. Tomer A. Human marrow megakaryocyte differentiation: multiparameter correlative analysis identifies von Willebrand factor as a sensitive and distinctive marker for early (2N and 4N) megakaryocytes. Blood. 2004;104:2722-2727.
23. Nagata Y, Muro Y, Todokoro K. Thrombopoietin-induced polyploidization of bone marrow megakaryocytes is due to a unique regulatory mechanism in late mitosis. J Cell Biol. 1997;139:449-457.
24. Tao H, Gaudry L, Rice A, Chong B. Cord blood is better than bone marrow for generating megakaryocytic progenitor cells. Exp Hematol. 1999;27:293-301.
25. Giammona LM, Fuhrken PG, Papoutsakis ET, Miller WM. Nicotinamide (vitamin B3) increases the polyploidisation and proplatelet formation of cultured primary human megakaryocytes. Br J Haematol. 2006;135:554-566.
26. Keighren M, West JD. Analysis of cell ploidy in histological sections of mouse tissues by DNA-DNA in situ hybridization with digoxigenin-labelled probes. Histochem J. 1993;25:30-44.
27. Decordier I, Cundari E, Kirsch-Volders M. Mitotic checkpoints and the maintenance of the chromosome karyotype. Mutat Res. 2008;651:3-13.
28. Roy L, Coullin P, Vitrat N, et al. Asymmetrical segregation of chromosomes with a normal metaphase/anaphase checkpoint in polyploid megakaryocytes. Blood. 2001;97:2238-2247.
29. Schipper LF, Brand A, Reniers NC, Melief CJ, Willemze R, Fibbe WE. Effects of thrombopoietin on the proliferation and differentiation of primitive and mature haemopoietic progenitor cells in cord blood. Br J Haematol. 1998;101:425-435.
30. Broudy VC, Lin NL, Kaushansky K. Thrombopoietin (c-mpl ligand) acts synergistically with erythropoietin, stem cell factor, and interleukin-11 to enhance murine megakaryocyte colony growth and increases megakaryocyte ploidy in vitro. Blood. 1995;85:1719-1726.
31. Carow CE, Fox NE, Kaushansky K. Kinetics of endomitosis in primary murine megakaryocytes. J Cell Physiol. 2001;188:291-303.
32. Debili N, Issaad C, Masse JM, et al. Expression of CD34 and platelet glycoproteins during human megakaryocytic differentiation. Blood. 1992;80:3022-3035.
33. Proulx C, Boyer L, Hurnanen DR, Lemieux R. Preferential ex vivo expansion of megakaryocytes from human cord blood CD34+-enriched cells in the presence of thrombopoietin and limiting amounts of stem cell factor and Flt-3 ligand. J Hematother Stem Cell Res. 2003;12:179-188.
34. Boyer L, Robert A, Proulx C, Pineault N. Increased production of megakaryocytes near purity from cord blood CD34+ cells using a short two-phase culture system. J Immunol Methods. 2008;332:82-91.

35. Gonzalez RC, Woods RE. Digital image processing (ed 2nd). Upper Saddle River, N.J.: Prentice Hall; 2002.
36. Gonzalez RC. Digital Image Processing Using Matlab. Upper Saddle River: PRENTICE HALL PTR; 2004.
37. McAndrew A. Introduction to digital image processing with Matlab. Boston, MA.: Thomson Course Technology; 2004.
38. Semmlow JL. Biosignal and biomedical image processing : MATLAB-based applications. New York: Marcel Dekker; 2004.

5.8. Tables and Figures

5.8.1. Tables

Table 5.1: Fates of megakaryocytes derived in CB- and BM-CD34$^+$ TPO cultures. Mean percentage of cumulative results shown for two observation time windows (day 0 - 5 and 5 - 10).

Ploidy Class	MK Fates	Cord Blood MK r = 5[a], N = 2,320[b]	Bone Marrow MK r = 5, N = 1,214
		n = 1,772[c]	n = 567
2N	Endomitosis	12.47% [9.3-27.1%][d]	17.81% [11.4-33.7%]
	Mitosis	75.1% [69.3-76.9%]	72.84% [49.1-82.4%]
	Proplatelet	6.04% [1.5-8.2%]	2.12% [0.0-7.4%]
	Death	7.28% [2.0-10.2%]	6.70% [6.2-8.0%]
		n = 340	n = 407
4N	Endomitosis	49.71% [44.4-71.4]	76.66% [75.3-78.1%]**
	Mitosis	27.35% [12.3-38.7%]	6.63% [6.5-6.8%]**
	Proplatelet	15.59% [9.5-18.8%]	10.81% [9.9-11.6%]**
	Death	3.82% [2.1-7.4%]	5.90% [5.2-6.5%]*
		n = 208	n = 240
8N	Endomitosis	41.83% [22.2-59.5%]	78.33% [76.5-81.3%]**
	Mitosis	8.17% [2.7-11.3%]	1.25% [1.1-1.3%]**
	Proplatelet	43.27% [22.6-65%]	16.67% [16.5-16.8%]**
	Death	4.81% [2.7-6.2%]	3.75% [1.1-5.4%]

[a]r: number of independent experiments; [b]N: total number of tracked cells, [c]n: number of individual cells. [d]: range observed [minimum-maximum]; *student t-Test P-Value (CB- vs. BM-cells) < 0.05; ** p < 0.001; MK: Megakaryocyte.

5.8.2. Figures
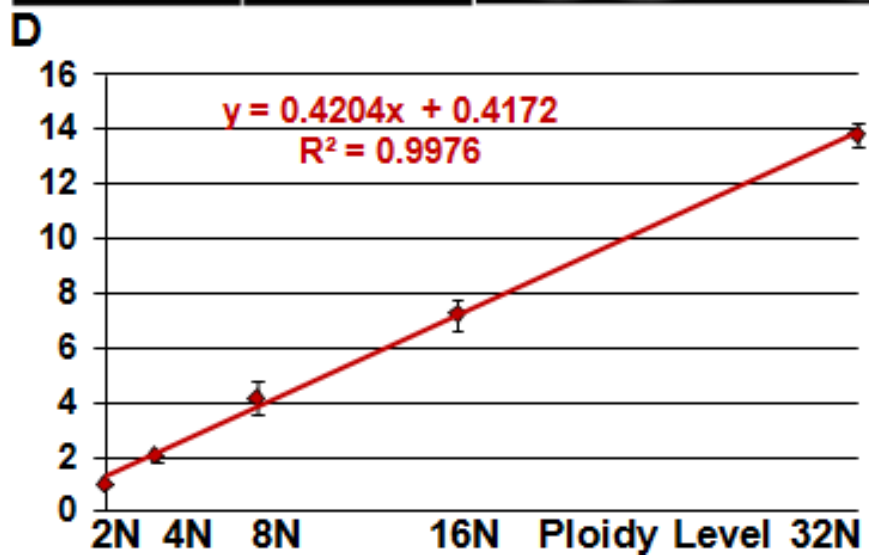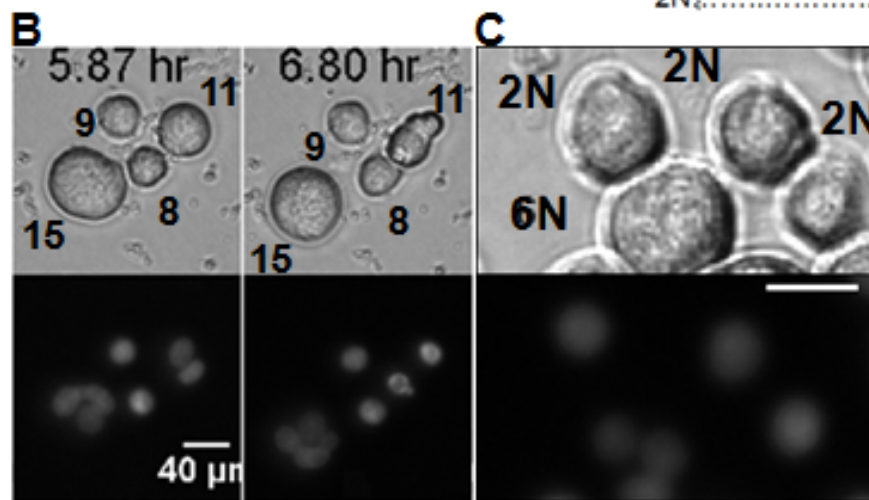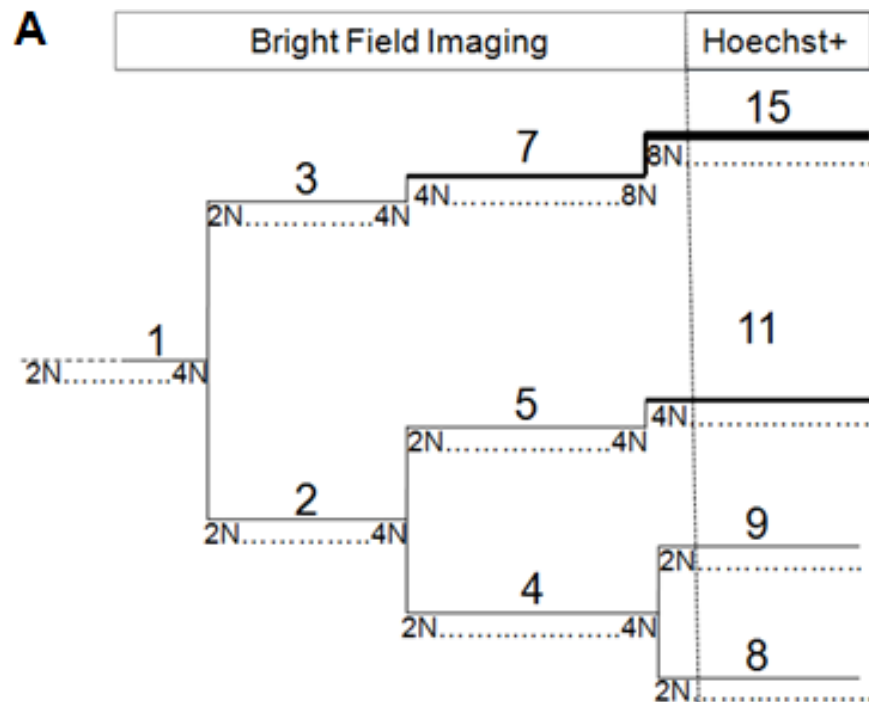
Figure 5.1: Ploidy levels of imaged cells were determined by three complementary methods. **A)** Cell lineage tree constructed based on morphological observations (bright field imaging at 20X) depicting the history of a CB-tetraploid cell and that of its descendants. In this instance, cells 8 and 9 were scored as diploids since their ancestors showed only 2N mitosis events, while cells 11 and 15 were classified as 4N and 8N since they underwent one and two rounds of endomitosis, respectively. Ploidy levels are shown below each line. Hoechst dye was added at the end of the culture. **B)** Examples of ploidy level determination by Hoechst staining. Stained nuclei of two CB-diploids, one CB-tetraploid, and one CB-octaploid corresponding to cells 8, 9, 11 and 15 in panel A, respectively. Cells 8 and 9, 11, and 15 show clearly one, two and four nuclear lobes, respectively. Bright field and corresponding fluorescent images shown. **C)** Example of Hoechst staining of a putative CB-hexaploid cell with a three-lobbed nucleus **D)** Linear correlation between ploidy level and CB-MK size (mean normalized volume ± SD of at least 40 observations per ploidy class is shown). Cell volume (V) was computed based on the projected cell surface (A) through $V \propto A^{3/2}$ (see last paragraph of supplementary Text B for details). Scale bar: 40 μm. See supplementary video 5.1B.
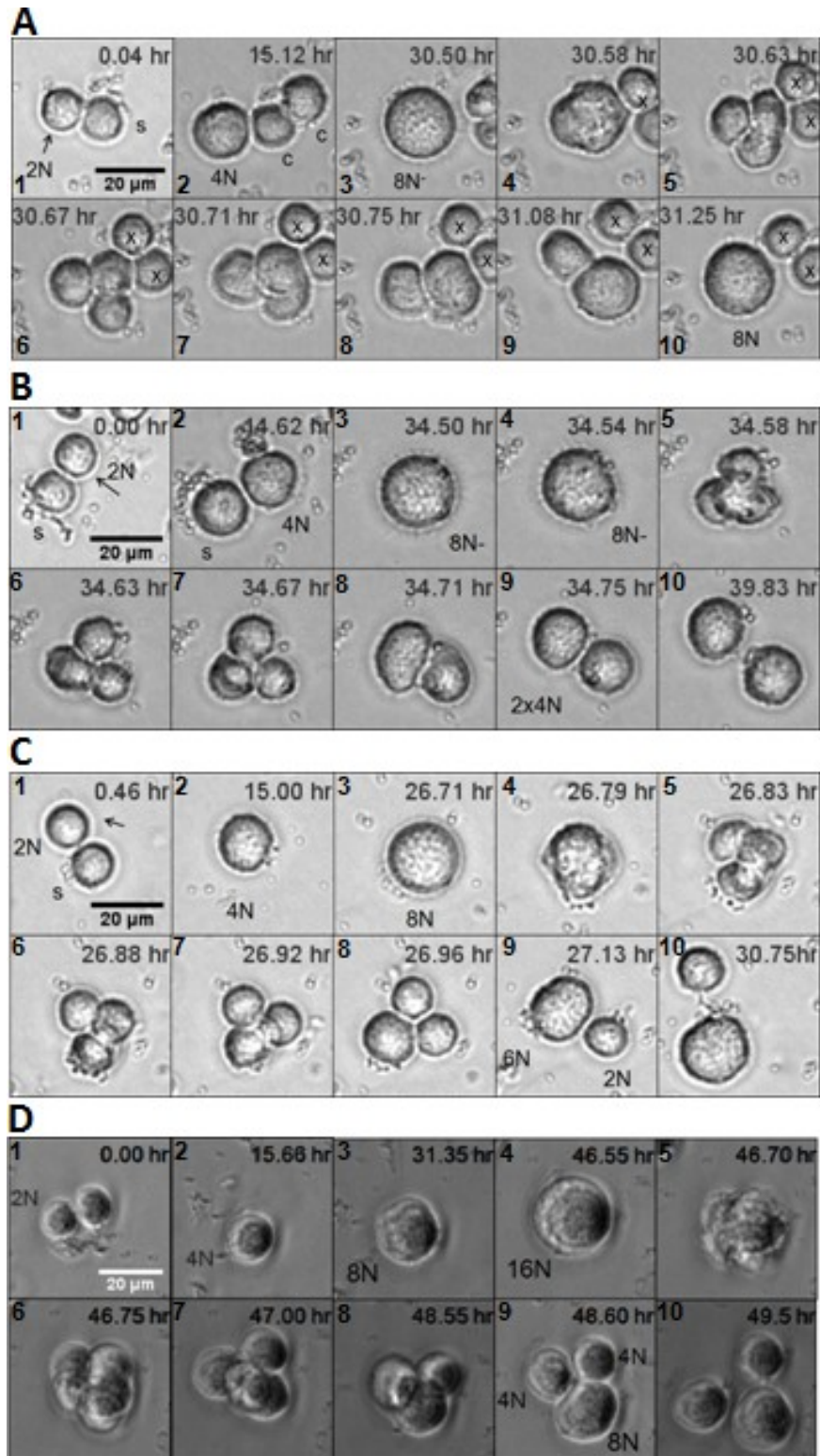
Figure 5.2: Polyploid CB-MKs can complete cytokinesis and undergo cell division in culture. **A)** A 4N cell undergoes endomitosis and forms an 8N cell. **B)** Symmetrical division of a tetraploid cell into two tetraploid cells; a parental 2N cell (frame 1) successfully completed endomitosis giving rise to a tetraploid cell (frame 2). This cell entered cell cycle (frame 3) and initiated cleavage furrow ingression (frames 4-8). During furrow regression,

two pairs of putative daughter cells reunified to form a symmetrical bi-polar 2x4N cell (frame 8) which successfully completed cytokinesis and cell abscission (frame 9), resulting in the formation of two 4N daughter cells (frame 9). These cells remained separated for the rest of the culture (frame 10). **C)** Asymmetrical division of a 4N cell into one 2N and one 6N cells; a 2N cell (frame 1) underwent endomitosis and formed a 4N cell (frame 2) which then initiated cleavage furrow ingression displaying four pseudo 2N daughter cells (frames 4 - 7). Two of these merged (frame 8) and less than 3 minutes later, one of the two remaining diploids regressed with the 4N leading to the formation of an asymmetrical bi-polar cell consisting of one 2N and one 6N pseudo cells which successfully completed cytokinesis (frame 9) producing one large 6N and one small 2N cells, which remained independent (frames 10). **D)** Asymmetrical division of a CB-8N MK into two 4Ns and one 8N. A 2N cell successfully completed two rounds of endomitosis producing one 8N (frames 1-3), which entered cell cycle and initiated cleavage furrow ingression (frame 4-5). The pseudo daughter cells regressed back together asynchronously (frames 6-7) leading to the formation of a three-lobbed asymmetrical cell (frame 8) consisting of two 4Ns and one 8N pseudo daughter cells, which became independent entities following completion of cytokinesis (frames 9-10). In the first frame of panel **A**, a sister cell marked as "s" underwent mitosis and produced two cousin cells marked as "c" in the second frame. Times indicated in hours (hr), x = unknown cell. Scale bar: 20 μm. See supplementary videos 5.2A-D. The frame number for each frame is indicated in Arabic number.
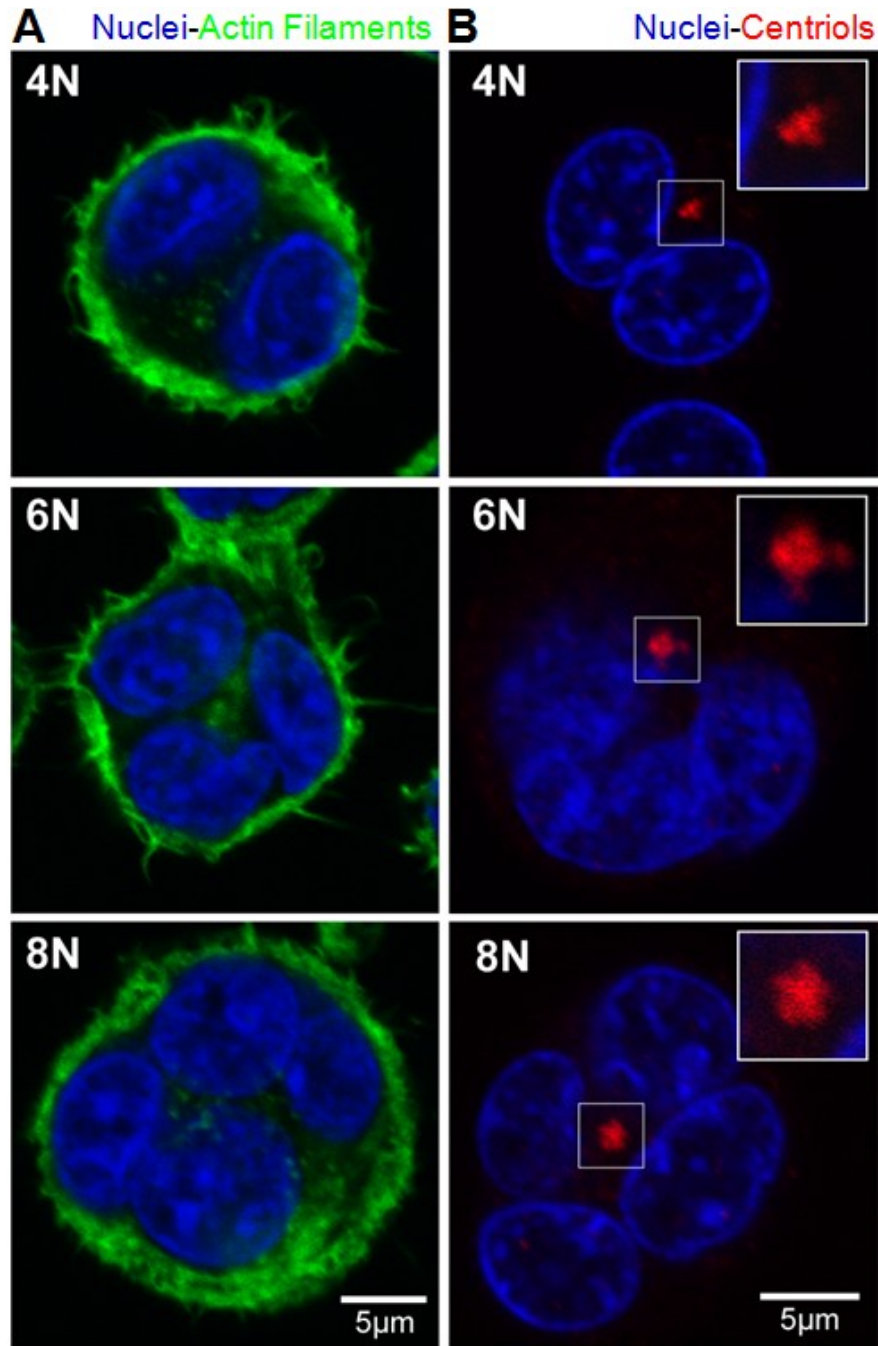
Figure 5.3: Immunostaining of polyploid CB-MKs confirms the existence of tri-lobular hexaploids (6N) in regular TPO cultures. CD41$^+$ cells of ploidy equal or greater than 4N cells were sorted at day 10, fixed and stain with Hoechst (cell nuclei in blue) and phalloidin ALEXA 488 (**A**, actin filaments in green) or anti-gamma tubulin (**B**, centrioles in red) and examined under confocal microscopy using 60x oil 1.42 NA objective (representative images shown, n = 3). Scale bar: 5 µm. See supplemental videos. The confocal experiments were performed by Amélie Robert with my collaboration.
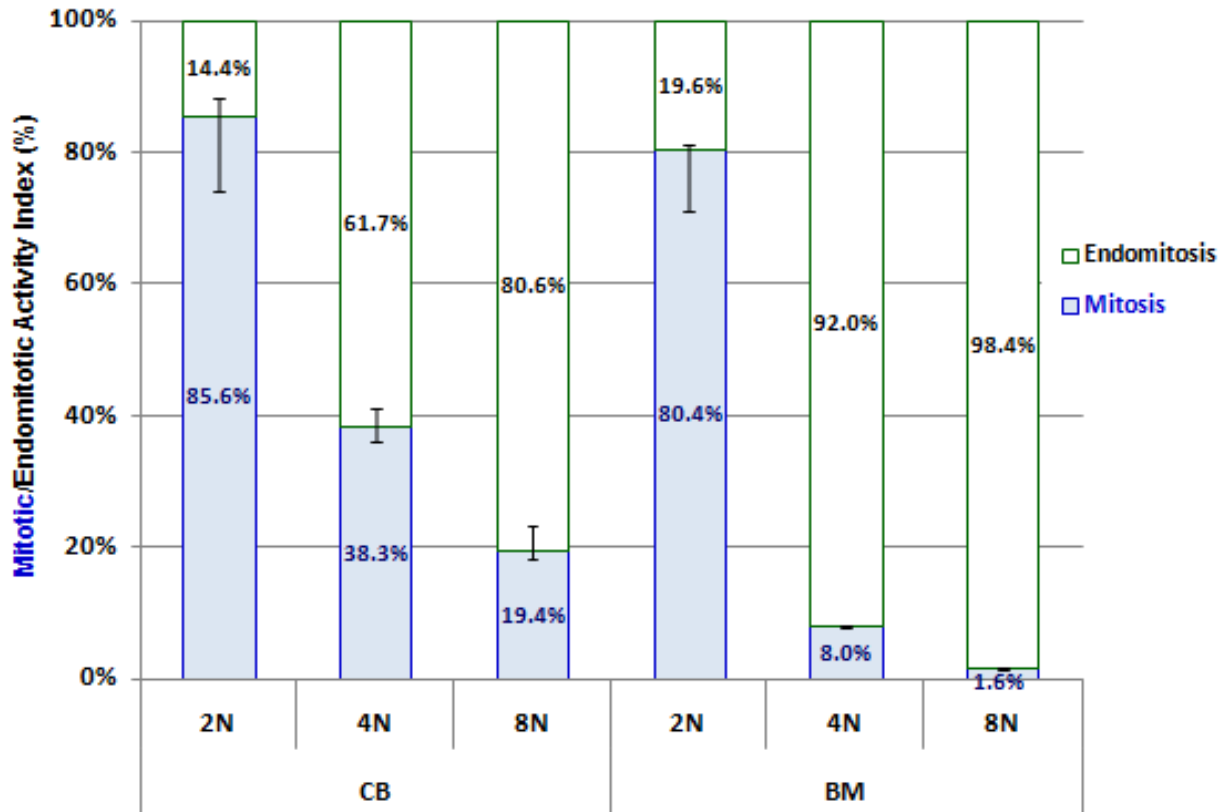
Figure 5.4: Mitotic completion index as a function of the source of the MKs and their ploidy class. Comparison of mitotic and endomitotic frequencies in different ploidy classes of CB- and BM-MKs in the absence of cell death and proplatelet formation. The frequencies were calculated as the ratio of cells that completed cell division or endomitosis over the sum total of both outcomes (based on data presented in Table 5.1). Mean of at least 5 independent experiments presented. The range is also provided in the form of error bars.
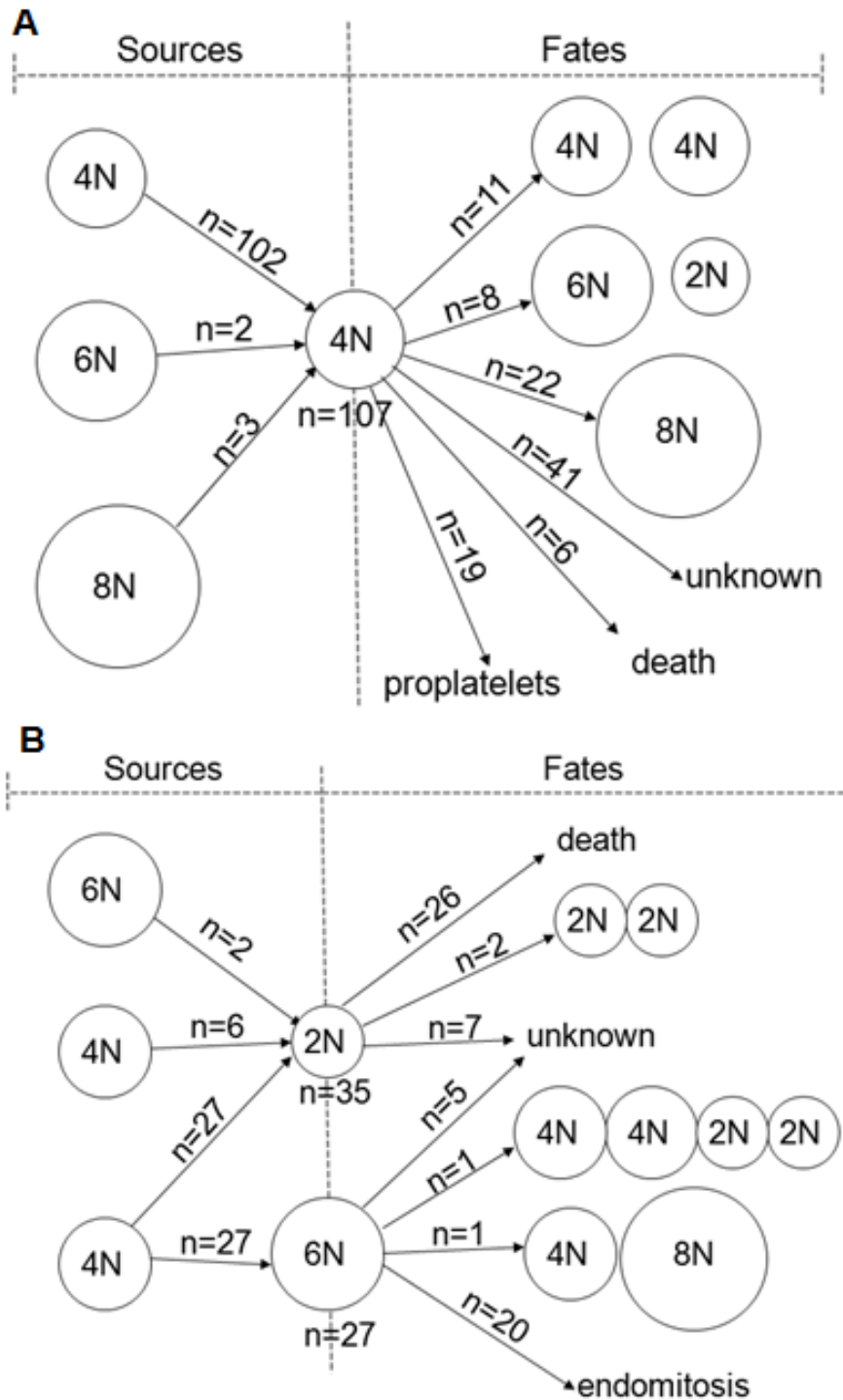
Figure 5.5: Sources and fates of CB-MKs generated through polyploid cell mitosis. **A)** Sources and fates for 107 tetraploids formed following mitosis of polyploid MKs. **B)** Sources and fates for 34 diploid and 27 hexaploid cells following asymmetrical divisions of polyploid MKs. Cumulative results of 5 independent experiments shown.
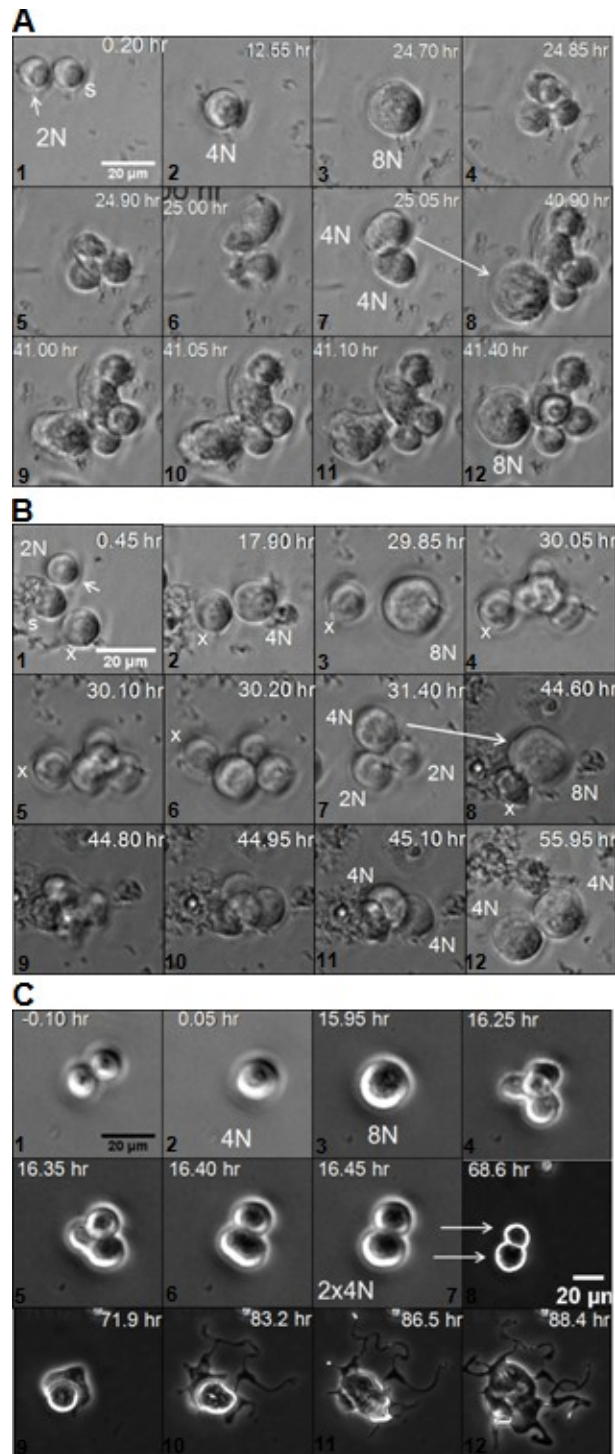
Figure 5.6: Fates of polyploid MK formed following mitosis of a polyploid MK. **A)** A CB-tetraploid cell divides to two tetraploids (frames 4 - 7). One of the tetraploids then enters cell cycle and eventually undergoes endomitosis (frames 8 - 12) and gives an 8N cell. **B)** A CB-tetraploid cell, after 30 hours, undergoes mitosis and divides gradually into three cells (one 4N and two 2Ns). The newly formed tetraploid then enters cell cycle and eventually divides into two tetraploids (frames 9 - 10). **C)** A BM-tetraploid cell (frame 2), after 16 hours, undergoes mitosis and divides gradually into two 4Ns (frames 3 - 7). The newly

formed tetraploids (frame 7) then enter cell cycle and eventually form proplatelets (frames 8 - 12). Legend: s = sister cell, x = unknown cell. Scale bar: 20 μm. The frame number for each frame is indicated in Arabic number.

5.9. Supplemental Data

TEXT A. Live Cell Imaging

Image Acquisition

Two Plexiglas chambers were designed; 1) a large dark outer chamber encompassing the whole optical system which allowed precise temperature control (37 ± 0.1°C) by hot air circulation, and 2) a small gas-tight chamber located on the stage where humidified air mixture (10% CO_2/90% air) was fed. Cells were seeded at a cell density of 0.25 - 0.40 x 10^4 cells/ml in 24-well plates (1ml/well) and monitored for 5 days at 20X magnification. Bright field images were captured every 2.0 - 3.0 minutes. Imaging of $CD34^+$ cell cultures took place with an initial cell density of 0.25 - 0.4 x 10^4 cells/ml, from day 0 to day 5 or from day 5 to day 10 with an initial cell density of 4 x 10^4 cells/ml at day 0.

The large fields of view used for cell tracking were obtained by tiling 5 x 5, 7 x 7 or 9 x 7 digital images with pixel resolution of 1,600 x 1,200 (pixel size of 7.4 μm at 1X, 12 bits/pixel). The captured area after tiling was therefore 2.96 x 2.22, 4.14 x 3.11, or 4.00 x 4.14 mm^2, respectively (at 20X magnification), i.e. 3.8, 7.5, 9.63% of the total surface area of a 24-well plate, respectively. For each experiment, the area of culture captured by the camera was adjusted to ensure that 2-4 cells were initially present within each field of view in tiled images. At least three independent experiments were performed for both CB- and BM-cell sources and for both time windows. Cells difficult to track such as those leaving the field of view or those forming colonies were kept in the analysis only if they could be tracked individually for over 90% of the experiment duration. Only a marginal number of cells were left out (less than 1%).

Image Processing and Analysis

When analyzing the images, the frame number, a unique cell ID number, and time were recorded in a spreadsheet when the following events occurred: cell division, cell polyploidization, proplatelet formation, cell death, elongation, colony formation, entrance or exit from the field of view. A set of custom Matlab R2008b (MathWork Inc.) scripts

were developed to analyze the recorded data, construct cell lineage trees and compile statistics. An integrated tool was also developed to extract regions of interest around predetermined sets of cells to prepare smaller videos of the most interesting and representative phenomena observed. Different steps were required to discriminate the cells from the background among acquired images[35]. Cell segmentation was performed by using a combination of mathematical morphological operators[36-38] using the Matlab software. Once either the cell or its DNA was successfully segmented, several features were defined to characterize each segmented specimen. Some cell features were also quantified by manual segmentation using ImageJ software (National Institute of Health).

TEXT B. Correlation between Ploidy Level and Cell Size

One of the important questions during the polyploid cell tracking is the determination of daughter cell ploidy level, particularly in the case of asymmetric division. Assuming that 1) each cell is ideally in a sphere shape; where the correlations between surface (A) and volume (V) and that of diameter (D) and volume are a power of 2/3 and 1/3, respectively; and 2) each daughter cell has an equal mass or volume; i.e. half of that of a parent cell; Therefore each cell has a rational diameter and surface to parent as $(1/2)^{1/3} =$ and $(1/2)^{2/3} =$. Using a similar argument, it is easily concluded a 4N cell at the end of cell cycle, which is 8N, should give a 2N with $(2/8)^{1/3} =$ diameter or $(2/8)^{2/3}=0.4$ surface of the parent and a 6N cell with $(6/8)^{1/3} =$ diameter or $(6/8)^{2/3}=0.83$ surface of that. Table 5.S1 summarizes this computation and compares these values with empirical sizes of cells with known ploidy levels.

Table 5.S1. Correlation between parent and daughter cell sizes.

Ploidy Level		Measured				Theory
Parent cell	Daughter cells	Number of cells	Diameter of daughter cell 1 (smaller)	Diameter of daughter cell 2 (larger)	Mean ± S.D	Diameter
4N	2N & 2N	17	$75.94 \pm 2.97\%$	$79.20 \pm 2.59\%$	$77.57 \pm 3.20\%$	$(2/4)^{1/3} =$
8N	4N & 4N	12	$76.13 \pm 0.01\%$	$78.84 \pm 0.03\%$	$77.49 \pm 0.04\%$	$(4/8)^{1/3} =$
8N	2N & 6N	7	$64.86 \pm 3.39\%$	$88.86 \pm 2.08\%$	---	$(2/8)^{1/3} =$ $(6/8)^{1/3} =$

To verify our assumptions: first, the ratio of two daughter cells' volume from symmetrical division was found 0.50 ± 0.04, which confirmed that each new daughter cell has around equal cytoplasm volume; Second, the ratio of sum volumes of daughter cells per that of the parent cell was 0.94 ± 0.09 which is close to unity. It is important to consider that the cell rotates over time and displays variable surfaces which results in measurement error. Furthermore, manual cell segmentation usually leads to some estimation errors of the projected surface. Using an average value from several frames reduces the level of errors and improves this ratio. Another possible reason is the correlation between the cell surface and volume which could be deviated from 2/3 assuming perfect spherical shape.

To find a correlation between ploidy level and cell size, cells were first identified by image segmentation (see *Text A*) and then their sizes were quantified by measurements of the projected cell surface area (A). Cell volume (V) and diameter (D) were then estimated based on spherical assumption ($V \propto A^{3/2}$ and $D \propto A^{1/2}$). Linear correlation between cell size (volume) and ploidy level was demonstrated by: 1) identifying a series of cells undergoing polyploidization continuously from 2N up to 16N following the observation of up to 3 rounds of endomitosis; 2), computing the relative cell volume for each of these cells and normalizing by division to the volume of 2N cells just after birth; 3) then plotting the relative cell volume vs. ploidy level. This investigation showed i) a strong linear relationship between cell volume and ploidy level determined at birth ($R^2 = 0.9969$), and ii) that each doubling in ploidy led to a 1.94 ± 0.15 –fold increase in cell volume of an individual cell (from 2N to 16N class of MK). In practice, ploidy level determination following mitosis or endomitosis was done by calculating the volume of the parental cells just before starting cleavage furrow (average of 2 - 4 frames) and the volume of the daughter cells right after birth (average of 3 - 5 frames).
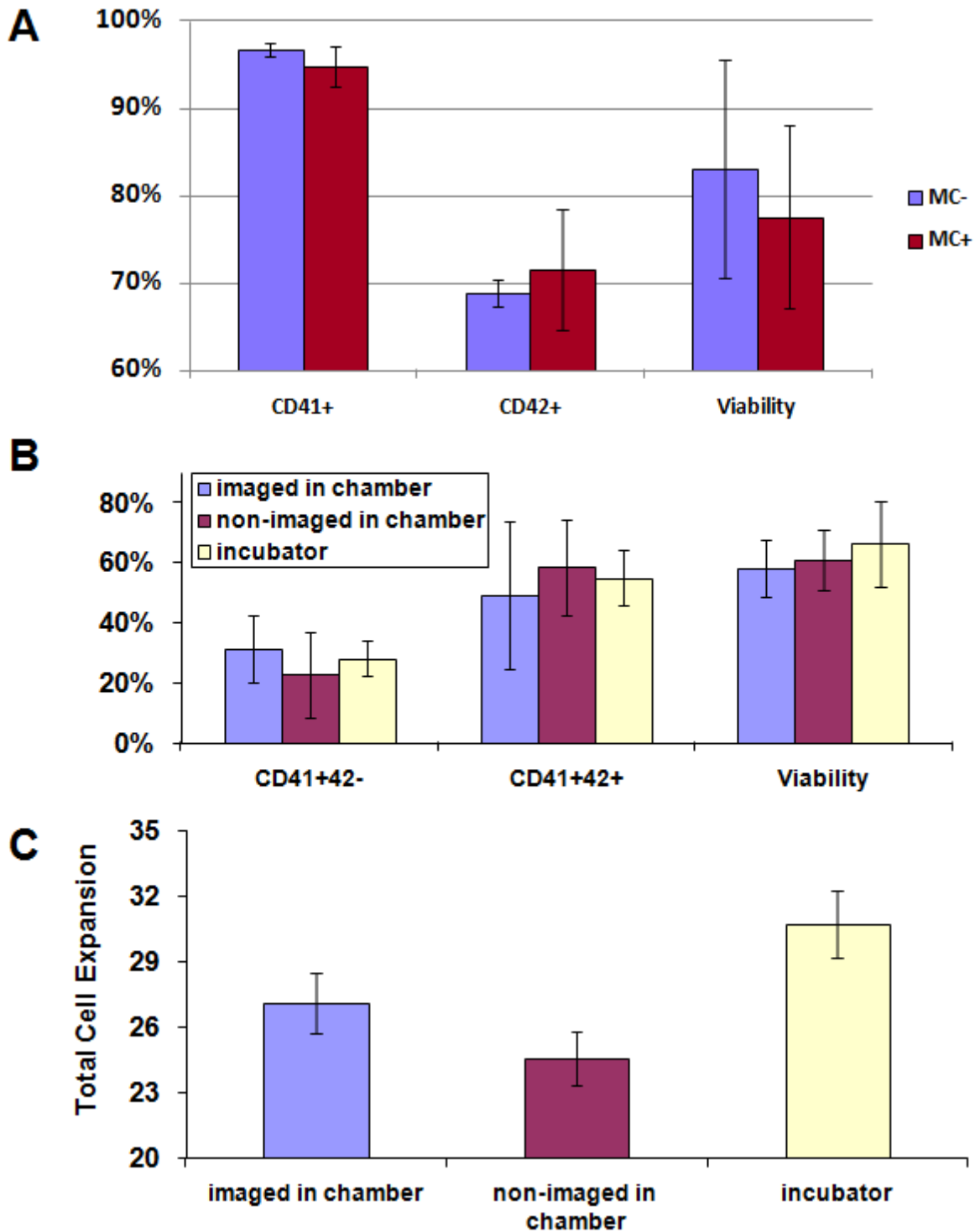
Figure 5.S1: Normal cell expansion, viability and MK cell differentiation of CB-CD34$^+$ cells under the live cell imaging condition used. **A)** Comparison of methylcellulose (MC) addition on cell phenotype and viability in a standard incubator. **B and C)** Comparison of cell phenotypes, viability (panel **B**), and cell expansion (panel **C**) between cultures in the presence of MC in a regular incubator or custom-made chamber with or without light exposure. Mean ± SD of duplicate culture of a representative experiment shown (n = 3).
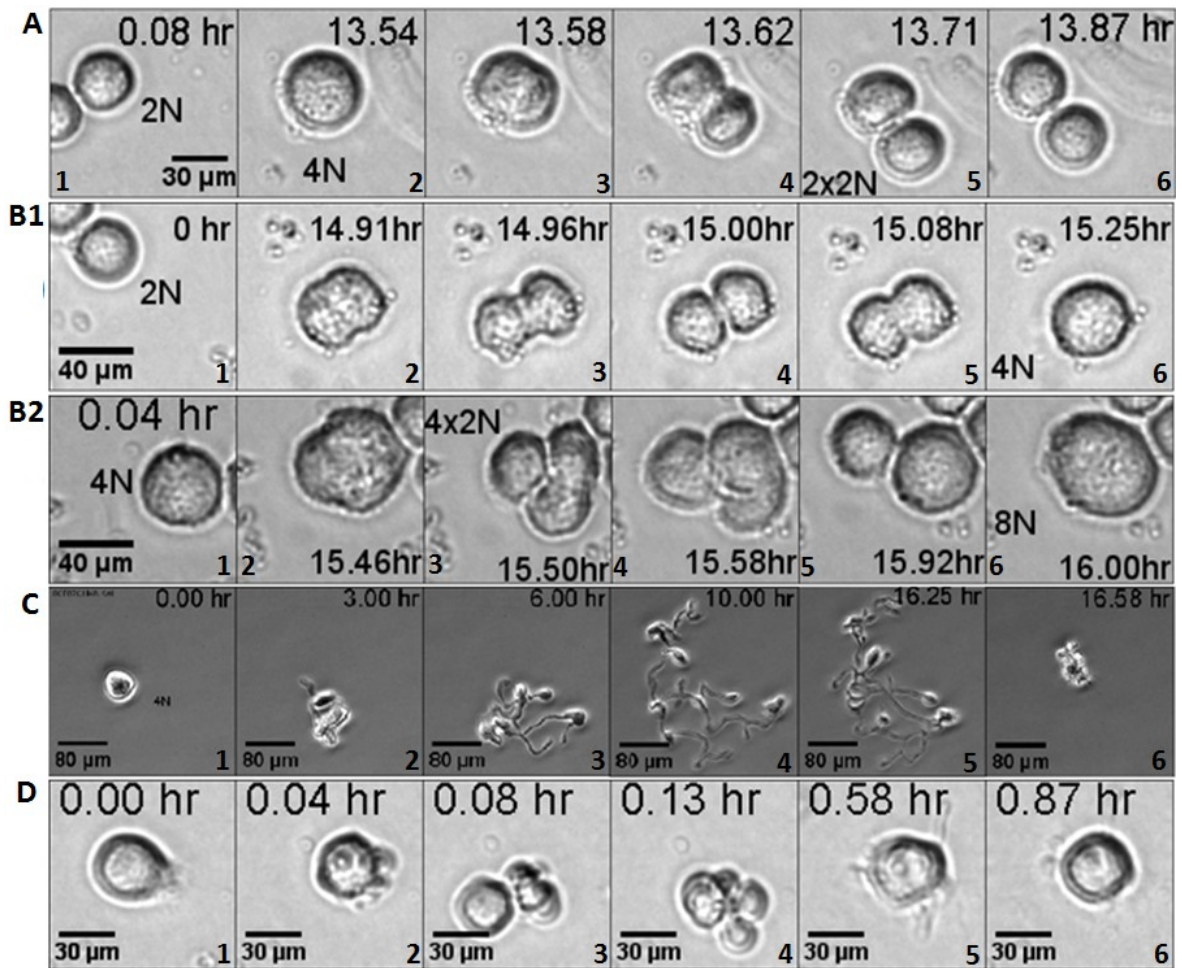
Figure 5.S2: Principal cellular events observed during the megakaryocytic differentiation and maturation of CD34$^+$ cells. CB- or BM-CD34$^+$ cells were induced to undergo MK differentiation in TPO cultures. Live cell imaging was conducted between day 0 - 5 or day 5 - 10 (bright field, 20X). **A)** Mitosis: a diploid cell finishes its cytokinesis and cell abscission to divide gradually into two 2N daughter cells. **B)** Endomitosis: B1) a diploid cell at the end of cell cycle undergoes endomitosis and forms a tetraploid cell. This series of frames demonstrate that cytokinesis is indeed initiated but is prematurely terminated during endomitosis, and its regression (so called backward movement) leads to the formation of a single daughter cells; B2) a 4N cell undergoes polyploidization and forms an 8N cell. **C)** Proplatelet formation with a mature CB-MK. **D)** Cell death of a mature MK. Time at which the pictures were taken is indicated in hours (hr). The frame number for each frame is indicated in Arabic number.
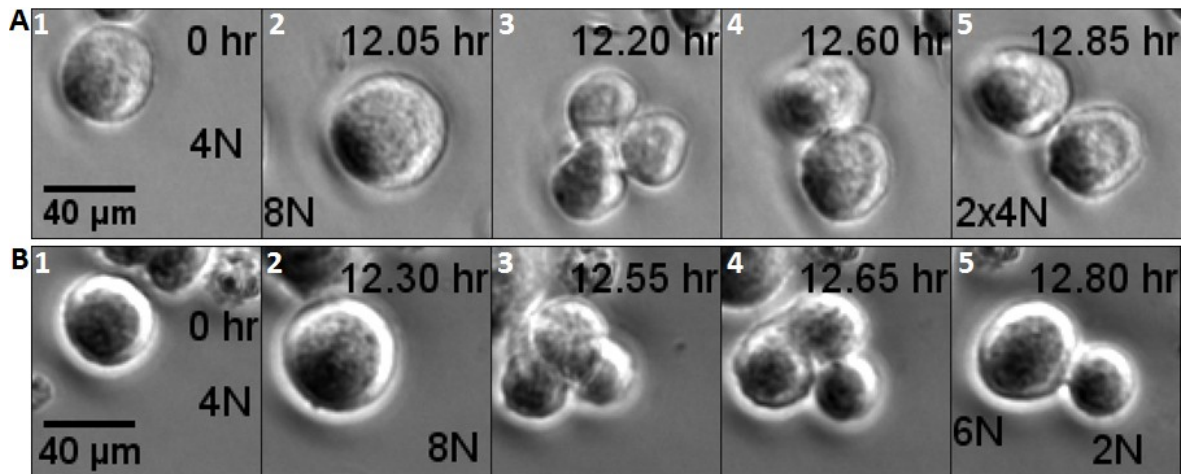
Figure 5.S3: Mitosis of BM-derived tetraploid MKs. **A)** Symmetrical division of a tetraploid cell into two tetraploid cells. A tetraploid cell (frame 1) enters cell cycle and completes DNA replication (frame 2), undergoes partial cleavage furrow ingression (frames 3-4). During cleavage furrow regression, two pairs of putative daughter cells fuses together to form bi-polar 2x4N cells (frame 4) which successfully complete furrow ingression, cytokinesis and cell abscission (frame 5), resulting in the formation of two tetraploid daughter cells (frame 5). These daughter cells remain permanently separated. **B)** Asymmetrical division of a tetraploid cell produces one diploid and one hexaploid cells; a tetraploid cell (frame 1) replicates its DNA (frame 2) and initiates cleavage furrow ingression (frame 3) by displaying two diploid and one tetraploid pseudo-daughter cells (frames 3-4). One of the diploids fuses with the tetraploid cell and forms a hexaploid cell (frame 5). These two cells successfully completed cytokinesis and remained independent. Time at which the pictures were taken is indicated in hours (hr). Scale bar: 40 μm. See supplemental online videos 5.S3A and S3B. The frame number for each frame is indicated in Arabic number.
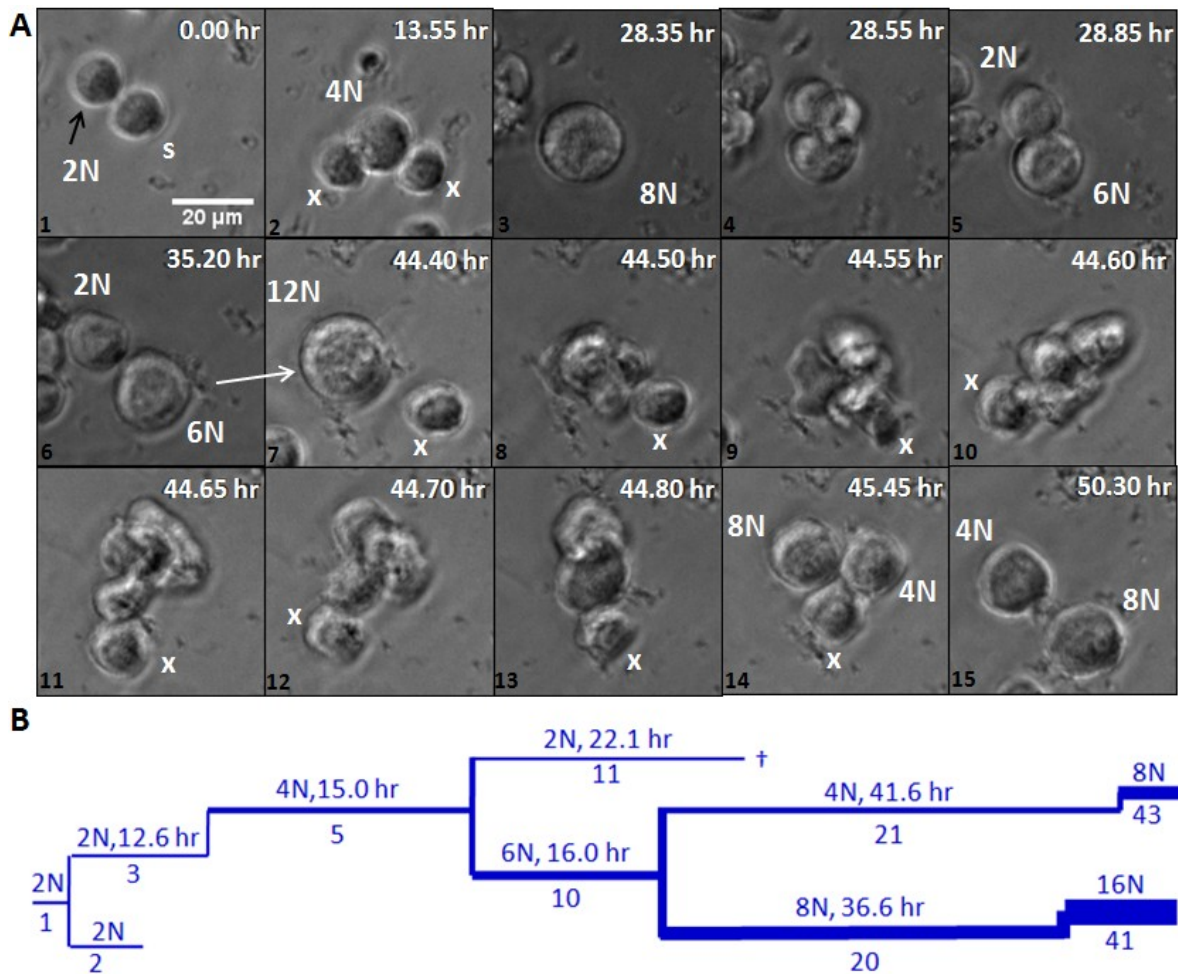
Figure 5.S4: Fates of a hexaploid MK formed following mitosis of a tetraploid MK. **A)** A tetraploid cell divides to a diploid (2N) and hexaploid (6N) (frames 3-5). The hexaploid then enter cell cycle and eventually divides into one tetraploid and one octaploid cell (frames 7-15). Legend: s = sister cell, x = unknown cell; scale bar: 20 μm. The frame number for each frame is indicated in Arabic number. **B)** Lineage tree of the cellular events shown partially in panel A. See supplemental online video 5.S4.
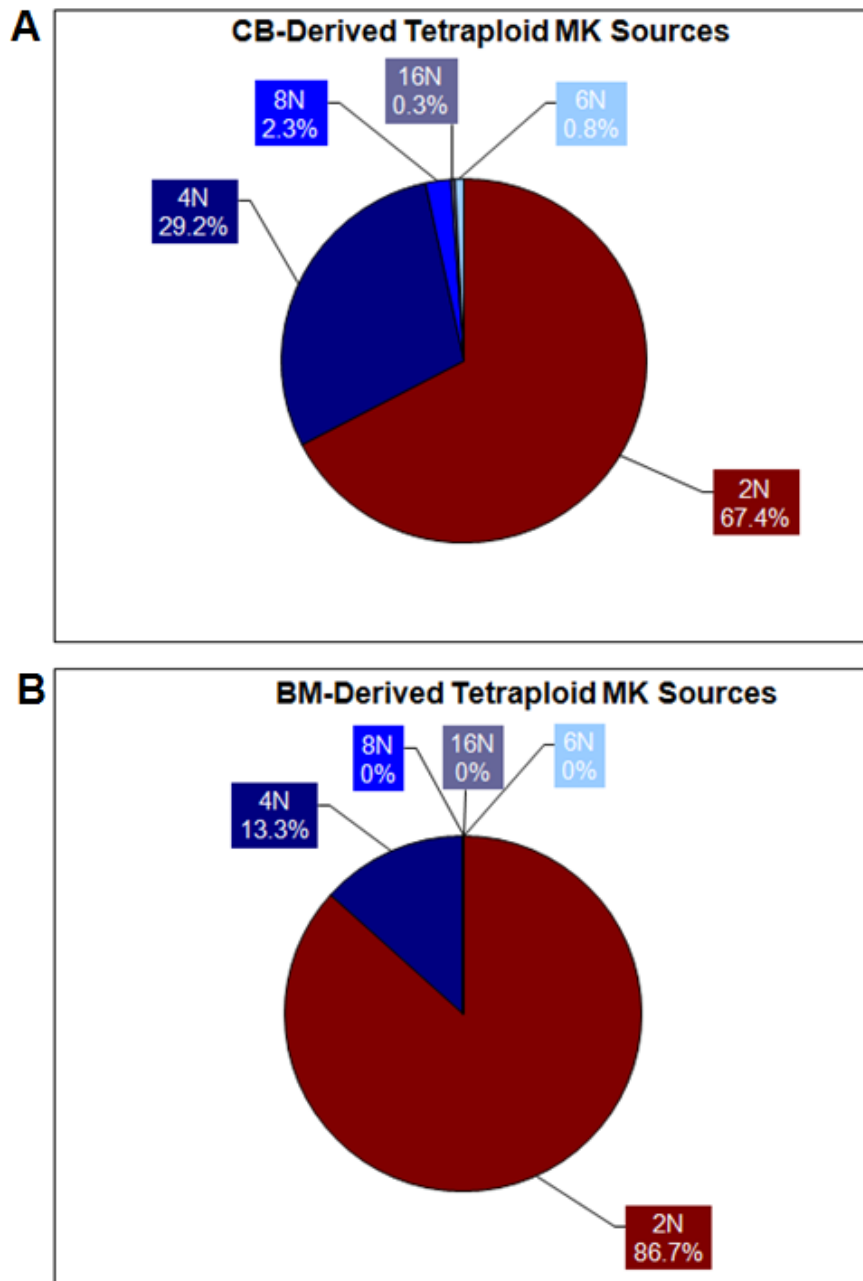
Figure 5.S5: Comparison of the various source of tetraploids in CB- (n = 311) and BM-cell (n = 405) cultures (cumulative results of 5 independent experiments). 2N indicates the proportion of 4N derived from endomitosis, while 4N and above indicates the proportion derived from the mitosis of polyploid MKs.

5.10. Movies

Movie 5.1B. Ploidy levels of tracked CB-cells were determined by Hoechst staining.

Movie 5.2A. A CB-4N undergoes endomitosis and forms an 8N cell.

Movie 5.2B. Symmetrical division of a CB-4N cell into two tetraploid cells.

Movie 5.2C. Asymmetrical division of a CB-4N cell into one 2N and one 6N cells.

Movie 5.2D. Asymmetrical division of a CB-8N MK into two 4Ns and one 8N.

Movie 5.3A. Z-stack slices of trilobular hexaploid CB-MK stained with Hoechst (cell nuclei/blue) and phalloidin ALEXA 488 (actin filaments/green).

Movie 5.3B. Z-stack slices of trilobular hexaploid CB-MK stained with Hoechst (cell nuclei/blue) and anti-gamma tubulin (centrioles/red).

Movie 5.6A. A CB-tetraploid cell divides to two tetraploids. One of the tetraploids then enters cell cycle and eventually undergoes endomitosis and gives an 8N cell. Two parts.

Movie 5.6B. A CB-tetraploid cell, after 30 hours, undergoes mitosis and divides gradually into three cells (one 4N and two 2Ns). The newly formed tetraploid enters cell cycle and eventually divides into two tetraploids. Two parts.

Movie 5.6C. A tetraploid BM-MK, after 16 hours, undergoes mitosis and divides gradually into two 4Ns. Two parts.

Movie 5.S3A. Symmetrical division of a BM-tetraploid cell into two tetraploid cells.

Movie 5.S3B. Asymmetrical division of a BM-tetraploid cell produces one diploid and one hexaploid cells.

Movie 5.S4. A tetraploid cell divides to a diploid (2N) and hexaploid (6N). The hexaploid then enters cell cycle and eventually divides into one tetraploid and one octaploid cell. Two parts.

6. Single Cell Level Analysis of Megakaryocyte Growth and Development[$]

Younes Leysi-Derilou[1,2], Carl Duchesne[1], Alain Garnier[1], and Nicolas Pineault[2*]

[1]Department of Chemical Engineering, Laval University, Québec, QC, Canada G1V 0A6

[2]R&D Department, Héma-Québec, Québec, QC, Canada G1V 5C3

*Correspondence and Reprint Requests: Dr. Nicolas Pineault, PhD

Héma-Québec, Research and Development Department, Laval University, Québec, QC
Canada G1V 5C3

Telephones: (418) 780-4362 # 3253. Fax: (418) 780-2091

E-Mails: Nicolas.Pineault@hema-quebec.qc.ca

Contact for offprint: Dr. Nicolas Pineault

6.1. Abstract/ Résumé

Several fundamental questions surrounding megakaryocyte (MK) growth and development can be answered by carefully recording the history of the cells. Long-term and large-field live cell imaging was used to study megakaryopoiesis at the single cell level, from human CD34^{+} cord blood (CB)- or adult bone marrow (BM)-cells in the presence of thrombopoietin with or without nicotinamide (NIC). Overall, over 9,300 cells were tracked and their fates analyzed. NIC treatment resulted in increased polyploidization of CB-MKs up to level normally observed with BM-MKs without NIC. Despite this, NIC failed to enhance platelet production, which correlated with a 7- and 31- fold reduction in proplatelet formation among tetraploid and octaploid CB-MKs, respectively. Surprisingly, significant fractions of diploid and polyploid CB-MKs were observed to undergo complete proplatelet regression. Though rare, reversal of proplatelet formation led to the formation of regular round cells that could then undergo endomitosis, mitosis or cell death. Cell cycle measurements of tracked cells undergoing mitosis and endomitosis demonstrated that the cell fate and ploidy level have major impacts on cell cycling time. Finally, global analysis of the tracked cells was used to developed MK lineage trees, which led to the identification of four recurrent cell lineage types for cells undergoing MK differentiation.

Plusieurs questions fondamentales entourant la croissance et le développement des cellules mégakaryocytaires (MKs) peuvent être répondues en analysant attentivement l'historique des MKs. Un système complexe d'imagerie cellulaire à grande échelle et à long terme a été utilisé pour étudier la mégakaryopoïèse au niveau unicellulaire. Pour ce faire, les cellules CD34^{+} issues de sang de cordon (CB) et cellules de la moelle osseuse (BM) adulte ont été mises en culture en présence de la thrombopoïétine, avec ou sans nicotinamide (NIC). Dans l'ensemble, plus de 9,300 cellules ont été suivies, et ce, jusqu'à la fin de leurs vies. Ainsi, le traitement avec NIC permettait une augmentation de la polyploïdisation des cellules MKs provenant de CB à un niveau normalement observé avec les cellules MKs provenant de la BM sans traitement de NIC. Malgré cette observation, le traitement à la NIC n'a pas permis d'augmenter le niveau de production des plaquettes provenant de SC, résultat qui est en

corrélation avec une réduction de 7 - et 31- fois la formation des proplaquettes à partir des MKs tétraploïdes et octoploïdes respectivement. De plus, nous avons observé une régression complète des filaments de proplaquettes sur des CB-MKs diploïdes et polyploïdes. Bien que rare, l'inversion de la formation des proplaquettes conduit à la formation de cellules rondes régulières qui pouvaient alors entrer en endomitose, en mitose ou en mort cellulaire. De plus, la mesure de la durée du cycle cellulaire de cellules en mitose et en endomitose a permis de démontrer que le devenir des cellules et le niveau de ploïdie ont un impact majeur sur la durée du cycle cellulaire. Finalement, l'analyse globale de ces cellules a permis l'élaboration d'arbres générationels des MKs, qui ont conduit à l'identification de quatre types de lignage cellulaire pour les cellules MKs ayant entamé le processus de différenciation.

6.2. Introduction

Although global population-based study is a common approach to understand cell biology, many biologists and engineers are now focusing their research work at the single cell level. For instance, the analysis of single-cell gene expression by RT-PCR[1-3], flow cytometry[4-6] or time-lapse video microscopy[7-9] have been reported to allow a better understanding of the cell biology. Our group has recently developed a long-term and large-field live cell imaging platform capable of maintaining and observing cell cultures over periods of up to 5 days. This tool was first used to study the complex phenomenon of megakaryocyte (MK) differentiation and maturation from cord blood (CB)- and adult bone marrow (BM)-CD34$^+$ cells[10].

MKs are derived in the marrow from multipotent progenitor cells. During maturation, MK undergo polyploidization through endomitosis, a process by which DNA is replicated, but the cell fails to proceed through the last stage of cell division, cytokinesis[11]. Using our live cell imaging platform on CB- and BM-CD34$^+$ cells undergoing MK differentiation, it was shown that polyploid MK could still complete cytokinesis and give rise to polyploid daughter cells with normal developmental fates[10]. This process was found more frequent in CB-derived MKs but occurred at a lower rate in BM-derived MKs and/or in MKs of greater ploidy levels for both CB- and BM-MKs[10].

The properties of MKs produced *ex vivo* depend largely upon the origin of the HSCs from which they are derived. For instance, the mean ploidy level of MKs derived from human CB-CD34$^+$ cells is significantly lower than that of adult HSCs. Around 80 - 85% of CB-MK remain diploid, while more than 50% of adult peripheral blood (PB)- and BM-MK reaches a ploidy equal or greater than 4N[12-15]. In addition, the maximum ploidy level reached by CB-MK is normally of 16N, while adult derived MK can reach 64N and sometime 128N[14,16-18]. Ploidy level of MK also varies between species, as the modal ploidy level for human MK is usually of 16N versus 32N in some mouse species[16,19].

Nicotinamide (NIC, vitamin B$_3$) has been shown to enhance the process of MK polyploidization of PB-MKs[20]. Giammona et al. showed that this effect was dose-dependent, and that the treated cells were larger, highly lobulated and reached ploidy level

up to 64N (compared to 16N for the NIC-free control)[20], without altering MK ultrastructure[21]. Interestingly, *in vitro* platelet production is lower for CB-MKs compared to PB-MKs due to their reduced ploidy level[14]. Hence, it was hypothesized that platelet yields from CB-CD34$^+$ cells could be improved by increasing MK ploidy level using NIC. However, the impact of NIC treatment on platelet production and polyploidization of CB-MKs has yet to be assessed.

The objectives of this work were: i) to further investigate polyploid MK division and whether or not it is responsible for ploidy distribution, ii) to quantify the single-cell level analysis of MK differentiation *ex vivo*, and iii) introduce MK cell lineage tree patterns. In this study, quantitative analysis of cell development and fates during MK differentiation was performed on approximately 9,300 individual cells. These included ~4,900 CB- and BM-derived MKs originally tracked[10], ~1,700 CB-cells treated with NIC, ~1,100 CB-cells cultured with the MK differentiation cytokine cocktail BS1[22], and ~1,600 murine BM-cells undergoing MK differentiation to investigate whether division of polyploid MKs also occurred in this specie. Finally, a comprehensive global analysis of cell fate of CB-MK undergoing differentiation and maturation led to the development of cell lineage trees that provide a new insight into the existing patterns and process of megakaryopoiesis *ex vivo*.

6.3. Results

Impact of Cytokine Cocktail on the Mitosis and Endomitosis Rates of CB-MK *Ex Vivo*

Long-term and large-field time-lapse video microscopy was carried out on CB- or BM-CD34$^+$-enriched cells ($\geq$ 90% purity) induced to undergo megakaryocytic differentiation. MK cell differentiation, maturation and viability were previously shown to proceed normally with this system[10]. MK differentiation of tracked cells was followed in real time between day-0 and day-5, or between day-5 and day-9 or day-10.

Our group has previously showed that the cytokine cocktail BS1 composed of TPO (30 ng/ml), SCF (1 ng/ml), IL-6 (7.5 ng/ml) and IL-9 (13.5 ng/ml) promotes CB-MK expansion and platelet release[22]. First, it was investigated whether such a cocktail could change the rate of mitosis of polyploid MK in comparison to MK produced in culture supplemented

with TPO alone. In all, 1,148 CB-cells cultured with BS1 (989 x 2N, 110 x 4N, 4 x 6N, 34 x 8N, 10 x 16N, 1 x 32N) in two independent experiments were tracked from culture day-0 to day-5, and day-5 to day-9 (Table 6.1). When compared to our original results obtained in TPO cultures using the same experimental set-up[10], the cytokine cocktail BS1 significantly increased the viability and mitotic rate of diploids, which resulted in greater cell expansion (Table 6.1 and data not shown) as previously reported[22,23]. As expected based on the predominance of diploid cells (the dominant ploidy class) in the BS1 culture, mitosis was the dominant fate of diploids MKs (mean of 83.52 ± 7.15%). The cytokine cocktail BS1 had a moderate impact on the mitotic rate of tetraploids (4N) or octaploids (8N) MKs (Table 6.1). Nonetheless, but consistent with our previous observations in CB-MK cultures with TPO[10], a significant fraction of the tetraploids (30.91%) and octaploids (8.82%) completed cytokinesis (Table 6.1).

In contrast to mitosis, the cytokine cocktail BS1 significantly reduced the endomitosis rate of diploid MKs (Table 6.1), and increased the proplatelet formation rate significantly among tetraploids and slightly in other ploidy classes (Table 6.1) when compared to culture complemented with TPO, demonstrating the advantage of using BS1 cocktail.

To better compare the decision of cells to complete or not mitosis as a function of cell source, ploidy level and the cytokines to which they were exposed, a mitotic activity index was defined as the ratio of the number of cells that completed cytokinesis to the total number of cells that entered the M phase. As shown in Figure 6.1, the mitotic activity index reduced monotonously with the ploidy level and reached plateau at 32N level for both CB-MKs cultured with TPO or BS1 ($R^2 \geq 0.96$). As shown in Table 6.1, the mitotic activity index of diploid CB-MKs cultured with the cytokine cocktail BS1 was significantly higher than that cultured in TPO alone ($p < 0.05$). Nonetheless, this index for higher ploidy MKs was not altered significantly by the cytokine combinations used. In brief, this result shows that: i) the polyploid MK mitotic rate was not influenced by the use of a cytokine cocktail, ii) the previously observed increased MK expansion[22] with the BS1 cocktail was due mainly to the greater mitotic rate of diploid MKs, and iii) mitosis of polyploid MKs was also observed in culture supplemented with BS1 at the same level as TPO alone culture.

Impacts of NIC Treatment on the Mitotic and Endomitotic Rates of CB-MKs in Culture

Several drugs have been shown to influence the ploidy level of MKs in culture, such as the Src kinase inhibitor SU6656[17,24], the MAPK kinase inhibitor PD98059[25], and NIC[17,24]. To this date, the effect of NIC has only been shown on adult derived-MKs, from mobilized CD34$^+$ cells[17]. Hence, it was tested whether addition of NIC to CB-TPO cultures could alter the different cell fate frequencies (endomitosis, mitosis, proplatelet formation or death) for MKs of different ploidy levels. In all, 1,690 CB-cells treated with NIC (1225 x 2N, 218 x 4N, 10 x 6N, 72 x 8N, 66 x 16N, 55 x 32N and 44 x 64N) were tracked from culture day 0 to day 4.5, and day 4.5 to day 9. NIC treatment reduced the viability of diploid cells early in culture (data not shown), which reduced cell expansion as previously reported[17]. Addition of NIC later e.g. at day 4 in comparison to day 0, reduced the cell death but did not influence much the mean ploidy therefore this strategy was not continued (data not shown). Although it significantly reduced the frequency of mitosis for diploid MKs from 74% to 64% (Table 6.1, $p < 0.05$), mitosis still remained the dominant fate of diploid NIC-treated MKs. NIC treatment also reduced the mitotic rate of tetraploid ($p < 0.08$) and octaploid ($p < 0.001$) MKs by 35% and 72%, respectively (Figure 6.1 and Table 6.1). Nonetheless, a significant proportion of the tetra and octaploid MKs completed cytokinesis. MKs of ploidy levels greater or equal to 16N derived in the presence of NIC never completed cytokinesis (Table 6.1).

While NIC had little impact on the overall endomitotic rate of diploids between day-0 and day-4.5 it significantly enhanced this fate in diploids during the second phase of culture (day-4.5 and day-9) as shown in Figure 6.2A. Consistent with this, the mitotic rate of NIC-treated diploids tended to be reduced in the second phase of the culture compared to the control ($p < 0.09$, Figure 6.2A). In addition, the reduction of the mitotic and the increase of the endomitotic rates observed in the controls during the second phase of culture is consistent with the normal maturation kinetics of MKs derived from undifferentiated CD34$^+$ cells, which turned their activity from mitosis to endomitosis as culture progressed.

NIC also had a major influence on the endomitotic rate of polyploid CB-MKs (Table 6.1). Hence, a strong increase in the fraction of highly polyploid MKs was observed in NIC-

containing CB-cultures (Figures 6.2B and 6.S1, and Movie 6.S1, p < 0.05). Consistent with this, the maximal ploidy level obtained with NIC was increased to 64N, comparatively to 16N for untreated cells (Figure 6.2B). To validate the effect of NIC on polyploidization, ploidy of CB-MKs derived in bulk cultures with or without NIC was analyzed by flow cytometry. As shown in Figure 6.2C-D, these analyses confirmed the strong impact of NIC on the polyploidization of CB-MKs; a significant reduction in diploids accompanied by a considerable increase in ≥ 8N cells were observed at day 10 for CD41$^+$ MKs (p < 0.05). Taken together, these results demonstrate that NIC can increase the ploidy of CB-MKs by promoting the endomitosis rate and reducing the mitotic activity.

Further analysis, using curve fitting, showed that the mitotic activity index reduced monotonously with ploidy level in treated CB-MK as untreated CB- and BM-MK did. The mitotic activity indexes of BM- and NIC-treated CB-MKs were significantly lower than that of untreated CB-MK (p < 0.01, Figure 6.1), which is consistent in part with our previous study[10]. Taken together, these analyses demonstrate that NIC significantly promote endomitosis over mitosis in polyploid CB-MKs that brought to the level of BM-MK cultured in TPO (Figure 6.1).

Impact of NIC Treatment on Platelet Shedding

Next, it was investigated whether the increase in MK polyploidization observed in NIC treated CB-cultures would enhance platelet production. First, it was analyzed the live cell imaging data to determine the impact of NIC on proplatelet formation, the last step in MK maturation prior to platelet release. In contrast to polyploidization, NIC treatment significantly reduced (7 - 30 folds) proplatelet formation of CB-MKs in the TPO cultures, independently of their ploidy level (Table 6.1). Consistent with this, NIC reduced platelet production by 60% in bulk NIC CB-cultures supplemented with the optimized cytokine cocktail BS1[22] (Figure 6.3, p < 0.05). This reduction was not the result of reduced overall MK production as shown in Figure 6.3. Taken together these results demonstrate that NIC treatment fails to increase platelet production despite the increase in highly polyploid CB-MKs. Since an increase in ploidy is generally associated with increased platelet production, it appeared that NIC may have a negative impact on proplatelet formation and platelet release that together counterbalance the positive effect on polyploidization.

Proplatelet Formation is perhaps also a Reversible Phenomenon

The correlation between MK ploidy level and platelet production has been discussed to some extent in the literature[14]. It is generally believed that highly polyploid MKs produce more platelets[14,26]. The frequency of proplatelet formation amongst the tracked untreated MKs correlated positively with ploidy level, though proplatelet formation was not restricted to polyploid cells ($\geq$ 4N) since it was observed in a significant fraction of diploid cells (6.04% [1.5 - 8.2%]) , as presented in Table 6.1 and Figure 6.4A.

Proplatelet formation is closely associated with the induction of apoptosis in the terminally mature MKs[27]. To verify this correlation, 293 untreated CB-MK (107 x 2N, 53 x 4N, 90 x 8N and 43 x 16N) undergoing proplatelet extensions were analyzed (extracted from Table 6.1). Indeed, the majority of the CB-MKs that formed proplatelets died shortly after regardless of their ploidy levels (see Figure 6.4B and Movie 6.4B). However, 45% of the tracked diploids (48 out of 107), 11% of the tetraploids (6 out of 53) and 1% of the octaploids (1 out of 90) that underwent proplatelet formation survived. For these, the proplatelet filaments regressed completely leading to the formation of regular round shape cells (Figure 6.4C and Movie 6.4C). Fate analysis of these regenerated cells showed that these were then able to either i) undergo endomitosis and increase their ploidy level (6 of 48 x 2N and 1 of 6 x 4N), ii) complete cytokinesis (1 of 48 x 2N and 1 of 6 x 4N) or, iii) remain alive for a significant length of time (> 8 hours) (41 of 48 x 2N, 4 of 6 x 4N, and 1 of 1 x 8N). From the all possible cell fates, the reversal of proplatelet formation appeared to be a very rare phenomenon since it only occurred at a rate of 2.7%, 1.8% and 0.5% in diploids, tetraploids and octaploids, respectively. Despite tracking 125 BM-MK (12 x 2N, 44 x 4N, 40 x 8N and 29 x 16N) cells, this phenomenon was never observed in the BM-TPO cultures. These observations suggest that, contrary to the general belief[28,29], proplatelet formation can be a reversible phenomenon. However, more investigations are needed to clarify whether this phenomenon is a *bona fide* event, as opposed to a culture artifact and whether this can also occur in BM-derived MKs.

Murine Polyploid BM-MKs Do Not Undergo Cell Division in Culture

Murine BM-MKs appear to have an increased propensity to undergo endomitosis in culture since a significant proportion of murine MKs have been reported to reach ploidy level of 64N and even 128N[30,31], which is rarely observed with human MKs[14,15,32]. Given our unexpected finding that polyploid human MK can complete cytokinesis in *ex vivo* culture[10], it was investigated whether polyploid murine MK could also complete cell division. This was addressed by performing live cell imaging on murine BM-derived MKs. Despite following 1568 murine cells (980 x 2N, 196 x 4N, 196 x 8N, 196 x16N) from two experiments, division of polyploid murine cells was never observed, whereas mitosis of diploid cells (n = 608) and endomitosis of diploid (n = 196) and polyploid cells (n = 588) were frequently observed. These results suggest that division of polyploid MKs may not occur in murine MK, or may occur at a very low frequency (< 0.5%).

Impact of Cell Fate and Ploidy Level on MK Cell Cycling Time

Live cell imaging represents a useful approach to measure cell cycle duration. Analysis of the cell cycle time length distribution included 466 untreated (416 x 2N, 35 x 4N and 15 x 8N) and 227 NIC-treated CB-MKs (193 x 2N, 19 x 4N and 15 x 8N). In general, increases in ploidy level tended to increase cycling time for cells undergoing mitosis (Figure 6.5A) but not for those undergoing endomitosis (Figure 6.5B). Interestingly, addition of NIC strongly reduced the cycling time of cells undergoing either process (p < 0.05). In addition, contrary to untreated cells, the cycling times for both processes in the presence of NIC were identical and unaffected by polyploidization (Figure 6.5A-B).

Next, it was analyzed whether cell fate decision had an impact on cell cycle time. This was investigated by plotting the cycling time of mitotic cells vs the mitotic potential index (Figure 6.5C), and the cycling time of endomitotic cells vs endomitotic potential index (Figure 6.5D). The cell cycle duration for endomitosis and mitosis showed a negative linear correlation with the corresponding indexes for untreated CB-MKs, while this trend was abolished upon NIC treatment. Cell cycle time measurements also led to the demonstration that the time required for cells to complete a non-dominant fate is longer than that of the dominant fate. Hence, the time required for diploids to undergo endomitosis was greater

than that needed for mitosis (dominant fate, Table 6.1 and Figure 6.5B); whereas the cell cycle duration for polyploids undergoing mitosis was greater than that required for endomitosis (dominant fate, Table 6.1 and Figure 6.5A). Although addition of NIC resulted in reduction of cell cycling time, it did not alter the impact of the dominant fate on the cell cycle time duration.

Furthermore, analyses of the cumulative data of MK lineage trees (described below) showed that untreated CB-MKs displayed a maximum of 7 divisions during 5 days of imaging (between culture day 5 to 10, n = 97), while NIC-treated CB-MK divided a maximum of 9 times during 4 days of tracking (between culture days 4 to 8, n = 25). While the time-window are not exactly identical, estimation of cell cycling time from this data confirmed the cycle time reduction for cells treated with NIC (17.1 ± 1.88 vs 10.7 ± 1.12 hours for untreated cells, p < 0.01).

Impact of Culture Time on the Size of Diploid and Polyploid MKs

Another parameter that can be studied using live cell imaging is cell size distribution and evolution as a function of culture time. Several studies have shown that MK size increases importantly while maturing due to polyploidization and cytoplasmic maturation[33,34]. However, little is known about the details of these relationships. Consistent with other studies[33], our group previously showed that the cell size volume is increased by 2-fold (1.94 ± 0.15, n ≥ 40 for each ploidy class) following each round of endomitosis for polyploid cells[10]. This ratio becomes important after a number of rounds of endomitosis. For instance, a 32N cell, after four rounds of endomitosis, is 13.5 ± 0.44 times (not 16 times) larger than a 2N cell (n ≥ 40 for each ploidy class). As shown in Figure 6.6, diploids expanded over 2-fold (2.42 ± 0.24 on average over 8 divisions) following each round of mitosis. This increase in cell volume was even greater during the first divisions early in culture as it sometimes exceeded 3.5-fold (Figure 6.6).

Megakaryocytic Cell Lineage Trees

The cumulative information originally obtained from tracking TPO-derived CB-MKs[10] was then used to construct MK lineage trees. These represent the history of the cells within two

time windows: i) from day-0 to day-5 and ii) from day-5 to day-10 of the culture. Details on the construction and interpretations of the lineage trees are provided below and in *Supplementary Materials Text A*. A representative MK pedigree in the second time window is presented in Figure 6.7A. In this case, the unsynchronized original ancestral diploid cell (cell #1 from generation 1, or identification number (ID) of 1DT1) and the next two generations underwent mitosis leading to the formation of eight diploids (cells with IDs of 4DT8 to 4DT15 inclusively). This occurred asynchronously due to differences in cycling time for the cells in the second and subsequent generations (cycling times are indicated in hours after "=" sign). Distinct fates were observed for cells of the fourth generation as cousin cells with IDs of #4DT8 and #4DT10 underwent endomitosis and became 4N (thicker line width shows the cell size increase) while the other six divided to generate twelve 2N cells (Figure 6.7A).

After constructing lineage trees for a number of cells (97 original cells), it was investigated whether distinct recurrent patterns existed or not. Based on mitosis and endomitosis events, four major types of MK lineage tree patterns were observed and classified: i) the "*proliferative*'' lineage pattern, where an original 2N parent cell and all its descendants divided symmetrically into 2 x 2N daughter cells until either death or the end of an experiment (Figure 6.7B), ii) the "*polyploidization*" pattern, where an original parent cell and its descendants exclusively underwent endomitosis (Figure 6.S2A); iii) the "*quiescent*" pattern, where cells remained inactive till death (Figure 6.S2B); and iv) a "*mixed*" pattern of proliferation and polyploidization, where a portion of an original parent cell descendants divided or underwent polyploidization (Figures 6.7A and 6.S2C).

Finally, it was investigated whether the cell fates for the descendants were dictated in a deterministic or stochastic fashion. The mixed pattern was found highly diversified, in which the fates of the sister cells were often different from each other, the parent and the cousin cells, and also different from another individual cell who displayed such pattern by that stage of development. For instance, as shown in Figure 6.7A, two out of eight cells during the fourth generation underwent polyploidization that can vary from zero (as the case of Figure 6.S2C) to eight. In this dominant pattern (increased from 37.2% at day 5 to 88.5% at day 10), the switch from a mitotic to endomitotic cycle (polyploidization event)

and vice-versa (polyploid cell divisions) in the mixed patterns were not found correlated to generation number per se within an individual pattern or among individuals. These events together with proplatelet formation were observed during all generations. In addition, endomitosis was observed within the first generation of the culture at day 0, presumably due to the contaminating $CD41^+$ cells (~1.5%). These results demonstrate that polyploidization or proplatelet formation of a given cell might be partially determined by the decision of its ancestor to enter a given fate pathway, together with other factors (intrinsic or extrinsic) that must also influence the fate decision of a cell. Regardless of the high diversity of mixed patterns, few mixed patterns of CB-MK lineage trees showed predictable fates for the descendents (Figure 6.S3). Indeed, the fate of each descendent in this typical mixed pattern was found quite similar to that of the cousin or parent cells. However, this type of lineage tree was observed rarely ($\leq 1.33\%$).

In summary, the incorporation of the information derived from the global analysis of cell fates throughout multiple generations into lineage trees has made possible the identification of four distinct recurrent cell lineage patterns for CB-cells undergoing MK differentiation and maturation that could be useful for correlation studies.

6.4. Discussion

Several fundamental questions surrounding megakaryocytic cell growth and development can be answered by carefully recording the history of the cells through multiple generations. In this study, it was demonstrate that long-term and large-field live cell imaging technique is a useful approach to study life and fates of a cell in general and as done in this work, in the context of multipotent cells undergoing MK differentiation. The presented multiple analyses of megakaryocytic cell life at the single cell level provided the basis to study the impact of NIC on polyploidization and proplatelet formation of CB-MKs, investigate cell cycle time duration as a function of ploidy level and cell fate. This study also reveals that proplatelet formation is in some cases a reversible phenomenon. Within every step of this analysis, hundreds of individual cells were analyzed and results were compared between diploid and polyploid MKs. Finally, global analysis of the fate of the MKs in culture led to the identification of four types of cell lineage tree patterns.

Comparison of the major cell fates of CB-MK of various ploidy classes derived in TPO or in the optimized cytokine cocktail BS1 revealed that the cytokine combination used in BS1 had some direct impact on the fate of the MK in culture. Among the differences observed, there was a reduction in endomitotic rate and an increase in the mitotic rate for diploid MKs with BS1. Proplatelet formation rates were also found increased by BS1 for both tetra and octaploid MKs. These result are certainly consistent with the improved MK and platelet yields achieved following BS1 optimization[22].

In contrast to cytokine stimulus, it was shown that NIC treatment could raise the ploidy level of CB-MKs. This increase in ploidy was the direct results of increase endomitotic rate observed in diploids and polyploid MKs. On the other hand, NIC significantly reduced proplatelet formation for all ploidy level. The reduction in proplatelet formation observed with CB-MKs is opposite to what Giammona et al. originally reported with adult-derived MKs[17]. The reason for this discrepancy is currently unknown but it might reflect another different property of CB-derived MKs from adult MKs in terms of response to their environment[13,35], or perhaps due to differences in the culture medium and experimental set-up used. Consistent with our result, platelet production decreased significantly in CB-cultures treated with NIC. It remains to be determined whether complete removal of NIC before the onset of proplatelet formation and platelet production (~ day 10 - 12, maximal at day 14) would restore normal platelet production. However, preliminary results (Marine Tymen in N. Pineault's laboratory) confirmed the reduction in platelet production in bulk CB-cultures treated with NIC for just 4 days (between days 3 - 7).

Long-term and large-field live cell imaging also confirmed that CB- and BM-MKs of low ploidy levels (2N and 4N) were capable of proplatelet formation. However, it was also observed that some polyploid CB-MKs that had initiated proplatelet formation could revert to a regular circular shape, indicating that in some cases proplatelet formation is also a reversible process. The regenerated cells were then able to undergo a normal development program, such as endomitosis or mitosis. Whether such phenomenon is due to a culture artifact cannot be ruled out at this time. The underlying mechanism responsible for this is unclear at this time, but perhaps this occurs following a late failure of apoptosis[27]. In the marrow, proplatelet filaments can extend into the circulation where shear stress leads to

their fragmentation[36]. Since reversal of proplatelet formation was, as for the division of polyploid MKs, inversely correlated with ploidy level, it is possible that such mechanism limits proplatelet formation from diploids or low polyploid MKs. These data support the previously postulated idea that the mechanism regulating polyploidization might be independent from that regulating cytoplasmic maturation[16,37].

Contrary to what had been observed with human MKs, mitosis of polyploid murine MKs was never visualized. Hence, endomitosis was the dominant fate for murine polyploid MKs that initiated DNA replication. This concords with other studies that have used time-lapse video microscopy to study murine MK endomitosis[38-40]. This significant difference between the two species may explain in part why murine MKs have a greater propensity to become highly polyploid in culture and why their modal ploidy level is greater than that of human MKs[19,30,31]. Hence this study and our previous findings[10] demonstrating that CB-MKs have a greater polyploid cell division rate, suggest that there exist an inverse correlation between the ploidy potential of the MKs and their polyploid cell division rate, which are dictated by the origin of the stem cells from which MKs are derived. Taken together, this further supports the hypothesis that the polyploidization potential of MKs is likely dictated by their proliferative capacity.

Theoretically, one could assume that the duration of an endomitotic cycle could be slightly shorter than that of a mitotic cycle due to an incomplete M phase and since it was previously shown that the time for DNA duplication is identical for both processes[16]. However, our results suggest that the cell cycle time duration is rather dependent on the ploidy level and fate of the cells. Indeed, it was demonstrated that the cycling time is longer if that fate is not the dominant one, as diploid cells displayed longer endomitotic cycle while polyploid cell showed longer mitotic cycles. Treatment of CB-MKs with NIC resulted in reduced cell cycling time. Similar influence of NIC on other HSC lineage differentiations such as myeloid has also been reported[41]. It has been shown that p53 is a key regulator of cell cycle arrest and apoptosis in response to DNA damage[42] and NIC downregulates p53[43]. NIC depletion in cultured cancer cells caused decreased p53 (the tumor suppressor protein)[44]. Furthermore, it was shown that NIC deficiency in human may contribute to increased frequency of gastrointestinal cancers in certain populations and NIC

supplementation in animal models has opposing effect on carcinogenesis[45]. Thus, NIC supplementation in MK culture may have influenced the progression of cells in maturation steps by regulating the genes related to checkpoint controls in the cell cycle and/or involved in cell endomitosis and apoptosis that disable the cell platelet production capacity.

Recording and classification of all cellular events together with the analysis of cell lineage trees also made possible the identification of recurrent patterns of MK growth and development. Cell lineage trees have been often constructed and described in the literature for different cell types[46,47]. It is however reported here for the first time for megakaryopoiesis. Lineage tree patterns were mainly defined based on the mitotic or endomitotic fates of the tracked cells (not proplatelet formation), and classified into four pattern types of quiescent, proliferative, polyploidizing or mixed. Few if any studies have used such an approach to shed some light on the complex fate-decision dilemma that takes place when multipotent stem cells undergo unilineage differentiation. This approach provided valuable information on the fates of CD34$^+$ cells and their descendants. Among other things, it demonstrated that not all ancestors and their descendents are capable of undergoing mitosis (i.e. proliferative pattern), endomitosis (i.e. polyploidization pattern), or a mix of both (i.e. mixed pattern), while other remained quiescent. The precise mechanism regulating MK fates and pattern distributions *ex vivo* still remains unclear, however our results provide indications on what these fates are and on their likelihood. To date, several genes have been identified as regulator of megakaryopoiesis (e.g. GATA-1, FOG-1 etc[48]), whether these are involved in cell fate determination remains to be investigated in the future. The development of this type of analyses combined with cell surface markers and exogenous gene expression or gene-reporter technologies opens a new powerful avenue to investigate such questions.

In summary, this study exploited the use of live cell imaging to carry out a series of quantitative analysis at the single cell level on the process of MK differentiation *ex vivo*. Our results of CB-cells treatment with NIC and murine marrow MK support the previous finding that polyploid MK division is a potential mechanism responsible for ploidy distribution[10]. It was also shown that proplatelet formation is potentially a reversible phenomenon. Whether this occurs *in vivo* remains to be addressed in future studies.

Construction of cell lineage trees should provide a valuable approach to deepen our understanding of complex cell behaviours such as those observed with stem cells. Combination of long-term live cell imaging with genetic inquiries will definitely open a new paradigm in cancer and stem cell development.

6.5. Materials and Methods

CD34-Enriched CB- and BM-Cells

Human umbilical CB-cells were collected and cryopreserved as previously described[10,23,49], following a protocol approved by Héma-Québec and Laval University ethical committees. Cryopreserved human BM-CD34$^+$ cells ($\geq$ 90% purity) were obtained from Lonza (Chicago, IL, USA). CD34-enriched cells ($\geq$ 90%) were cultured in a serum free medium[23] supplemented with either TPO alone (100 ng/ml) or the cytokine cocktail BS1: SCF (1 ng/ml), TPO (30 ng/ml), IL-9 (13.5 ng/ml) and IL-6 (7.5 ng/ml)[22] (Peprotech, Rocky Hill, NJ). Imaging culture cells were initiated with 2.5 – 3.6 x 10^3 cells/ml, supplemented with 3.75 g/L methylcellulose (Sigma-Aldrich) and 1% penicillin-streptomycin solution (Invitrogen), as previously described[10]. In some CB-culture, NIC (Sigma-Aldrich, St-Louis, MO, USA) was added at day 0 and day 4 at 4.5 mM to the TPO culture. Murine BM-cells (wild-type female BALB/c mice) were gifts by Dr. Renée Bazin and were treated like human BM-MKs, except the TPO concentration during the cell culture was of 200 ng/ml.

Flow Cytometry Analysis

Samples from the cultures were taken frequently and analyzed by flow cytometry using FACS-Calibur (Becton Dickinson Immunocytometry Systems, San Jose, CA) to measure MK and platelet counts and surface expressions as previously described[10,23,49]. Murine BM-cells were analyzed using rat anti-mouse CD41 conjugated with Fluorescein Isothiocyanate (catalogue # 553848, Becton Dickinson Immunocytometry Systems, San Jose, CA). Ploidy analysis was done on CD41$^+$ cells at day-10 as previously described[49].

Live Cell Imaging

Long-term and large-field live cell imaging was performed using an automated inverted microscope (IX81, Olympus, Canada), and cells were maintained in custom built chambers, as previously described[10].

Cell Size Measurements

Cells were first identified by image segmentation as described in *Supplementary Text B* and as previously reported[10], and then their sizes were quantified by measurements of the projected cell surface area (A). Cell volume (V) and diameter (D) were then estimated based on spherical assumption of cell shape ($V \propto A^{3/2}$ and $D \propto A^{1/2}$). The relative cell volume for each cell was computed and normalized, dividing by the initial cell volume (immediately after mitosis or endomitosis). Cell sizes were quantified by calculating the volume (average of 2 - 5 frames) of the parental cells just before starting cleavage furrow and that of the daughter cells right after birth.

Statistical Analysis

Comparisons were analyzed using the Student t-test. Results were regarded as significant when p-values were below 0.05.

Acknowledgments

Abbreviations

CB	Cord Blood
BS1	Best platelet production culture medium found at Héma-Québec
BM	Bone Marrow
DNA	Deoxyribonucleic Acid
DT	Division Time (hour) in cell lineage tree
HSC	Hematopoietic Stem Cell
IL	Interleukin

LT	Life Time (hour) in cell lineage tree
MAPK	Mitogen-activated protein (MAP) kinases
MK	Megakaryocyte
NIC	Nicotinamide
PB	Peripheral Blood
PT	Ploidy Time or endomitosis cycling time (hour) in cell lineage tree
SCF	Stem Cell factor
Src	Sarcoma
TPO	Thrombopoietin

6.6. References

1. Sakhinia E, Weaver DL, Nunez C, Brunet C, Bostock V, Brady G. Single-cell RT-PCR cDNA subtraction. Methods Mol Biol. 2008;461:667-674.
2. Muller D, Jones PM, Persaud SJ. Single-cell RT-PCR identification of genes expressed by human islet endocrine cells. Methods Mol Biol. 2009;560:73-86.
3. Toledo-Rodriguez M, Markram H. Single-cell RT-PCR, a technique to decipher the electrical, anatomical, and genetic determinants of neuronal diversity. Methods Mol Biol. 2007;403:123-139.
4. Duhamel S, Gregori G, Van Wambeke F, Mauriac R, Nedoma J. A method for analysing phosphatase activity in aquatic bacteria at the single cell level using flow cytometry. J Microbiol Methods. 2008;75:269-278.
5. Perez OD, Nolan GP. Phospho-proteomic immune analysis by flow cytometry: from mechanism to translational medicine at the single-cell level. Immunol Rev. 2006;210:208-228.
6. Prussin C. Cytokine flow cytometry: understanding cytokine biology at the single-cell level. J Clin Immunol. 1997;17:195-204.
7. Ecker RC, Steiner GE. Microscopy-based multicolor tissue cytometry at the single-cell level. Cytometry A. 2004;59:182-190.
8. Errington RJ, Marquez N, Chappell SC, Wiltshire M, Smith PJ. Time-lapse microscopy approaches to track cell cycle progression at the single-cell level. Curr Protoc Cytom. 2005;Chapter 12:Unit 12 14.
9. Nancharaiah YV, Rajadurai M, Venugopalan VP. Single cell level microalgal ecotoxicity assessment by confocal microscopy and digital image analysis. Environ Sci Technol. 2007;41:2617-2621.
10. Leysi-Derilou Y, Robert A, Duchesne C, Garnier A, Boyer L, Pineault N. Polyploid megakaryocytes can complete cytokinesis. Cell Cycle. 2010;9:2589-2599.
11. Lordier L, Jalil A, Aurade F, et al. Megakaryocyte endomitosis is a failure of late cytokinesis related to defects in the contractile ring and Rho/Rock signaling. Blood. 2008;112:3164-3174.
12. Bornstein R, Garcia-Vela J, Gilsanz F, Auray C, Cales C. Cord blood megakaryocytes do not complete maturation, as indicated by impaired establishment of endomitosis and

low expression of G1/S cyclins upon thrombopoietin-induced differentiation. Br J Haematol. 2001;114:458-465.

13. van den Oudenrijn S, von dem Borne AE, de Haas M. Differences in megakaryocyte expansion potential between CD34(+) stem cells derived from cord blood, peripheral blood, and bone marrow from adults and children. Exp Hematol. 2000;28:1054-1061.

14. Mattia G, Vulcano F, Milazzo L, et al. Different ploidy levels of megakaryocytes generated from peripheral or cord blood CD34+ cells are correlated with different levels of platelet release. Blood. 2002;99:888-897.

15. Miyazaki R, Ogata H, Iguchi T, et al. Comparative analyses of megakaryocytes derived from cord blood and bone marrow. Br J Haematol. 2000;108:602-609.

16. Cramer EM, Vainchenker W. Chapter 25. Platelet Production: Cellular and Molecular Regulation (ed 5th). Philadelphia, PA: Lippincott Williams & Wilkins; 2006.

17. Giammona LM, Fuhrken PG, Papoutsakis ET, Miller WM. Nicotinamide (vitamin B3) increases the polyploidisation and proplatelet formation of cultured primary human megakaryocytes. Br J Haematol. 2006;135:554-566.

18. Ravid K, Lu J, Zimmet JM, Jones MR. Roads to polyploidy: the megakaryocyte example. J Cell Physiol. 2002;190:7-20.

19. Papadantonakis N, Ravid K. Chapter 5. Development of Megakaryocytes. In: Kee AWaB, ed. Molecular Basis of Hematopoiesis: Springer Science + Business Media; 2009:95-126.

20. Giammona LM, Papoutsakis E, Miller WM. Nicotinamide Enhances the Polyploidization of Primary Megakaryocytes; 2005.

21. Giammona LM, Panuganti S, Kemper JM, et al. Mechanistic studies on the effects of nicotinamide on megakaryocytic polyploidization and the roles of NAD+ levels and SIRT inhibition. Exp Hematol. 2009;37:1340-1352 e1343.

22. Cortin V, Garnier A, Pineault N, Lemieux R, Boyer L, Proulx C. Efficient in vitro megakaryocyte maturation using cytokine cocktails optimized by statistical experimental design. Exp Hematol. 2005;33:1182-1191.

23. Boyer L, Robert A, Proulx C, Pineault N. Increased production of megakaryocytes near purity from cord blood CD34+ cells using a short two-phase culture system. J Immunol Methods. 2008;332:82-91.

24. Lannutti BJ, Blake N, Gandhi MJ, Reems JA, Drachman JG. Induction of polyploidization in leukemic cell lines and primary bone marrow by Src kinase inhibitor SU6656. Blood. 2005;105:3875-3878.

25. Guerriero R, Parolini I, Testa U, et al. Inhibition of TPO-induced MEK or mTOR activity induces opposite effects on the ploidy of human differentiating megakaryocytes. J Cell Sci. 2006;119:744-752.

26. Kaushansky K. The enigmatic megakaryocyte gradually reveals its secrets. Bioessays. 1999;21:353-360.

27. Clarke MC, Savill J, Jones DB, Noble BS, Brown SB. Compartmentalized megakaryocyte death generates functional platelets committed to caspase-independent death. J Cell Biol. 2003;160:577-587.

28. Battinelli EM, Hartwig JH, Italiano JE, Jr. Delivering new insight into the biology of megakaryopoiesis and thrombopoiesis. Curr Opin Hematol. 2007;14:419-426.

29. Italiano JE, Jr., Lecine P, Shivdasani RA, Hartwig JH. Blood platelets are assembled principally at the ends of proplatelet processes produced by differentiated megakaryocytes. J Cell Biol. 1999;147:1299-1312.

30. Broudy VC, Lin NL, Kaushansky K. Thrombopoietin (c-mpl ligand) acts synergistically with erythropoietin, stem cell factor, and interleukin-11 to enhance murine megakaryocyte colony growth and increases megakaryocyte ploidy in vitro. Blood. 1995;85:1719-1726.

31. Carow CE, Fox NE, Kaushansky K. Kinetics of endomitosis in primary murine megakaryocytes. J Cell Physiol. 2001;188:291-303.

32. Debili N, Issaad C, Masse JM, et al. Expression of CD34 and platelet glycoproteins during human megakaryocytic differentiation. Blood. 1992;80:3022-3035.

33. Arriaga M, South K, Cohen JL, Mazur EM. Interrelationship between mitosis and endomitosis in cultures of human megakaryocyte progenitor cells. Blood. 1987;69:486-492.

34. Tomer A. Human marrow megakaryocyte differentiation: multiparameter correlative analysis identifies von Willebrand factor as a sensitive and distinctive marker for early (2N and 4N) megakaryocytes. Blood. 2004;104:2722-2727.

35. De Bruyn C, Delforge A, Martiat P, Bron D. Ex vivo expansion of megakaryocyte progenitor cells: cord blood versus mobilized peripheral blood. Stem Cells Dev. 2005;14:415-424.

36. Junt T, Schulze H, Chen Z, et al. Dynamic visualization of thrombopoiesis within bone marrow. Science. 2007;317:1767-1770.

37. Chang Y, Bluteau D, Debili N, Vainchenker W. From hematopoietic stem cells to platelets. J Thromb Haemost. 2007;5 Suppl 1:318-327.

38. Geddis AE, Fox NE, Tkachenko E, Kaushansky K. Endomitotic megakaryocytes that form a bipolar spindle exhibit cleavage furrow ingression followed by furrow regression. Cell Cycle. 2007;6:455-460.

39. Geddis AE, Kaushansky K. Endomitotic megakaryocytes form a midzone in anaphase but have a deficiency in cleavage furrow formation. Cell Cycle. 2006;5:538-545.

40. Papadantonakis N, Makitalo M, McCrann DJ, et al. Direct visualization of the endomitotic cell cycle in living megakaryocytes: differential patterns in low and high ploidy cells. Cell Cycle. 2008;7:2352-2356.

41. Skokowa J, Lan D, Thakur BK, et al. NAMPT is essential for the G-CSF-induced myeloid differentiation via a NAD(+)-sirtuin-1-dependent pathway. Nat Med. 2009;15:151-158.

42. Oren M. Decision making by p53: life, death and cancer. Cell Death Differ. 2003;10:431-442.

43. Spronck JC, Nickerson JL, Kirkland JB. Niacin deficiency alters p53 expression and impairs etoposide-induced cell cycle arrest and apoptosis in rat bone marrow cells. Nutr Cancer. 2007;57:88-99.

44. Jacobson EL, Shieh WM, Huang AC. Mapping the role of NAD metabolism in prevention and treatment of carcinogenesis. Mol Cell Biochem. 1999;193:69-74.

45. Surjana D, Halliday GM, Damian DL. Role of nicotinamide in DNA damage, mutagenesis, and DNA repair. J Nucleic Acids. 2010; Jul 25,157591.

46. Ramunas J, Illman M, Kam A, et al. True monolayer cell culture in a confined 3D microenvironment enables lineage informatics. Cytometry A. 2006;69:1202-1211.

47. Ramunas J, Montgomery HJ, Kelly L, Sukonnik T, Ellis J, Jervis EJ. Real-time fluorescence tracking of dynamic transgene variegation in stem cells. Mol Ther. 2007;15:810-817.

48. Wang X, Crispino JD, Letting DL, Nakazawa M, Poncz M, Blobel GA. Control of megakaryocyte-specific gene expression by GATA-1 and FOG-1: role of Ets transcription factors. Embo J. 2002;21:5225-5234.

49. Pineault N, Boucher JF, Cayer MP, et al. Characterization of the effects and potential mechanisms leading to increased megakaryocytic differentiation under mild hyperthermia. Stem Cells Dev. 2008;17:483-493.

50. Gonzalez RC, Woods RE. Digital image processing (ed 2nd). Upper Saddle River, N.J.: Prentice Hall; 2002.

51. Gonzalez RC. Digital Image Processing Using Matlab. Upper Saddle River: Prentice Hall; 2004.

52. McAndrew A. Introduction to digital image processing with Matlab. Boston, MA.: Thomson Course Technology; 2004.

53. Semmlow JL. Biosignal and biomedical image processing : Matlab-based applications. New York: Marcel Dekker; 2004.

6.7. Tables and Figures

6.7.1. Tables

Table 6.1: Fates of megakaryocytes derived in CB- and BM-CD34$^+$ TPO or BS1 cultures, with or without treatment by nicotinamide (NIC). Mean percentage of cumulative results shown for two observation time windows (day 0 - 5 and 5 - 10).

Ploidy Level	CB-MK Fates N = 4,968	TPO$^\$$ r = 5^a, N = 2,320^b	BS1 Cocktail r = 2, N = 1,133	TPO+NIC r = 2, N = 1,515
	N = 3,986	**n = 1,772^c**	**n = 989**	**n = 1,225**
2N	Endomitosis	12.47% [9.3-27.1%]^d	7.38% [5.1-9.2%]*	13.63% [13.3-16%]
	Mitosis	74.21% [69.3-76.9%]	83.52% [76.6-90.9%]*	63.84% [56.2-66.7%]*
	Proplatelet	6.04% [1.5-8.2%]	7.79% [3.6-9.7%]	0.33% [0.3-0.4%]*
	Death	7.28% [2.0-10.2%]	2.79% [2.1-3.8]*	22.20% [19.6-29.1%]**
	N = 668	**n = 340**	**n = 110**	**n = 218**
4N	Endomitosis	49.71% [46-71.4]	43.64% [31.0-51.5%]	74.31% [68.2-77.0%]**
	Total Mitosis:	30.88% [12.3-38.7%]	30.91% [25.0-40.5%]	20.18% [17.8-24.2%]
	Division to 2x4N	18.82% [4.8-24.6%]	21.82% [13.2-35.7%]	11.93% [11.8-12.1%]
	Division to 2N & 6N	9.71% [4.8-10.6%]	3.64% [2.4-6%]*	4.59% [3.3-7.6%]
	Division to 2x2N & 4N	2.35% [1.0-4.8%]	5.45% [2.4%-7.4%]	3.21% [2.6-4.5%]
	Division to 4x2N	0%	0%	0.46% [0.0-0.7%]**
	Proplatelet	15.59% [9.5-18.8%]	21.82% [20.6-23.8]*	2.29% [2.0-3.0%]**
	Death	3.82% [2.1-7.4%]	3.64% [2.9-4.8%]	3.21% [2.6-4.5%]
	N = 352	**n = 208**	**n = 72**	**n = 72**
8N	Endomitosis	41.83% [22.2-59.5%]	29.41% [16.7-36.4%]*	91.67% [88.2-94.7%]**
	Total Mitosis:	10.10% [2.7-11.3%]	8.82% [8.3-9.1%]	2.78% [2.6-2.9%]**
	Division to 2x8N	3.85% [2.5-5.7%]	0%**	0%**
	Division to 4N & 12N	4.81% [2.5-9.4%]	5.88% [4.5-8.3%]	2.78% [2.6-2.9%]*
	Division to 2x4N & 8N	1.44% [0-2.7%]	2.94% [0-4.5%]%	0%**
	Proplatelet	43.27% [22.6-64.2%]	55.88% [50.0-66.7%]	1.39% [0-2.9%]**
	Death	4.81% [2.7-6.2%]	5.88% [4.5-8.3%]	4.17% [2.6-5.9%]

$^\$$Details of the experiment are as previously published[10]. a: r: number of independent experiments; b: N: total number of tracked cells, c: n: number of tracked cells; d: range observed [minimum - maximum]; *student t-Test P-Value (CB-TPO vs. CB-TPO+NIC or vs. CB-BS1), * p < 0.05, ** p < 0.0001.

6.7.2. Figures
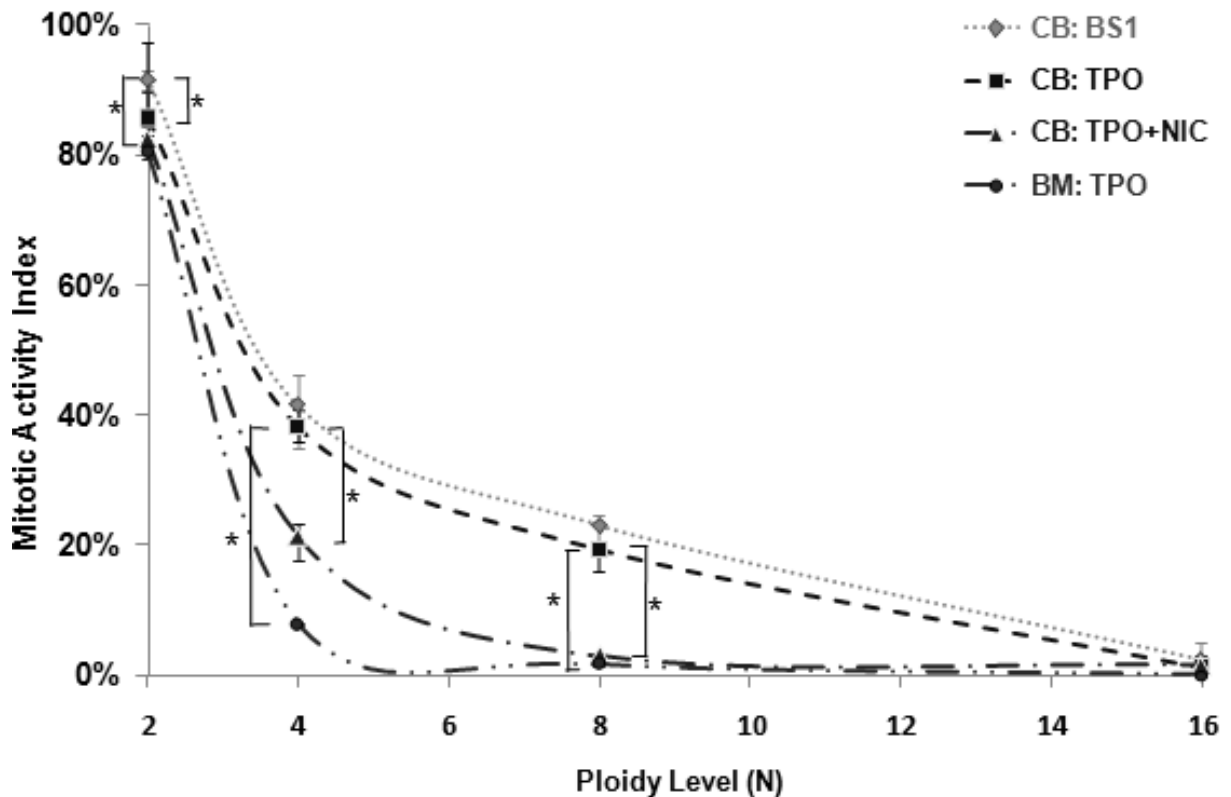
Figure 6.1: Comparison of mitotic activity index of polyploid MKs derived from CB- and BM-CD34$^+$-enriched cells. The mitotic activity index was defined as the ratio of the number of cells that completed cytokinesis to the total number of cells that entered M phase. The analysis included 2,320 CB-cells cultured with TPO (mean ± SEM, r = 5), 1,133 CB-cells cultured with BS1 cytokine cocktail (r = 2), 1,515 CB-cells cultured with TPO and treated with NIC (r = 2), and 1,214 BM-cells cultured with TPO (r = 5), in which r shows the number of experiments and * $p < 0.05$.
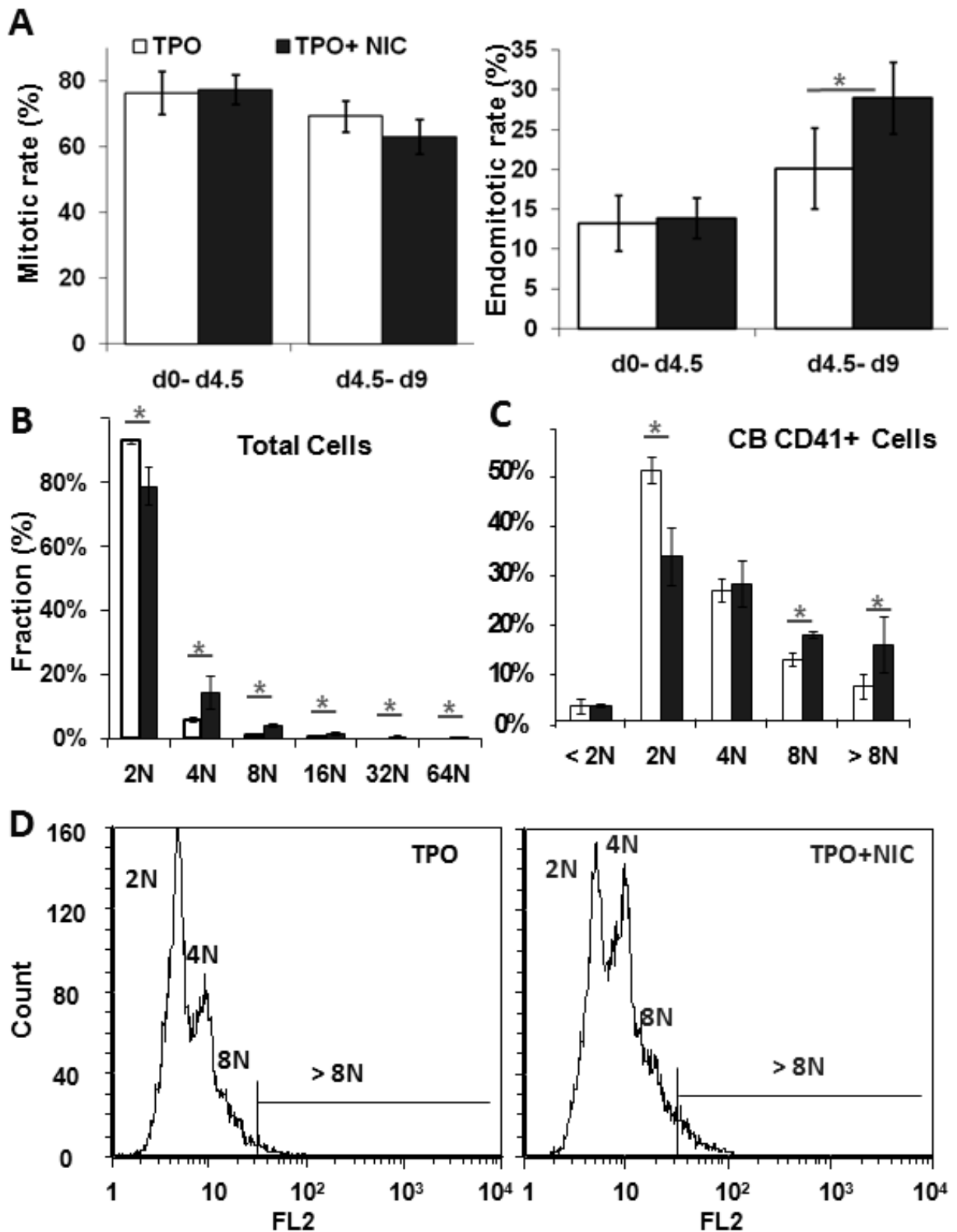
Figure 6.2: Addition of nicotinamide (NIC) to CB-TPO cultures increases the ploidy level of the MKs. **A)** Mitotic and endomitotic rate of CB-cells grown in TPO-culture treated or not with NIC (mean ± SEM shown). **B)** Ploidy level distribution of tracked CB-cells in TPO culture with/without 4.5 mM NIC (mean ± SEM, r = 2) from day 0 until day 9. **C)**

Ploidy level distribution of day-10 CB-CD41$^+$ cells in bulk TPO culture with or without NIC evaluated by flow cytometry (mean ± SEM of 3 independent experiments). **D)** ploidy histograms of CD41$^+$ cells derived in CB-TPO cultures with or without NIC treatment by flow cytometry (representative result shown, r = 3). * indicates that the difference between the TPO and TPO+NIC culture are significant p < 0.05.
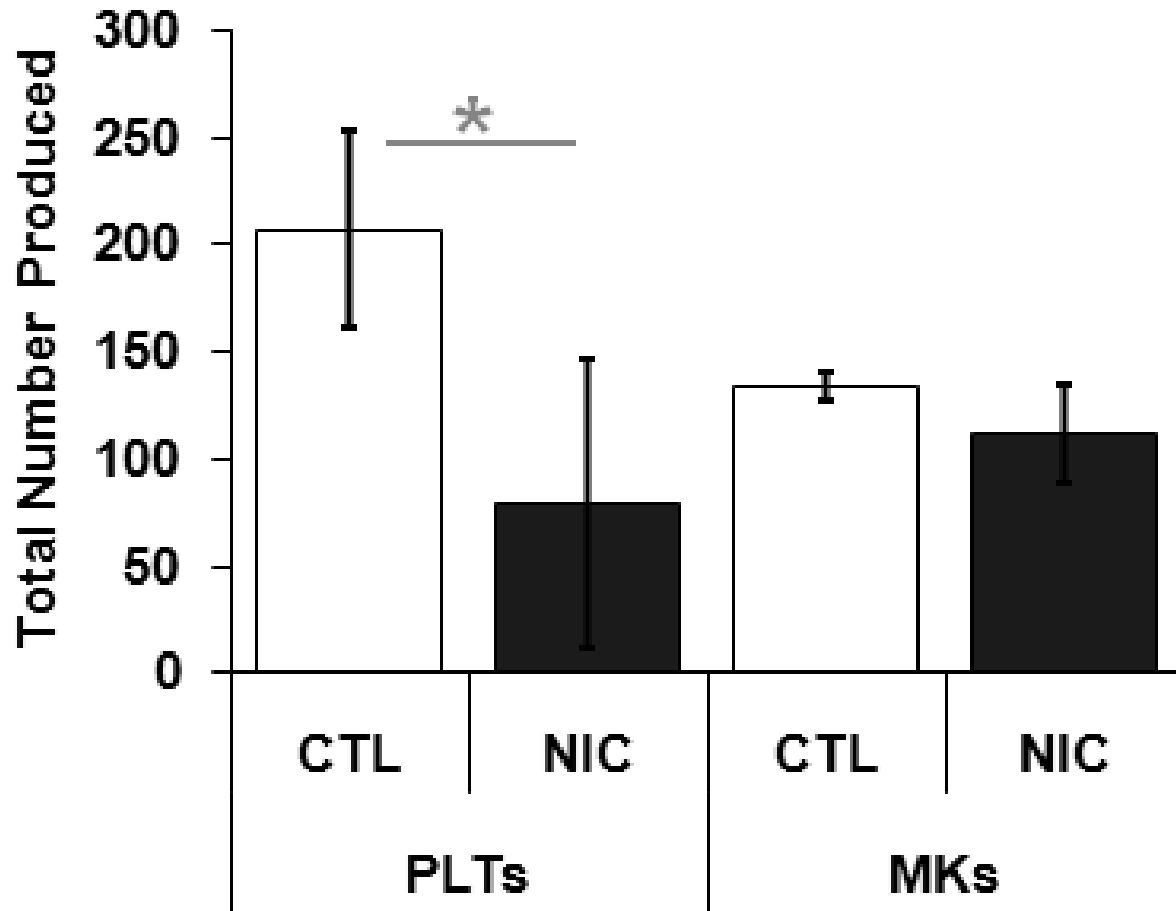
Figure 6.3: Impact of NIC treatment on final MK and platelet (PLT) yields in bulk CB-cultures. Total number per seeded cell shown (mean ± SEM, * $p < 0.05$, r = 3). CB-CD34$^+$ cells grown for 14 days in serum free medium supplemented with the cocktail BS1^{22} with or without NIC treatment from day 7 to 14 (NIC concentration of 4.5 and 1.5 µM between day 7 - 10 and 10 - 14, respectively).
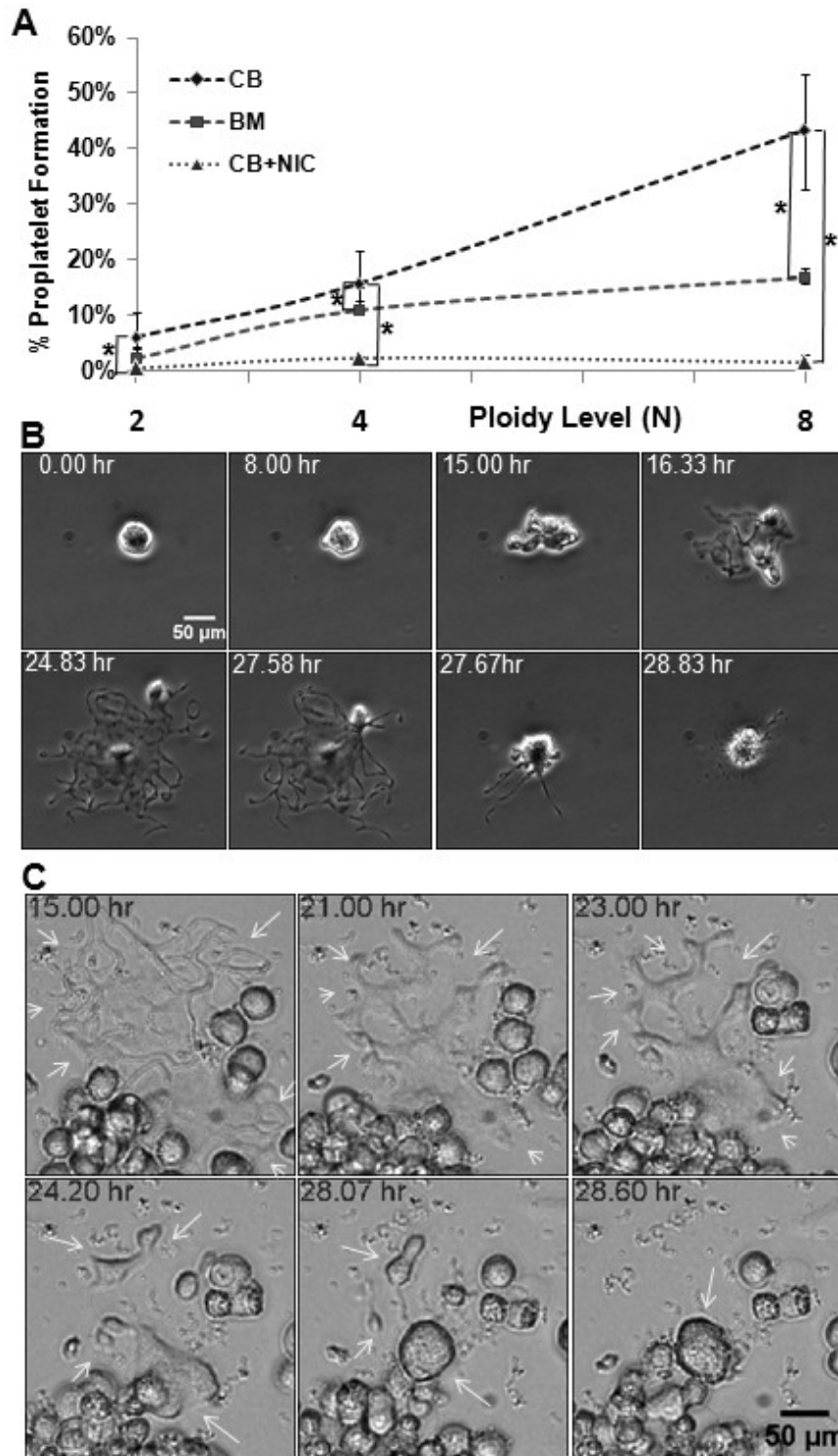
Figure 6.4: Proplatelet formation of CB-MK increases with ploidy level and is a reversible process. **A)** Correlation of proplatelet formation with ploidy level. Analysis included 250 CB- (107 x 2N, 53 x 4N, 90 x 8N) and 96 BM-MK (12 x 2N, 44 x 4N, 40 x 8N), extracted from 2,320 CB- and 1,515 BM-cells presented in Table 6.1. **B)** Example of a mature CB-MK undergoing proplatelet that ends with programmed cell death. See supplemental Video 6.4B. **C)** Reversible proplatelet formation. A mature tetraploid CB-MK that has already

formed proplatelets regress to a regular round shape, highlighted by the arrows. Later, this cell undergoes further endomitosis and becomes octaploid. See supplemental Video 6.4C.
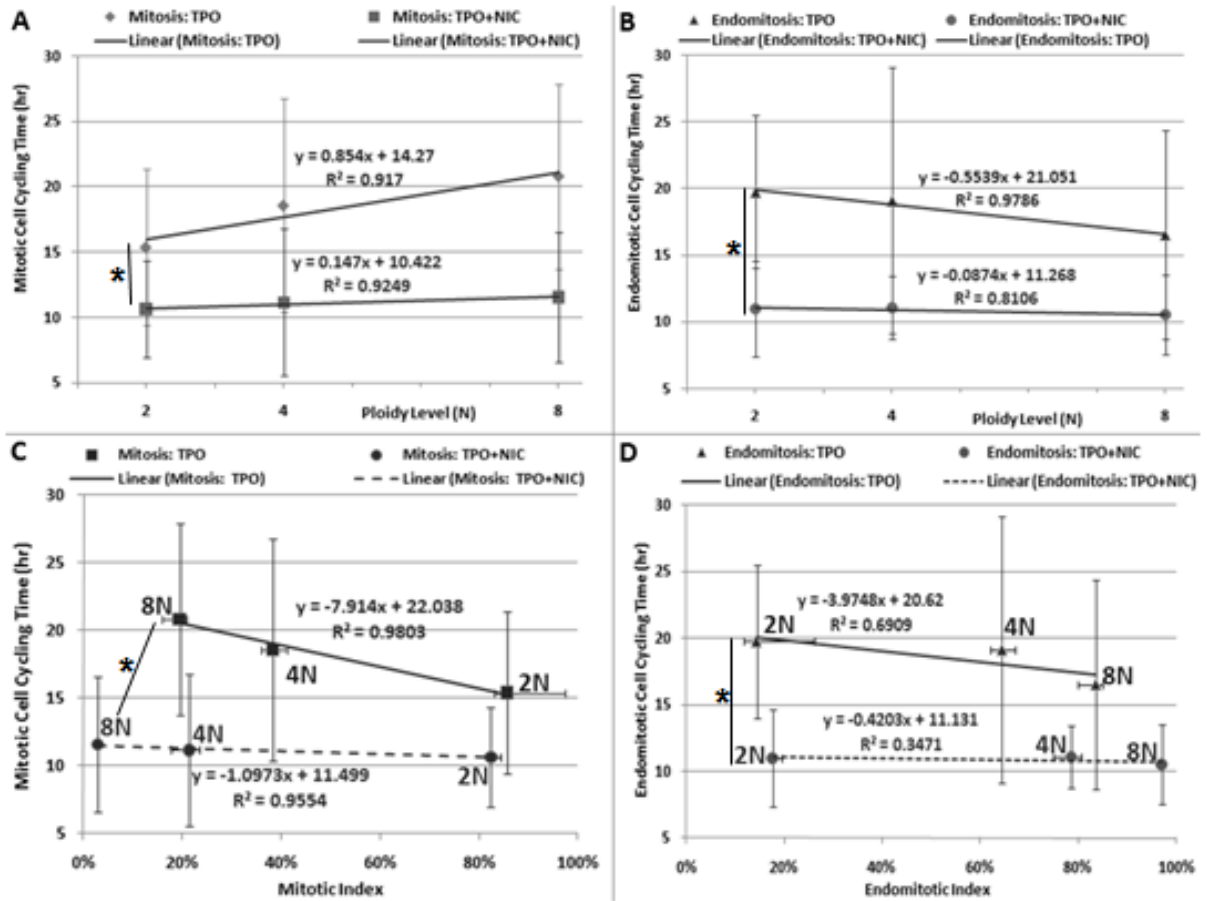
Figure 6.5: Comparison of mitotic and endomitotic cell cycling periods of CB-MKs treated or not with NIC. Mitotic cell cycling as a function of ploidy level **(A)** and mitotic index **(C)**. Endomitotic cycling time is dependent on ploidy level **(B)** and endomitotic index **(D)**. Mean of cumulative data from five experiments shown. Representative result shown for TPO (r = 3) and TPO+NIC culture (r = 2), mean ± SEM, * $p < 0.05$.
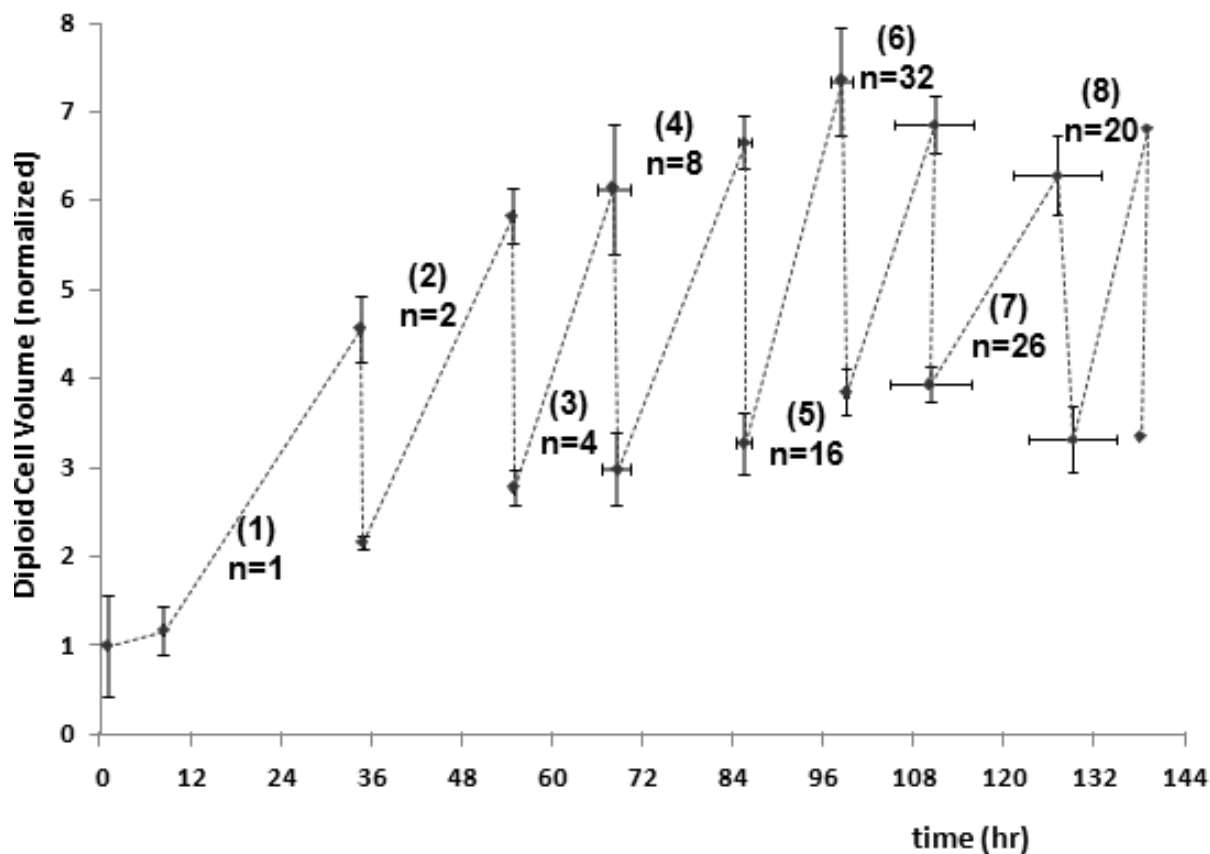
Figure 6.6: Kinetic of CB-MK cell size changes over culture time and division for proliferative diploids. The numbers inside parentheses shows the generation number, and *n* is the number of tracked cells (representative result is shown). Cell size volume was measured at the birth and end of the cell cycle. Average size (computed from surface area) of 3 - 4 frames for every cell was considered. Average size of the sister or cousin cells from each generation is shown. See *Cell Size Measurements* for details.
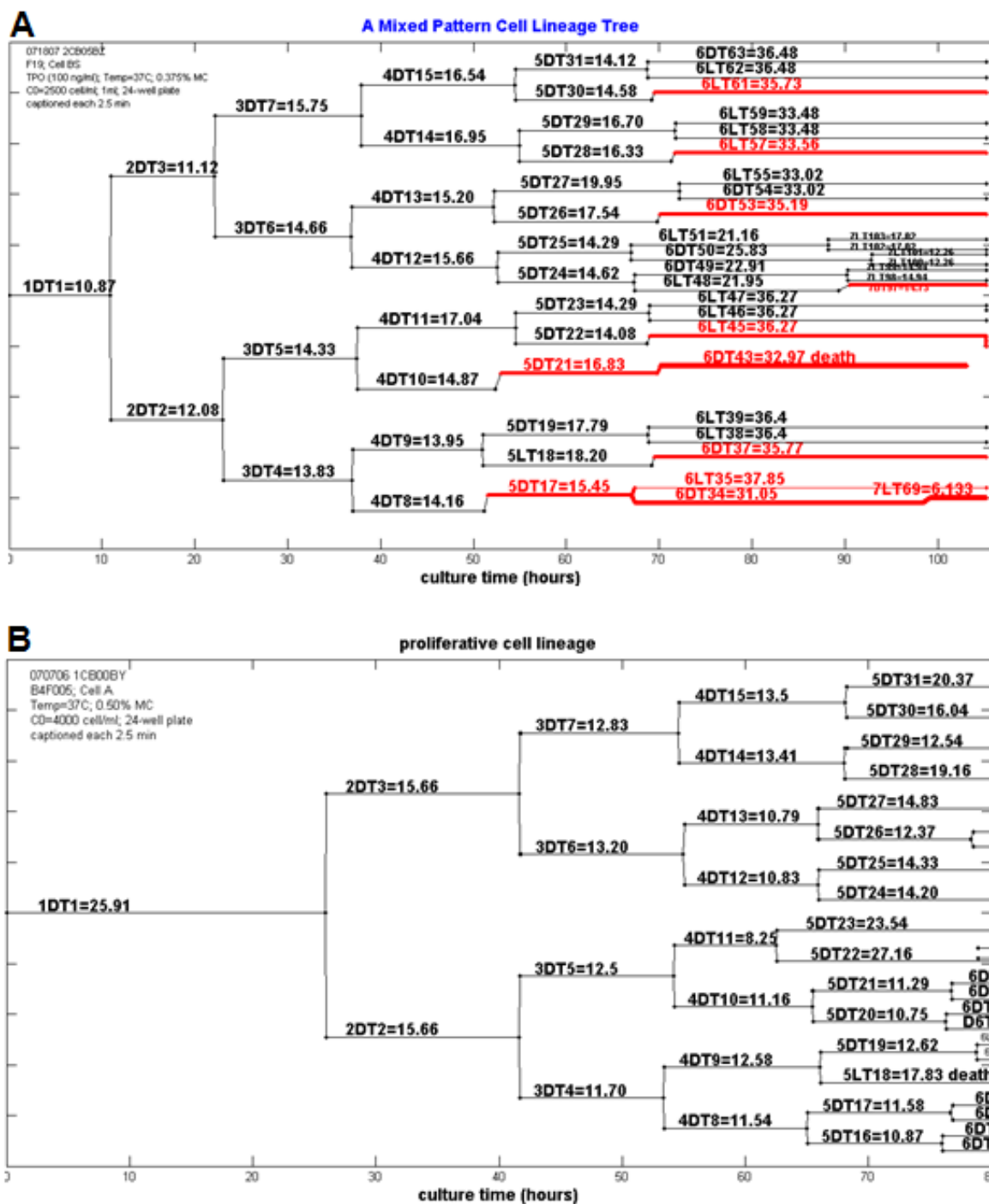
Figure 6.7: Representative cell lineage trees of CB-cells undergoing MK differentiation in TPO culture. **A)** a 7-generation mixed lineage tree, **B)** a 6-generation proliferative lineage tree. A large area (5x5 tiling) of a culture was followed and monitored from day 5 until day 10 using a 20X objective. The initial cell number was 96 in the imaged region (average of 3 cells per field), and ended over 650 cells after 5 days culture. Ploidy level of the tracked cells was determined by morphological changes, DNA staining, and cell size-ploidy level correlation, as previously reported[10]. See the text and supplementary materials for the further details.

6.8. Supplementary Materials

TEXT A. Cell Lineage Tree

In the cell lineage trees, as shown in Figure 6.7, each horizontal line represents the life of a cell. The history of all generated daughter cells is written with a set of characters above the horizontal lines, for example 4DT10=14.87 in Figure 6.6. The first character (number 4) shows the cell generation number, starting with 1 for the first generation. The second and third characters are two letters corresponding to the following abbreviations. DT: division time (mitosis cycling time, hour); PT: ploidy time (endomitosis cycling time, hour); LT: life time (hour). The last character is another number (10 in this example) corresponding to a unique cell ID of this experiment. Finally, the computed life span of the cell in hours is provided after the equal sign (i.e. 14.87 hours in the example). Furthermore, each individual cell is given a name based on its location in a field (a two-digit number after "F") from a large tiled image. The line width represents the ploidy class: 1 - 4, 6, and 8 for 2N, 4N, 6N, 8N, 12N and 16N, respectively. The color of each line represents a cell fate: diploid cells undergoing mitosis: black; a cell undergoing endomitosis: red; proplatelet formation: green. For cell death or a cell leaving the field of view (i.e. lost cell), these events were written at the end of the line corresponding to that cell. Cell division is indicated by a horizontal line splitting in two. When a parent cell divides into two separate cells with clear boundaries, or becomes a single cell with a regular round shape, that time point (or frame number) is the end of the connecting line and the beginning of the next daughter(s) cell life. The cells undergo endomitosis, the horizontal line shifts up to show the ploidy level is increased, while it is shown in red and the line width is also enlarged.

TEXT B. Image Processing and Analysis

During video image analysis, the frame numbers at which the following events occurred were recorded on a spreadsheet together with a unique cell ID number and time of occurrence: cell division, cell polyploidization, proplatelet formation, cell death, elongation, forming colony, entering or going out of the field of view. A set of custom Matlab R2008b (MathWork Inc.) scripts were developed to analyze the recorded data, construct cell lineage trees and compile statistics.

Different steps were required to discriminate the cells among acquired images[50]. The cell segmentation was performed by a combination of mathematical morphological operators[51-53] using Matlab software. Once either the cell or its DNA successfully segmented, several features were defined to characterize each segmented specimen. Some cells were manually segmented using ImageJ software.
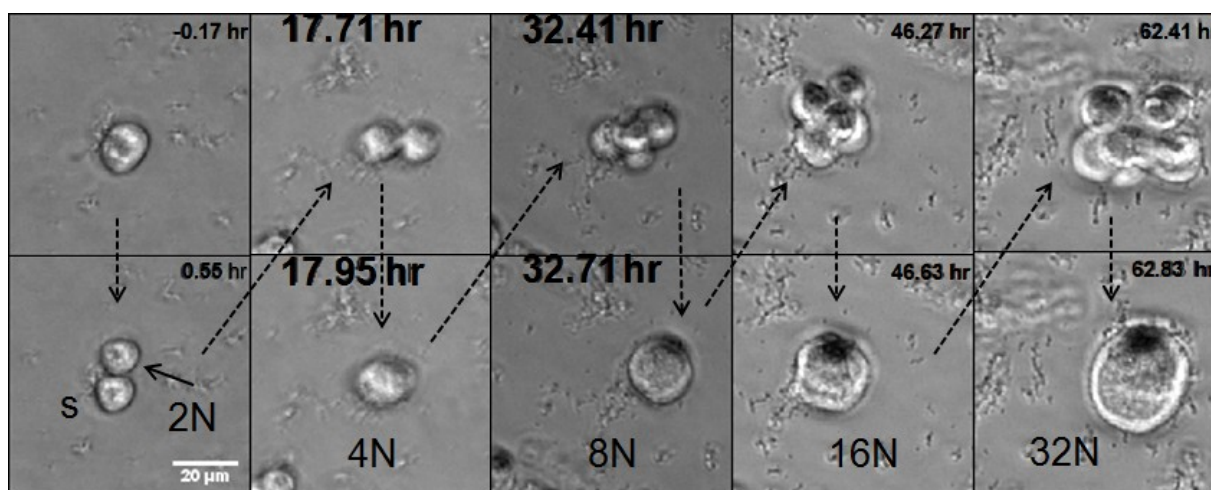
Figure 6.S1: NIC-treated CB-MKs undergoes several continuous rounds of endomitosis. The first and second row show furrow ingression during cytokinesis and the MKs after completion of endomitosis, respectively. Legend: s = sister cell; scale bar: 20 µm.

A Polyploidizing Lineage Tree

071807 2CB05BZ
TPO (100 ng/ml); Temp=37C; 0.375% MC
C0=2500 cell/ml; 1ml; 24-well plate
captioned each 2.5 min

culture time (hours)

B Quiscent Lineage Tree

071807 2CB05BZ
TPO (100 ng/ml); Temp=37C; 0.375% MC
C0=2500 cell/ml; 1ml; 24-well plate
captioned each 2.5 min

culture time (hours)

C Mixed Lineage Tree

070807 2CB05BZ
F01; Cell AA
TPO (100 ng/ml); Temp=37C; 0.375% MC
C0=4000 cell/ml; 1ml; 24-well plate
captioned each 2.5 min

culture time (hours)

Figure 6.S2: Megakaryocyte cell lineage tree patterns for cord blood cell culture in TPO. **A)** Examples of polyploidization pattern. **B)** Examples of quiescent patterns. **C)** A representative mixed pattern. A large area of the culture at day 5 (5 x 5 tiling) of 1 ml culture in 24-well plate using a 20X objective, was captured every 2.5 minutes and monitored until day 10. The initial cell number was 96 in the imaged region, i.e. averagely 3 cells per field (range of 1 - 6), and ended up over 650 cells after 5 days culture and imaging. All of these cells were tracked carefully and their ploidy level determined either by Hoechst staining at the end of imaging and/or by cell size measurement. See the text and supplementary materials for the further details.

Figure 6.S3: A typical mixed pattern of CB-derived MK lineage tree. As presented, the first cell (#1) underwent symmetrical division and produced two daughter cells (#2 and #3). These cells then divided asymmetrically to form two pairs of cells (#4 and #5, or #6 and #7). In each pair, one of the daughter cells underwent endomitosis (#4 and #6) while the other one (#5 and #7) divided asymmetrically as their parent did. See the text and supplementary materials for the further details.

6.9. Movies

Movie 6.4B: Example of a mature CB-MK undergoing proplatelet that ends with programmed cell death.

Movie 6.4C: Reversible proplatelet formation. A mature tetraploid CB-MK that has already formed proplatelets regress to a regular round shape. Later, this cell undergoes further endomitosis and becomes octaploid.

Movie 6.S1: NIC-treated CB-MKs undergoes several continuous rounds of endomitosis.

7. Complementary Data

This chapter contains complementary data which can be viewed as supplementary data for the results presented in *Chapters 4-6* or contains raw data (with minimal explanation) that were referred as "data not shown" in those chapters.

7.1. Parameter Estimability of the 5-C Model

Parameter estimability of the 5-C model was performed using sensitivity analysis improved by Yao et al.[169], in which sensitivity coefficients were obtained by varying one parameter at a time with ± 1% perturbation around their most likely optimal values (absolute values) at several local minima. This allowed investigating which parameters were always estimable, e.g. globally identifiable, and those that could only be estimated locally around few local minima. This analysis was applied on sets of parameter solutions which had SS/SS_{min} values of 1.01, 1.05, 1.10, 1.18, 1.50 and 1.77 (Table 7.1A), therefore within the approximate 95% confidence region (~7500 solution sets)[173]. Furthermore, 6 sets of parameter values were chosen in which one of the responses had the highest R^2 value. The result is shown in Table 7.1B.

Table 7.1: Parameter estimability of the 5-C model through sensitivity analyses on global and local minima. Parameters were ranked from the most to the least estimable, in which a ± 1% perturbation was applied. **A)** Parameter ranking at different values of SS/SS_{min}. **B)** Parameter ranking when multi-response (R^2_T) and single response (A to P) is considered to fit the experimental data.

A) Parameter ranking at different values of SS/SS_{min}.

	SS/SS_{min}								
	1.00			**1.01**	**1.05**	**1.10**	**1.18**	**1.50**	**1.77**
	p [a]	SS_R [b]	%est. [c]	p	P	p	p	p	p
1	μ_{maxI}	7653.01	100%	μ_{maxI}	μ_{maxI}	μ_{maxI}	μ_{maxI}	t_A	μ_{maxA}
2	t_A	1353.78	17.69%	t_A	t_A	t_A	t_A	μ_{maxI}	μ_{maxI}
3	μ_{maxA}	317.148	4.14%	μ_{maxA}	μ_{maxA}	μ_{maxA}	μ_{maxA}	μ_{maxA}	t_A
4	t_I	129.081	1.69%	t_I	t_I	t_I	r_A	r_A	r_A
5	r_A	45.7321	0.60%	r_A	r_A	r_A	X_{max}	X_{max}	y_{AI}
6	X_{max}	13.5454	0.18%	X_{max}	X_{max}	S_{AE}	t_I	μ_{maxE}	S_{IM}
7	r_I	7.0967	0.09%	S_{AE}	r_I	r_I	μ_{maxE}	y_{AI}	r_I
8	S_{AE}	2.8266	0.04%	r_I	S_{AE}	μ_{maxE}	r_I	t_I	X_{max}
9	μ_{maxE}	1.1334	0.01%	μ_{maxE}	μ_{maxE}	X_{max}	y_{AI}	r_I	μ_{maxE}
10	μ_{maxM}	0.0251	0.0003%	μ_{maxM}	μ_{maxM}	y_{AI}	μ_{maxM}	μ_{maxM}	μ_{maxM}
11	$K_L Y_{X/L}$	1.8E-10	2.3E-12%	$K_s Y_{x/s}$	$K_s Y_{x/s}$	S_{IM}	S_{AE}	S_{AE}	$K_s Y_{x/s}$
12	S_{IM}	3.6E-18	4.7E-20%	S_{IM}	S_{IM}	$K_s Y_{x/s}$	$K_s Y_{x/s}$	$K_s Y_{x/s}$	S_{AE}
13	y_{AI}	4.5E-22	5.9E-24%	y_{AI}	y_{AI}	μ_{maxM}	S_{AI}	S_{AI}	t_I
14	S_{AI}	5.0E-24	6.5E-26%	S_{AI}	S_{AI}	S_{AI}	S_{IM}	S_{IM}	S_{AI}

a) p: Parameter, b) The sum of squares of the residuals matrix (R) in Yao et al. method in *Sensitivity Analysis*, c) %Estimability was defined as 100% for the parameter with the highest SS_R value. White, light gray and dark gray regions represent the estimable, less-estimable, and non-estimable parameters, respectively. Two cut-off values of 0.1% and 0.0001% estimability were defined for this classification.

B) Parameter ranking when multi-response (R^2_T) and single response (A to P) fits to the experimental data.

	R^2_T	R^2_A	R^2_I	R^2_M	R^2_E	R^2_P	R^2_X
1	μ_{maxI}	μ_{maxI}	μ_{maxI}	μ_{maxI}	μ_{maxI}	μ_{maxI}	μ_{maxI}
2	t_A	μ_{maxM}	t_A	t_A	μ_{maxM}	t_A	t_A
3	μ_{maxA}	t_A	t_I	μ_{maxA}	t_A	μ_{maxA}	μ_{maxA}
4	t_I	μ_{maxA}	μ_{maxA}	t_I	μ_{maxA}	X_{max}	X_{max}
5	r_A	r_A	r_A	r_A	r_A	r_A	r_A
6	X_{max}	X_{max}	r_I	r_I	X_{max}	t_I	t_I
7	r_I	t_I	μ_{maxM}	S_{AE}	t_I	S_{AE}	r_I
8	S_{AE}	μ_{maxE}	μ_{maxE}	X_{max}	μ_{maxE}	μ_{maxE}	S_{AE}
9	μ_{maxE}	S_{AE}	y_{AI}	μ_{maxE}	S_{AE}	r_I	μ_{maxE}
10	μ_{maxM}	$K_L Y_{X/L}$	S_{AE}	μ_{maxM}	$K_L Y_{X/L}$	$K_L Y_{X/L}$	$K_L Y_{X/L}$
11	$K_L Y_{X/L}$	r_I	X_{max}	y_{AI}	r_I	μ_{maxM}	μ_{maxM}
12	S_{IM}	y_{AI}	$K_L Y_{X/L}$	$K_L Y_{X/L}$	y_{AI}	y_{AI}	S_{IM}
13	y_{AI}	S_{IM}	S_{IM}	S_{IM}	S_{IM}	S_{IM}	y_{AI}
14	S_{AI}	S_{AI}	S_{AI}	S_{AI}	S_{AI}	S_{AI}	S_{AI}

7.2. Effects of Rock Inhibitor

Several drugs have been shown to influence the ploidy level of MKs in culture[30,209]. Among these, Rho/Rock inhibitor was recently shown to increase the ploidy of MK derived from BM-CD34^{+} cells[30]. The effects of inhibiting the Rho/Rock pathway on MK polyploid cell division were investigated, since this pathway is essential for cytokinesis. CB- and BM-TPO cultures were treated at day 6 with the Rock inhibitor Y27632 (50 µM), in all the fates of 214 CB- and 309 BM-MKs were analyzed. Though only one test was done with BM- and CB-cells, these results were essentially identical; Rock almost completely inhibited mitosis of diploid cells and completely inhibited the division of polyploid MKs in CB- and BM-TPO cultures (Table 7.2). Due to its toxic effect, inhibition of Rock failed to promote endomitosis and the formation of highly polyploid MKs.

Table 7.2: Fates of megakaryocytes derived from CB-CD34^{+} TPO cultures treated with Rock inhibitor Y27632. The cultures were treated at day 6.

Ploidy Class	MK Fates N = 323	CB+Y27632 r = 1[a], N = 214[b]	BM+Y27632 r = 1, N = 309
2N	N = 323	n = 150[c]	n = 173
	Endomitosis	22.67%	21.39%
	Mitosis	0.67%	0.58%
	Proplatelet	0.00%	1.49%
	Death	76.67%	78.03%
4N	N = 143	n = 40	n = 103
	Endomitosis	60.00%	25.24%
	Mitosis	0.00%	0.00%
	Proplatelet	0.00%	0.72%
	Death	40.00%	74.76%
8N	N = 57	n = 24	n = 33
	Endomitosis	33.33%	9.09%
	Mitosis	0.00%	0.00%
	Proplatelet	0.00%	0.00%
	Death	66.67%	90.91%

[a]r: number of independent experiments; [b]N: total number of tracked cells, [c]n: number of tracked cells;

7.3. Cell Expansion Kinetic: Single Cell vs. Bulk Population

The raw data from the tracked cells was reanalyzed to compare the cell life dynamic of an individual cell and compared to that of bulk population. Cell number is a good indicator for such a comparison. Thus, as an example, the kinetic of viable cell number over around 5 days of culture is presented in Figure 7.1. This shows how tracking of a single cell and measurement of its cell life associated parameters can be applied to a big population. Furthermore, the number and frequency of descendent cells in each generation were calculated, as shown in Figure 7.2. The resulting information allows to determine more precisely the generation dynamics than what can be generally obtained by other techniques such as CFSE staining dye[115-117]. Thus, several mathematical models such as age-maturity structure, cell-cycle distribution, cell growth kinetics, etc can be applied directly on the data obtained from cell imaging and lineage trees and the effects of environmental factors can be investigated. In addition, this sort of data analysis allows directly measuring the parameters introduced in a mathematical model, like the probability of proliferation or differentiation.
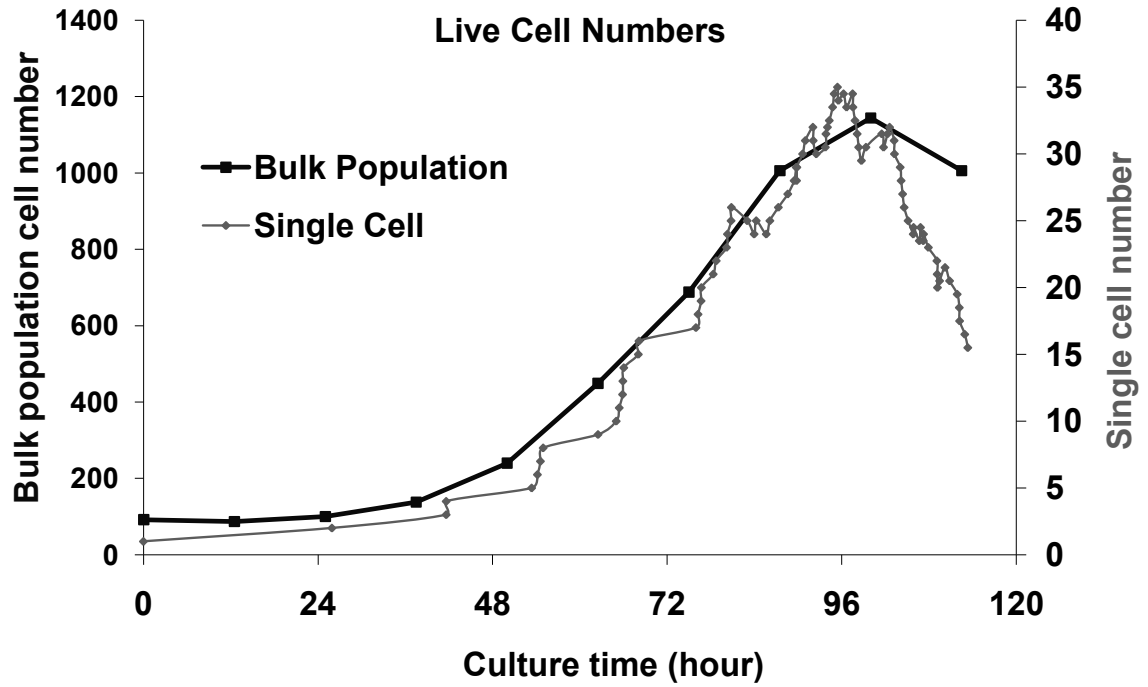
Figure 7.1: Evolution of the viable CB-MK number, compared between a single cell and the whole population. The result is extracted from a representative mixed pattern cell lineage tree for the single cell and the counted total cells for the whole population (both measured by live cell imaging.
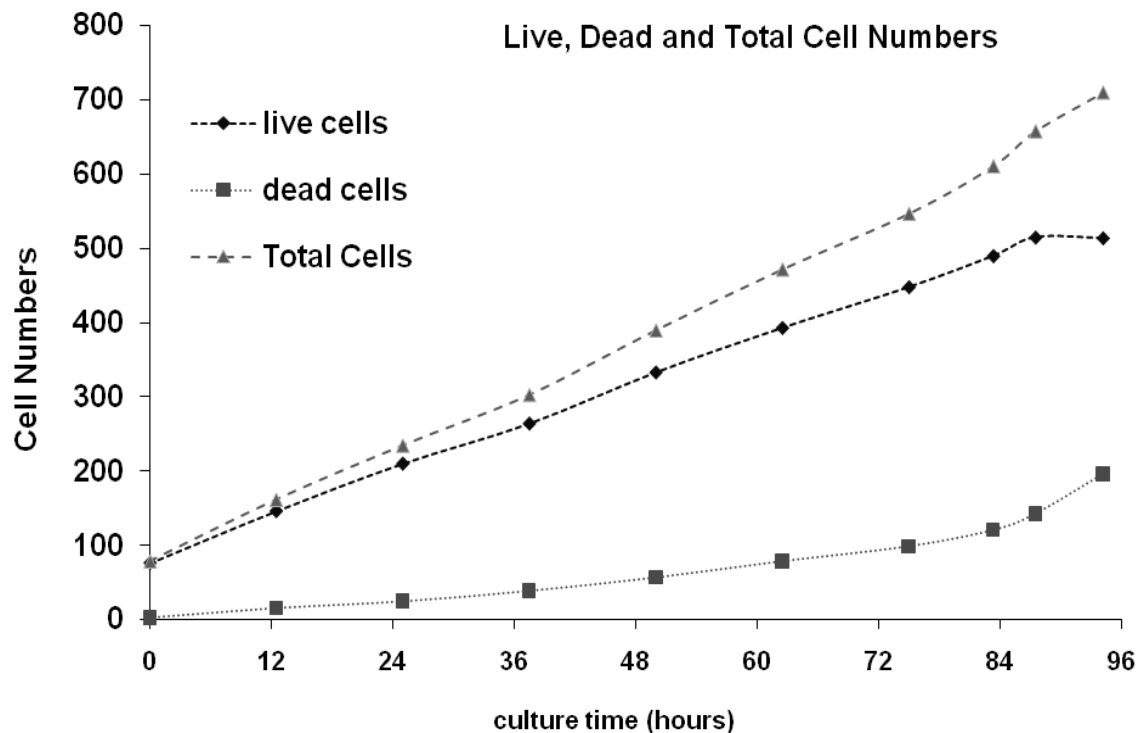
Figure 7.2: Kinetic of the total, live and dead CB-MKs cells, tracked during the time windows of 5 - 10 culture days (representative data).

8. Discussion, Conclusion and Perspectives

The development of the MK mathematical model together with the live cell imaging culture system in this thesis show how the merging of biological research with quantitative analyses can lead to new discoveries, knowledge and methods to gain further insights into complex biological processes such as megakaryopoiesis. Looking back to the objectives of this thesis (*Chapter 2*), one can summarize the results as follows.

8.1. Mathematical Modelling of Megakaryopoiesis

A mathematical model of megakaryopoiesis *ex vivo*, reflecting the growth and development of MK progenitors and MK from the stage of CD34$^+$ cells, enriched in HSCs, with capability to proliferate and differentiate to the blood platelets was developed (Objective #1). The basic structure of the model contained most cell differentiation stages previously shown to occur during the process of megakaryopoiesis[19,159]. The model was based on flow cytometry data and contained five major compartments: HSC, immature MK, mature MK, non-MK cells and platelets. Importantly, the approach of 3-D mathematical modeling (*Chapter 4*) can be easily formulated for every stem cell population balance in general to study the cell fates.

The proposed mathematical model fitted reasonably well the experimental data and provided a deeper understanding of the differentiation and proliferation pathways and estimation of the various rates, such as proliferation and differentiation of multiple subpopulations together with specific platelet production rate and symmetrical differentiation coefficients. This model sheds light on the impact of mild hyperthermia on the specific proliferation, differentiation and death rates of CB cells undergoing MK differentiation. However, the confidence ranges of these parameters were found too large to compare statistically these incubation temperatures. To derive the model, specific death rates of each compartment together with the specific platelet production rate were first estimated directly using the available experimental data. This resulted in a significant reduction in the number of parameters to be estimated. Next, it was attempted to estimate the remaining parameters describing cell fates and symmetrical division coefficients, in

which a hybrid stochastic optimization algorithm was used to search thousands of solutions, from random initial guesses for parameter values. An empirical 95% confidence interval was defined and introduced, that included 1,200 solution sets among 11,000 collected sets of parameters representing sum of square local minima. The optimum and acceptable range of parameter values were chosen for both incubation temperature data sets and compared. To evaluate the parameter estimability, global and local sensitivity analyses (using an improvement over Yao et al. method[169]) were applied which also brought additional information (Objective #2). The parameter estimation was robust enough to evaluate the order of magnitude of the rates and the relative importance of the different steps, for the cellular events occurring during megakaryopoiesis. This also showed that just two parameters (S_{AI} and S_{IM}) could not be estimated among the 14 of the model, using the available data. These two parameters needed to be measured using different methods or just simply kept fixed. Furthermore, applying PCA on the solution matrix, which included 1,200 sets of the 14 parameters, resulted in an interesting finding of the highly correlative interactions among the parameters which meant that their estimation was not easily achievable and the non-linear structure of the model should have been considered. Among these and in agreement with the findings of sensitivity analysis, those two parameters were found to be less interactive or important in creating the parameter solution space. It would be worth to fix the values, either arbitrarily or from prior knowledge, of the non-estimable parameters, and then try estimating the remaining parameters and performing a sensitivity analysis. This might lead to the discovery of the non-estimability of other sets of parameters that might need repeating this step further. This procedure can help to define the lowest dimension of the model. Since lowering the number of parameters led loosing the resolution of curve-fitting (as experienced during the estimation of 5-C model with/without specific death rates), this step was not followed in this work.

Applying long-term and large-field microscopy system, as summarized in the next section, allowed us to take into account the proliferation rate of the HSC precursors that represents a very important fate of the cells in the model structure. Previously, many investigators simulated the proliferation fate only for the first compartment (enriched HSC) which could differentiate into the precursors that only differentiated or died, thus neglecting the differentiated cell proliferation[133,135]. It was attempted to fit that type of structure into our

case, but this approach showed a poor regression. Applying time-lapse video microscopy increased our understanding of megakaryopoiesis process, in which it was observed that polyploid or mature MK did proliferate. Thus, the message of that approach was that immature MK expansion was not solely due to the differentiation of MK progenitors because the proliferation of immature MK was observed to occur at high frequency. This was interpreted mathematically that the proliferation fate for the HSC precursors was required to be taken into account in the model structure (Objective #10). Following this finding, the proliferation fates were considered for both immature and mature MK compartments.

Next, the estimated parameter values of the model between two incubation temperatures were compared (Objective #3). Our results were consistent with the previous studies demonstrating that the incubation of CB-CD34$^+$ cells at 39°C resulted in accelerated MK differentiation and maturation and increase in the number of MKs and platelets. Our model could describe values of parameters that cannot be measured directly or experimentally. For instance, the specific production and death rates of platelets was estimated 1.2- and 1.3-fold higher, respectively at the elevated temperature. Furthermore, the comparison of the optimal values showed that maximum total cell concentration, maximum specific growth rates of HSC and immature MK, symmetrical differentiation of immature to mature MK and specific death rates of all compartments increased with incubation temperature shift from 37 to 39°C. Nonetheless, it was found that this temperature alteration had no significant impact on two of the parameters t_I (time constant in sigmoidal differentiation function of immature MK) and k_{dM} (specific death rate of mature MK). In summary, the model provides new information and insight on culture incubation temperature effects on megakaryopoiesis process.

The proposed model was used to predict the cell fates of MK progenitors and MK *ex vivo* based on three cell surface marker staining. This model can be easily adapted for other lineages of blood stem cells or different stem cells and/or based on different markers. Increased model complexity is essential for quantitative precise conclusions. In the aim of providing a practical tool to understand the cellular complexity, it would be good to consider the effects of cytokine concentration changes over time into the current model

structure, for instance using Hill function[130,222], which will change the model type from descriptive to predictive. This can be achieved by comparing the optimal parameter values of the current or new model at different cytokine or chemokine combinations or concentrations to investigate which parameters are sensitive and play an important role when a stimulus is changed. The model proposed here was a deterministic type, while cell functions are known to be stochastic, which causes large variations of cell behaviours from cell lot to cell lot or from one experiment to the other. Therefore, a mixture of stochastic and deterministic models[137,180] might be more suitable and give better regression results. For instance, Kirouac et al. introduced recently a deterministic compartmental model on HSC which can be viewed as a stochastic model, since the proliferation fraction of subpopulations followed a Gaussian distribution[180]. Adding stochastic parameters into the current model might improve the model fitting to experimental data. To improve the parameter estimation, a pseudo-experimental approach would be an exciting and useful tool to be applied, e.g. generating experimental data by a computer simulation of the model. This will help to check i) how far a global minimum is achieved, i.e. compare the optimal values of the parameters found by the optimizer with that of the used values; ii) model prediction error and how to reduce, i.e. the best achievable R^2 and SS_{min}; iii) importantly how many initial guesses are required to have a reasonable and/or the best regression and how this varies based on the lower-upper bounds definitions; and v) how parameter estimability varies with artificial experimental data (different trials). Furthermore to estimate some parameters independently, it would be better to visualize the differentiation of HSC to MK using some fluorescent marker(s) under the regulation of a promoter of a MK specific gene, such as CD41a and using lentivirus to genetically modified CD34+ cells with a GFP-fused gene providing better visualization of cell division or differentiation[29]. If such a technique is developed, it will allow the direct estimation of the differentiation rates and asymmetrical differentiation coefficients, which were a dominant part of the model parameters. Getting benefits of technology improvements, another interesting approach will be to sort each subpopulation with the minimal effects of sorting and then culture to be able to independently estimate the parameters of the proliferation, differentiation or death rates of that subpopulation.

8.2. Live Cell Imaging Study of Megakaryopoiesis

In this work, long-term and large-field live cell imaging was developed and used to study megakaryopoiesis *ex vivo*, from the initial minutes of the cell growth and maturation. First, few factors needed to be considered and developed for the experimental design, such as i) the development of an incubating chamber that could be mounted on the microscope stage, ii) optimization of the culture condition that would enable the tracking of the generated cells over long period, such as initial cell concentration and using methylcellulose to control the cell movements, and iii) using tiling technique for large-field imaging to increase the number of events that can be observed for statistical. In addition, many efforts were devoted to develop a reliable set of methods to determine the ploidy level of the imaged cells (Hoechst staining of cell nuclei, cell history and cell size-ploidy level correlation). Using this system, a large number of MKs (> 9,300 total and > 3,200 polyploid MK) were recorded and their fates were analyzed for the first time for two consecutive periods of culture of 5 days. This technique definitely proved useful as it not only confirmed recent observations from previous studies[29,30,102,108], but it also identified a new series of cellular events that occur with MKs *ex vivo*.

The principal discovery of this work is that a significant fraction of polyploid MKs can in fact complete cytokinesis and undergo cell division as diploids do (Objective #4). The division of polyploid MKs was unexpected given the universally accepted belief that polyploid MKs undergo abortive cytokinesis[18,19]. Two similar studies recently reported new insights into endomitosis[29,30]. Our results confirm their observations that partial cleavage furrow ingression followed by regression and cytokinesis failure is an unambiguous hallmark of MK endomitosis. However, none of these two studies reported complete cytokinesis in polyploid MKs. This could be due to differences in experimental designs. Using long-term instead of short-term time-lapse video microscopy in this work enabled us to visualize the development of a much greater number of polyploid MKs (> 3,200 polyploid MK) up to 5 days, while the other studies followed far fewer polyploid MKs (50 and ~20) over a shorter period of time (6 - 24 hours)[29,30]. The previous studies used exclusively BM-MKs, from murine or human, in which polyploid cell division occurs at low frequency as reported here.

It was initially observed that CB-derived polyploid MKs underwent division at high frequency; it was investigated whether this property was unique to the neonate-derived cells. This was refuted since polyploid MK division did occur in BM-derived cells but at a much lower rate. Consistent with this, CB- and BM-MKs also diverged significantly in their mean ploidy level. This study clearly shows that the proliferation rate amongst polyploid MKs is inversely correlated to their ploidy level, and that this phenomenon is much more frequent in CB-derived MKs than in their adult BM counterpart (Objective #5). This finding partially explain why CB-derived MKs remain either diploid or in low ploidy class[101,105,192].

Given this unexpected finding, it was certainly important to demonstrate that this new phenomenon was not an artefact of the imaging conditions (Objective #6). The main sources for such errors could have been due to i) addition of methylcellulose used to slow down the cell movement to be able to track the cells for long-term; and ii) effect of long-term light exposure. Control experiments demonstrated that neither of these parameters was responsible for the division of polyploid MKs. Next, a reverse engineering approach was used to demonstrate that 6N cells, a by-product of the asymmetrical division of a 4N cell did exist. The existence of 6N cells could explain the small intermediate peak observed sometimes between 4N and 8N cells in cytometry DNA histogram analyses of CB- or BM-MK cultures apparent in previous reports[30,99,102,191], for which none of the authors addressed their existence. Z-series stack of confocal slices clearly demonstrated the presence of three well-defined nuclear lobes of similar size contained within the same cell (so called tri-lobular MKs) derived in regular TPO cultures (without methylcellulose and light exposure).

All previous reports on MK ploidy reported a doubling series of ploidy levels (2N, 4N, 8N,…)[18,19]. Another novel finding provided by our work is the existence of MKs with ploidy levels of 6N (product of 4N division to 2N and 6N) and 12N (asymmetrical division of 8N to 4N and 12N or endomitosis of 6N). Whether such cells exist *in vivo* remains unknown at this time. Furthermore, it was investigated whether polyploid MKs formed following mitosis of polyploid MKs had a development program comparable to those generated through endomitosis. The fate analysis of these cells showed that polyploid MK mitosis did not result in any abnormal fates for the newly derived polyploid daughter cells,

while the resulting diploid cells were for the most part non viable for unknown reasons. What determines asymmetrical divisions of polyploid MK that result in non-doubling series of ploidy level is not known at this stage.

Next, it was investigated whether the proliferation of polyploid MKs had a significant impact on the origin of polyploid cells in MK cultures (Objective #7). The contribution of various cell sources on polyploid MKs was studied. Our quantitative analysis shows that division of polyploid MKs represents a new and significant source of polyploid MKs expansion. Endomitosis was identified as the dominant fate of polyploid BM-MKs, while this was less accentuated for polyploid CB-MK. No other study has ever reported this finding, which demonstrates the power of the live cell approach to study complex cellular development.

The effect of few agents, such as addition of cytokines or NIC, on the polyploid MK division rate was investigated (Objective #8). Valerie Cortin and colleagues at Héma-Québec R&D department have previously showed that the cytokine cocktail BS1 promotes CB-MK expansion and platelet release[82]. First, it was investigated whether that cocktail could change the rate of mitosis of polyploid MK in comparison to MK produced in culture supplemented with TPO alone. The cytokine cocktail BS1 significantly increased the viability and mitotic rate of diploids, which resulted in greater cell expansion as previously reported[82,158]. The cytokine cocktail BS1 only had moderate impact on the mitotic rate of tetraploid (4N) or octaploid (8N) MKs, but there was no significant difference with that of TPO cultures. Interestingly, treatment of CB-MKs with NIC altered endomitosis and mitosis rates among polyploid MKs. Furthermore, NIC treatment of CB-MK resulted in a significant increase in maximal ploidy level (up to 64N) and reduction in mitotic activity index of all ploidy levels of CB-MK which was close to that of BM-MK treated with TPO alone.

Based on live cell imaging observations, it was noticed that, besides mitosis and endomitosis, CB- and BM-MKs of low ploidy levels (2N and 4N) were capable of proplatelet formation. However, it was also observed that some polyploid CB-MKs that had initiated proplatelet formation could revert to a regular circular shape, indicating that in some cases proplatelet formation might also be a reversible process. The regenerated cells

were then able to undergo a normal development program, including further division. Whether such phenomenon is due to a culture artifact cannot be answered at this time. Loss of cell shape might be due to other factors than reversion of proplatelet formation. Immunofluorescent staining might help to answer this question. Dr Amy Geddis, Professor at UCSD, has also seen similar events with murine BM-MK and by immunofluorescent staining. She showed that these cells at the stage of irregular shape with extended filaments displayed mitochondria and nucleus (personal discussion via email). The regulating mechanism is not clear at this moment, but perhaps this occurs following a late failure of apoptosis[171]. In the BM, proplatelet filaments can extend into the circulation where shear stress plays a critical role in MK fragmentation[45]. Our observation was under less shear stress than what is present in vivo due to the methyl cellulose usage in the culture However, Dr Geddis experiment was performed under a certain level of shear stress since she didn't use methyl cellulose. Thus, the absence of shear stress might not be the major factor for such an important observation. Since reversal of proplatelet formation was, as for the division of polyploid MKs, inversely correlated with ploidy level, it is possible that such mechanism limits proplatelet formation for diploids or low polyploid MKs. These data support the previously postulated idea that the mechanism regulating polyploidization might be independent from that regulating cytoplasmic maturation[18,212].

Live cell imaging also gave us an opportunity to measure the duration of a cell cycle. Theoretically, one could assume that an endomitotic cycle could be slightly shorter than that of a mitotic cycle due to an incomplete cytokinesis and since it was previously shown that the time for DNA duplication is identical for both processes[18]. However, our results suggest that this is not entirely true as the cell cycle time duration is rather dependent on the ploidy level and also cell fates. Indeed, it was demonstrated that the cycling time is longer if that fate is not the dominant one. For instance in TPO cultures, 2N CB-MK displayed longer endomitotic cycle while polyploid CB-MK showed longer mitotic cycles. Treatment of these cells with NIC resulted in reduced cell cycling time. Nonetheless, no significant differences between mitotic and endomitotic cell cycle durations were observed among treated CB-MK with NIC. Similar influence of NIC on other HSC lineage differentiations such as myeloid has also been reported[214]. At this step, it is unclear why NIC has such an influence on cell cycle duration. One may postulate that NIC supplementation in MK

culture may influence the progression of cells through the maturation steps by regulating the genes related to checkpoint controls in the cell cycle and/or involved in cell endomitosis and apoptosis that disable the cell platelet production capacity.

Recording and classification of all cellular events together with the analysis of cell lineage trees also made possible the identification of recurrent patterns of MK growth and development (Objective #9). Cell lineage trees have been often constructed and described in the literature for different cell types[219,220]. It is however reported for the first time on megakaryopoiesis. Lineage tree patterns were mainly defined based on major cellular events of the mitotic or endomitotic fates of the tracked cells (not proplatelet formation), and classified into four pattern types of quiescent, proliferative, polyploidizing or mixed. This tool provided valuable information on the fates of CD34$^+$ cells and their descendants. Among other things, it demonstrated that not all ancestors and their descendents are capable of undergoing mitosis, endomitosis, or a mixed of both events, while other remained quiescent. The precise mechanism regulating MK fates and lineage tree pattern distributions *ex vivo* still remains unclear. At this step, the development stages of the cells in lineage trees are not known, particularly for diploids that can be MK or MK progenitor. It would be great to develop a strategy to visualize the cell surface marker expression for each cell shown in the lineage tree. The development of this type of analyses combined with cell surface markers opens a new powerful avenue to investigate new questions.

The molecular mechanism responsible for polyploid MK mitosis remains unclear at this moment. However, addition of the Rock inhibitor Y27632 completely blocked mitosis of polyploid and diploid MKs in both CB and BM sources. The Rho/Rock pathway is responsible among other things for the activation of the actomyosin contractile ring. This result demonstrates that polyploid MKs can complete cytokinesis as diploids dependent on the Rho/Rock pathway. It would be good to investigate the effects of some proteins which are known to play important roles in MK endomitosis and formation of cleavage furrow such as Aurora-B Kinase, Mitotic Kinesin-Like Protein 1(MKLP1)*,* MKLP2, MgcRacGAP, Ect2 or RhoA[29,186].

8.3. Conclusion

The overall goal of this thesis was to perform a quantitative assessment and investigation of megakaryopoiesis. Toward this, a flow cytometry-based mathematical model and an automated imaging system were developed as tools to describe and investigate various stages of MK expansion and maturation and to improve the understanding of MK growth and development. A mathematical model of megakaryopoiesis *ex vivo*, predicting the proliferation, differentiation and death rates of MK progenitors and MK was developed. The basic structure of the model considered the major cell differentiation stages previously shown to occur during the process and based on cell staining with three surface markers. Applying time-lapse video microscopy helped to consider a major modification in the model structure, in which proliferation fate for the immature and mature MK was considered. The developed model fit well to both data sets at two incubation temperatures. Comparison of the optimal values of the parameters at two incubation temperatures provided different perspectives of the mild hyperthermia impact on megakaryopoiesis which was inconsistent with the previous reports by our colleagues[104,109]. Sensitivity analysis showed all parameters except two were identifiable either locally or globally. However, searching thousands of solution sets and finding the acceptable range for each parameter within approximate 95% confidence intervals gave larger range of parameter values. Thus, the precise values of parameters might be achieved using different measurements which might be subsequently possible with the benefits of technology improvements over time. The approach of 3-D mathematical modeling can be easily adapted for every stem cell population balance in general and predictively simulate the cell fates and dynamic characteristics. According to our best knowledge, this is the first flow cytometry-based mathematical model on megakaryopoiesis. The model provides insight into phenomena that would otherwise be difficult to interpret. This model can be used as a platform for future stem cell engineering and the rational design of stem cell bioprocesses.

Several fundamental questions surrounding megakaryocytic cell growth and development were also effectively answered by carefully recording the history of the cells (at the single cell level) through multiple-step analyses. New fundamental divergence in fate decision between CB- and BM-derived MKs were revealed, and new insight into the impact of cell

fate on cell cycle duration were notably revealed. This study also demonstrates for the first time that polyploid human MKs can undergo cell division following successful completion of cytokinesis, and give rise to polyploid daughter cell(s) that subsequently have normal fates. Hence, this study brings a new paradigm to the field of megakaryopoiesis as it challenges the concept that polyploid MKs are derived solely from cells undergoing endomitosis. Our results support the notion that endomitosis is the exclusive mechanism by which polyploidization is initiated and by which MKs increase their ploidy levels. This together with the results of CB-MK treatment with NIC demonstrates division of polyploid MKs could perhaps represent a mechanism responsible for the propagation of low ploidy MKs. Whether this occurs *in vivo* remains to be addressed in future studies, although many processes observed in TPO cultures were subsequently confirmed *in vivo*[3,45,99,105]. It was also shown that proplatelet formation is potentially a reversible phenomenon. Whether this occurs *in vivo* remains to be addressed in future studies. Finally, global analysis of the fate of the MKs in culture led to the identification of four types of cell lineage tree patterns. Taken together, this work demonstrates that time-lapse video microscopy is a powerful approach to study life and fates of a cell in general and as done in this work, in the context of multipotent cells undergoing MK differentiation.

8.4. Perspectives and Future Work

Despite the numerous findings made during this research work, like other cases of investigating a subject in depth, a number of ideas for future work and new questions were raised. Based on the number of cellular events occurring during megakaryopoiesis which can be visualized, two mathematical models could also be proposed. The first one can be easily fed by live cell imaging data without any improvement to the method that has been developed. The second one could be identified if the cell type could be recognized, either using surface markers or cell-type specific promoters controlling the expression of reporter genes.

During the development of the long-term imaging microscopy system, tools was also made to add gently and directly Hoechst to stain the cell nuclei at the end of a 5-day culture imaging. A couple of factors need to be considered in the future for many other applications such as (but not limited to): i) for longer period of imaging, the culture might need to be

refreshed. This can be implemented by coupling the current system with a syringe pump to gently add and/or remove the culture medium, for which a small modification in the current design might be required. This would allow to run the culture for longer term, such as two weeks experiments as it is done for MK culture and many other cells; ii) add any other antibodies, particularly cell surface markers, to occasionally determine the cell phenotypes. This experiment can be done for 5 - 15 minutes every 1 - 2 days of the long-term imaging to integrate the phonotypical information into the current system; iii) visualize the dynamic proplatelets formation or platelet release under shear stress using a perfusion system or simply a syringe pump coupled with a microfluidic device.

The long-term and large-field imaging approach developed here can be easily used as a platform to shed light on the growth and development of many other stem cells such as other blood cell lineages such as erythrocytes or granulocytes. Recently, Schwertz et al reported that blood platelets can also undergo division and produce functional platelet progenitors, through a process that resembled extension of proplatelet evolution[184]. Our system can be easily applied to determine whether the observed events were really the extension of proplatelet formation or that the produced platelets can undergo consecutive division(s). This is an important question in developmental and fundamental biology, since the human platelets lack of nucleus and it will be an exciting discovery to visualize an anucleated cell division process.

The major finding of this research work is that mature MK undergoes complete cytokinesis. Whether polyploid MK division occurs *in vivo* remains unanswered at this moment. Some steps can be followed to clarify that: i) it would be good to show whether the small 6N peak (between 4N and 8N) observed occasionally in fresh BM samples from humans or mice is due to the individual 6Ns which can be confirmed by flow cytometry or ImageStream (recently developed advanced technology which combines microscopy and flow cytometry) which allows simultaneous DNA contents analysis and imaging of thousands of individual cells; ii) sorting the high polyploid MKs such as 8N or above (without contamination of any diploids) and then perform proliferation assays such CFSE dyes[115-117]; iii) use intravital confocal microscopy to visualize *in vivo* occurrence of endomitosis and/or polyploid MK division in mice or zebrafish since a transparent zebrafish was developed recently[223].

Obviously, the major discovery of this research is that a significant fraction of low polyploid MK derived from CB undergo mitosis. Whether this finding can be translated directly to a clinical application remains unanswered at this time. Some steps might be taken to answer this question. First, isolate the low ploidy level of CB-MK without contamination of diploids, expand and then produce platelets. Comparison of the generated platelets quantity and quality with that of unsorted MK and also that of high ploidy level MK (that have experienced less or no mitosis) might help to address the question. If it was found that the polyploidy MK undergoing mitosis gives highly functional platelets and/or in high amounts, the next step would be to find a way to increase the proliferation of high ploidy level MKs (8N and above).

Answering one question in this thesis raises new ones: What determines the return of MK to normal cell cycling after it begins polyploidization? How is the cell decision to switch between mitosis and endomitosis regulated? Does polyploid MK division occur *in vivo*? Is polyploid MK mitosis useful or not? How is the polyploid MK proliferation rate in pathological conditions? How can the differentiation of CD34$^+$ cells to MK be better visualized? Does MK (whether diploid or polyploid) differentiate to non-MK cells? Are there any other cells beside MK that can generate platelets?

Based on the number of cellular events occurring during megakaryopoiesis which can be easily observed using time-lapse video microscopy, developed and described here, a new and simple version of mathematical model can be applied which is shown in Figure 8.1. The first compartment contains all diploid cells, either HSC or MK, while the second to fourth compartments represent 4N, 8N, and 16N or higher polyploid MKs, respectively. Released platelets from every ploidy class of MK are pooled into one compartment. The main advantages of this model are (but not limited to): i) all cellular events, e.g. mitosis, endomitosis, proplatelet formation and death, can be observed and quantified directly using bright-field microscopy (without staining or using a fluorescent protein), and ii) any parameters describing directly the cellular events and cell numbers can be estimated, thus the model identifiability can be tested accordingly.
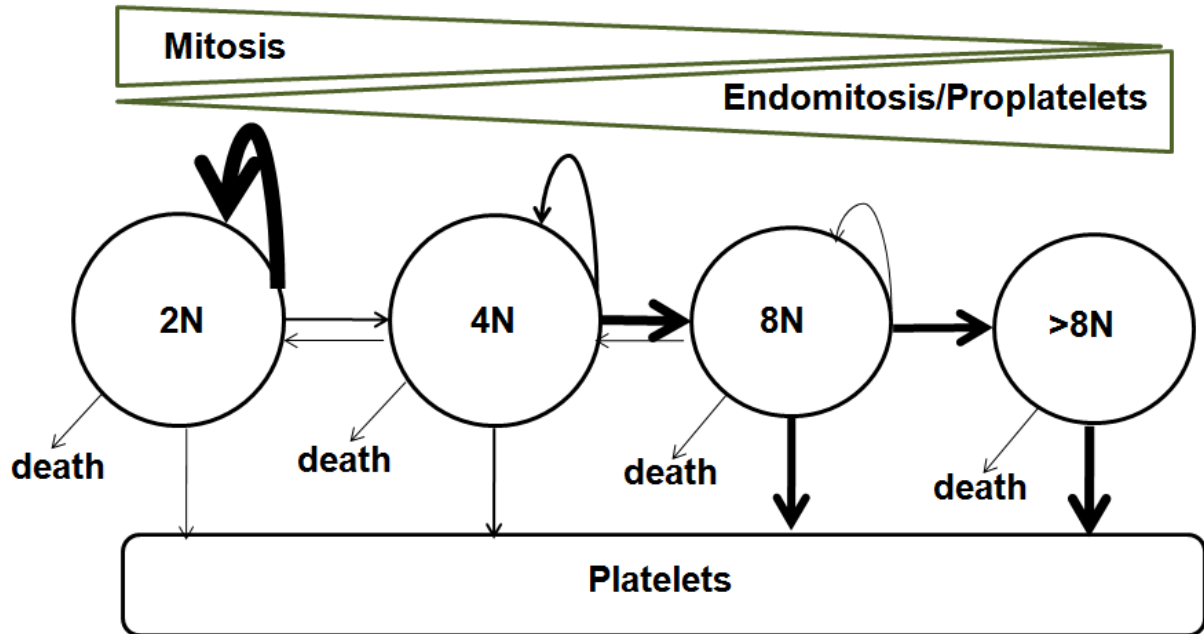
Figure 8.1: Proposed mathematical model of MK growth and development based on observable live cell imaging data.

Based on the findings of this study from the mathematical model and microscopic analysis (*Chapters 4-6 and Appendix*) as well as the conceptual model of megakaryopoiesis process in the literature (*Chapter 1*), an entirely new model is described as shown in Figure 8.2. Megakaryopoiesis in general consists of four major compartments; hematopoietic stem cells, immature MK, mature MK and platelets. It is assumed that HSCs are diploids while immature and mature MKs are mixed of diploids and polyploids. HSCs are highly proliferative cells and can commit to immature MK (2N). Immature MKs have the capability of mitosis, endomitosis and differentiation to mature MK. Immature and mature MK are recognized by expression of the CD42 marker. A diploid immature MK can have four fates: i) proliferates and gives two 2N immature MK (CD41^{+}42^{-}), ii) undergoes endomitosis that becomes 4N immature MK (CD41^{+}42^{-}), iii) differentiates to 2N mature MK that expresses CD41^{+}42^{+}, or iv) simultaneously undergoes polyploidization and differentiates (4N mature MK CD41^{+}42^{+}). Tetraploid and octaploid immature MKs can have four fates with similar fashion. Mitosis capacity of immature MKs is lower than that of HSC and is reduced by increased ploidy level, while endomitosis potential is increased. Mature MKs undergo endomitosis without division and have the capacity to produce platelets. A mixture of stochastic and deterministic models can be applied to quantify the

observed events. It is important to validate the parameters experimentally, which might be performed using conventional fluorescent or confocal microscopy imaging together with flow cytometry. In addition, ImageStream technology (an advanced imaging flow cytometry technology) may help to directly estimate some of the parameters for each compartment.
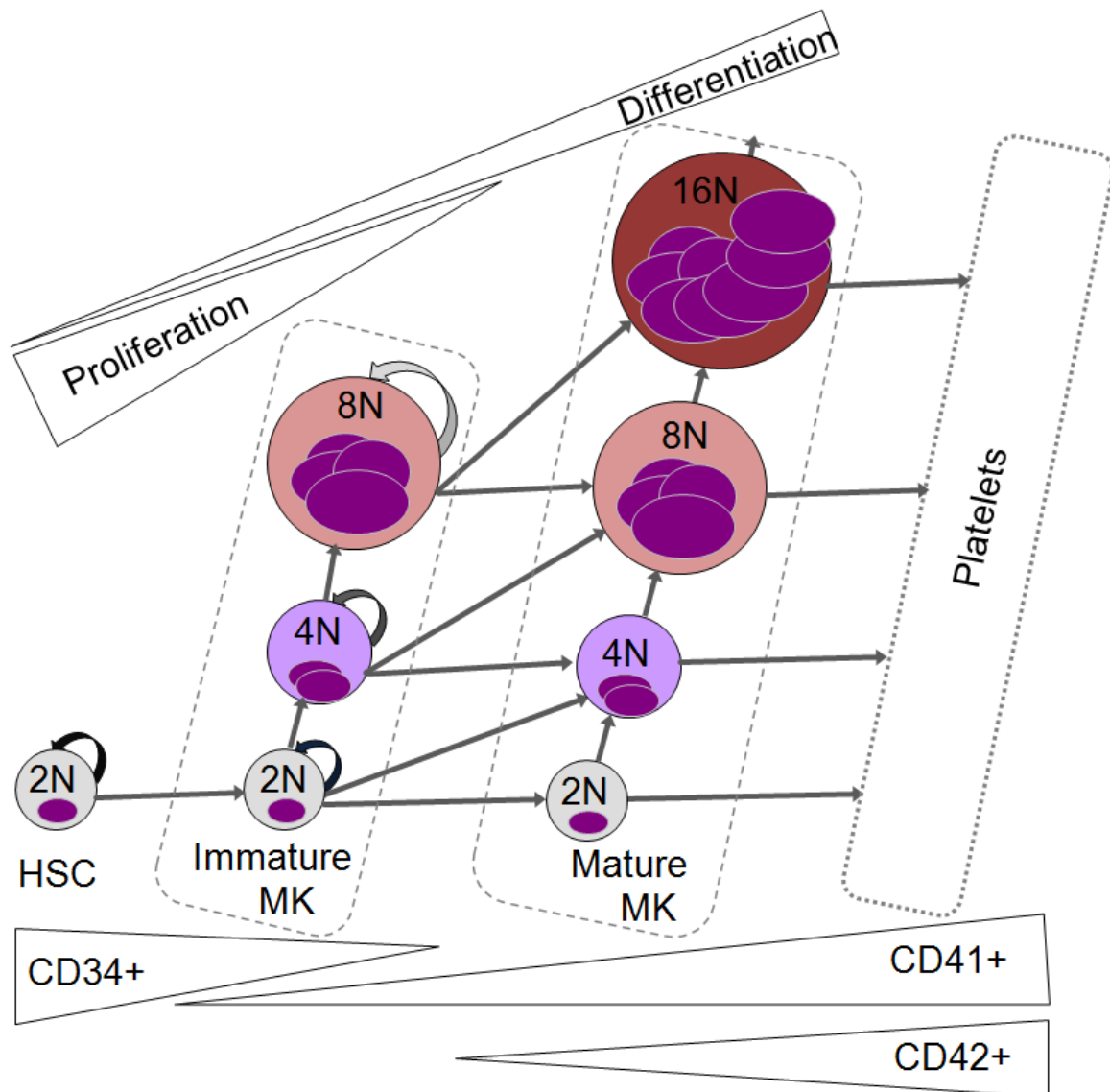
Figure 8.2: Proposed schematic model of MK growth, differentiation and polyploidization for future studies. The model shows diploid HSC CD34^{+} has the capability to proliferate or commit to immature MK (CD41^{+}). Immature MK can proliferate, polyploidize or differentiate to mature MK. Mature MK (CD42^{+}) cannot proliferate but can increase their ploidy level or release platelets. Mitosis rate is reduced by commitment from HSC toward mature MK.

References

1. Michelson AD. Platelets (ed 2nd). Amsterdam ; Boston: Academic Press/Elsevier; 2007.
2. Wright JH. Studies on the histogenesis of blood platelets. J Morphol. 1910;21:263–277.
3. Italiano JE, Jr., Lecine P, Shivdasani RA, Hartwig JH. Blood platelets are assembled principally at the ends of proplatelet processes produced by differentiated megakaryocytes. J Cell Biol. 1999;147:1299-1312.
4. Eils R, Athale C. Computational imaging in cell biology. J Cell Biol. 2003;161:477-481.
5. Hamilton N, Kerr MC, Burrage K, Teasdale RD. Analyzing real-time video microscopy: the dynamics and geometry of vesicles and tubules in endocytosis. Curr Protoc Cell Biol. 2007;Chapter 14:Unit 4 16.
6. Bryant JA, Francis D. The eukaryotic cell cycle. New York: Taylor & Francis; 2008.
7. Hunter T. Regulation of the eukaryotic cell cycle. Introduction. Ciba Found Symp. 1992;170:1-6.
8. Morgan DO. The cell cycle: principles of control. London, Sunderland, MA: New Science Press; Sinauer Associates; 2007.
9. Smith OP. Chapter9. Haematological Problems (ed 5th): Springer Berlin Heidelberg; 2009.
10. Kondo M, Wagers AJ, Manz MG, et al. Biology of hematopoietic stem cells and progenitors: implications for clinical application. Annu Rev Immunol. 2003;21:759-806.
11. Debili N, Coulombel L, Croisille L, et al. Characterization of a bipotent erythro-megakaryocytic progenitor in human bone marrow. Blood. 1996;88:1284-1296.
12. Baum CM, Weissman IL, Tsukamoto AS, Buckle AM, Peault B. Isolation of a candidate human hematopoietic stem-cell population. Proc Natl Acad Sci U S A. 1992;89:2804-2808.
13. Spangrude GJ, Heimfeld S, Weissman IL. Purification and characterization of mouse hematopoietic stem cells. Science. 1988;241:58-62.
14. Koestenbauer S, Zisch A, Dohr G, Zech NH. Protocols for hematopoietic stem cell expansion from umbilical cord blood. Cell Transplant. 2009;18:1059-1068.
15. Martinez-Agosto JA, Mikkola HK, Hartenstein V, Banerjee U. The hematopoietic stem cell and its niche: a comparative view. Genes Dev. 2007;21:3044-3060.
16. NIH. Regenerative Medicine. In: Services DoHaH ed. Vol. 139; 2006.
17. Ng YY, Baert MR, de Haas EF, Pike-Overzet K, Staal FJ. Isolation of human and mouse hematopoietic stem cells. Methods Mol Biol. 2009;506:13-21.
18. Cramer EM, Vainchenker W. Chapter 25. Platelet Production: Cellular and Molecular Regulation (ed 5th). Philadelphia, PA: Lippincott Williams & Wilkins; 2006.
19. Battinelli EM, Hartwig JH, Italiano JE, Jr. Delivering new insight into the biology of megakaryopoiesis and thrombopoiesis. Curr Opin Hematol. 2007;14:419-426.
20. Kaushansky K. The enigmatic megakaryocyte gradually reveals its secrets. Bioessays. 1999;21:353-360.
21. Handagama PJ, George JN, Shuman MA, McEver RP, D.F. B. Incorporation of a circulating protein into megakaryocyte and platelet granules. PNAS. 1987;84: 861-865

22. Youssefian T, Cramer EM. Megakaryocyte dense granule components are sorted in multivesicular bodies. Blood. 2000;95:4004-4007.
23. Breton-Gorius J, Vainchenker W, Nurden A, Levy-Toledano S, Caen J. Defective alpha-granule production in megakaryocytes from gray platelet syndrome: ultrastructural studies of bone marrow cells and megakaryocytes growing in culture from blood precursors. Am J Pathol. 1981;102:10-19.
24. Debili N, Issaad C, Masse JM, et al. Expression of CD34 and platelet glycoproteins during human megakaryocytic differentiation. Blood. 1992;80:3022-3035.
25. Odell TT, Jr., Jackson CW, Gosslee DG. Maturation of rat megakaryocytes studied by microspectrophotometric measurement of DNA. Proc Soc Exp Biol Med. 1965;119:1194-1199.
26. Ravid K, Lu J, Zimmet JM, Jones MR. Roads to polyploidy: the megakaryocyte example. J Cell Physiol. 2002;190:7-20.
27. Nagata Y, Muro Y, Todokoro K. Thrombopoietin-induced polyploidization of bone marrow megakaryocytes is due to a unique regulatory mechanism in late mitosis. J Cell Biol. 1997;139:449-457.
28. Vitrat N, Cohen-Solal K, Pique C, et al. Endomitosis of human megakaryocytes are due to abortive mitosis. Blood. 1998;91:3711-3723.
29. Geddis AE, Fox NE, Tkachenko E, Kaushansky K. Endomitotic megakaryocytes that form a bipolar spindle exhibit cleavage furrow ingression followed by furrow regression. Cell Cycle. 2007;6:455-460.
30. Lordier L, Jalil A, Aurade F, et al. Megakaryocyte endomitosis is a failure of late cytokinesis related to defects in the contractile ring and Rho/Rock signaling. Blood. 2008;112:3164-3174.
31. Bath PM, Carney C, Markandu ND, MacGregor GA. Platelet volume is not increased in essential hypertension. J Hum Hypertens. 1994;8:457-459.
32. Behnke O. An electron microscope study of the megacaryocyte of the rat bone marrow. I. The development of the demarcation membrane system and the platelet surface coat. J Ultrastruct Res. 1968;24:412-433.
33. Ebbe S, Bentfeld-Barker M, Adrados C, et al. Functionally abnormal stromal cells and megakaryocyte size, ploidy, and ultrastructure in Sl/Sld mice. Blood Cells. 1986;12:217-232.
34. Nakao K, Angrist AA. Membrane surface specialization of blood platelet and megakaryocyte. Nature. 1968;217:960-961.
35. Yamada E. The fine structure of the megakaryocyte in the mouse spleen. Acta Anat (Basel). 1957;29:267-290.
36. Harrison P, Cramer EM. Platelet alpha-granules. Blood Rev. 1993;7:52-62.
37. Bond J, Fliendre T, Archambeau J. Mammalian radiation lethality. London: Academic Press; 1965.
38. van den Oudenrijn S, von dem Borne AE, de Haas M. Differences in megakaryocyte expansion potential between CD34(+) stem cells derived from cord blood, peripheral blood, and bone marrow from adults and children. Exp Hematol. 2000;28:1054-1061.
39. Choi ES, Nichol JL, Hokom MM, Hornkohl AC, Hunt P. Platelets generated in vitro from proplatelet-displaying human megakaryocytes are functional. Blood. 1995;85:402-413.
40. Geddis AE, Kaushansky K. Immunology. The root of platelet production. Science. 2007;317:1689-1691.

41. Radley JM, Scurfield G. The mechanism of platelet release. Blood. 1980;56:996-999.

42. Patel SR, Richardson JL, Schulze H, et al. Differential roles of microtubule assembly and sliding in proplatelet formation by megakaryocytes. Blood. 2005;106:4076-4085.

43. Kosaki G. In vivo platelet production from mature megakaryocytes: does platelet release occur via proplatelets? Int J Hematol. 2005;81:208-219.

44. Kosaki G. Platelet production by megakaryocytes: protoplatelet theory justifies cytoplasmic fragmentation model. Int J Hematol. 2008;88:255-267.

45. Junt T, Schulze H, Chen Z, et al. Dynamic visualization of thrombopoiesis within bone marrow. Science. 2007;317:1767-1770.

46. Avecilla ST, Hattori K, Heissig B, et al. Chemokine-mediated interaction of hematopoietic progenitors with the bone marrow vascular niche is required for thrombopoiesis. Nat Med. 2004;10:64-71.

47. Lee KG, Miller T, Anastassov I, Cohen WD. Shape transformation and cytoskeletal reorganization in activated non-mammalian thrombocytes. Cell Biol Int. 2004;28:299-310.

48. Gregory M, Jagadeeswaran P. Selective labeling of zebrafish thrombocytes: quantitation of thrombocyte function and detection during development. Blood Cells Mol Dis. 2002;28:418-427.

49. Jagadeeswaran P, Sheehan JP, Craig FE, Troyer D. Identification and characterization of zebrafish thrombocytes. Br J Haematol. 1999;107:731-738.

50. Pang L, Weiss MJ, Poncz M. Megakaryocyte biology and related disorders. J Clin Invest. 2005;115:3332-3338.

51. Kato T, Ogami K, Shimada Y, et al. Purification and characterization of thrombopoietin. J Biochem (Tokyo). 1995;118:229-236.

52. Farese AM, Hunt P, Boone T, MacVittie TJ. Recombinant human megakaryocyte growth and development factor stimulates thrombocytopoiesis in normal nonhuman primates. Blood. 1995;86:54-59.

53. Mu SX, Xia M, Elliott G, et al. Megakaryocyte growth and development factor and interleukin-3 induce patterns of protein-tyrosine phosphorylation that correlate with dominant differentiation over proliferation of mpl-transfected 32D cells. Blood. 1995;86:4532-4543.

54. Toombs CF, Young CH, Glaspy JA, Varnum BC. Megakaryocyte growth and development factor (MGDF) moderately enhances in-vitro platelet aggregation. Thromb Res. 1995;80:23-33.

55. Ulich TR, del Castillo J, Yin S, et al. Megakaryocyte growth and development factor ameliorates carboplatin-induced thrombocytopenia in mice. Blood. 1995;86:971-976.

56. Vaickus L, Breitmeyer JB, Schlossman RL, Anderson KC. Platelet transfusion and alternatives to transfusion in patients with malignancy. Stem Cells. 1995;13:588-596.

57. Yamasaki K, Jamal N, Mann KG, Messner HA. Megakaryocyte colony growth-supporting activities in human plasma: modification by platelets and platelet membranes. J Cell Physiol. 1987;133:337-343.

58. Enomoto K, Kawakita M, Kishimoto S, Katayama N, Miyake T. Thrombopoiesis and megakaryocyte colony stimulating factor in the urine of patients with aplastic anaemia. Br J Haematol. 1980;45:551-556.

59. Williams N, McDonald TP, Rabellino EM. Maturation and regulation of megakaryocytopoiesis. Blood Cells. 1979;5:43-55.

60. Kaushansky K, Lok S, Holly RD, et al. Promotion of megakaryocyte progenitor expansion and differentiation by the c-Mpl ligand thrombopoietin. Nature. 1994;369:568-571.

61. Zeigler FC, de Sauvage F, Widmer HR, et al. In vitro megakaryocytopoietic and thrombopoietic activity of c-mpl ligand (TPO) on purified murine hematopoietic stem cells. Blood. 1994;84:4045-4052.

62. Banu N, Wang JF, Deng B, Groopman JE, Avraham H. Modulation of megakaryocytopoiesis by thrombopoietin: the c-Mpl ligand. Blood. 1995;86:1331-1338.

63. Broudy VC, Lin NL, Kaushansky K. Thrombopoietin (c-mpl ligand) acts synergistically with erythropoietin, stem cell factor, and interleukin-11 to enhance murine megakaryocyte colony growth and increases megakaryocyte ploidy in vitro. Blood. 1995;85:1719-1726.

64. Chen J, Herceg-Harjacek L, Groopman JE, Grabarek J. Regulation of platelet activation in vitro by the c-Mpl ligand, thrombopoietin. Blood. 1995;86:4054-4062.

65. Kuter DJ, Beeler DL, Rosenberg RD. The purification of megapoietin: a physiological regulator of megakaryocyte growth and platelet production. Proc Natl Acad Sci U S A. 1994;91:11104-11108.

66. Kuter DJ, Rosenberg RD. Appearance of a megakaryocyte growth-promoting activity, megapoietin, during acute thrombocytopenia in the rabbit. Blood. 1994;84:1464-1472.

67. Doshi PD, Giri JG, Abegg AL, et al. Promegapoietin, a family of chimeric growth factors, supports megakaryocyte development through activation of IL-3 and c-Mpl ligand signaling pathways. Exp Hematol. 2001;29:1177-1184.

68. Kuter DJ. Thrombopoietin: biology, clinical applications, role in the donor setting. J Clin Apher. 1996;11:149-159.

69. Wendling F, Han ZC. Positive and negative regulation of megakaryocytopoiesis. Baillieres Clin Haematol. 1997;10:29-45.

70. Zauli G, Vitale M, Falcieri E, et al. In vitro senescence and apoptotic cell death of human megakaryocytes. Blood. 1997;90:2234-2243.

71. Kuter DJ. Chapter 54: Thrombopoietin: Academic Press; 2002.

72. Harker LA, Marzec UM, Hunt P, et al. Dose-response effects of pegylated human megakaryocyte growth and development factor on platelet production and function in nonhuman primates. Blood. 1996;88:511-521.

73. Choi ES, Hokom MM, Chen JL, et al. The role of megakaryocyte growth and development factor in terminal stages of thrombopoiesis. Br J Haematol. 1996;95:227-233.

74. Oda A, Miyakawa Y, Druker BJ, et al. Thrombopoietin primes human platelet aggregation induced by shear stress and by multiple agonists. Blood. 1996;87:4664-4670.

75. Sitnicka E, Lin N, Priestley GV, et al. The effect of thrombopoietin on the proliferation and differentiation of murine hematopoietic stem cells. Blood. 1996;87:4998-5005.

76. Kobayashi M, Laver JH, Kato T, Miyazaki H, Ogawa M. Thrombopoietin supports proliferation of human primitive hematopoietic cells in synergy with steel factor and/or interleukin-3. Blood. 1996;88:429-436.

77. Gurney AL, Carver-Moore K, de Sauvage FJ, Moore MW. Thrombocytopenia in c-mpl-deficient mice. Science. 1994;265:1445-1447.

78. Carver-Moore K, Broxmeyer HE, Luoh SM, et al. Low levels of erythroid and myeloid progenitors in thrombopoietin-and c-mpl-deficient mice. Blood. 1996;88:803-808.

79. Ballmaier M, Germeshausen M, Schulze H, et al. c-mpl mutations are the cause of congenital amegakaryocytic thrombocytopenia. Blood. 2001;97:139-146.

80. Fitzgerald KA, O'Neil LAJ, Gearing AJH, Callard RE. The cytokine facts book (ed second): Academic Press; 2001.

81. Orazi A, Cooper RJ, Tong J, et al. Effects of recombinant human interleukin-11 (Neumega rhIL-11 growth factor) on megakaryocytopoiesis in human bone marrow. Exp Hematol. 1996;24:1289-1297.

82. Cortin V, Garnier A, Pineault N, Lemieux R, Boyer L, Proulx C. Efficient in vitro megakaryocyte maturation using cytokine cocktails optimized by statistical experimental design. Exp Hematol. 2005;33:1182-1191.

83. Sigurjonsson OE, Gudmundsson KO, Haraldsdottir V, Rafnar T, Agnarsson BA, Gudmundsson S. Flt3/Flk-2 ligand in combination with thrombopoietin decreases apoptosis in megakaryocyte development. Stem Cells Dev. 2004;13:183-191.

84. Lefebvre P, Winter JN, Meng Y, Cohen I. Ex vivo expansion of early and late megakaryocyte progenitors. J Hematother Stem Cell Res. 2000;9:913-921.

85. LaIuppa JA, Papoutsakis ET, Miller WM. Evaluation of cytokines for expansion of the megakaryocyte and granulocyte lineages. Stem Cells. 1997;15:198-206.

86. Teramura M, Katahira J, Hoshino S, Motoji T, Oshimi K, Mizoguchi H. Clonal growth of human megakaryocyte progenitors in serum-free cultures: effect of recombinant human interleukin 3. Exp Hematol. 1988;16:843-848.

87. Mazur EM, Cohen JL, Bogart L, et al. Recombinant gibbon interleukin-3 stimulates megakaryocyte colony growth in vitro from human peripheral blood progenitor cells. J Cell Physiol. 1988;136:439-446.

88. Gordon MS, Hoffman R. Growth factors affecting human thrombocytopoiesis: potential agents for the treatment of thrombocytopenia. Blood. 1992;80:302-307.

89. Leven RM, Clark B, Tablin F. Effect of recombinant interleukin-6 and thrombopoietin on isolated guinea pig bone marrow megakaryocyte protein phosphorylation and proplatelet formation. Blood Cells Mol Dis. 1997;23:252-268.

90. Fujiki H, Kimura T, Minamiguchi H, et al. Role of human interleukin-9 as a megakaryocyte potentiator in culture. Exp Hematol. 2002;30:1373-1380.

91. Weich NS, Wang A, Fitzgerald M, et al. Recombinant human interleukin-11 directly promotes megakaryocytopoiesis in vitro. Blood. 1997;90:3893-3902.

92. Gordon MS, McCaskill-Stevens WJ, Battiato LA, et al. A phase I trial of recombinant human interleukin-11 (neumega rhIL-11 growth factor) in women with breast cancer receiving chemotherapy. Blood. 1996;87:3615-3624.

93. Schlerman FJ, Bree AG, Kaviani MD, et al. Thrombopoietic activity of recombinant human interleukin 11 (rHuIL-11) in normal and myelosuppressed nonhuman primates. Stem Cells. 1996;14:517-532.

94. Vainchenker W, Debili N, Mouthon MA, Wendling F. Megakaryocytopoiesis: cellular aspects and regulation. Crit Rev Oncol Hematol. 1995;20:165-192.

95. Kie JH, Yang WI, Lee MK, et al. Decrease in apoptosis and increase in polyploidization of megakaryocytes by stem cell factor during ex vivo expansion of human cord blood CD34+ cells using thrombopoietin. Stem Cells. 2002;20:73-79.

96. Pineault N. Individual and synergistic cytokine effects controlling the expansion of cord blood CD34+ cells and megakaryocyte progenitors in culture Cytotherapy. 2010;Epub ahead of print.

97. Shaw PH, Olszewski M, Kletzel M. Expansion of megakaryocyte precursors and stem cells from umbilical cord blood CD34+ cells in collagen and liquid culture media. J Hematother Stem Cell Res. 2001;10:391-403.

98. De Bruyn C, Delforge A, Martiat P, Bron D. Ex vivo expansion of megakaryocyte progenitor cells: cord blood versus mobilized peripheral blood. Stem Cells Dev. 2005;14:415-424.

99. Bornstein R, Garcia-Vela J, Gilsanz F, Auray C, Cales C. Cord blood megakaryocytes do not complete maturation, as indicated by impaired establishment of endomitosis and low expression of G1/S cyclins upon thrombopoietin-induced differentiation. Br J Haematol. 2001;114:458-465.

100. Mattia G, Vulcano F, Milazzo L, et al. Different ploidy levels of megakaryocytes generated from peripheral or cord blood CD34+ cells are correlated with different levels of platelet release. Blood. 2002;99:888-897.

101. Miyazaki R, Ogata H, Iguchi T, et al. Comparative analyses of megakaryocytes derived from cord blood and bone marrow. Br J Haematol. 2000;108:602-609.

102. Giammona LM, Fuhrken PG, Papoutsakis ET, Miller WM. Nicotinamide (vitamin B3) increases the polyploidisation and proplatelet formation of cultured primary human megakaryocytes. Br J Haematol. 2006;135:554-566.

103. Garcia Vela JA, Delgado I, Bornstein R, et al. Comparative intracellular cytokine production by in vitro stimulated T lymphocytes from human umbilical cord blood (HUCB) and adult peripheral blood (APB). Anal Cell Pathol. 2000;20:93-98.

104. Proulx C, Dupuis N, St-Amour I, Boyer L, Lemieux R. Increased megakaryopoiesis in cultures of CD34-enriched cord blood cells maintained at 39 degrees C. Biotechnol Bioeng. 2004;88:675-680.

105. Hegyi E, Nakazawa M, Debili N, et al. Developmental changes in human megakaryocyte ploidy. Exp Hematol. 1991;19:87-94.

106. Rocha V, Labopin M, Sanz G, et al. Transplants of umbilical-cord blood or bone marrow from unrelated donors in adults with acute leukemia. N Engl J Med. 2004;351:2276-2285.

107. Giammona LM, Papoutsakis E, Miller WM. Nicotinamide Enhances the Polyploidization of Primary Megakaryocytes; 2005.

108. Giammona LM, Panuganti S, Kemper JM, et al. Mechanistic studies on the effects of nicotinamide on megakaryocytic polyploidization and the roles of NAD+ levels and SIRT inhibition. Exp Hematol. 2009;37:1340-1352 e1343.

109. Pineault N, Boucher JF, Cayer MP, et al. Characterization of the effects and potential mechanisms leading to increased megakaryocytic differentiation under mild hyperthermia. Stem Cells Dev. 2008;17:483-493.

110. Sherley JL, Stadler PB, Scott Stadler J. A quantitative method for the analysis of mammalian cell proliferation in culture in terms of dividing and non-dividing cells. Cell Proliferation. 1995;28:137-144.

111. Deasy BM, Jankowski RJ, Payne TR, et al. Modeling stem cell population growth: incorporating terms for proliferative heterogeneity. Stem Cells. 2003;21:536-545.

112. Deasy BM, Qu-Peterson Z, Greenberger JS, Huard J. Mechanisms of muscle stem cell expansion with cytokines. Stem Cells. 2002;20:50-60.

113. Deasy BM, Gharaibeh BM, Pollett JB, et al. Long-term self-renewal of postnatal muscle-derived stem cells. Mol Biol Cell. 2005;16:3323-3333.
114. Deasy BM, Jankowski RJ, Huard J. Muscle-derived stem cells: characterization and potential for cell-mediated therapy. Blood Cells Mol Dis. 2001;27:924-933.
115. Pierelli L, Scambia G, Fattorossi A, et al. Functional, phenotypic and molecular characterization of cytokine low-responding circulating CD34+ haemopoietic progenitors. Br J Haematol. 1998;102:1139-1150.
116. Ko KH, Odell R, Nordon RE. Analysis of cell differentiation by division tracking cytometry. Cytometry A. 2007;71:773-782.
117. Lyons AB. Analysing cell division in vivo and in vitro using flow cytometric measurement of CFSE dye dilution. J Immunol Methods. 2000;243:147-154.
118. Allison PD, SAS Institute. Logistic regression using the SAS system : theory and application. Cary, N.C.: SAS Institute; 2003.
119. Hosmer DW, Lemeshow S. Applied logistic regression (ed 2nd). New York: Wiley; 2000.
120. Menard SW. Applied logistic regression analysis. Thousand Oaks, Calif.: Sage Publications; 1995.
121. Pampel FC. Logistic regression : a primer. Thousand Oaks, Calif.: Sage Publications; 2000.
122. Jolicoeur P, Pontier J. Population growth and dcecline: a four-parameter generalization of the logistic curve. Theor Biol. 1989;141:563-571.
123. Goudar CT, Joeris K, Konstantinov KB, Piret JM. Logistic equations effectively model Mammalian cell batch and fed-batch kinetics by logically constraining the fit. Biotechnol Prog. 2005;21:1109-1118.
124. Graves WG, Peckham B, Pastor J. A bifurcation analysis of a differential equations model for mutualism. Bull Math Biol. 2006;68:1851-1872.
125. Haegeman B, Loreau M. A mathematical synthesis of niche and neutral theories in communityecology. J Theor Biol. 2010.
126. Kooi BW, Kuijper LD, Kooijman SA. Consequences of symbiosis for food web dynamics. J Math Biol. 2004;49:227-271.
127. Loeffler M, Wichmann HE. A comprehensive mathematical model of stem cell proliferation which reproduces most of the published experimental results. Cell Tissue Kinet. 1980;13:543-561.
128. Nielsen LK, Papoutsakis ET, Miller aWM. Modeling ex vivo hematopoiesis using chemical engineering metaphors. Chem Eng Sci. 1998;53:1913-1925.
129. Bernstein SH, Jusko WJ, Krzyzanski W, Nichol J, Wetzler M. Pharmacodynamic modeling of thrombopoietin, platelet, and megakaryocyte dynamics in patients with acute myeloid leukemia undergoing dose intensive chemotherapy. J Clin Pharmacol. 2002;42:501-511.
130. Colijn C, Mackey MC. A mathematical model of hematopoiesis--I. Periodic chronic myelogenous leukemia. J Theor Biol. 2005;237:117-132.
131. da Silva CL, Goncalves R, Lemos F, et al. Modelling of ex vivo expansion/maintenance of hematopoietic stem cells. Bioprocess Biosyst Eng. 2003;25:365-369.
132. Goncalves R, da Silva CL, Ferreira BS, et al. Kinetic analysis of the ex vivo expansion of human hematopoietic stem/progenitor cells. Biotechnol Lett. 2006;28:335-340.

133. Hardy K, Stark J. Mathematical models of the balance between apoptosis and proliferation. Apoptosis. 2002;7:373-381.

134. Jin F, Krzyzanski W. Pharmacokinetic model of target-mediated disposition of thrombopoietin. AAPS PharmSci. 2004;6:E9.

135. Peng C-A, Koller MR, Palson aBO. Unilineage model of hematopoiesis predicts self-renewal of stem and progenitors cells based on ex vivo growth data. Biotechnol Bioeng. 1996;52:24-33.

136. Prudhomme WA, Duggar KH, Lauffenburger DA. Cell population dynamics model for deconvolution of murine embryonic stem cell self-renewal and differentiation responses to cytokines and extracellular matrix. Biotechnol Bioeng. 2004;88:264-272.

137. Viswanathan S, Zandstra PW. Towards predictive models of stem cell fate. Cytotechnology. 2003;41:75-92.

138. Santillan M, Mahaffy JM, Belair J, Mackey MC. Regulation of platelet production: the normal response to perturbation and cyclical platelet disease. J Theor Biol. 2000;206:585-603.

139. Kuter DJ. The physiology of platelet production. Stem Cells. 1996;14 Suppl 1:88-101.

140. Harker LA, Roskos LK, Marzec UM, et al. Effects of megakaryocyte growth and development factor on platelet production, platelet life span, and platelet function in healthy human volunteers. Blood. 2000;95:2514-2522.

141. Camille NA, Marshall AL. Structure of the marrow New York: McGraw Hill; 1995.

142. Chaudhry MA, Bowen BD, Eaves CJ, Piret JM. Empirical models of the proliferative response of cytokine-dependent hematopoietic cell lines. Biotechnol Bioeng. 2004;88:348-358.

143. Sung MH, McNally JG. Live cell imaging and systems biology. Wiley Interdiscip Rev Syst Biol Med. 2010.

144. Rieder CL, Khodjakov A. Mitosis through the microscope: advances in seeing inside live dividing cells. Science. 2003;300:91-96.

145. Bajer AS, Bajer JM. Spindle dynamics and chromosome movements. Int Rev Cytol. 1972;3:1-271.

146. Hinchcliffe EH. Using long-term time-lapse imaging of mammalian cell cycle progression for laboratory instruction and analysis. Cell Biol Educ. 2005;4:284-290.

147. Dykstra B, Ramunas J, Kent D, et al. High-resolution video monitoring of hematopoietic stem cells cultured in single-cell arrays identifies new features of self-renewal. Proc Natl Acad Sci U S A. 2006;103:8185-8190.

148. Day D, Pham K, Ludford-Menting MJ, et al. A method for prolonged imaging of motile lymphocytes. Immunol Cell Biol. 2009;87:154-158.

149. Iyer G, Michalet X, Chang YP, Weiss S. Tracking single proteins in live cells using single-chain antibody fragment-fluorescent quantum dot affinity pair. Methods Enzymol. 2010;475:61-79.

150. Jaiswal JK, Mattoussi H, Mauro JM, Simon SM. Long-term multiple color imaging of live cells using quantum dot bioconjugates. Nat Biotechnol. 2003;21:47-51.

151. Michalet X, Pinaud FF, Bentolila LA, et al. Quantum dots for live cells, in vivo imaging, and diagnostics. Science. 2005;307:538-544.

152. Trache A, Lim SM. Integrated microscopy for real-time imaging of mechanotransduction studies in live cells. J Biomed Opt. 2009;14:034024.

153. Wang Y, Shyy JY, Chien S. Fluorescence proteins, live-cell imaging, and mechanobiology: seeing is believing. Annu Rev Biomed Eng. 2008;10:1-38.

154. Xie M, Tataw M, Venugopala Reddy G. Towards a functional understanding of cell growth dynamics in shoot meristem stem-cell niche. Semin Cell Dev Biol. 2009;20:1126-1133.

155. Cutler SR, Somerville CR. Imaging plant cell death: GFP-Nit1 aggregation marks an early step of wound and herbicide induced cell death. BMC Plant Biol. 2005;5:4.

156. Mechali M, Lutzmann M. The cell cycle: now live and in color. Cell. 2008;132:341-343.

157. Proulx C, Boyer L, Hurnanen DR, Lemieux R. Preferential ex vivo expansion of megakaryocytes from human cord blood CD34+-enriched cells in the presence of thrombopoietin and limiting amounts of stem cell factor and Flt-3 ligand. J Hematother Stem Cell Res. 2003;12:179-188.

158. Boyer L, Robert A, Proulx C, Pineault N. Increased production of megakaryocytes near purity from cord blood CD34+ cells using a short two-phase culture system. J Immunol Methods. 2008;332:82-91.

159. Cortin V, Pineault N, Garnier A. Ex vivo megakaryocyte expansion and platelet production from human cord blood stem cells. Methods Mol Biol. 2009;482:109-126.

160. Norol F, Vitrat N, Cramer E, et al. Effects of cytokines on platelet production from blood and marrow CD34+ cells. Blood. 1998;91:830-843.

161. Cybernetics M. In vivo User Guides Version 3.2. Silver Spring, MD; 2006.

162. Gonzalez RC, Woods RE. Digital image processing (ed 2nd). Upper Saddle River, N.J.: Prentice Hall; 2002.

163. Gonzalez RC. Digital Image Processing Using Matlab. Upper Saddle River: PRENTICE HALL PTR; 2004.

164. McAndrew A. Introduction to digital image processing with Matlab. Boston, MA.: Thomson Course Technology; 2004.

165. Semmlow JL. Biosignal and biomedical image processing : MATLAB-based applications. New York: Marcel Dekker; 2004.

166. Robert A, Boyer L, Pineault N. Glycoprotein Ibα Receptor Instability Is Associated with Loss of Quality in Platelets Produced in Culture. Stem Cells and Development. 2010; Sep 15. [Epub ahead of print].

167. Wichmann HE, Gerhardts MD, Spechtmeyer H, Gross R. A mathematical model of thrombopoiesis in rats. Cell Tissue Kinet. 1979;12:551-567.

168. Skomorovski K, Harpak H, Ianovski A, et al. New TPO treatment schedules of increased safety and efficacy: pre-clinical validation of a thrombopoiesis simulation model. Br J Haematol. 2003;123:683-691.

169. Yao KZ, Shaw BM, Kou B, McAuley KB, Bacon aDW. Modeling Ethylene/Butene Copolymerization with Multi-site Catalysts: Parameter Estimability and Experimental Design Polymer reaction Engineering. 2003;11:563-588.

170. Yue H, Brown M, Knowles J, Wang H, Broomhead DS, Kell DB. Insights into the behaviour of systems biology models from dynamic sensitivity and identifiability analysis: a case study of an NF-kappaB signalling pathway. Mol Biosyst. 2006;2:640-649.

171. Clarke MC, Savill J, Jones DB, Noble BS, Brown SB. Compartmentalized megakaryocyte death generates functional platelets committed to caspase-independent death. J Cell Biol. 2003;160:577-587.

172. Leysi-Derilou Y, Robert A, Duchesne C, Garnier A, Boyer L, Pineault N. Polyploid Megakaryocytes Can Complete Cytokinesis. Cell Cycle. 2010;9:2589-2599.

173. Bates DM, Watts DG. Nonlinear regression analysis and its applications. New York ; Toronto: Wiley; 1988.

174. Blanco M, Coello J, Iturriaga H, Maspoch S, Riba J, Rovira E. Kinetic spectrophotometric determination of Ga(III)-Al(III) mixtures by stopped-flow injection analysis using principal component regression. Talanta. 1993;40:261-267.

175. Chester VL, Wrigley AT. The identification of age-related differences in kinetic gait parameters using principal component analysis. Clin Biomech (Bristol, Avon). 2008;23:212-220.

176. Vajda S, Valko P, TURANYI T. Principal Component Analysis of Kinetic Models International Journal of Chemical Kinetics. 1985;17:55-81.

177. Morris MD. Factorial sampling plans for preliminary computational experiments. Technometrics. 1991;33:161-174.

178. Saltelli A, Ratto M, Tarantola S, Campolongo F. Sensitivity analysis for chemical models. Chem Rev. 2005;105:2811-2828.

179. Wilson A, Laurenti E, Oser G, et al. Hematopoietic stem cells reversibly switch from dormancy to self-renewal during homeostasis and repair. Cell. 2008;135:1118-1129.

180. Kirouac DC, Madlambayan GJ, Yu M, Sykes EA, Ito C, Zandstra PW. Cell-cell interaction networks regulate blood stem and progenitor cell fate. Mol Syst Biol. 2009;5:293.

181. Galipeau PC, Cowan DS, Sanchez CA, et al. 17p (p53) allelic losses, 4N (G2/tetraploid) populations, and progression to aneuploidy in Barrett's esophagus. Proc Natl Acad Sci U S A. 1996;93:7081-7084.

182. Falcieri E, Bassini A, Pierpaoli S, et al. Ultrastructural characterization of maturation, platelet release, and senescence of human cultured megakaryocytes. Anat Rec. 2000;258:90-99.

183. Otto SP. The evolutionary consequences of polyploidy. Cell. 2007;131:452-462.

184. Schwertz H, Koster S, Kahr WH, et al. Anucleate platelets generate progeny. Blood. 2010.

185. Chu K, Teele N, Dewey MW, Albright N, Dewey WC. Computerized video time lapse study of cell cycle delay and arrest, mitotic catastrophe, apoptosis and clonogenic survival in irradiated 14-3-3sigma and CDKN1A (p21) knockout cell lines. Radiat Res. 2004;162:270-286.

186. Geddis AE, Kaushansky K. Endomitotic megakaryocytes form a midzone in anaphase but have a deficiency in cleavage furrow formation. Cell Cycle. 2006;5:538-545.

187. Tomer A, Harker LA, Burstein SA. Flow cytometric analysis of normal human megakaryocytes. Blood. 1988;71:1244-1252.

188. Worthington RE, Nakeff A, Micko S. Flow cytometric analysis of megakaryocyte differentiation. Cytometry. 1984;5:501-508.

189. Zhang Y, Nagata Y, Yu G, et al. Aberrant quantity and localization of Aurora-B/AIM-1 and survivin during megakaryocyte polyploidization and the consequences of Aurora-B/AIM-1-deregulated expression. Blood. 2004;103:3717-3726.

190. Levine RF, Hazzard KC, Lamberg JD. The significance of megakaryocyte size. Blood. 1982;60:1122-1131.

191. Tomer A. Human marrow megakaryocyte differentiation: multiparameter correlative analysis identifies von Willebrand factor as a sensitive and distinctive marker for early (2N and 4N) megakaryocytes. Blood. 2004;104:2722-2727.

192. Tao H, Gaudry L, Rice A, Chong B. Cord blood is better than bone marrow for generating megakaryocytic progenitor cells. Exp Hematol. 1999;27:293-301.

193. Keighren M, West JD. Analysis of cell ploidy in histological sections of mouse tissues by DNA-DNA in situ hybridization with digoxigenin-labelled probes. Histochem J. 1993;25:30-44.

194. Decordier I, Cundari E, Kirsch-Volders M. Mitotic checkpoints and the maintenance of the chromosome karyotype. Mutat Res. 2008;651:3-13.

195. Roy L, Coullin P, Vitrat N, et al. Asymmetrical segregation of chromosomes with a normal metaphase/anaphase checkpoint in polyploid megakaryocytes. Blood. 2001;97:2238-2247.

196. Schipper LF, Brand A, Reniers NC, Melief CJ, Willemze R, Fibbe WE. Effects of thrombopoietin on the proliferation and differentiation of primitive and mature haemopoietic progenitor cells in cord blood. Br J Haematol. 1998;101:425-435.

197. Carow CE, Fox NE, Kaushansky K. Kinetics of endomitosis in primary murine megakaryocytes. J Cell Physiol. 2001;188:291-303.

198. Sakhinia E, Weaver DL, Nunez C, Brunet C, Bostock V, Brady G. Single-cell RT-PCR cDNA subtraction. Methods Mol Biol. 2008;461:667-674.

199. Muller D, Jones PM, Persaud SJ. Single-cell RT-PCR identification of genes expressed by human islet endocrine cells. Methods Mol Biol. 2009;560:73-86.

200. Toledo-Rodriguez M, Markram H. Single-cell RT-PCR, a technique to decipher the electrical, anatomical, and genetic determinants of neuronal diversity. Methods Mol Biol. 2007;403:123-139.

201. Duhamel S, Gregori G, Van Wambeke F, Mauriac R, Nedoma J. A method for analysing phosphatase activity in aquatic bacteria at the single cell level using flow cytometry. J Microbiol Methods. 2008;75:269-278.

202. Perez OD, Nolan GP. Phospho-proteomic immune analysis by flow cytometry: from mechanism to translational medicine at the single-cell level. Immunol Rev. 2006;210:208-228.

203. Prussin C. Cytokine flow cytometry: understanding cytokine biology at the single-cell level. J Clin Immunol. 1997;17:195-204.

204. Ecker RC, Steiner GE. Microscopy-based multicolor tissue cytometry at the single-cell level. Cytometry A. 2004;59:182-190.

205. Errington RJ, Marquez N, Chappell SC, Wiltshire M, Smith PJ. Time-lapse microscopy approaches to track cell cycle progression at the single-cell level. Curr Protoc Cytom. 2005;Chapter 12:Unit 12 14.

206. Nancharaiah YV, Rajadurai M, Venugopalan VP. Single cell level microalgal ecotoxicity assessment by confocal microscopy and digital image analysis. Environ Sci Technol. 2007;41:2617-2621.

207. Leysi-Derilou Y, Robert A, Duchesne C, Garnier A, Boyer L, Pineault N. Polyploid Megakaryocytes Can Complete Cytokinesis. Cell Cycle. 2010;9: 2587-2597.

208. Papadantonakis N, Ravid K. Chapter 5. Development of Megakaryocytes. In: Kee AWaB, ed. Molecular Basis of Hematopoiesis: Springer Science + Business Media; 2009:95-126.

209. Lannutti BJ, Blake N, Gandhi MJ, Reems JA, Drachman JG. Induction of polyploidization in leukemic cell lines and primary bone marrow by Src kinase inhibitor SU6656. Blood. 2005;105:3875-3878.

210. Guerriero R, Parolini I, Testa U, et al. Inhibition of TPO-induced MEK or mTOR activity induces opposite effects on the ploidy of human differentiating megakaryocytes. J Cell Sci. 2006;119:744-752.

211. Arriaga M, South K, Cohen JL, Mazur EM. Interrelationship between mitosis and endomitosis in cultures of human megakaryocyte progenitor cells. Blood. 1987;69:486-492.

212. Chang Y, Bluteau D, Debili N, Vainchenker W. From hematopoietic stem cells to platelets. J Thromb Haemost. 2007;5 Suppl 1:318-327.

213. Papadantonakis N, Makitalo M, McCrann DJ, et al. Direct visualization of the endomitotic cell cycle in living megakaryocytes: differential patterns in low and high ploidy cells. Cell Cycle. 2008;7:2352-2356.

214. Skokowa J, Lan D, Thakur BK, et al. NAMPT is essential for the G-CSF-induced myeloid differentiation via a NAD(+)-sirtuin-1-dependent pathway. Nat Med. 2009;15:151-158.

215. Oren M. Decision making by p53: life, death and cancer. Cell Death Differ. 2003;10:431-442.

216. Spronck JC, Nickerson JL, Kirkland JB. Niacin deficiency alters p53 expression and impairs etoposide-induced cell cycle arrest and apoptosis in rat bone marrow cells. Nutr Cancer. 2007;57:88-99.

217. Jacobson EL, Shieh WM, Huang AC. Mapping the role of NAD metabolism in prevention and treatment of carcinogenesis. Mol Cell Biochem. 1999;193:69-74.

218. Surjana D, Halliday GM, Damian DL. Role of nicotinamide in DNA damage, mutagenesis, and DNA repair. J Nucleic Acids. 2010;[Epub ahead of print].

219. Ramunas J, Illman M, Kam A, et al. True monolayer cell culture in a confined 3D microenvironment enables lineage informatics. Cytometry A. 2006;69:1202-1211.

220. Ramunas J, Montgomery HJ, Kelly L, Sukonnik T, Ellis J, Jervis EJ. Real-time fluorescence tracking of dynamic transgene variegation in stem cells. Mol Ther. 2007;15:810-817.

221. Wang X, Crispino JD, Letting DL, Nakazawa M, Poncz M, Blobel GA. Control of megakaryocyte-specific gene expression by GATA-1 and FOG-1: role of Ets transcription factors. Embo J. 2002;21:5225-5234.

222. Colijn C, Mackey MC. A mathematical model of hematopoiesis: II. Cyclical neutropenia. J Theor Biol. 2005;237:133-146.

223. White RM, Sessa A, Burke C, et al. Transparent adult zebrafish as a tool for in vivo transplantation analysis. Cell Stem Cell. 2008;2:183-189.

Appendix. Live Cell Imaging Reveals New Insight Into Megakaryopoiesis[$]

Younes Leysi-Derilou,[1,2] Carl Duchesne,[1] Nicolas Pineault,[2] and Alain Garnier[1*]

[1]Département de Génie Chimique, Université Laval, Québec, QC, Canada, G1V 0A6;

[2]Département de R&D, Héma-Québec, Québec, QC, Canada G1V 5C3

*Correspondence and Reprint Requests:

Dr. Alain Garnier

Department of Chemical Engineering, Laval University, Québec, QC, Canada G1V 0A6

Telephone: (418) 656-3106. Fax: (418) 656-3993

E-Mails: alain.garnier@gch.ulaval.ca

A.1. Abstract/ Résumé

Megakaryocyte (MK) undergoes polyploidization through endomitosis during its normal development. To better characterize the cellular events occurring in this process and their frequencies, we have performed long-term and large-field live cell imaging of *in vitro* MK cultures. In this work, we first report that a considerable proportion of polyploid MKs (4N to 16N) can complete mitosis and contribute significantly to the expansion of the polyploid MK population. Furthermore, we demonstrate that polyploid MK mitosis depends on the cell source, is inversely related to the ploidy level and can be controlled by the addition of chemicals. These new findings explain in part the unresolved issue of lower ploidy level of cord-blood derived MKs and contest the concept by which polyploid MKs do not divide or that MK polyploidization results exclusively from interrupted cytokinesis. The imaging data have been further analyzed by plotting lineage trees of the observed cells. This allowed classification of cell fate into four typical patterns, which frequencies determination permitted to deepen the understanding of megakaryopoiesis dynamics. We illustrate the applicability of such a data mining approach by highlighting cell-age effects on MK dynamics.

Les cellules mégacaryocytaires (MKs) subissent au cours de leur développement une polyploïdisation à travers l'endomitose. Afin de mieux caractériser les événements cellulaires survenant dans ce processus complexe et leurs fréquences, nous avons mis au point un système d'imagerie microscopique à long terme et à grande échelle, ceci dans le but de mettre des cellules MKs viables en cultures *in vitro*. Dans ce travail, nous avons démontré en premier lieu, qu'une proportion considérable des cellules MKs polyploïdes (4N à 16N) peuvent compléter la mitose et aussi contribuer de manière significative à l'expansion de la population des cellules MKs polyploïdes. Deuxièmement, nous avons également démontré que la mitose des cellules MKs polyploïdes dépend de la source de cellules $CD34^+$ utilisée, et ceci est inversement relié au niveau de ploïdie des MKs. Ainsi, l'ajout de produits chimiques peut contribuer au contrôle de ce phénomène. Ces nouveaux résultats permettent d'expliquer d'une part, la question non résolue du niveau de ploïdie

inférieure des MKs provenant de sang du cordon et d'une d'autre part, contestent la théorie par lequel les cellules MKs polyploïdes ne se divisent pas ou que la polyploïdisation des cellules MKs résulte exclusivement de l'interruption de la cytocinèse. Par ailleurs, les données d'imagerie ont été analysées en traçant un arbre de lignage cellulaire. Cela a permis de faire une classification du devenir des cellules en quatre modèles typiques, laquelle a permis de déterminer les fréquences des divisions autorisées et a également permis d'approfondir la compréhension de la dynamique de la mégakaryopoïèse. Pour terminer, nous avons illustré l'applicabilité des données d'une telle approche en mettant en évidence les effets de l'âge des cellules dans la dynamique de la mégakaryopoïèse.

A.2. Introduction

To date, among the mammalian marrow cells, megakaryocytes (MK) are the only cells known to undergo polyploidization during their normal development, through a process called endomitosis[1]. MK endomitosis has been recently reported to be an interruption of cytokinesis, either at the anaphase midzone formation[2] or at the cleavage furrow ingression stages[3]. Using time-lapse confocal microscopy, Lordier et al. (2008) confirmed very recently that cleavage furrow ingression occurs in all of the sightings of diploid MKs undergoing endomitosis. Given that cellular division is interrupted at such a late stage of mitosis, it could be hypothesized that in some instances, polyploid MKs could complete cytokinesis and divide. However, polyploid MK division has not yet been reported[1,4].

A.3. Materials and Methods

To study megakaryocytic differentiation and maturation, long-term video microscopy was performed on cord blood (CB)- or bone marrow (BM)-Hematopoietic Stem Cells (HSC, $CD34^+$-enriched, $\geq$ 90% purity) induced to undergo specific megakaryocytic differentiation with the addition of thrombopoietin (TPO), the principal stimulator of megakaryopoiesis. The culture strategy was applied as previously reported[5]. Imaging was conducted during two culture time windows; from day 0 to day 5 and from day 5 to day 10. The goal of the first imaging experiment (day 0 − 5) was to study HSC differentiation and the onset of polyploid cell formation, while that of the second experiment (day 5 − 10) was to monitor a greater number of polyploid MKs in order to analyze this process in more details.

A.4. Results

It is generally believed and accepted that once a MK has reach the endomitosis stage of maturation and undergone polyploidization, this cell ceases to undergo mitosis. However, contrary to such expectation complete division of polyploid MKs were frequently observed in CB-cultures. The peak of polyploid MK division occurred with tetraploid cells (4N) and in different forms such as divisions into: i) 2 x 4N cells, ii) 1 x 2N and 1 x 6N, and iii) 2 x 2N and 1 x 4N. Furthermore, divisions of 6N, 8N and 16N cells were also observed. To

investigate whether the capacity of polyploid MKs to complete mitosis was exclusive to MKs derived from CB-HSC; similar experiments were performed with adult human BM-HSC. Overall, a total of 1,723 CB-MKs (1,180 x 2N, 301 x 4N, 186 x 8N, 24 x 6N, 16 x 12N, and 16 x 16N) and 1,322 adult human BM-cells (677 x 2N, 405 x 4N, and 240 x 8N) were observed and included in our analyses. The results showed that BM-tetraploid and octaploid MKs were also able to undergo complete mitosis, however this occurred at a much lower frequency than for CB-MKs. To better compare cell decision to complete or not mitosis as a function of cell source and ploidy level, a mitosis completion index was defined (Figure A.1). These results clearly show that polyploid CB- and BM-derived MKs differ significantly in their capacity to undergo mitosis, but that the capacity of all polyploid MKs to undergo mitosis is inversely related to their ploidy level.
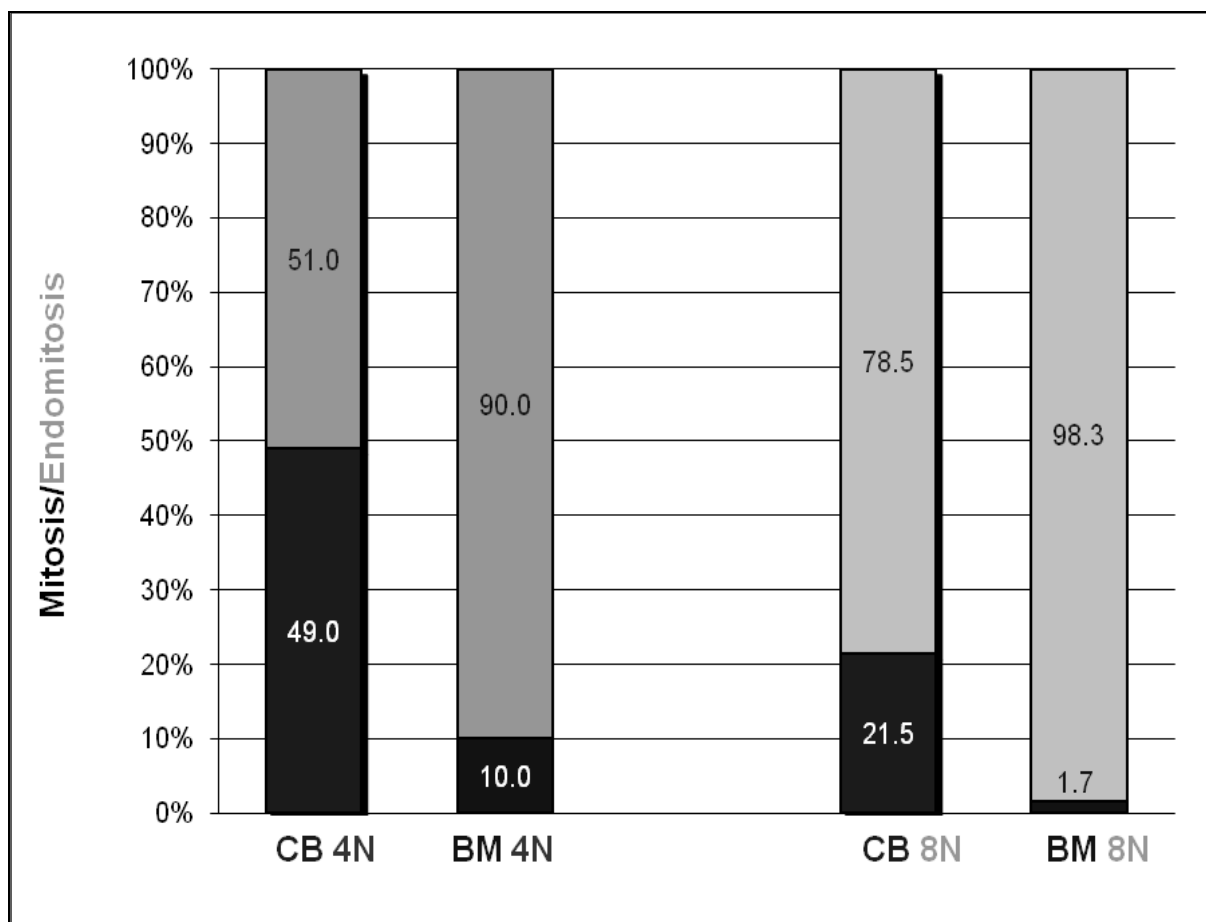
Figure A.1: Comparison of mitosis vs. endomitosis activity index for 4N and 8N polyploid megakaryocytes derived from cord blood and bone marrow CD34$^+$ cells. In this analysis,

the index was defined as the ratio of cells that completed mitosis or endomitosis over the total of both outcomes.

The monitoring of cell fates and their descendant's was used to construct MK lineage trees representing cell life history from the initial hours to the end of the live cell imaging experiments. Based on cell division and polyploidization events, four recurrent MK lineage tree patterns were observed: i) the "*proliferative*'' lineage pattern, where an original 2N parent cell and all its descendants divided symmetrically into 2 x 2N daughter cells until either death or the end of the experiment; ii) the "*polyploidizing*" pattern, where an original parent cell and its descendants exclusively underwent endomitosis; iii) the "*quiescent*" pattern; where cells neither divided nor underwent polyploidization; and iv) the "*mixed*" pattern of proliferation and polyploidization; where an original parent cell and/or its descendants either divided or underwent polyploidization (Figure A.2). In the *mixed* pattern, the descendants exhibited both mitotic and endomitotic activities and a polyploid cell could often divide into two (or sometimes more than two) daughter cells with identical or different ploidy levels. In general, the life of descendents in all patterns ended either directly by death or indirectly through proplatelet formation followed by death. In the mixed pattern, fates of daughter cells were different from those of the parent and even sister cells had different fates from each other, leading to either mitosis or endomitosis. The switch from a mitotic to endomitotic cycle and vice-versa in the mixed patterns was not found related to generation per se. These results together with dividing polyploid cell fate analyses indicate that polyploidization of a given cell is partially determined by the decision of its ancestor's, but also by some unknown, still undetermined factors.
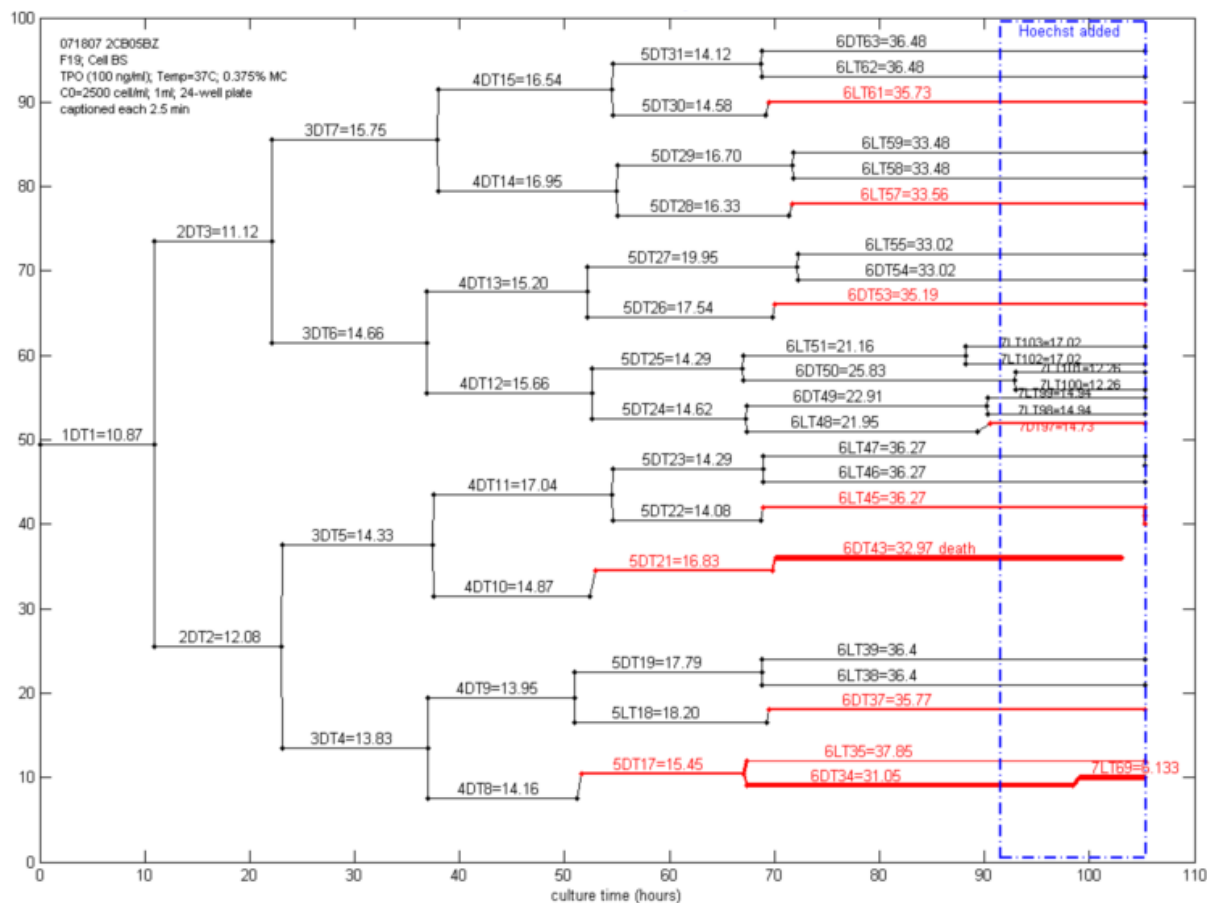
**Figure A.2:** A representative CB-derived MK lineage tree (mixed pattern).

Another simple way to analyze imaging-based data is to measure the cell cycle duration. For instance, it could be interesting to know if the endomitotic cell cycle is shorter or longer that the mitotic cycle. Analysis of the whole cell cycle period including cytokinesis stage and before cleavage furrow formation in diploid and polyploid CB-MK was performed over hundreds of single cells. Contrary to expectation, the result (Figure A.3) showed that the endomitotic cycle was significantly (p < 0.0001) longer than the mitotic cycle for 2Ns either for the whole cell cycle or the specific duration of cytokinesis as such (anaphase midzone and cleavage furrow formation). These differences were not found significant among 4Ns. Furthermore, cell cycle time slightly but significantly increases with ploidy level from 2N to 4N for mitosis (p < 0.1) but not for endomitosis.
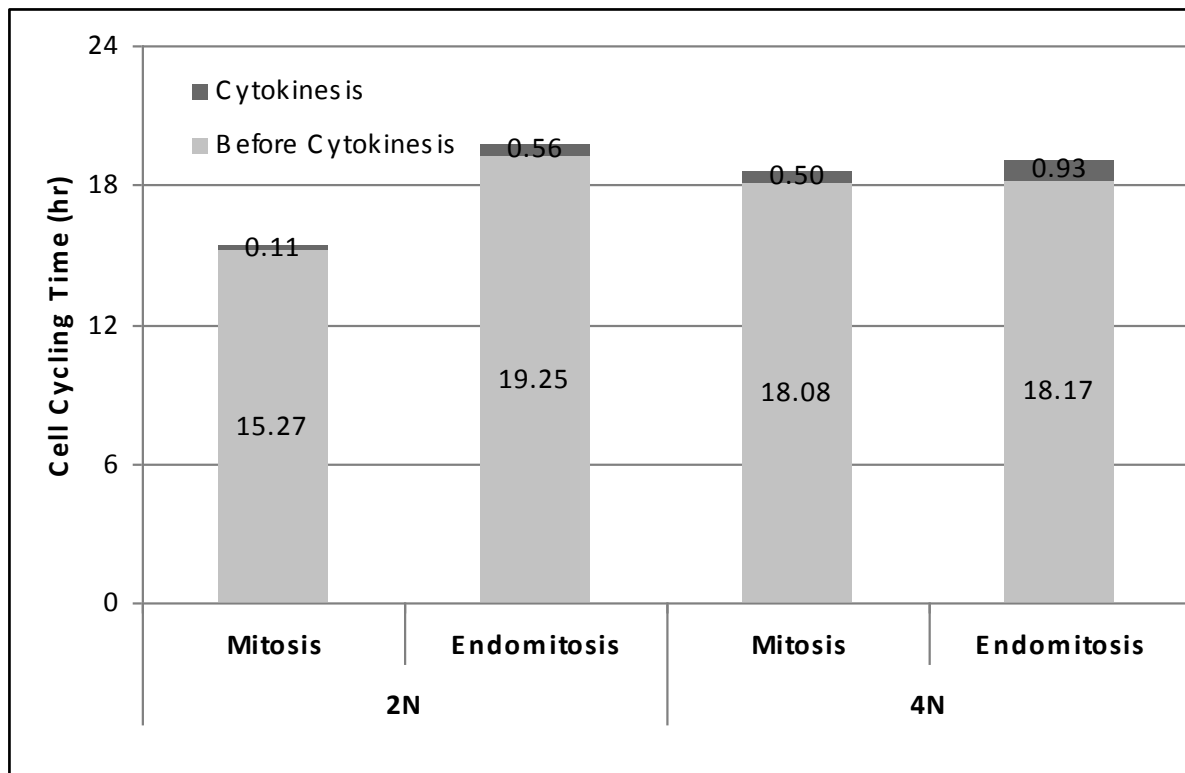
Figure A.3: Comparison of mitosis and endomitosis cell cycling periods for diploid and polyploid CB-derived MK. The analysis included 370 mitosing and 50 endomitosing 2N cells, and 7 mitosing and 30 endomitosing 4N cells. Numbers on each bar shows the average duration.

The number of descendent cells in each generation (Figure A.4A), as well as their frequencies (Figure A.4B) can also be calculated from live cell imaging data. The resulting information allows determining generation dynamics much more precisely than what is generally obtained by techniques such as CFSE staining, as soon as the number of initial cells used for the calculation exceeds 5 cells. From that point, several mathematical models such as age-maturity structure, cell-cycle distribution, cell growth kinetics, etc can be applied on the obtained data from cell imaging and lineage trees and the effects of environmental factors can be studied.
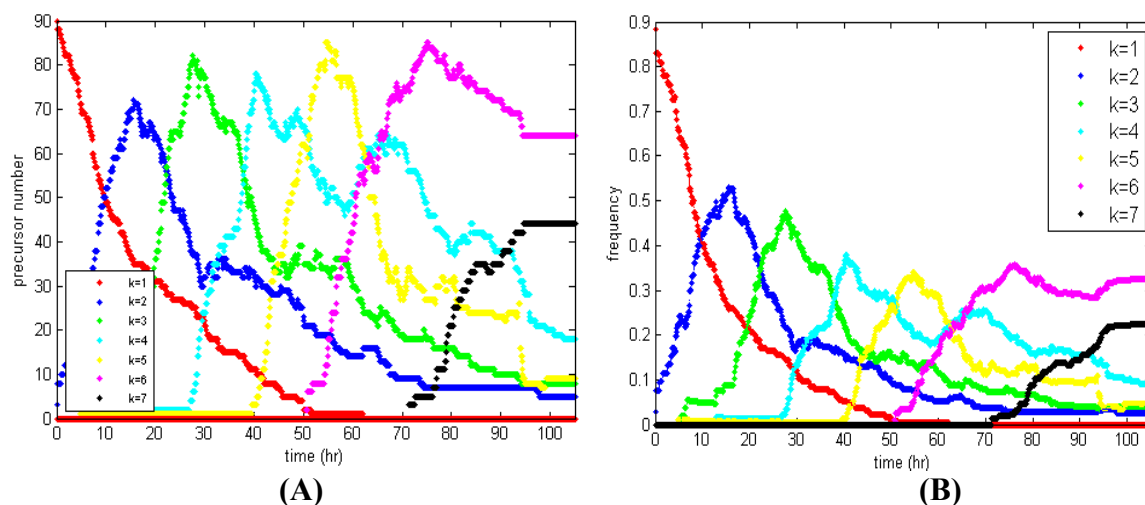
Figure A.4: Distribution of CB-derived MK generations over time: **A)** dynamics of descendent cell numbers, **B)** dynamics of descendent frequency (n = 90).

A.5. Discussion

The main objective of this study was to quantify in detail the formation and the fates of a large number of polyploid MKs in order to better describe and understand the complex phenomenon of MK polyploidization. Long-term and large-field live cell imaging was used to follow the differentiation and maturation of MKs from immature CD34^{+} progenitor cells. Our observations confirmed that polyploidization follows the failure of cytokinesis[2,3,6]. However, the main discovery of this work is that a large number of polyploid MKs (4N, 6N, 8N, and 16N) can complete mitosis thereby producing additional polyploid MKs. Though little is known at this time on this process and its regulation, this finding nonetheless challenges the concept that polyploid MKs are only derived from diploid cells undergoing repeated endomitosis. This unexpected phenomenon was not specific to CB-derived MKs as it was also observed in MKs derived from adult BM-HSCs, though at a lower frequency. This finding explains partially the lower ploidy levels of CB-derived MKs generally observed[7-9].

Recording and classification of all cellular events together with the analysis of cell lineage trees made possible the identification of recurrent patterns of MK growth and development. Few if any studies have used such approach to shed some light on the complex fate-decision dilemma that takes place when multipotent stem cells undergo differentiation. This approach provided valuable information on the fates of CD34^{+} cells and their descendants

in both quantitative and qualitative forms. The precise mechanism regulating MK fates and pattern distributions *ex vivo* still remains unclear; however, our results provide indications on the nature and the frequencies of these fates.

A.6. Conclusion

In summary, a large body of evidences presented in this study demonstrates that polyploid CB- and BM-derived MKs can undergo complete mitosis. The molecular mechanism responsible for this new process is at this time unknown and needs to be studied further. Our findings also confirm that endomitosis remains the main mechanism to initiate polyploidization of diploid MKs and to further increase the ploidy of pre-established polyploid MKs, while polyploid MK division is perhaps a new mechanism that can be used to propagate low polyploid MKs.

A.7. References

1. Cramer EM, Vainchenker W. Chapter 25. Platelet Production: Cellular and Molecular Regulation (ed 5th). Philadelphia, PA: Lippincott Williams & Wilkins; 2006.
2. Geddis AE, Kaushansky K. Endomitotic megakaryocytes form a midzone in anaphase but have a deficiency in cleavage furrow formation. Cell Cycle. 2006;5:538-545.
3. Geddis AE, Fox NE, Tkachenko E, Kaushansky K. Endomitotic megakaryocytes that form a bipolar spindle exhibit cleavage furrow ingression followed by furrow regression. Cell Cycle. 2007;6:455-460.
4. Battinelli EM, Hartwig JH, Italiano JE, Jr. Delivering new insight into the biology of megakaryopoiesis and thrombopoiesis. Curr Opin Hematol. 2007;14:419-426.
5. Cortin V, Garnier A, Pineault N, Lemieux R, Boyer L, Proulx C. Efficient in vitro megakaryocyte maturation using cytokine cocktails optimized by statistical experimental design. Exp Hematol. 2005;33:1182-1191.
6. Lordier L, Jalil A, Aurade F, et al. Megakaryocyte endomitosis is a failure of late cytokinesis related to defects in the contractile ring and Rho/Rock signaling. Blood. 2008;112:3164-3174.
7. Hegyi E, Nakazawa M, Debili N, et al. Developmental changes in human megakaryocyte ploidy. Exp Hematol. 1991;19:87-94.
8. Miyazaki R, Ogata H, Iguchi T, et al. Comparative analyses of megakaryocytes derived from cord blood and bone marrow. Br J Haematol. 2000;108:602-609.
9. Tao H, Gaudry L, Rice A, Chong B. Cord blood is better than bone marrow for generating megakaryocytic progenitor cells. Exp Hematol. 1999;27:293-301.